KAERI/TR-1619/2000

SSC-K 전산코드 사용자 지침서 (Rev.0)

SSC-K Code User's Manual (Rev.0)

2000. 7

한 국 원 자 력 연 구 소

PLEASE BE AWARE THAT
ALL OF THE MISSING PAGES IN THIS DOCUMENT
WERE ORIGINALLY BLANK

제 출 문

한국원자력연구소장 귀하

본 보고서를 2000 년도 "액체금속로 안전해석 기술개발" 과제의 기술보고서로 제출합니다.

제목: SSC-K 전산코드 사용자 지침서 (Rev.0)
SSC-K Code User's Manual (Rev.0)

2000. 7

과 제 명 : 액체금속로 안전해석 기술개발
주 저 자 : 권영민
공 저 자 : 이용범
장원표
한도희

요 약 문

한국원자력연구소 (KAERI)는 Pool 형 액체금속로인 KALIMER 의 다양한 비정상 조건 및 사고를 분석하기 위하여 최적열수력 전산코드인 SSC-K (Supper System Code of KAERI)를 개발하고 있다. SSC-K 는 미국 BNL 에서 루프형 액체금속로의 안전해석을 위해 개발된 SSC-L 을 기반으로 하여 KALIMER 와 같은 풀형 원자로에 적용할 수 있도록 개발되었다. 현재 SSC-K 코드는 루프형과 풀형의 액체금속로를 모두 모의할 수 있다. SSC-K 는 과도상태의 열수력, 핵 및 기계적 모델을 포함하고 있으므로 사고시 노심과 냉각재, 핵연료의 거동 및 구조물의 온도변화를 을 모의할 수 있다.

본 보고서는 SSC-K 를 위하여 새로이 개발된 여러 현상학적인 모델들을 기술하고 있으며 부록에는 코드입력에 대한 설명을 포함하고 있다. 풀형 원자로 열수력 계산을 위해 개발된 정상상태 및 과도상태의 모델을 2 장과 3 장에 상세히 설명하였다. 4 장에는 기존 SSC-L 코드의 IHX 모델을 풀형의 원자로 구성에 적합하도록 변경한 중간열전달교환기 (IHX) 모델에 대해서 기술하였다. 5 장에는 전자펌프 모델을 설명하였으며, SSC-K 는 기존의 원심펌프 외에 KALIMER 설계에 도입된 전자펌프 모델을 선택적으로 사용 가능하다. 6 장에는 노심에서 발생되는 붕괴열을 원자로 벽면과 압력용기 벽면을 통하여 주변의 공기로 제거하는 PSDRS 모델을 기술하였다. 7 장에는 도플러와 소듐밀도 변화에 의한 반응도 모델 및 노심의 기하학적 변형에 의한 여러 반응도 궤환 모델에 대하여 설명하였다. 마지막으로 8 장에는 SSC-K 에 사용되는 상관식 및 물성치에 대하여 기술하였다. 참고로 부록 A 와 B 에는 코드 입력에 대한 설명 및 SSC-K 에 사용된 Subroutines 을 포함시켰다.

시험계산을 통하여 개발된 SSC-K 코드의 예측능력에 대한 타당성을 정성적으로 확인하였다. 전형적인 액체금속로 사고들에 대하여 SSC-K 를 사용한 안전해석 결과는 별도의 보고서로 발간될 예정이다. 시험해석 결과에 의하면 개발된 SSC-K 코드는 향후 KALIMER 예비 안전해석에 사용할 수 있을 것으로 판단된다. SSC-K 코드는 계속 개발 중에 있으므로 사용자 지침서 역시 앞으로 개정될 예정이다.

SUMMARY

The Supper System Code of KAERI (SSC-K) is a best-estimate system code for analyzing a variety of off-normal or accidents in the heat transport system of a pool type LMR design. It is being developed at Korea Atomic Energy Research Inititution (KAERI) on the basis of SSC-L, originally developed at BNL to analyze loop-type LMR transients. SSC-K can handle both designs of loop and pool type LMRs. SSC-K contains detailed mechanistic models of transient thermal, hydraulic, neutronic, and mechanical phenomena to describe the response of the reactor core, icoolant, fuel elements, and structures to accident conditions.

This report provides an overview of recent model developments of the SSC-K computer code, focusing on phenomenological model descriptions for new thermal, hydraulic, neutronic, and mechnaical modules. A comprehensive description of the models for pool-type reactor is given in Chapters 2 and 3; the steady-state plant characterization, prior to the initiation of transient is described in Chapter 2 and their transient counterparts are discussed in Chapter 3. In Chapter 4, a discussion on the intermediate heat exchanger (IHX) is presented. The IHX model of SSC-K is similar to that used in the SSC-L, except for some changes required for the pool-type configuration of reactor vessel. In Chapter 5, an electromagnetic (EM) pump is modeled as a component. There are two pump choices available in SSC-K; a centrifugal pump which was originally imbedded into the SSC-L, and an EM pump which was introduced for the KALIMER design. In Chapter 6, a model of passive safety decay heat removal system (PSDRS) is discussed, which removes decay heat through the reactor and containment vessel walls to the ambient air heat sink. In Chapter 7, models for various reactivity feedback effects are discussed. Reactivity effects of importance in fast reactor include the Doppler effect, effects of sodium density changes, effects of dimensional changes in core geometry. Finally in Chapter 8, constitutive laws and correlations required to execute the SSC-K are described.

Test runs for typical LMFBR accident analyses have been performed for the qualitative verification of the developed SSC-K modules. The analysis results will be issued as a separate report. It was found that the present version of SSC-K would be used for the priliminary safety analysis of KALIMER. However, the further validation of SSC-K is required for real applications. It is noted that the user's manual of SSC-K will be revised later with the further development of SSC-K code.

Table of Contents

List of Figures

List of Tables

1. INTRODUCTION

The Supper System Code of KAERI (SSC-K) is a best-estimate system code for analyzing a variety of off-normal or accidents in KALIMER [1-1] which is a pool type design. It is developed at Korea Atomic Energy Research Inititution (KAERI) on the basis of SSC-L [1-2] developed at BNL to analyze loop-type LMR transients. Because of inherent difference between the pool and loop design, the major modifications of SSC-L has been made for the safety analysis of KALIMER.

The major difference between KALIMER and general loop type LMRs exists in the primary heat transport system as shown in Fig. 1.2. In KALIMER, all of the essential components consisted of the primary heat transport system are located within the reactor vessel. This includes reactor, four EM pumps, primary side of four intermediate heat exchangers, sodium pools, cover gas blanket, and associated pipings. This is contrast to the loop type LMRs, in which all the primary components are connected via piping to form loops attached externally to the reactor vessel. KALIMER has only one cover gas space. This eliminates the need for separate cover gas systems over liquid level in pump tanks and upper plenum. The IHX outlet is directly connected to cold pool instead of the piping into pump suction which is a typical configuration in loop type LMRs. Since the sodium in hot pool is separated from cold pool by insulated barrier in KALIMER, the liquid level in hot pool is different from that in the cold pool mainly due to hydraulic losses and pump suction heads occuring during flow through the circulation pathes. In some accident conditions the liquid in the hot pool is flooded into cold pool and it forms the natural circulation flow path. During the loss of heat sink transients, this will provided as a major heat rejection mechanism with the passive decay heat removel system. Since the pipes in the primary system exist only between pump discharge and core inlet plenum and are submerged in cold pool, a pipe rupture accident becomes less severe due to a constant back pressure exerted against the coolant flow from break. The intermediate and steam generator systems of both designs are generally identical (Fig. 1.3).

The SSC-K is designed to predict plant response under various off-normal and accident conditions until sodium boiling occurs. This code can also perform the steady-state initialization.

This feature is provided so that user can easily obtain the various preaccident initial conditions based on user-specified design parameters and minimum operating values.

This report provides an overview of recent model developments in the SSC-K comput code, focusing on phenomenological model descriptions for new thermal, hydraulic, neutronic, and mechnaical modules. Since SSC-K is developed on the basis of SSC-L, many portions of SSC-K utilized the same methods and models as its parent code SSC-L. Therefore, the primary emphasis in the development and its description in the report has been focused on the differences between the two codes.

A comprehensive description of the models for pool-type reactor is given in Chapters 2 and 3; the steady-state plant characterization, prior to the initiation of transient is described in Chapter 2 and their transient counterparts are discussed in Chapter 3. In Chapter 4, a discussion on the intermediate heat exchanger (IHX) is presented. The IHX model of SSC-K is similar to that used in the SSC-L, except some changes required for the pool-type configuration of reactor vessel. In Chapter 5, an electromagnetic (EM) pump is modeled as a component. There are two pump choices available in SSC-K; a centrifugal pump which was originally imbedded into the SSC-L, and an EM pump which was introduced for the KALIMER design. In Chapter 6, a model of passive safety decay heat removal system (PSDRS) is discussed, which removes decay heat through the reactor and containment vessel walls to the ambient air heat sink. In Chapter 7, models for various reactivity feedback effects are discussed. Reactivity effects of importance in fast reactor include the Doppler effect, effects of sodium density changes, effects of dimensional changes in core geometry. Finally in Chapter 8, constitutive laws and correlations required to execute the SSC-K are described.

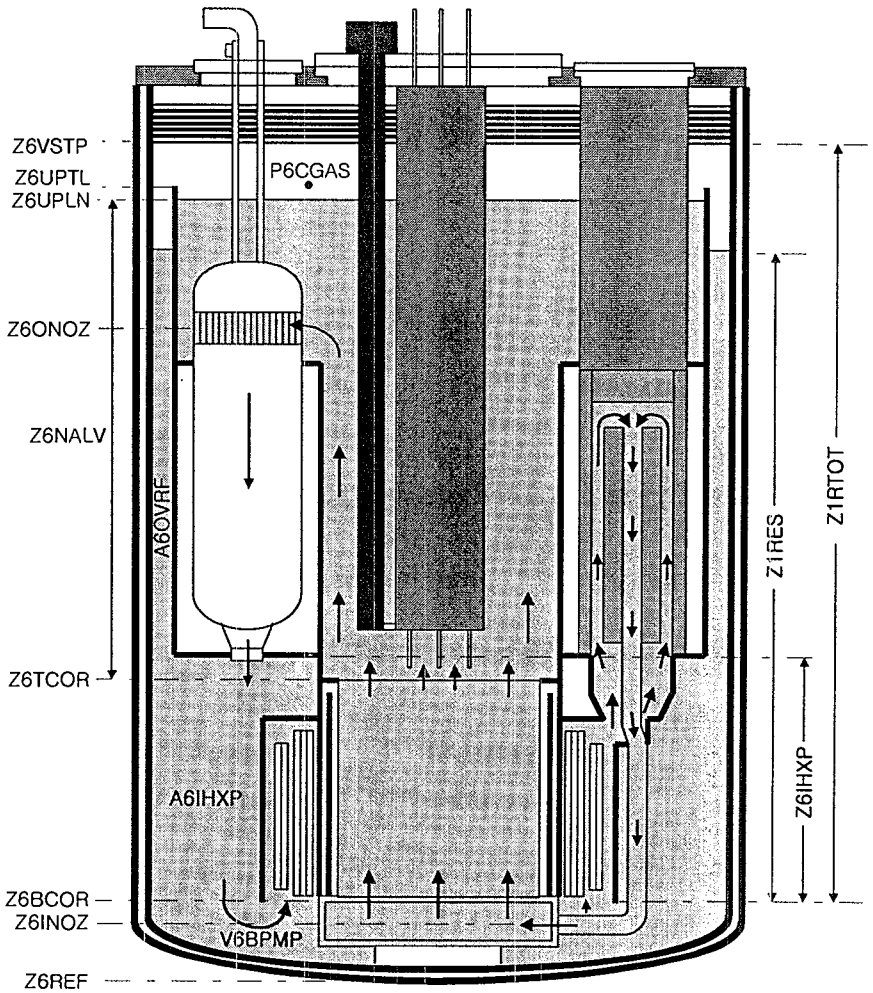

Fig. 1.1 KALIMER Primary System

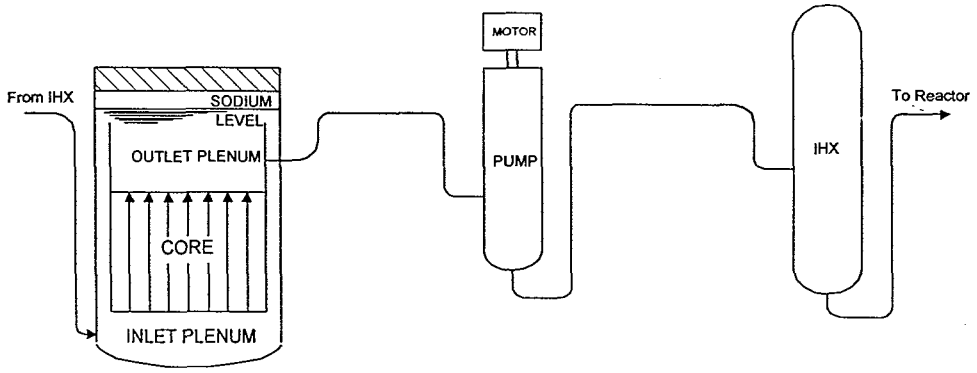

(a) Loop-type LMR

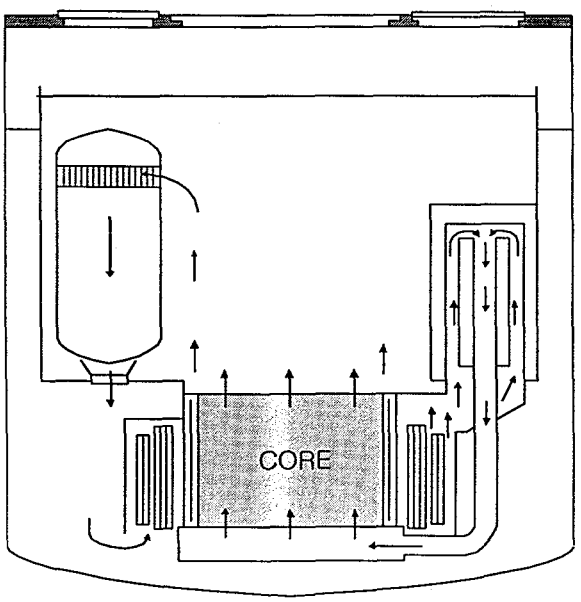

(b)Pool-type LMR

Fig. 1.2 Primary System Schematics

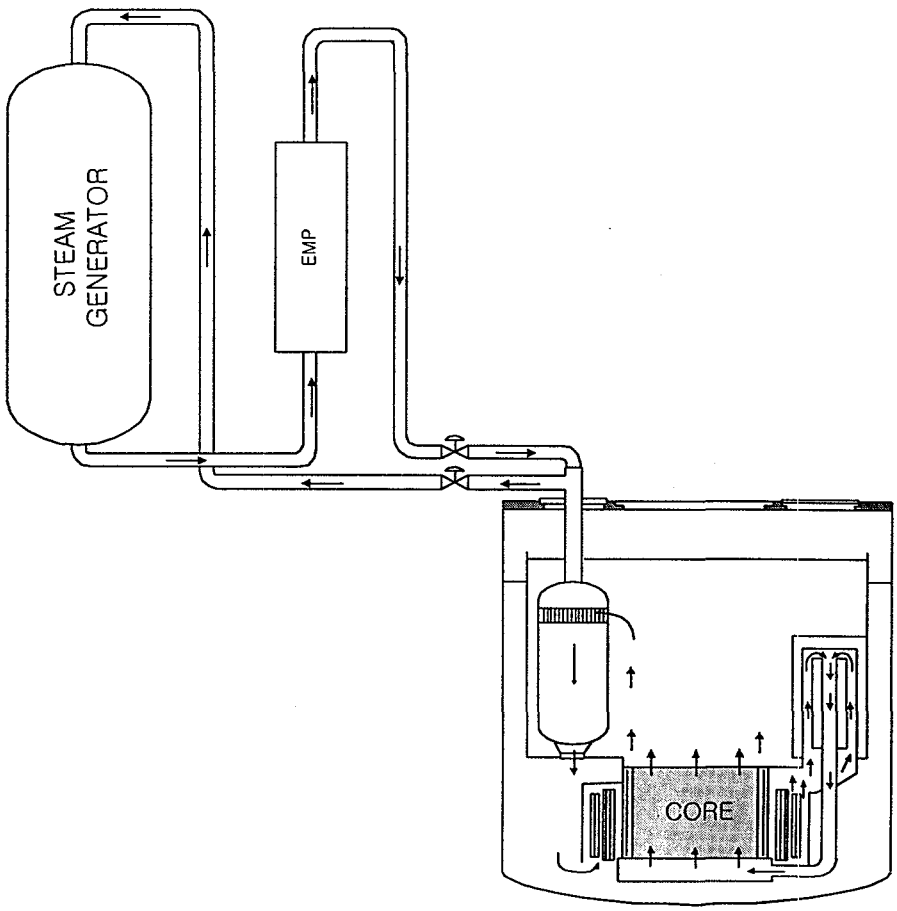

Fig. 1.3 Schematic Diagram of KALIMER System

2. STEADY-STATE MODELS

In the initial part of the transient calculation, a stable and unique steady state or pre-transient solution for entire plant must be obtained. As a result, the continuity, energy, and momentum conservation equations in time-independent form are reduced to a set of nonlinear algebraic equations. These equations are solved in two steps. First, the global parameters are obtained. More detailed characterization is achieved by using the global conditions obtained in the first step, as boundary conditions. Since the SSC-K is developed based on SSC-L, the most of the steady-state routine in SSC-L is used with minimum changes. Some modifications are required due to including the cold pool model into SSC-K. The flow chart for steady-state solution routine is in Fig. 2.1.

2.1 Global Heat Balance

At steady state, the fluid and metal in the core inlet plenum are assumed to be thermal equilibrium. The temperatures are then equal to the user specified fluid temperature at the inlet nozzle, i.e.,

$$T_{lplenum} = T_{metal} = T_{6inlt} \tag{2-1}$$

The core inlet temperature is specified as input. The hot pool sodium enthalpy and temperature can be obained using known values of core power and mass flow rate:

$$h_{6outl} = h_{6inlt}(T_{6inlt}) + P_{core} / W_{6tot} \tag{2-2}$$

$$T_{6outl} = f(h_{6outl}) \tag{2-3}$$

The IHX inlet and outlet temperatures are determined according to the location of pump in

order to account the temperature rise due to pump heat generation.

$$\begin{cases} T_{INIHX} = T_{6outl} + \Delta T_{1pump} & \text{if pump is between hot pool and IHX} \\ T_{INIHX} = T_{6outl} & \text{if pump is located after IHX} \end{cases} \quad (2\text{-}4)$$

$$\begin{cases} T_{OUHX} = T_{6inlt} - \Delta T_{1pump} & \text{if pump is between IHX and core inlet plenum} \\ T_{OUHX} = T_{6inlt} & \text{if pump is located before IHX} \end{cases} \quad (2\text{-}5)$$

The total heat removal rate by IHX can be calculated as following:

$$Q_{TOINT} = W_{loop}\left[h(T_{INIHX}) - h(T_{OUHX})\right] \quad (2\text{-}6)$$

2.1.1 Steady State Calculation in IHX

To start the steady state calculations for IHX, the boundary temperatures at one end of IHX, in this case T_{1INHX}, T_{2IHXO} and W_{2loop}, must been known. T_{INHX} is known from global thermal balance calculations. The IHX outlet temperature and flow rate for intermediate side are guessed for first pass:

$$\begin{cases} W_{2loop} = W_{1loop} + 1.0 \\ T_{2IHXO} = T_{1INHX} - 20 \qquad \text{where } T_{2IHXI} = \text{known} \end{cases} \quad (2\text{-}7)$$

The iteration procedure for the temperature distribution of IHX is as following:

Step 1. Find out the node length and heat transfer areas for tube and shell sides:

Δx : length of IHX node

A_2 : primary side (shell side) heat transfer area for each IHX node

$= \pi \cdot (IHX\ tube\ outer\ diameter) \cdot \Delta x \cdot (\#\ tubes)$

A_1 : intermediate side (tube side) heat transfer area for each IHX node

Step 2. Compute the constants for computation of Peclet numbers:

$$A_{PEP} = (diameter)(velocity)(density) = P_e \cdot k / c_p = \frac{W_{1loop} \cdot d_1}{A_{1IHX}} \tag{2-8}$$

$$A_{PES} = (diameter)(velocity)(density) = P_e \cdot k / c_p = \frac{W_{2loop} \cdot d_2}{A_{2IHX}} \tag{2-9}$$

Step 3. Guess the tube structure temperature (Fig. 2.2):

$$TT = \frac{T_{i,p} + T_{i,s}}{2}$$

$$T_{po} = T_{pi}, \quad T_{so} = T_{si} \tag{2-10}$$

Step 4: Calculate the node average sodium temperatures:

$$\overline{T}_p = \frac{T_{po} + T_{pi}}{2}, \qquad \overline{T}_s = \frac{T_{so} + T_{si}}{2} \tag{2-11}$$

Step 5: Find out the non-dimensional numbers for heat transfer coefficients:

Peclet numbers for primary and intermediate sides

$$P_{ep} = A_{PEP} \cdot c_{p_p} / k_p, \quad P_{es} = A_{PES} \cdot c_{p_s} / k_s \tag{2-12}$$

Nusselt number

$$Nu_p = a + b \cdot P_e^c \qquad \text{Shell side (primary)} \tag{2-13}$$

Aoki's correlation for tube side (intermediate)

$$Nu_s = 6.0 + 0.025 \cdot (\overline{\Psi} Pe_s)^{0.8} \tag{2-14}$$

where

$$\overline{\Psi} = \frac{0.014(1 - e^{-71.8x})}{x} \tag{2-15}$$

$$x = \frac{1}{Re_s^{0.45} \cdot Pr_s^{0.2}} \tag{2-16}$$

$$Re_s = \frac{\rho u d}{\mu} = \frac{A_{PES}}{\mu_s} \tag{2-17}$$

$$Pr_s = \frac{\nu}{\alpha} = \frac{c_{p_s} \cdot \mu_s}{k_s} \tag{2-18}$$

Step 6: Calcualte the overall heat transfer coefficients:

$$U_{pt} = \frac{1}{\frac{D_{h,p}}{Nu_p \cdot k_p} + r_{wall,p} + r_{foul,p}} \tag{2-19}$$

$$U_{st} = \frac{1}{\frac{D_{h,s}}{Nu_s \cdot k_s} + r_{wall,s} + r_{foul,s}} \tag{2-20}$$

Step 7: Calculate the node outlet temperatures for primary and intermediate sides:

$$e_{po1} = e_{pi} + \frac{A_2 \cdot U_{pt}(TT - \overline{T}_p)}{W_{1loop}} \tag{2-21}$$

$$e_{so1} = e_{si} + \frac{A_1 \cdot U_{st}(TT - \overline{T}_s)}{W_{2loop}} \tag{2-22}$$

$$T_{pol} = T(e_{pol}) \tag{2-23}$$

$$T_{sol} = T(e_{sol}) \tag{2-24}$$

Step 8: Calculate the node average sodium temperatures and tube temperature based on the calculated node exit temperatures:

$$\overline{T}_p = \frac{T_{pol} + T_{pi}}{2} \tag{2-25}$$

$$\overline{T}_s = \frac{T_{sol} + T_{si}}{2} \tag{2-26}$$

$$TT_l = \frac{A_l U_{st} \overline{T}_s + A_2 U_{pt} T_p}{A_l U_{st} + A_2 U_{pt}} \tag{2-27}$$

Step 9: Perform the convergence test for the node:

$$\text{if} \quad \left|T_{po} - T_{pol}\right| > \varepsilon \quad \text{and} \quad \left|T_{so} - T_{sol}\right| > \varepsilon \quad \text{and} \quad \left|TT - TT_l\right| > \varepsilon \quad \text{then} \tag{2-28}$$

$$T_{pol} \rightarrow T_{po}, \quad T_{sol} \rightarrow T_{so}, \quad TT_l \rightarrow TT \tag{2-29}$$

go to Step 4 and iterate again.

Step 10: Reset the node exit temperatures into the inlet temperatures for next node until $i = nihx1$:

$T_{pol} \rightarrow T_{pi}$, $T_{sol} \rightarrow T_{si}$, $TT_l \rightarrow TT$ and go to Step 4 and continue for next node.

Step 11. Perform the error checking if the energy gain is equal to energy loss:

$$T_{1OUHX} = T(e_{po}) \tag{2-30}$$

$$T_{2INHX} = T(e_{so}) \tag{2-31}$$

$$Q_{1loss} = W_{1loop}(e_{p,in} - e_{po}) \tag{2-32}$$

$$Q_{2gain} = W_{2loop}(e_{s,out} - e_{s,in}) \tag{2-33}$$

$$\text{if } \left|1 - \frac{Q_{2gain}}{Q_{1loss}}\right| > \varepsilon \qquad \text{error} \tag{2-34}$$

Step 12. Check for convergence based on total energy balance:

The heat rejection from IHX should equal to the reactor heat plus heat addition at the pump within specified limits:

$$\text{if } \left|\frac{Q_{TOINT} - Q_{2gain}}{Q_{TOINT}}\right| < \varepsilon \quad \text{quit interation} \tag{2-35}$$

Step 13. If not, the secondary outlet temperature and flow rate have to be reselected and the computation repeated until convergence is obtained:

Log-mean temperature difference

$$\Delta\overline{T} = \frac{(T_{1OUHX} - T_{2INHX}) - (T_{1INHX} - T_{2OUHX})}{ln[(T_{1OUHX} - T_{2INHX})/(T_{1INHX} - T_{2OUHX})]} \tag{2-36}$$

$$UA = Q_{2gain} / \Delta\overline{T} \tag{2-37}$$

Assuming UA constant, determine new *lmtd* guess

$$\Delta\bar{T}_{new} = Q_{TOINT} / UA \quad . \tag{2-38}$$

$$\Delta T_A = T_{1OUHX} - T_{2INHX} \tag{2-39}$$

$$\Delta\bar{T}_{new} = \frac{\Delta T_A - \Delta T_B}{ln[\Delta T_A / \Delta T_B]} \quad \rightarrow \text{Find } \Delta T_B \text{ using root finding scheme.} \tag{2-40}$$

$$T_{2OUHX} = T_{1INHX} - \Delta T_B \tag{2-41}$$

$$W_{2loop} = \frac{Q_{TOINT}}{[e(T_{2OUHX}) - e(T_{2INHX})]} \quad \text{Return to Step 1} \tag{2-42}$$

After calculating the temperature distribution of IHX, the similar process is performed for the energy balance for steam generator.

2.2 Hot Pool Pressure Distribution

Subroutine PINT1S calculates the interface pressure between the hot pool and IHX.

$$P_{1INLT} = P_{6CGAS} + \rho(T_{6OUTL}) \cdot g(Z_{6UPLN} - Z_{6ONOZ}) \tag{2-43}$$

where Z_{6UPLN} : relative height of sodium in vessel upper plenum to Z_{6REF}

Z_{6ONOZ} : elevation of vessel outlet nozzle above Z_{6REF}

$$T_{1INLT} = T_{6OUTL} \tag{2-44}$$

$$P_{6OUTL} = P_{1INLT} \tag{2-45}$$

$$P_{6INTL} = P_{6OUTL} + P_{1PDRV} \tag{2-46}$$

where P_{1PDRV} : pressure drop between core inlet and IHX inlet

2.3 Thermal-Hydraulics for Fuel Assembly Region

2.3.1 Core Thermal-Hydraulics

The core region is divided into *N6CHAN* parallel channels. These channels represent either fuel, blanket, or control rods. The flow rate for each channel is obtained by user specified flow fraction of the total flow through these channels.

$$W_{6CHAN_j} = W_{6TOT} \cdot F_{6FLOW_j} \tag{2-47}$$

$$G_{6I_j} = \frac{W_{6CHAN_j}}{N_{6RODS_j} \cdot A_{6ROD_j}} \tag{2-48}$$

where G_{6I_j} : mass flux of channel j

N_{6RODS_j} : number of rods in channel j

A_{6ROD_j} : sodium flow area per rod in channel j

Each of the flow channels is divided into a user-controlled number of axial slices. The axial distributions of coolant enthalpy and pressure in all channels are determined in this subroutine.

$$F_{CONSI} = \frac{P_{6TPOW} \cdot F_{6TPOW_j}}{Z_{6CHAN} \cdot W_{6CHAN_j}} \tag{2-49}$$

where F_{6TPOW_j} : Total normalized power fraction in channel j from fission and decay heating

$$Q_{FACT_{ji}} = \frac{dh}{dz}\Delta z = \frac{1}{W_{6CHAN_j}} \frac{P_{6TPOW} \cdot F_{6TPOW_j} \cdot F_{6NPWA_{ji}} \cdot Z_{6DELT_{ji}}}{Z_{6CHAN} \cdot} = F_{CONSI} \cdot F_{6NPWA_{ji}} \cdot Z_{6DELT_{ji}} \tag{2-50}$$

where $Q_{FACT_{j,i}}$: enthalpy change in axial slice i of channel j

$F_{6NPWA_{j,i}}$: normalized axial power in axial slice i of channel j

$Z_{6DELT_{j,i}}$: length of axial slice i in channel j

$$T_{AVG} = \frac{T_{in} + T_{OLD}}{2} \tag{2-51}$$

$$T_{OUT} = T_{in} + Q_{FACT_{j,i}} / C_p(T_{AVG}) \tag{2-52}$$

where T_{in} : inlet temperature of axial slice i in channel j (known)

T_{OLD} : outlet temperature of axial slice i in channel j (unknown)

T_{OUT} : calculated outlet temperature of axial slice i in channel j

if the temperature difference between initial guessing value and calculated value, $|T_{OUT} - T_{OLD}|$, is greater than user specified limit, T_{OLD} is reseted to T_{OUT} and T_{OUT} is calculated again unitl $|T_{OUT} - T_{OLD}|$ is less than the limit. Then, the friction and heat transfer coefficients are calculated based upon the new outlet temperature of the axial slice.

$$f_{6FRIC_{j,i}} = f\left[D_h, G_{6I_j}, \mu(T_{OUT}), (P/D)_{rod}, (P/D)_{wire\ wrap}, L_{6ATYP}\right] \tag{2-53}$$

$$h_{6NODE_{j,i}} = \frac{Nu\left[D_h, G_{6I_j}, T_{AVG}, (P/D)_{rod}\right] \cdot K(T_{AVG})}{D_h} \tag{2-54}$$

After completing the calculations for the current axial slice, the same calculations performs for the next axial slice.

2.3.2 Core Pressure Distribution

Because the current version of SSC-K simulates single phase flow, the flow is assumed to be incompressiable. The axial distributions of coolant pressure in all channels are determined by momentum equations.

The pressure of the core bottom is obtained from the pressure of core inlet plenum by substracting the pressure drop due to form loss and gravitational loss:

$$G_{LPLN} = W_{6TOT} / A_{6LPLN} \tag{2-55}$$

$$\Delta P_{grav}^{LP} = \rho g \cdot (Z_{6BCOR} - Z_{6INOZ}) \tag{2-56}$$

$$\Delta P_{loss}^{LP} = -F_{6PKLP} \tag{2-57}$$

where G_{LPLN} : mass flux of lower plenum

ΔP_{grav}^{LP} : gravitation pressure drop from inlet nozzle to bottom of core

ΔP_{loss}^{LP} : pressure drop due to form loss from inlet nozzle to bottom of core

F_{6PKLP} : user specified pressure drop due to form loss from inlet nozzle to bottom of core

$$P_{6BCOR} = P_{6INLT} - \Delta P_{loss}^{LP} - \Delta P_{grav}^{LP} \tag{2-58}$$

$$K_{6LP} = 2\rho \cdot \Delta P_{loss}^{LP} / (G_{LPLN} \cdot |G_{LPLN}|) \tag{2-59}$$

where P_{6BCOR} : Pressure of the core bottom

K_{6LP} : Equivalent form loss coef. from inlet nozzle to bottom of core

The pressure of the core top is obtained from the cover gas pressure by adding the pressure drop due to form loss and gravitational loss:

$$G_{UPLN} = W_{6TOT} / A_{6UPLF} \tag{2-60}$$

$$\Delta P_{grav}^{UP} = \rho g \cdot (Z_{6UPLN} - Z_{6TCOR}) \tag{2-61}$$

$$\Delta P_{loss}^{UP} = -F_{6PKUP} \tag{2-62}$$

where G_{UPLN} : mass flux of upper plenum

ΔP_{grav}^{UP} : gravitation pressure drop from top of core to top of hot pool

ΔP_{loss}^{UP} : pressure drop due to form loss from top of core to top of hot pool

F_{6PKUP} : user specified pressure drop due to form loss from top of core to top of hot pool

$$P_{6TCOR} = P_{6CGAS} + \Delta P_{grav}^{UP} + \Delta P_{loss}^{UP} \tag{2-63}$$

$$K_{6UP} = 2\rho \cdot \Delta P_{loss}^{UP} / (G_{UPLN} \cdot |G_{UPLN}|) \tag{2-64}$$

where P_{6TCOR} : Pressure of the core bottom

K_{6UP} : equivalent form loss coef. from inlet nozzle to bottom of core

Before calculating the pressure distribution for the active core region, the pressre drop in inlet orifice zone has to be estimated:

$$\Delta P_{grav}^{INOZ} = \rho g \Delta Z_{6INZ} \tag{2-65}$$

$$W_{INOZ_j} = \frac{W_{6TOT} \cdot F_{6FLOW_j}}{N_{5ASSY_j}}$$

where ΔP_{grav}^{INOZ} : Pressure drop for inlet orifice zone

W_{INOZ_j} : flow rate per subassembly for channel j

F_{6FLOW_j} : flow fraction for channel j

Because the pressure drop due to friction in inlet orifice zone is given by user, the hydraulic diameter for orifice zone can be found by Bisection or Newton's method (YHYD6S).

1. Guess the initial value for D_h^n

2. Calculate the pressure drop due to friction

$$\Delta P_{fric}^{calc} = f(D_h, G, \mu)\frac{\Delta Z_{6INZ}}{D_h}\frac{G|G|}{2\rho} \tag{2-66}$$

3. Find the difference between user specified pressure drop and calculated pressure drop

$$\Delta P^{n+1} = \Delta P_{fric}^{INOZ} - \Delta P_{fric}^{calc} \tag{2-67}$$

4. Reset the upper and lower limits for Bisection method.

$$\begin{cases} \Delta P^{UP} = \Delta P^{n+1} & \text{if } \Delta P^{n+1} > 0.0 \\ \Delta P^{LOW} = \Delta P^{n+1} & \text{if } \Delta P^{n+1} < 0.0 \end{cases} \tag{2-68}$$

5. Convergence test

$$\text{if } \Delta P^{n+1} < 1.0 \text{ then } \quad D_h^{INOZ} = D_h \text{ and terminate the iteration} \tag{2-69}$$

6. Find the hydraulic diameter for next iteration:

$$D_h^{n+1} = D_h^n + \Delta P^n \left| \frac{D_h^{n-1} - D_h^n}{\Delta P^n - \Delta P^{n-1}} \right| \tag{2-70}$$

7. Test if D_h^{n+1} is within the bounds.

$$\begin{cases} \text{Reset the values and return to step2} & \text{if } D_h^{LOW} < D_h^{n+1} < D_h^{UP} \\ D_h^{n+1} = \dfrac{D_h^{LOW} + D_h^{UP}}{2} & \text{else} \\ \quad \text{Reset the values and return to step2} \end{cases} \tag{2-71}$$

Because the form loss coefficient due to expansion and contraction in inlet orifice zone is given by user, the pressure drop in orifice zone can be obtained such as:

Mass flux for inlet orifice zone is obtained from the calculated hydraulic diameter:

$$G_{INOZ} = \frac{4 \cdot W_{INOZ}}{\pi \cdot D_h^{INOZ}} \tag{2-72}$$

The pressure drop drop to form loss:

$$\Delta P_{loss}^{INOZ} = F_{6\,LSA} \cdot \frac{G_{INOZ} \cdot |G_{INOZ}|}{2\rho} \tag{2-73}$$

The pressure at the bottom of active core region is:

$$P_{6\,NODE_{j,i}} = P_{6\,BCOR} - \Delta P_{grav}^{INOZ} - \Delta P_{loss}^{INOZ} - \Delta P_{fric}^{INOZ} \tag{2-74}$$

The constant for calculation of the pressure distribution in active core region:

$$\rho_{j,\Delta i} = \frac{\rho_{j,i} + \rho_{j,i+1}}{2} \tag{2-75}$$

where $\rho_{j,\Delta i}$: average density for nodes i and $i+1$ in channel j

$$\Delta P_{j,\Delta i}^{grav} = \rho_{j,\Delta i} g \Delta Z_{j,\Delta i} \tag{2-76}$$

$$\Delta P_{j,\Delta i}^{fric} = f_{6\,FRIC} \frac{\Delta Z_{j,\Delta i}}{D_h} \frac{G_{6I}|G_{6I}|}{2\rho_{j,\Delta i}} \tag{2-77}$$

$$\Delta P_{j,\Delta i}^{mflux} = \frac{G_{6I}^2}{\rho_{j,i+1}} - \frac{G_{6I}^2}{\rho_{j,i}} \tag{2-78}$$

The pressure at node $i+1$ is:

$$P_{6\,NODE_{j,i+1}} = P_{6\,NODE_{j,i}} - \Delta P_{j,\Delta i}^{grav} - \Delta P_{j,\Delta i}^{fric} - \Delta P_{j,\Delta i}^{mflux} \tag{2-79}$$

2.3.3. Upper Plenum Thermal-Hydraulics

The core region is divided into *N6CHAN* parallel channels. These channels represent either fuel, blanket, or control rods. The flow rate for each channel is obtained by user specified flow fraction of the total flow through these channels.

$$W_{6CT} = \sum_{j}^{N6CHAN} W_{6CHAN_j} \tag{2-80}$$

$$E_{6\,AVER} = \sum_{j}^{N6CHAN} \left(W_{6CHAN_j} \cdot E_{6\,NODE_j}\right) \Big/ W_{6CT} \tag{2-81}$$

$$T_{AVER} = \left(\sum_{j}^{N6CHAN} T_{6\,NODE_j}\right) \Big/ N_{6CHAN} \tag{2-82}$$

$$Q_{IN} = \sum_{j}^{N6CHAN} \left(W_{6CHAN_j} \cdot E_{6\,NODE_j}\right) \tag{2-83}$$

The temperatures for cover gas, internal structure, thermal liner and vessel closure head can be found by solving the governing energy equations for hot pool region by iterative procedure:

1. Guess thermal liner temperature, T_{6M2} same as hot pool sodium temperature:

$$T_{6M2} = T_{6OUTL};\quad T_{UP} = T_{6OUTL};\quad T_{LOW} = -1.$$
$$E_{6BPUI} = E_{6BPLI};\quad T_{6BPUI} = T(E_{6BPUI}) \tag{2-84}$$

2. Compute the temperatures for cover gas, internal structure, thermal liner from user-specified heat transfer coefficients and the assmued thermal liner temperature:

$$T_{6CGAS} = T_{6M2} - U_{ALM2}(T_{6OUTL} - T_{6M2})/U_{AGM2} \tag{2-85}$$

$$T_{6M3} = (U_{AGM3}T_{6CGAS} + U_{AGM3}T_{6BPUI})/2 \cdot U_{AGM3} \tag{2-86}$$

$$T_{6M1} = (U_{ALM1}T_{6OUTL} + U_{AGM1}T_{6CGAS})/(U_{ALM1} + U_{AGM1}) \tag{2-87}$$

3. Compute T_{6M2}

$$T^{*}_{6M2} = T_{6CGAS} - \frac{U_{ALGL}(T_{6OUTL} - T_{6CGAS}) + U_{AGM1}(T_{6M1} - T_{6CGAS}) + U_{AGM3}(T_{6M3} - T_{6CGAS})}{U_{AGM2}} \tag{2-88}$$

4. If computed T^{*}_{6M2} is not equal to assumed T_{6M2}, reset and iterate.

In order to calculate the pressure drop for outlet module, the core outlet pressure has to be found.

$$P_{6OUTL} = P_{6CGAS} + \rho(T_{6OUTL})g \cdot (Z_{6UPLN} + Z_{6ONOZ}) \tag{2-89}$$

$$P_{6TCOR} = P_{6OUTL} + \rho(T_{6OUTL})g \cdot (Z_{6ONOZ} + Z_{6TCOR}) \tag{2-90}$$

where P_{6OUTL} : IHX inlet pressure

P_{6TCOR} : core outlet pressure

2.3.4 Core Outlet Module Hydraulics

This subrutine calculates the pressure equalization loss coefficient at outlet module.

$$W_{INOZ_j} = W_{6TOT} \cdot F_{6FLOW_j} / N_{5ASSY_j} \tag{2-91}$$

$$G_{OUZ_j} = W_{INOZ} / (A_{6ROD_j} \cdot N_{5AROD_m}) \tag{2-92}$$

where W_{INOZ_j} : flow rate per assembly in channel j

G_{OUZ_j} : mass flux per assembly in channel j

$$\Delta P^{OUT}_{grav_j} = \rho \cdot g \cdot \Delta Z_{6OUZ} \tag{2-93}$$

$$\Delta P^{OUT}_{kloss_j} = \frac{F_{6LSA_j}}{2} \frac{G_{OUZ_j} \left| G_{OUZ_j} \right|}{\rho} \tag{2-94}$$

where $\Delta P^{OUT}_{kloss_j}$: pressure drop for outlet module zone in channel j due to contraction and expansion

F_{6LSA_j} : k-loss factor for outlet module zone in channel j due to contraction and expansion

$$\Delta P_{\varepsilon} = P_{6NODE_{lastnode}} - P_{6TCOR} - \Delta P^{OUT}_{grav_j} - \Delta P^{OUT}_{kloss_j} \tag{2-95}$$

$$K_{OUT_j} = F_{6LSA4_j} = 2 \cdot \Delta P_{\varepsilon} \cdot \rho / (G_{OUZ_j} \cdot \left| G_{OUZ_j} \right|) \tag{2-96}$$

where F_{6LSA4_j} : k-loss factor for outlet module in channel j except k-loss due to expansion and contraction

2.4 Loop Hydraulics

2.4.1 Hydraulics for IHX

This subroutine solves the steady state pressure drop and/or k-loss factor for the IHX.

The pressure drop due to flow differnece:

$$\Delta P_{frow} = \left(\frac{1}{\rho_{IHX,O}} - \frac{1}{\rho_{IHX,I}} \right) \frac{W_{IHX}|W_{IHX}|}{A_{IHX}^2} \tag{2-97}$$

$$Re = \frac{W \cdot De}{A_x \cdot \mu} \tag{2-98}$$

$$f = f(Re) \tag{2-99}$$

The pressure drop due to wall friction:

$$\Delta P_{fric} = f \frac{\Delta x}{D_h} \frac{W_{IHX}|W_{IHX}|}{2\rho \cdot A_{IHX}^2} \tag{2-100}$$

The pressure drop due to gravitation:

$$\Delta P_{grav} = g\left(\rho_{IHX,I} \cdot \sin\phi_{IHX,I} \Delta x_{IN} + \rho_{IHX,O} \cdot \sin\phi_{IHX,O} \Delta x_{OUT} + \sum_{i}^{N_{INODE}} \rho_i \cdot \sin\phi_i \Delta x_i \right) \tag{2-101}$$

The pressure drop due to contraction or expansion at IHX inlet:

$$\Delta P_{loss,in} = K_{in} \frac{W_{IHX}|W_{IHX}|}{2\rho_{in} \cdot A_{in}^2} \tag{2-102}$$

The pressure drop due to contraction or expansion at IHX outlet:

$$\Delta P_{loss,out} = K_{out} \frac{W_{IHX}|W_{IHX}|}{2\rho_{out} \cdot A_{out}^2} \tag{2-103}$$

The total pressure drop except the pressure drop due to k-loss factor inside IHX:

$$\Delta P_{SUM} = \Delta P_{flow} + \Delta P_{fric} + \Delta P_{grav} + \Delta P_{loss,in} + \Delta P_{loss,out} \tag{2-104}$$

The total k-loss factor for IHX except k-loss due to contraction and expansion:

$$K_{IHX} = 2\rho_{IHX}(P_{1PDHX} - \Delta P_{SUMs}) \frac{A_{IHX}^2}{W_{IHX}|W_{IHX}|} \tag{2-105}$$

2.4.2 Hydraulics for Pipes

This subroutine solves the steady state flow equations for a pipe in the coolant loop. It is assumed that the diameter is constant, and the pipe wall is in thermal equilibrium with the coolant.

$$\Delta x_{node} = \Delta x_{pipe} / N_{1NODE} \tag{2-106}$$

$$sin_{SUM} = \sum_{i}^{N_{1NODE}-1} sin\,\phi_i \tag{2-107}$$

$$E_{OD} = (Roughness)/D_e \tag{2-108}$$

$$f = f(Re, E_{OD}) \tag{2-109}$$

The total pressure drop in a pipe can be expressed in two different forms depend on locations. The pipe between IHX exit and pump inlet is not a real pipe and is used to minimize the modification of the SSC-L. Therefore, the pressure drop for the pipe between IHX exit and

pump inlet includes the pressure drop due to gravitaion only. The density used in gravitational force calculation is assumed as the cold pool sodium density.

$$\Delta P_{drop}^{PIPE} = \rho_{cldp} \cdot g \cdot sin_{SUM} \cdot \Delta x_{node} \quad \text{if pipe is between IHX exit and pump inlet} \tag{2-110}$$

$$\Delta P_{drop}^{PIPE} = \left(f \frac{\Delta x_{pipe}}{D_e} + K \right) \frac{W|W|}{2\rho_{inlet} A^2} + \rho_{inlet} g \cdot sin_{SUM} \Delta x_{node} \quad \text{else} \tag{2-111}$$

2.4.3 Pump

The pump rotating speed is determined by matching pump head and total hydraulic head.

The required pressure rise across pump is obtained from:

$$\Delta P_{pp} = \sum_{i}^{N_{IPIPE}} \Delta P_{drop_i}^{pipe} + P_{IPDRV} + P_{IPDCV} \tag{2-112}$$

where $\Delta P_{drop_i}^{pipe}$: pressure drop for pipe i

P_{IPDRV} : pressure drop from core inlet to IHX inlet

P_{IPDCV} : pressure drop in check valve

The pump head:

$$H_{pump} = \Delta P_{pp} / (\rho \cdot g) \tag{2-113}$$

$$h = H_{pump} / H_r \tag{2-114}$$

$$v = (W_{IREF} / \rho) / Q_r \tag{2-115}$$

$$\alpha = \Omega / \Omega_r \tag{2-116}$$

The α is found based on the value of h/v^2 from pump homologous curve using root finding scheme and pump rotational speed is obtained from:

$$\Omega = \alpha \cdot \Omega_r \tag{2-117}$$

2.4.4 Pressure Distribution of Pipes

This subroutine set the pressure at the pipe end point.

$$P_{1OUT,1} = P_{1IN,1} - P_{DROP,1} \tag{2-118}$$

where $P_{1OUT,1}$: outlet pressure for pipe 1 in primary loop

$P_{1IN,1}$: inlet pressure for pipe 1 in primary loop (IHX inlet pressure)

$P_{DROP,1}$: pressure drop in pipe 1

For pipe 2 to N1PIPE, the $P_{1IN,i}$ is set to zero except the pipe after pump.

$$\begin{cases} P_{1IN,i} = \Delta P_{pump}^{rise} & \text{if } i = \text{pipe index for the pipe after pump} \\ P_{1IN,i} = 0 & \text{else} \end{cases} \tag{2-119}$$

Then, the pressure at a pipe inlet equals the sum of pressure at the previous pipe outlet and pressure drop due to any device (i.e., pump) between the pipes.

$$P_{1IN,i} = P_{1IN,i} + P_{1OUT,i-1} \qquad \text{for } i = 2, \quad N_{1PIPE} \tag{2-120}$$

$$P_{1IOUT,i} = P_{1IN,i} - P_{DROP,i} \qquad \text{for } i = 2, \quad N_{1PIPE} \tag{2-121}$$

2.4.5 Cold Pool Hydraulics

The sodium enthalpy in cold pool is assumed to the IHX exit enthalpy.

$$h_{cp} = h_{Xout} \tag{2-121}$$

The liquid level in cold pool is obtained from pressure difference between the cover gas pressure and the pump inlet pressure.

$$Z_{cp} = Z_{Pin} + \frac{P_{Pin} - P_{gas}}{\rho_{Pin} \cdot g} \tag{2-122}$$

Then, the cold pool sodium mass is obtained from the sodium level in cold pool by assuming that the cold pool can represented by two distinct regions with different cross-sectional area:

$$M_{cp} = \begin{cases} V_{b-pmp} + A_{cldp-c} \cdot Z_{cldp-c} + A_{ovf}(Z_{cp} - Z_{Xo}) & \text{if } Z_{cp} > Z_{Xo} \\ V_{b-pmp} + A_{cldp-c} \cdot (Z_{cp} - Z_{Pin}) & \text{if } Z_{cp} \le Z_{Xo} \end{cases} \tag{2-123}$$

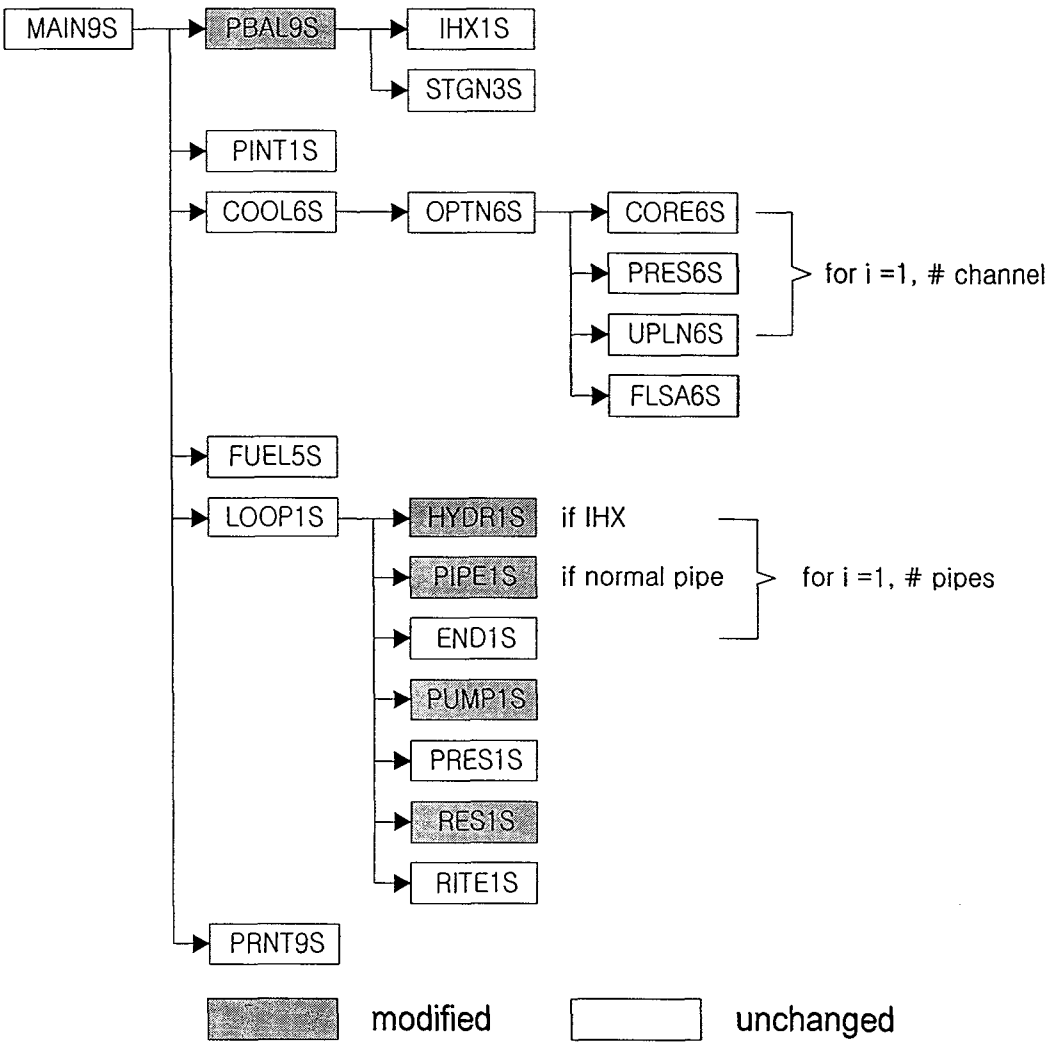

Fig. 2.1 Flowchart for Steady-State Calculation

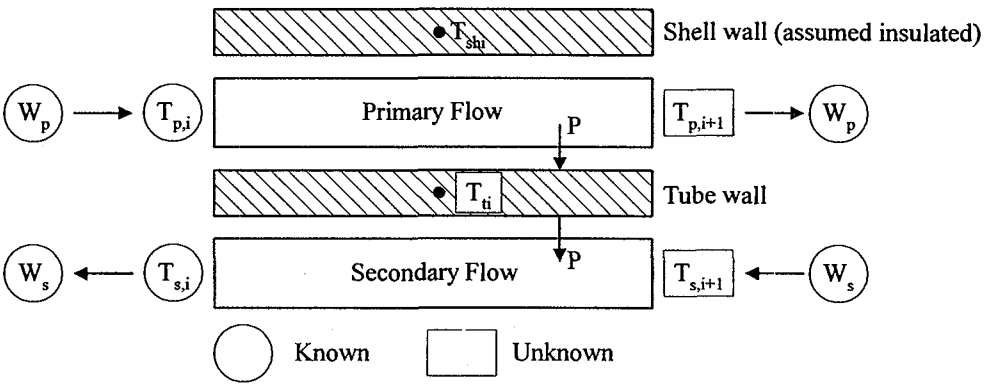

Fig. 2.2 Steady state Conditions for an IHX Nodal Section

3. TRANSIENT MODELS

The dynamic response of the primary coolant in a pool-type LMR, particularly the hot pool concept like KALIMER, can be quite different from response in the loop-type LMR. The difference arises primarily from the lack of direct piping connections between components in the hot and cold pools. Even through there are free surfaces in the reactor vessel and pump tank of loop-type designs, the direct piping connections permit the use of basically a single momentum equation to characterize the coolant dynamics in the primary loop, except in a transient initiated by pipe rupture or similar asymmetric initiator.

In KALIMER, both hot and cold pools have free surfaces and there is direct mixing of the coolant with these open pools prior to entering the next component. At least two different flows would have to be modeled to characterize the coolant dynamics of the primary system. During steady-state the two flow rates can be obtained by a simple algebraic equation. During a transient, however, the flow from the pump to hot pool would respond to the pump head and losses in that circuit including losses in the core; the IHX flow would respond to the level difference between the two pools, as well as losses and gravity gains in the IHX. The gravity gain could be significant for low-flow conditions, particularly if the IHX gets overcooled due to a mismatch of primary and secondary flows. The flow chart for transient routine is in Fig. 3.1.

3.1 Flow Equations

Since the primary system of KALIMER has same number of pumps and IHXs, the first version of SSK-K has developed with constraint that the number of pumps has to be same as the number of IHXs. In SSC-K, the concept of flow paths (N_{path}) is introduced and each flow path includes one pump and one IHX.

3.1.1 Intact System

For an intact system, volume-averaged momentum equations can be written as follows:

Pump Flow

$$\frac{dW_p(k)}{dt}\sum_p \frac{L(k)}{A(k)} = P_{Po}(k) - P_{Rin} - \sum_p \Delta P_{f,g}(k), \qquad k = 1,\cdots,N_{path} \tag{3-1}$$

In above equation, the pump exit pressure, P_{Po}, is obtained from

$$P_{Po} = P_{Pin} + \rho_{Pin} g\, H \tag{3-2}$$

where H is the pump head, obtained from the pump characteristics.

IHX Flow

$$\frac{dW_{1X}(k)}{dt}\sum_X \frac{L(k)}{A(k)} = P_{Xin} - P_{Xo} - \sum_X \Delta P_{f,g}(k), \qquad k = 1,\cdots,N_{path} \tag{3-3}$$

The IHX inlet and exit pressures, P_{Xin} and P_{Xo}, are obtained from static balance as

$$P_{Xin} = P_{gas} + \rho_h g(Z_{HP} - Z_{Xin}) \tag{3-4}$$

$$P_{Xo} = P_{gas} + \rho_c g(Z_{CP} - Z_{Xo}) \tag{3-5}$$

The core inlet pressure, P_{Rin}, is obtained from a complicated algebraic equation and the derivation will be discussed later.

3.1.2 Damaged System

In KALIMER, the pipe rupture can only happen in pump discharge line to reactor core. For the broken path, Eq. (3-1) has to be modified to:

$$\frac{dW_p}{dt}\sum_{uob}\frac{L}{A} = P_{Po} - P_{bin} - \sum_{uob}\Delta P_{f,g} \tag{3-6}$$

An additional equation is needed to describe the flow downsteam of the break:

$$\frac{dW_{dob}}{dt}\sum_{dob}\frac{L}{A} = P_{bo} - P_{Rin} - \sum_{dob}\Delta P_{f,g} \tag{3-7}$$

The inlet and outlet pressures at break location, P_{bin} and P_{bo}, respectively, are calculated by break model. The break model in SSC-K is same as that in SSC-L. The external pressure for the break, which is needed to compute these pressures, is obtained from static balance as

$$P_{ext} = P_{gas} + \rho_C g(Z_{CP} - Z_b) \tag{3-8}$$

This pressure acts as the back pressure opposing the flow out of the break. The value of this pressure is much larger than that for loop-type design, which is generally equal to atmospheric pressure until the sodium in guard vessel covers the break location. This will make the pipe break in pool-type designs less sever relative to loop-type designs.

3.2 Pump Suction Pressure

Fig. 3.1 shows a schematic of SSC-K Modeling for KALIMER. As you may be noticed, there is a pipe after IHX which does not exist in KALIMER. This pipe is included to minimize the modification of loop type version of SSC-K. This pipe is used to make the elevation of IHX exit same as the elevation of pump inlet. The pump surge tank model in loop-type version of SSC is used as a basis of the cold pool model in KALIMER. Pump surge tank in a loop-type LMR has similar characteristics with cold pool in pool-type LMR in many aspects. Both components include two distinct regions. In one region, the sodium is present in lower part while the second region is filled with noncondensable gas on the top of the sodium. The sodium levels in both components are changing with mass balance between IHX exit flow and pump inlet flow. However, some differences exist between two components. First, cover gas in pump surge tank is separated by cover gas in vessel while cover gas in cold pool is in common with cover gas above hot pool. Second, enthalpy in pump surge tank is assumed to be same as enthalpy of IHX exit

flow. This is a reasonable assumption for pump surge tank because of its small volume. However, it is not true in cold pool, which has relatively large sodium inventory. Therefore, energy equation is added in cold pool model to account the energy stored in sodium. And it is assumed that the entire pump inlet flow is from cold pool and no direct flow from IHX exit. The energy balance in cold pool will be discussed in later section.

As seen in Fig. 3.2, a few variables are newly defined to model a cold pool and their descriptions are as follows:

- V6BPMP: Volume below pump inlet
- Z6IHXP: Elevation change from pump suction to IHX exit
- A6IHXP: Average flow area from pump suction to IHX exit
- A6OVRF: Average flow area for overflow path
- B6CLDP: Sodium mass of cold pool
- E6CLDP: Sodium average enthalpy of cold pool
- T6CLDP: Sodium average temperature of cold pool
- D6CLDP: Sodium average density of cold pool

The pump inlet pressure is obtained by adding cover gas pressure with elevation head of cold pool:

$$P_{Pin} = P_{gas} + \rho_c g(Z_{CP} - Z_{Pin}) \tag{3-9}$$

3.3 Liquid Levels in Pools

The liquid levels in cold and hot pools can be obtained by mass balance at each pool. The total flow through all the IHXs and all the pumps can be determined from:

$$W_{Xtot} = \sum_{k=1}^{N_{path}} W_X(k) \tag{3-10}$$

and

$$W_{Ptot} = \sum_{k=1}^{N_{path}} W_P(k) \tag{3-11}$$

Total sodium mass in cold pool is obtained by mass balance at the cold pool:

$$\frac{d}{dt}(\rho V)_{CP} = W_{Xtot} - W_{Ptot} + W_{ovf} + W_b \tag{3-12}$$

Note that the break flow, W_b, is zero for an intact system and the overflow from hot pool, W_{ovf}, is zero if the hot pool level is below the top of thermal liner. Then, the cold pool level can be obtained from the sodium mass in cold pool by assuming that the cold pool can represented by two distinct regions with different cross-sectional area:

$$(\rho V)_{CP} = \begin{cases} \rho_{cp}\left\{V_{bpmp} + A_{IHXP} \cdot Z_{IHXP} + A_{ovf} \cdot \left(Z_{cp} - Z_{IHXP}\right)\right\} \\ \qquad\qquad \text{if} \quad (\rho V)_{CP} > \rho_{cp} \cdot (V_{bpmp} + A_{IHXP} \cdot Z_{IHXP}) \\ \rho_{cp}\left\{V_{bpmp} + A_{IHXP} \cdot Z_{cp}\right\} \\ \qquad\qquad \text{if} \quad (\rho V)_{CP} \le \rho_{cp} \cdot (V_{bpmp} + A_{IHXP} \cdot Z_{IHXP}) \end{cases} \tag{3-13}$$

where V_{bpmp} : Cold pool volume below flow skirt

A_{IHXP} : Average cold pool cross-sectional area between flow skirt botton and IHX exit

Z_{IHXP} : Height from flow skirt botton to IHX exit

A_{ovf} : Average cold pool cross-sectional area above IHX exit

The time rate change of sodium mass in hot pool is obtained by mass balance at the hot pool:

$$A_{HP}\frac{d}{dt}(\rho Z)_{HP} = W_C - W_{Xtot} - W_{ovf} \tag{3-14}$$

Eq. (3-14) assumes that all the level changes likely to occur during the transient are confined to a constant cross-sectional area. When equations (3-12), (3-13) and (3-14) are solved

simultaneously with the flow equations, the sodium levels for hot and cold pool during the transient can be obtained.

3.4 Reactor Internal Pressure

The reactor internal pressure, P_{Rin}, for both an intact and a damaged system is derived in the following section.

3.4.1 Intact System

Mass conservation at core inlet yields

$$W_C = \sum_{k=1}^{N_{path}} W_P(k) \tag{3-15}$$

Differentiating both sides with time yields

$$\frac{dW_C}{dt} = \sum_{k=1}^{N_{path}} \frac{dW_P(k)}{dt} \tag{3-16}$$

The core flow can be expressed in terms of channel flows as

$$W_C = \sum_{j=1}^{N_{ch}} W_j \tag{3-17}$$

where N_{ch} represents the number of channels simulated in the core. Differentiating both sides with time gives

$$\frac{dW_C}{dt} = \sum_{j=1}^{N_{ch}} \frac{dW_j}{dt} \tag{3-18}$$

Time rate of core flow change for each channel can be written from momentum balance

$$\frac{dW_j}{dt}\left(\sum\frac{L}{A}\right)_j = P_{Rin} - P_{Ro} - \left(\sum\Delta P_{f,g}\right)_j \tag{3-19}$$

$$P_{Ro} = P_g + \rho_H g(Z_{HP} - Z_{Ro})\,. \tag{3-20}$$

Combining Eqs. (3-16), (3-18) and (3-19) gives

$$\sum_{k=1}^{N_{path}}\frac{dW_P(k)}{dt} = \sum_j\left\{\frac{P_{Rin} - P_{Ro} - \left(\sum\Delta P_{f,g}\right)_j}{\left(\sum L/A\right)_j}\right\} \tag{3-21}$$

Substituting Eq. (3-1) into the left hand side of Eq. (3-21) gives

$$\sum_{k=1}^{N_{path}}\left[\frac{P_{Po}(k) - P_{Rin} - \sum_p\Delta P_{f,g}(k)}{\sum_p\frac{L(k)}{A(k)}}\right] = \sum_j\left\{\frac{P_{Rin} - P_{Ro} - \left(\sum\Delta P_{f,g}\right)_j}{\left(\sum L/A\right)_j}\right\} \tag{3-22}$$

Simplifying Eq. (3-22) yields the core inlet pressure as

$$P_{Rin} = \frac{A+B}{C+D} \tag{3-23}$$

where

$$A = \sum_j\left\{\frac{P_{Ro} + \left(\sum\Delta P_{f,g}\right)_j}{\left(\sum L/A\right)_j}\right\} \tag{3-24}$$

$$B = \sum_{k=1}^{N_{path}}\left[\frac{P_{Po}(k) - \sum_p\Delta P_{f,g}(k)}{\sum_p\{L(k)/A(k)\}}\right] \tag{3-25}$$

$$C = \sum_j \left\{ \frac{1}{\left(\sum L / A\right)_j} \right\} \tag{3-26}$$

$$D = \sum_{k=1}^{N_{path}} \left[\frac{1}{\sum_P \{L(k) / A(k)\}} \right] \tag{3-27}$$

3.4.2 Damaged System

In case of a pipe rupture in one of the pump discharge lines, mass conservation at core inlet has to account for the downstream flow of break to core.

$$W_C = \sum_{\substack{k=1 \\ \neq brk}}^{N_{path}} W_P(k) + W_{dob} \tag{3-28}$$

Differentiating both sides with time yields

$$\frac{dW_C}{dt} = \sum_{\substack{k=1 \\ \neq brk}}^{N_{path}} \frac{dW_P(k)}{dt} + \frac{dW_{dob}}{dt} \tag{3-29}$$

Combining Eqs. (3-19 and (3-29) gives

$$\sum_{\substack{k=1 \\ \neq brk}}^{N_{path}} \frac{dW_P(k)}{dt} + \frac{dW_{dob}}{dt} = \sum_j \left\{ \frac{P_{Rin} - P_{Ro} - \left(\sum \Delta P_{f,g}\right)_j}{\left(\sum L / A\right)_j} \right\} \tag{3-30}$$

Substituting Eqs. (3-1) and (3-7) into the left hand side of Eq. (3-30) gives

$$\sum_{\substack{k=1 \\ \neq brk}}^{N_{path}} \left[\frac{P_{Po}(k) - P_{Rin} - \sum_{p} \Delta P_{f,g}(k)}{\sum_{p} \frac{L(k)}{A(k)}} \right] + \frac{P_{bo}(k) - P_{Rin} - \sum_{dob} \Delta P_{f,g}(k)}{\sum_{dob} \frac{L(k)}{A(k)}} = \sum_{j} \left\{ \frac{P_{Rin} - P_{Ro} - \left(\sum \Delta P_{f,g} \right)_j}{\left(\sum L / A \right)_j} \right\} \quad (3\text{-}31)$$

Simplifying Eq. (3-31) yields the core inlet pressure as

$$P_{Rin} = \frac{A + B + C}{D + E + F} \quad (3\text{-}32)$$

where

$$A = \sum_{j} \left\{ \frac{P_{Ro} + \left(\sum \Delta P_{f,g} \right)_j}{\left(\sum L / A \right)_j} \right\} \quad (3\text{-}33)$$

$$B = \sum_{\substack{k=1 \\ \neq brk}}^{N_{path}} \left[\frac{P_{Po}(k) - \sum_{p} \Delta P_{f,g}(k)}{\sum_{p} \{ L(k) / A(k) \}} \right] \quad (3\text{-}34)$$

$$C = \frac{P_{bo}(k) - \sum_{dob} \Delta P_{f,g}(k)}{\sum_{dob} \{ L(k) / A(k) \}} \quad (3\text{-}35)$$

$$D = \sum_{j} \left\{ \frac{1}{\left(\sum L / A \right)_j} \right\} \quad (3\text{-}36)$$

$$E = \sum_{\substack{k=1 \\ \neq brk}}^{N_{path}} \left[\frac{1}{\sum_{p} \{ L(k) / A(k) \}} \right] \quad (3\text{-}37)$$

$$F = \frac{1}{\sum_{dob}\{L(k)/A(k)\}} \tag{3-38}$$

3.5 Energy Balance in Hot Pool

Thermal stratification can occur in the hot pool region if the entering coolant is colder than the existing hot pool coolant and the flow momentum is not large enough to overcome the negative buoyancy force. Since the fluid of hot pool enters IHXs, the temperature distribution of hot pool can alter the overall system response. Hence, it is necessary to predict the pool coolant temperature distribution with sufficient accuracy to determine the inlet temperature conditions for the IHXs and its contribution to the net buoyancy head.

During a normal reactor scram, the heat generation is reduced almost instantaneously while the coolant flow rate follows the pump coastdown. This mismatch between power and flow results in a situation where the core flow entering the hot pool is at a lower temperature than the temperature of the bulk pool sodium. This temperature difference leads to stratification when the decaying coolant momentum is insufficient.

The stratification of the core flow in the hot pool is represented by a two-zone model based on the model for mixing in the upper plenum of loop-type LMRs in SSC-L (Fig. 3.3). The hot pool is divided into two perfectly mixing zones determined by the maximum penetration distance of the core flow. This penetration distance is a function of the Froude number of the average core exit flow. The temperature of each zone is computed from energy balance considerations. The temperature of the upper portion, T_A, will be relatively unchanged; in the lower region, however, T_B will be changed and somewhat between the core exit temperature and the temperature of upper zone due to active mixing with core exit flow as well as heat transfer with the upper zone. The temperature of upper zone is mainly affected by interfacial heat transfer. Full penetration is assumed for flow with positive buoyancy.

The two-zone model in SSC-L has some difficulties to maintain the mass and energy conservation in the hot pool because it does not account for the mass and energy change due to

the variation of penetration height. Therefore, the following equations for energy balance is adopted in SSC-K.

The non-conservative form of energy balance equations which determine the various temperatures in the hot pool are given below:

3.5.1 Lower Mixing Zone B:

Case 1: $\frac{dz_j}{dt} > 0$

Mass conservation

$$\frac{d}{dt}(\rho V)_B = \frac{dz_j}{dt}\rho_A A + W_C - f_B \sum_{k=1}^{Npath} W_{IHX}(k) \tag{3-39}$$

Energy Conservation

$$\begin{aligned}\frac{d}{dt}(\rho EV)_B = {} & \frac{dz_j}{dt}\rho_A A E_A + W_C E_{Ro} - f_B \sum_{k=1}^{Npath} W_{IHX} E_B \\ & - UA_{bm2}(T_B - T_{m2}) - UA_{hm1}(1-f)(T_B - T_{m1}) - hA_{ba}(T_B - T_A)\end{aligned} \tag{3-40}$$

Expand derivative in energy equation for total mass and enthalpy:

$$\begin{aligned}(\rho V)_B \frac{dE_B}{dt} + E_B \frac{d}{dt}(\rho V)_B = {} & \frac{dz_j}{dt}\rho_A A E_A + W_C E_{Ro} - f_B \sum_{k=1}^{Npath} W_{IHX} E_B \\ & - UA_{bm2}(T_B - T_{m2}) - UA_{hm1}(1-f)(T_B - T_{m1}) - hA_{ba}(T_B - T_A)\end{aligned} \tag{3-41}$$

Combine above equation with mass conservation equation and rearrange the nonconservative form of energy equation:

$$\rho_B V_B \frac{dE_B}{dt} = \frac{dz_j}{dt}\rho_A A(E_A - E_B) + W_C(E_{Ro} - E_B) - UA_{bm2}(T_B - T_{m2}) - UA_{hm1}(1-f)(T_B - T_{m1}) - hA_{ba}(T_B - T_A) \quad (3\text{-}42)$$

Case 2: $\frac{dz_j}{dt} < 0$

Mass conservation

$$\frac{d}{dt}(\rho V)_B = \frac{dz_j}{dt}\rho_B A + W_C - f_B \sum_{k=1}^{Npath} W_{IHX}(k) \quad (3\text{-}43)$$

Energy Conservation

$$\frac{d}{dt}(\rho EV)_B = \frac{dz_j}{dt}\rho_B A E_B + W_C E_{Ro} - f_B \sum_{k=1}^{Npath} W_{IHX} E_B - UA_{bm2}(T_B - T_{m2}) - UA_{hm1}(1-f)(T_B - T_{m1}) - hA_{ba}(T_B - T_A) \quad (3\text{-}44)$$

Expand derivative in energy equation for total mass and enthalpy:

$$(\rho V)_B \frac{dE_B}{dt} + E_B \frac{d}{dt}(\rho V)_B = \frac{dz_j}{dt}\rho_B A E_B + W_C E_{Ro} - f_B \sum_{k=1}^{Npath} W_{IHX} E_B - UA_{bm2}(T_B - T_{m2}) - UA_{hm1}(1-f)(T_B - T_{m1}) - hA_{ba}(T_B - T_A) \quad (3\text{-}45)$$

Combine above equation with mass conservation equation and rearrange the nonconservative form of energy equation:

$$\rho_B V_B \frac{dE_B}{dt} = W_C(E_{Ro} - E_B) - UA_{bm2}(T_B - T_{m2}) - UA_{hm1}(1-f)(T_B - T_{m1}) - hA_{ba}(T_B - T_A) \quad (3\text{-}46)$$

3.5.2 Upper Mixing Zone A:

Case 1: $\frac{dz_j}{dt} > 0$

Mass conservation

$$\frac{d}{dt}(\rho V)_A = -\frac{dz_j}{dt}\rho_A A - f_A \sum_{k=1}^{Npath} W_{IHX}(k) - W_{orf} \tag{3-47}$$

Energy Conservation

$$\begin{aligned}\frac{d}{dt}(\rho EV)_A = &-\frac{dz_j}{dt}\rho_A A E_A - f_A \sum_{k=1}^{Npath} W_{IHX} E_A - W_{orf} E_A \\ &- UA_{am2}(T_A - T_{m2}) - UA_{hm1} f(T_A - T_{m1}) - UA_{hg}(T_A - T_g) + hA_{ba}(T_B - T_A)\end{aligned} \tag{3-48}$$

Expand derivative in energy equation for total mass and enthalpy:

$$\begin{aligned}(\rho V)_A \frac{dE_A}{dt} + E_A \frac{d}{dt}(\rho V)_A = &-\frac{dz_j}{dt}\rho_A A E_A - f_A \sum_{k=1}^{Npath} W_{IHX} E_A - W_{orf} E_A \\ &- UA_{am2}(T_A - T_{m2}) - UA_{hm1} f(T_A - T_{m1}) - UA_{hg}(T_A - T_g) + hA_{ba}(T_B - T_A)\end{aligned} \tag{3-49}$$

Combine above equation with mass conservation equation and rearrange the nonconservative form of energy equation:

$$\begin{aligned}(\rho V)_A \frac{dE_A}{dt} = &-UA_{am2}(T_A - T_{m2}) - UA_{hm1} f(T_A - T_{m1}) \\ &- UA_{hg}(T_A - T_g) + hA_{ba}(T_B - T_A)\end{aligned} \tag{3-50}$$

Case 2: $\frac{dz_j}{dt} < 0$

Mass conservation

$$\frac{d}{dt}(\rho V)_A = -\frac{dz_j}{dt}\rho_B A - f_A \sum_{k=1}^{Npath} W_{IHX}(k) - W_{orf} \tag{3-51}$$

Energy Conservation

$$\begin{aligned}\frac{d}{dt}(\rho EV)_A = &-\frac{dz_j}{dt}\rho_B A E_B - f_A \sum_{k=1}^{Npath} W_{IHX} E_A - W_{orf} E_A \\ &- UA_{am2}(T_A - T_{m2}) - UA_{hm1} f(T_A - T_{m1}) - UA_{hg}(T_A - T_g) + hA_{ba}(T_B - T_A)\end{aligned} \tag{3-52}$$

Expand derivative in energy equation for total mass and enthalpy:

$$\begin{aligned}(\rho V)_A \frac{dE_A}{dt} + E_A \frac{d}{dt}(\rho V)_A = &-\frac{dz_j}{dt}\rho_B A E_B - f_A \sum_{k=1}^{Npath} W_{IHX} E_A - W_{orf} E_A \\ &- UA_{am2}(T_A - T_{m2}) - UA_{hm1} f(T_A - T_{m1}) - UA_{hg}(T_A - T_g) + hA_{ba}(T_B - T_A)\end{aligned} \tag{3-53}$$

Combine above equation with mass conservation equation and rearrange the nonconservative form of energy equation:

$$\begin{aligned}(\rho V)_A \frac{dE_A}{dt} = &-\frac{dz_j}{dt}\rho_B A(E_B - E_A) - UA_{am2}(T_A - T_{m2}) \\ &- UA_{hm1} f(T_A - T_{m1}) - UA_{hg}(T_A - T_g) + hA_{ba}(T_B - T_A)\end{aligned} \tag{3-54}$$

3.5.3 Other Temperatures in Hot Pool

Upper internal structure (metal m1):

$$M_{m1} C_{m1} \frac{dT_{m1}}{dt} = UA_{hm1}[f T_A + (1-f) T_B - T_{m1}] - UA_{gm1}(T_{m1} - T_g) \tag{3-55}$$

Barrier (metal m2):

$$M_{m2}C_{m2}\frac{dT_{m2}}{dt}=UA_{hm2}\left[\frac{A_{am2}T_A+A_{bm2}T_B}{A_{hm2}}-T_{m2}\right]-UA_{cm2}(T_{m2}-T_{CP}) \tag{3-56}$$

U_{hm2} is not very sensitive to changes in sodium temperature, and so this equation is derived assuming $U_{bm2}=U_{am2}$.

Roof (metal m3):

$$M_{m3}C_{m3}\frac{dT_{m3}}{dt}=UA_{gm3}(T_g-T_{m3}) \tag{3-57}$$

The heat transfer from the roof to the ambient has been neglected.

Cover gas:

$$\begin{aligned}M_gC_g\frac{dT_g}{dt}=&UA_{hg}(T_A-T_g)-UA_{cg}(T_g-T_{CP})\\&+UA_{gm1}(T_{m1}-T_g)-UA_{gm3}(T_g-T_{m3})\end{aligned} \tag{3-58}$$

The auxiliary equations required by the above governing equations are

$$A_{ba}=\pi D^2/4 \tag{3-59}$$

$$f=1-z_j(t)/(Z_{HP}-Z_{Ro}) \tag{3-60}$$

3.6 Energy Balance in Cold Pool

Currently, perfect mixing of the IHX flow with the cold pool sodium is assumed. Energy balance equation for cold pool is derived as:

Mass Conservation

$$\frac{d}{dt}(\rho V)_{cp} = \sum_{N_{path}} W_{IHX} - \sum_{N_{path}} W_{pmp} + W_{ovf} + \sum_{N_{path}} W_{brk} \tag{3-61}$$

Energy Conservation

$$\frac{d}{dt}(\rho hV)_{cp} = \sum_{N_{path}} W_{IHX} h_{IHX} - \sum_{N_{path}} W_{pmp} h_{cp} + W_{ovf} h_{hp} + \sum_{N_{path}} W_{brk} h_{brk} \tag{3-62}$$

Expand derivative in energy equation for total mass and enthalpy:

$$\begin{aligned}(\rho V)_{cp} \frac{dh_{cp}}{dt} + h_{cp} \frac{d}{dt}(\rho V)_{cp} &= \sum_{N_{path}} W_{IHX} h_{IHX} \\ &- h_{cp} \sum_{N_{path}} W_{pmp} + W_{ovf} h_{hp} + \sum_{N_{path}} W_{brk} h_{brk}\end{aligned} \tag{3-63}$$

Combine above equation with mass conservation equation:

$$\begin{aligned}(\rho V)_{cp} \frac{dh_{cp}}{dt} + h_{cp} (\sum_{N_{path}} W_{IHX} - \sum_{N_{path}} W_{pmp} + W_{ovf}) \\ = \sum_{N_{path}} W_{IHX} h_{IHX} - h_{cp} \sum_{N_{path}} W_{pmp} + W_{ovf} h_{hp} + \sum_{N_{path}} W_{brk} h_{brk}\end{aligned} \tag{3-64}$$

Rearrange the nonconservative form of energy equation:

$$\begin{aligned}(\rho V)_{cp} \frac{dh_{cp}}{dt} = \sum_{N_{path}} W_{IHX} h_{IHX} - h_{cp} \sum_{N_{path}} W_{IHX} \\ + W_{ovf} h_{hp} - W_{ovf} h_{cp} + \sum_{N_{path}} W_{brk} h_{brk} - h_{cp} \sum_{N_{path}} W_{brk}\end{aligned} \tag{3-65}$$

Above equation can be expressed into two different equations depend on the direction of break flow.

$$(\rho V)_{cp}\frac{dh_{cp}}{dt}=$$

$$\begin{cases}\sum_{N_{path}} W_{IHX}h_{IHX}-h_{cp}\sum_{N_{path}} W_{IHX}+W_{ovf}(h_{hp}-h_{cp}) & \\ \qquad +\sum_{N_{path}} W_{brk}h_{brk}-h_{cp}\sum_{N_{path}} W_{brk} & if\ W_{brk}>0 \\ \sum_{N_{path}} W_{IHX}h_{IHX}-h_{cp}\sum_{N_{path}} W_{IHX}+W_{ovf}(h_{hp}-h_{cp}) & if\ W_{brk}\le 0\end{cases} \tag{3-66}$$

Discretize above equation in time:

$$h_{cp}^{t+\Delta t}-h_{cp}^{t}=$$

$$\begin{cases}\frac{\Delta t}{(\rho V)_{cp}}\left[\sum_{N_{path}} W_{IHX}h_{IHX}-h_{cp}^{t+\Delta t}\sum_{N_{path}} W_{IHX}+W_{ovf}h_{hp}\right. & \\ \qquad \left.-W_{ovf}h_{cp}^{t+\Delta t}+\sum_{N_{path}} W_{brk}h_{brk}-h_{cp}^{t+\Delta t}\sum_{N_{path}} W_{brk}\right] & if\ W_{brk}>0 \\ \frac{\Delta t}{(\rho V)_{cp}}\left[\sum_{N_{path}} W_{IHX}h_{IHX}-h_{cp}^{t+\Delta t}\sum_{N_{path}} W_{IHX}\right. & \\ \qquad \left.+W_{ovf}h_{hp}-W_{ovf}h_{cp}^{t+\Delta t}\right] & if\ W_{brk}\le 0\end{cases} \tag{3-67}$$

$$\begin{cases}h_{cp}^{t+\Delta t}\left\{1+\frac{\Delta t}{(\rho V)_{cp}}\left(\sum_{N_{path}} W_{IHX}+W_{ovf}+\sum_{N_{path}} W_{brk}\right)\right\} & \\ \quad =h_{cp}^{t}+\frac{\Delta t}{(\rho V)_{cp}}\left\{\sum_{N_{path}} W_{IHX}h_{IHX}+W_{ovf}h_{hp}+\sum_{N_{path}} W_{brk}h_{brk}\right\} & if\ W_{brk}>0 \\ h_{cp}^{t+\Delta t}\left\{1+\frac{\Delta t}{(\rho V)_{cp}}\left(\sum_{N_{path}} W_{IHX}+W_{ovf}\right)\right\} & \\ \quad =h_{cp}^{t}+\frac{\Delta t}{(\rho V)_{cp}}\left\{\sum_{N_{path}} W_{IHX}h_{IHX}+W_{ovf}h_{hp}\right\} & if\ W_{brk}\le 0\end{cases} \tag{3-68}$$

Solve for $h_{cp}^{t+\Delta t}$:

$$\begin{cases} h_{cp}^{t+\Delta t} = \dfrac{h_{cp}^{t} + \dfrac{\Delta t}{(\rho V)_{cp}} \left\{ \sum_{N_{path}} W_{IHX} h_{IHX} + W_{ovf} h_{hp} + \sum_{N_{path}} W_{brk} h_{brk} \right\}}{1 + \dfrac{\Delta t}{(\rho V)_{cp}} \left(\sum_{N_{path}} W_{IHX} + W_{ovf} + \sum_{N_{path}} W_{brk} \right)} & if\ W_{brk} > 0 \\ h_{cp}^{t+\Delta t} = \dfrac{h_{cp}^{t} + \dfrac{\Delta t}{(\rho V)_{cp}} \left\{ \sum_{N_{path}} W_{IHX} h_{IHX} + W_{ovf} h_{hp} \right\}}{1 + \dfrac{\Delta t}{(\rho V)_{cp}} \left(\sum_{N_{path}} W_{IHX} + W_{ovf} \right)} & if\ W_{brk} \le 0 \end{cases} \tag{3-69}$$

Lower structures (metal m4):

$$(MC)_{m4} \frac{dT_{m4}}{dt} = UA_{cm4} (T_{cp} - T_{m4}) \tag{3-70}$$

It should be noted that the heat transfer between structures and cold pool sodium is ignored in current version of SSC-K. The above equation will be adopted in later version.

Table 3-1 Code Modification List

Subroutine Name	Changes
CRDR9R	Inconsistent subroutine arguments: GENRD
DCODNC	Inconsistent data type with subroutine argument. • IVLU been set to real(8) from integer
END1T	Inlet/Outlet enthalpy of pipe segment in cold pool has been changed
EQIV1T	No pump surge tank option • head due to liquid level to zero • matrix element for head due to liquid level to zero • pump speed change rate to zero • liquid level change rate to zero Bypass flow calculation has been corrected Integrated values related to pool model has been changed
EQIV2T	No pump surge tank option • head due to liquid level to zero • matrix element for head due to liquid level to zero • pump speed change rate to zero • liquid level change rate to zero
ERRMSG	2nd argument of EXIT9U to 8 characters
FLOW1T	No pump surge tank option has been added
FLOW2T	No pump surge tank option has been added
GENRD	Inconsistent data type with subroutine argument. • IVLU been set to real(8) from integer
GVSL1T	External pressure for break flow calculation
HEAD1T	Discontinuity in pump head homologous curve removed
HYDR1S	Pressure drop calculations corrected
IHX1T	LOHS actuation at specified time by user
INIT1T	Initialization for no pump surge tank case • pump inlet pres. to vessel outlet pres. • head due to liquid level to zero Initialization for cold pool variables • Cold pool sodium mass • Pump inlet pressure Cover gas volume calculation Cold pool enthalpy calculation
INIT2T	Initialization for no pump surge tank case • Pump inlet pres. to preceeding pipe outlet pres. • Head due to liquid level to zero
INTG1T	Inconsistent data type with subroutine argument. • IVLU been set to real(8) from integer

Table 3-1 Code Modification List (continued)

Subroutine Name	Changes
ISETHM	Character variables can not be set to real variables directly. • Character variables are set to real variables using write statement.
LOOP1T	Cold pool enthalpy calculation
NSKIP	Inconsistent data type with subroutine argument. • IVLU been set to real(8) from integer.
PBAL9S	ERR9U arguments been changed • sequence of arguments has been changed
PIPE1S	Enthalpy and pressure drop calculation routine for cold pool added
PIPW1T	Pressure drop calculation routine for cold pool added
PRUP6T	Calculation for IHX inlet pressure been corrected
PUMP1S	Discontinuity of head homologous curve been corrected
PUMP1T	Discontinuity of head homologous curve been corrected EMP coastdown at specified time No enthalpy rise across EMP assumed
READ1R	GENRD arguments been changed : 19 places • 4th arg.: integer(id2) to real(d2)
READ7R	GENRD arguments been changed : 43 places • 4th arg.: integer(id2) to real(d2)
READ8R	GENRD arguments been changed : 1 place • 4th arg.: integer(id2) to real(d2) GENRD arguments been changed : 1 place • 3rd arg.: real(dum) to integer(idum) • 5th arg.: real(dum) to first real array element[a(1)] • 6th arg.: real(dum) to first int array element[ia(1)]
READ9R	int. array for data containment[ia(1)] been included GENRD arguments been changed : 7 places • 4th arg.: integer(id2) to real(d2)
READ9T	equivalence statement (A(1),IA(1)) been removed GENRD arguments been changed : 1 place • 3rd arg.: real(dum) to integer(idum) • 5th arg.: real(dum) to first real array element[a(1)] • 6th arg.: real(dum) to first int array element[ia(1)] GENRD arguments been changed : 3 places • 4th arg.: integer(id2) to real(d2) error message for excess of max. table length been removed
READHM	Character variables can not be set to real variables directly. • Character variables are set to real variables using write statement.
REPEAT	Inconsistent data type with subroutine argument. • IVLU been set to real(8) from integer.

Table 3-1 Code Modification List (continued)

Subroutine Name	Changes
RES1S	Steady state calculation for cold pool
RES1T	No pump surge tank option has been added • liquid level in pump tank to zero • pump inlet presssure to vessel outlet pres. • liquid level change rate to zero Cold pool option added • Time derivative of cold pool sodium mass • Cold pool level calculation • Pump inlet pressure
RES2S	No pump surge tank option • gas mass in surge tank to zero • liquid level in surge tank to zero
RES2T	No pump surge tank option • liquid level in pump tank to zero • pump inlet pres. to vessel outlet pres. • liquid level change rate to zero
RITE6U	int. variables HY, HI been defined definition for character STRING1 been changed
UPLS6T	• Overflow model added • Mass, energy equations changed to include overflow effect • Time derivative of enthalpy difference due to overflow modified
VERR9T	Dimension for character NAME been changed to character*6
VESL1T	Overflow rate calculation Cover gas volume
VRFY9T	character NC been defined VERR9T arguments been changed : 11 places • 4th arg.: integer(+0) to character(NC) VERR9T arguments been changed : 1 place • 4th arg.: null character to character(NC)
WIMPLT	Cover gas volume calculation

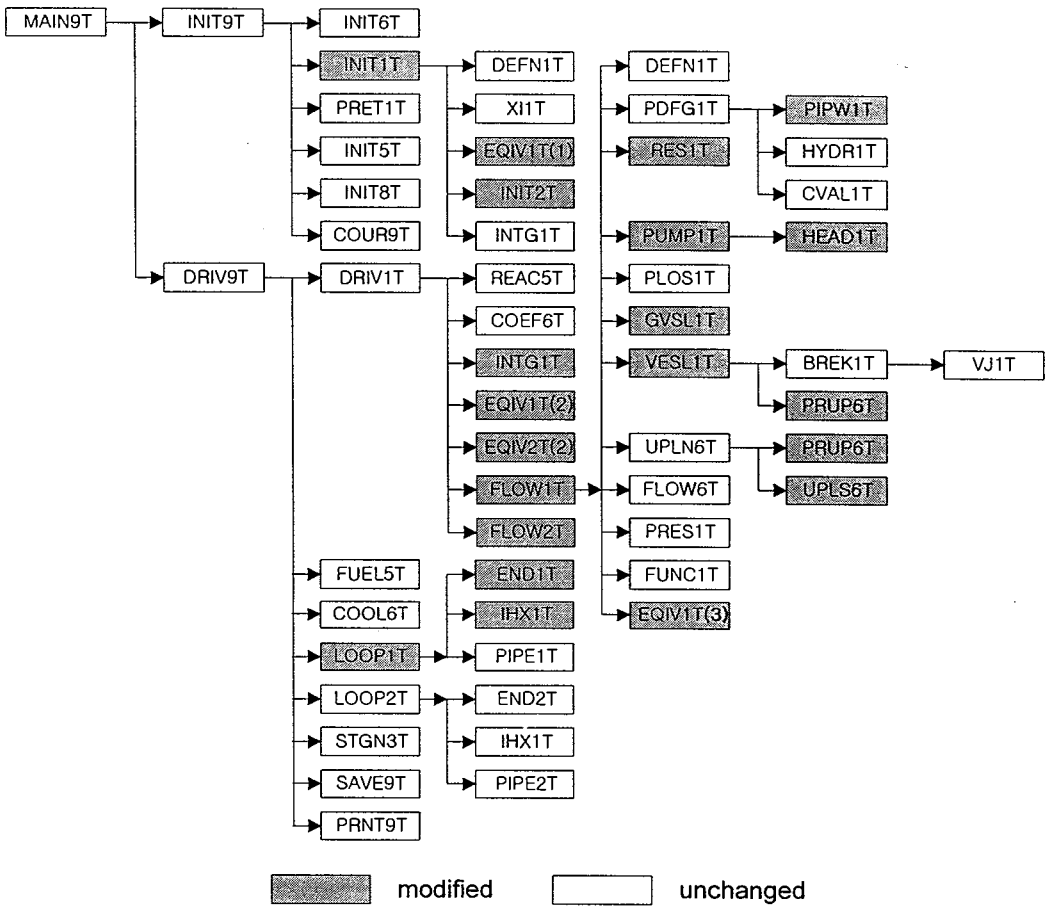

Fig. 3.1 Flowchart for Transient Calculation

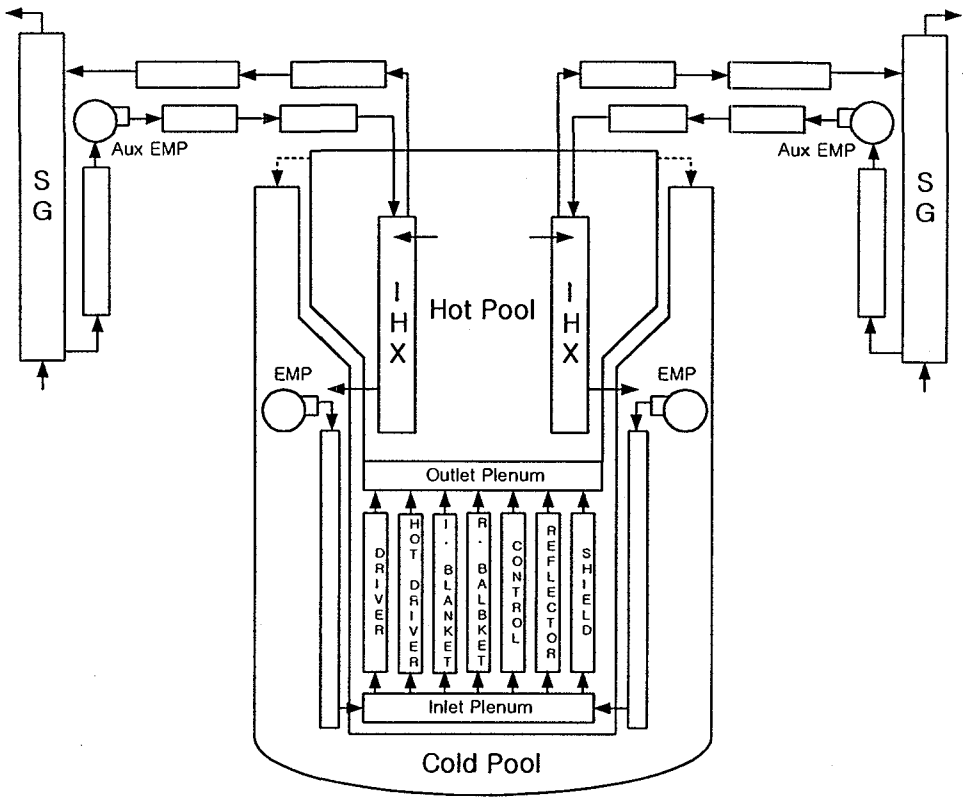

Fig. 3.2 Schematic of SSC-K Modeling for KALIMER

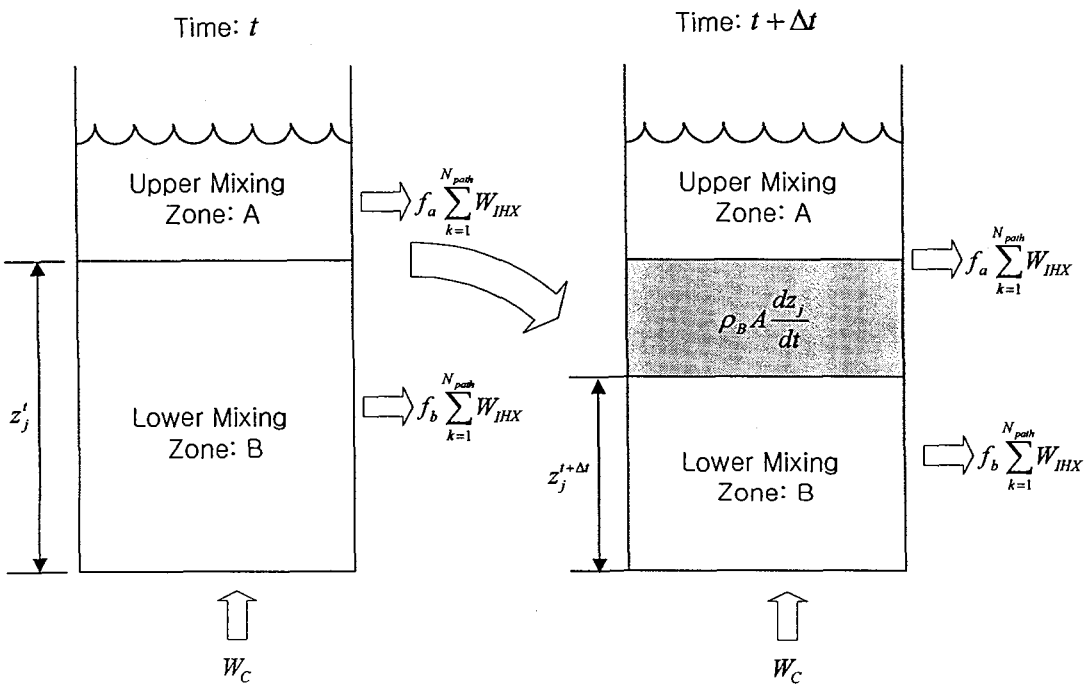

Fig. 3.3 Two Mixing Zone Model for Hot Pool

4. INTERMEDIATE HEAT EXCHANGER

4.1 Pool Type IHX

The intermediate heat exchangers (IHX) physically separate the radioactive primary coolant from the non-radioactive intermediate coolant while at the same time thermally connecting the two circuits in order to transfer the core heat to the steam generator. The IHX in pool type LMFBR is identical in function, and similar in design, to that in loop type design. The only difference arises from the different configuration in the primary system, where the IHX draws coolant from an open hot pool and discharges to another open cold pool. The liquid levels in the hot and cold pools reflect the hydraulic flow resistance through the IHXs. The liquid level difference in the KALIMER is about 5 m under normal operation. The low differential level requires the IHX to have a low pressure drop on the primary side. The main concern with a low pressure drop in the IHXs is its effect on flow distribution. Poor flow distribution can adversely affect operational reliability by causing temperature distributions and resultant thermal stress that could exceed design allowances.

Most of IHX in LMFBRs are of similar design. The IHX design of KALIMER is vertical, counter flow, shell-and-tube heat exchangers with basically straight tubes as shown in Fig. 4.1. Primary sodium flows downward on the shell side and exits at the bottom, with transferring heat to secondary coolant in the tubes. The secondary coolant flows in the tubes. The pressure losses in the primary side are limited as discussed above, it may be advantageous to send primary flow through the tubes to ensure good flow distribution. The higher pressure in the secondary side is to assure no radioactive coolant enters the secondary circuit in the event of a leak in any of the heat transfer tubes.

Principal differences in IHXs between the loop and pool systems appear at the entrance and exit flow nozzles. Tube bundle is mounted to allow for differential thermal expansion between the tubes and the shell. To accomplish this, the lower tube sheet is allowed to float and, therefore, is supported by the tube bundle. The tubes are supported by the upper tube sheet.

4.2 Heat Transfer Model

The IHX model of SSC-K is essentially unchanged from that of SSC-L. The energy equations are written using nodal heat balance with the donor-cell differencing scheme. Figure 3-2 is a nodal diagram for thermal model under counterflow arrangement. The active heat transfer tubes are modeled by one representative tube in the figure. The active heat transfer tube is divided into same axial distance by user specified number. Axial heat conduction in the metal wall is assumed negligible. As shown in Fig. 4.2, the IHX is modeled by four radial nodes, secondary coolant, tube metal, primary coolant and shell wall. Material properties and heat transfer coefficients are evaluated locally by specifying the material as user input. The tube and shell wall nodes lie in the mid-plane between the fluid nodal interfaces, giving rise to a staggered nodal arrangement.

The coolant equations are derived using the nodal heat balance method. It is assumed that ideal mixing plenums at the inlet and outlet of each coolant stream. The time dependent governing equations for thermal transportation of each section are described below.

1) Primary inlet plenum

$$\rho_{in} V_{in} \frac{d}{dt}(e_{p_1}) = W_p^{'}(e_{p_{in}} - e_{p_1}) \tag{4-1}$$

where

$$e_{p_{in}} = e(T_{p_{in}}) \quad \text{and} \quad e_{p_1} = e(T_{p_1}) \tag{4-2}$$

V_{in} is the stagnant sodium volume in the primary inlet plenum, and ρ_{in} is the average sodium density in the inlet plenum. Considering the fraction of flow bypassing the active heat transfer region, β_p, we have the following equation from mass conservation.

$$W_p^{'} = (1-\beta_p) W_p \tag{4-3}$$

1) Primary outlet plenum

$$\rho_{out} V_{out} \frac{d}{dt}(e_{p_{out}}) = W_p' e_{pN} + \beta_p W_p e_{pB} - W_p e_{p_{out}} \tag{4-4}$$

V_{out} is the sodium volume in the primary outlet plenum and ρ_{out} is the average sodium density in the outlet plenum.

3) Primary bypass plenum

$$\rho_{pB} V_{pB} \frac{d}{dt}(e_{pB}) = \beta_p W_p (e_{p_{in}} - e_{pB}) \tag{4-5}$$

Similar equations can be written for the inlet, outlet plenums and downcomer on the secondary side.

4) Active heat transfer region

For primary coolant

$$\rho V_p \frac{d}{dt}(e_{p_{i+1}}) = W_p'(e_{p_i} - e_{p_{i+1}}) - U_{pt} A_{pt} (T_{p_{i\,i+1}} - T_{t_i}) - U_{psh} A_{psh} (T_{p_{i\,i+1}} - T_{sh_i}) \tag{4-6}$$

For secondary side coolant

$$\rho V_s \frac{d}{dt}(e_{s_i}) = W_s (e_{s_{i+1}} - e_{s_i}) + U_{st} A_{st} (T_{t_i} - T_{s_{i\,i+1}}) \tag{4-7}$$

For tube wall

$$M_t C_{t_i} \frac{d}{dt}(T_{t_i}) = U_{pt} A_{pt} (T_{p_{i\,i+1}} - T_{t_i}) - U_{st} A_{st} (T_{t_i} - T_{s_{i\,i+1}}) \tag{4-8}$$

For shell wall

$$M_{sh} C_{sh_i} \frac{d}{dt}(T_{sh_i}) = U_{psh} A_{psh} (T_{p_{i\,i+1}} - T_{sh_i}) \tag{4-9}$$

In the above equations, V_p and V_s are the control volumes between interfaces i and i+1 on the primary and secondary sides, respectively. A_{pt}, A_{st} and A_{psh} are the areas per length Δx for heat transfer between primary coolant and tube wall, between secondary fluid and tube wall, and between primary coolant and shell wall, respectively, defined as

$$A_{pt} = \pi D_2 n_t \Delta x \tag{4-10}$$

$$A_{st} = \pi D_1 n_t \Delta x \tag{4-11}$$

$$A_{psh} = A_{sh} \Delta x / L \tag{4-12}$$

where n_t is number of active heat transfer tubes and A_{sh} is the shell heat transfer area given by user input. D_1 and D_2 are the IHX tube inner and outer diameters, respectively, and L is the length of the active heat transfer region.

In above equations, U_{pr}, U_{st}, and U_{psh} represent the overall heat transfer coefficient between primary coolant and tube wall, between secondary fluid and tube wall, and between primary coolant and shell wall, respectively. Those are defined based on the thermal resistance concept as:

$$\frac{1}{U_{pt}} = \frac{1}{h_{film,p}} + r_{wall,p} + \frac{1}{h_{foul,p}} \tag{4-13}$$

$$\frac{1}{U_{st}} = \frac{1}{h_{film,s}} + r_{wall,s} + \frac{1}{h_{foul,s}} \tag{4-14}$$

$$\frac{1}{U_{psh}} = \frac{1}{h_{film,p}} \tag{4-15}$$

where the film heat transfer coefficients are calculated in terms of Nusselt number Nu, which is obtained from the embedded correlations in SSC-K. Fouling is a time-dependent phenomenon, and the fouling resistances of $1/h_{foul,p}$ and $1/h_{foul,s}$ are provided as a user input quantity for the primary and secondary sided walls, respectively.

$$h_{film,p} = \frac{Nu_{pt} k_p}{D_{h,p}} \tag{4-16}$$

$$h_{film,s} = \frac{Nu_{st} k_s}{D_1} \tag{4-17}$$

The wall thermal resistance terms are defined by dividing the tube wall thickness equally between primary and secondary sides. The temperature of tube, T_t, is defined at the midpoint of wall thickness.

$$r_{wall,p} = \frac{D_2}{2k_t} \ell n(2D_2 / (D_1 + D_2)) \tag{4-18}$$

$$r_{wall,s} = \frac{D_1}{2k_t} \ell n((D_1 + D_2) / 2D_1) \tag{4-19}$$

where k_t is a thermal conductivity of tube wall which is calculated internally by specifying the material as input.

The overall heat transfer coefficients U_{pt} and U_{st} are dependent on material and flow properties, which are functions of temperature. Those are evaluated at each nodal section along with the temperatures. Referring to Fig. 4.2, for each i, k_t is evaluated at i on the tube wall node whereas all other variables (k_p, k_s, Nu_{pt}, Nu_{st}) are evaluated at the midpoint between the fluid nodal interfaces i and (i+1).

If a flow area on primary side of IHX is not provided as a user input, SSC-K calculates it by the following equation. The pitch-to-diameter P/D_2 is taken to be as the average value in case the pitch is not uniform throughout the tube bundle.

$$A_p = n_t \frac{\pi D_2^2}{4} \left[\frac{2\sqrt{3}}{\pi} (P / D_2)^2 - 1 \right] \tag{4-20}$$

Then, the hydraulic diameter of primary side is calculated as follows:

$$D_{h,p} = \frac{4A_p}{n_t \pi D_2} \tag{4-21}$$

The Reynolds number for the primary side and internal tube is defined as, respectively.

$$\mathrm{Re}_p = \frac{W_p D_{h,p}}{A_p \mu_p} \tag{4-22}$$

$$\mathrm{Re}_t = \frac{W_s D_1}{A_s \mu_s} \tag{4-23}$$

where, the flow area through the tubes is given as

$$A_s = n_t \frac{\pi D_1^2}{4} \tag{4-24}$$

4.3 Pressure Losses Model

Figure 4-1 shows the flow paths of KALIMER IHX. Primary coolant flows downward in the active heat transfer region and exits at the bottom of the tube unit. The secondary (intermediate) coolant flows down the central downcomer into the bottom header (inlet plenum region) where it turns upward to present a counterflow arrangement in the heat transfer region. In all cases, the primary flow is downward, and this helps to simplify the formulation. The sum of pressure losses on both primary and secondary sides of the IHX is expressed as follows:

$(\Delta P_{f,g})$IHX = (acceleration loss) + (frictional loss) + (gravity loss or gain) + (inlet loss)
+ (exit loss) + (contraction/expansion losses) +(other losses)

Note that a negative value obtained for gravity loss indicates a gain. The user should be cautious when specifying the value of ΔP_{IHX} if known, to ensure that it does not include the

gravity term. The SSC-K code adds on the gravity term to give the final ΔP_{IHX} for the hydraulic calculations.

For the primary side, the pressure losses are calculated as

$$(\Delta p_{f,g})_{IHX,p} = \frac{W_p^{\,2}}{A_p^2}\left(\frac{1}{\rho_N}-\frac{1}{\rho_1}\right)+\frac{1}{2}\frac{W_p|W_p|}{D_{h,p}A_p^2}\int_0^L \frac{f}{\rho}dx+\Delta p_g + k_{p_{in}}\frac{W_p|W_p|}{(\rho A^2)_{in}}+k_{p_{out}}\frac{W_p|W_p|}{(\rho A^2)_{out}}+k_p\frac{W_p|W_p|}{\bar{\rho}A_p^2} \tag{4-25}$$

where

$$\Delta p_g = g(\rho\sin\alpha\Delta x)_{inlet\ plenum}+g\int_0^L \rho\sin\alpha dx+g(\rho\sin\alpha\Delta x)_{outlet\ plenum} \tag{4-26}$$

$$W_p' = (1-\beta_p)W_p \tag{4-3}$$

$$\bar{\rho}=\frac{\rho_{in}+\rho_{out}}{2} \tag{4-27}$$

where $k_{p,in}$ and $k_{p,out}$ represent loss coefficients for expansion and contraction of flow, respectively, i.e., from the plenum to pipe or reverse direction. It also include inlet plenum losses due to turning, flow distribution, etc. k_p is an uncertainty absorber that is either calculated during steady state if $\Delta P_{IHX,p}$ is provided by user input. Once determined or known, the value of k_p remains constant throughout the transient. This is useful parameter especially to overcome the difficulty of determining accurately all the losses in the complex internal geometry of the IHX.

Similarly, for the secondary side of IHX,

$$(\Delta p_{f,g})_{IHX,s} = \frac{W_s^2}{A_s^2}\left(\frac{1}{\rho_1}-\frac{1}{\rho_N}\right)+\frac{1}{2}\frac{W_s|W_s|}{D_1A_s^2}\int_0^L \frac{f}{\rho}dx+\Delta p_g + k_{s,in}W_s|W_s|/(\rho A_{in}^2)+k_{s,out}W_s|W_s|/(\rho A^2)_{out} + \Delta p_{c,e}+k_s/W_s|W_s|/(\bar{\rho}A_s^2) \tag{4-28}$$

where

$$\Delta p_g = g(\rho \sin\alpha \Delta x)_{downcomer} + g(\rho \sin\alpha \Delta x)_{inlet\ plenum} + g\int_0^L \rho \sin\alpha dx + g(\rho \sin\alpha \Delta x)_{outlet\ plenum} \quad (4\text{-}29)$$

$$\Delta p_{c,e} = k_c \frac{W_s|W_s|}{(\rho A^2)_{tube\ in}} + k_e \frac{W_s|W_s|}{(\rho A^2)_{tube\ out}} \quad (4\text{-}30)$$

where k_s is the uncertainty absorber for the secondary side. The friction factor f in above equations is a function of Reynold number and the relative roughness of the channel. The same approach is used in the formulation of the hydraulics in the sodium side of the IHX.

4.4 Liquid Levels in Pools

During steady state, the level difference between hot and cold pools supports the net losses occurring in the IHX, thereby maintaining flow through it. A high level difference would be necessary to drive flow through a high pressure drop unit. During transient conditions, reduction in IHX losses will tend to increase flow through it. However, this will also reduce the level difference driving the flow. This competition between two opposing forces determining the dynamic state of levels and flow through the IHX. During flow coastdown transients, the levels approach each other, implying a net increase of cold pool mass at the expense of the hot pool. When the levels restabilize under low flow conditions, the level difference once again maintains the IHX losses.

If the IHX is overcooled due to very high intermediate flow, the resulting gravity head in the unit, available at much higher densities, is sufficient to overcome all frictional and losses. The levels then cross each other while the flow is maintained positive.

Mass balance at the cold pool gives

$$A_{cp} \frac{d(\rho_c Z_{cp})}{dt} = W_{IHX} - W_{core} + W_{bypass} + W_{break} \quad (4\text{-}31)$$

Note that W_b, the break flow, is zero for an intact loop. Z_{cp} in Eq. (4-31) is calculated based on the assumption that all the level changes likely to occur during a transient are confined to a constant cross-section area, A6OVRF in Fig. 1.1.

Mass balance in the hot pool gives

$$A_{hp}\frac{d\left(\rho_h Z_{hp}\right)}{dt} = W_{core} - W_{IHX} \tag{4-32}$$

When equations (4-31) and (4-32) are solved simultaneously with the flow equations, the results yield levels of cold pool (Z_{cp}) and hot pool (Z_{hp}) during the transient.

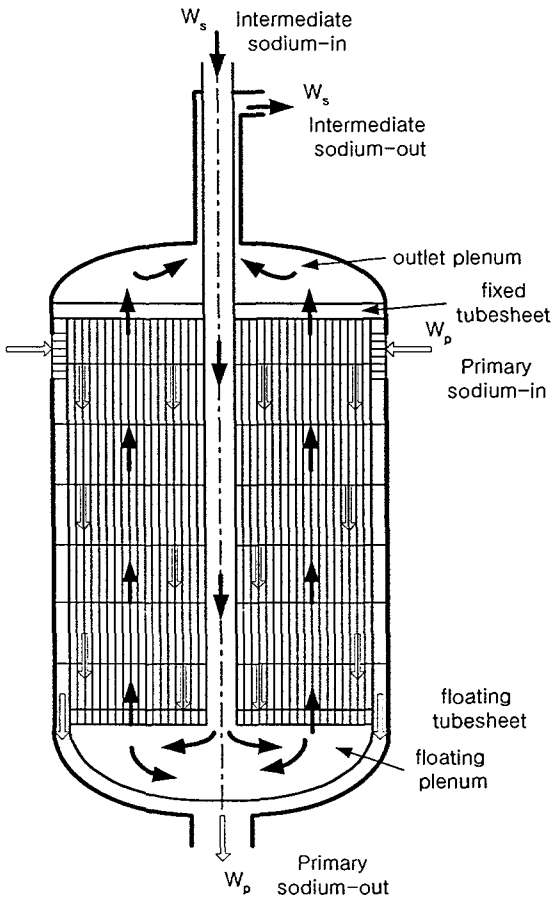

Fig. 4.1 Flow Paths of KALIMER IHX

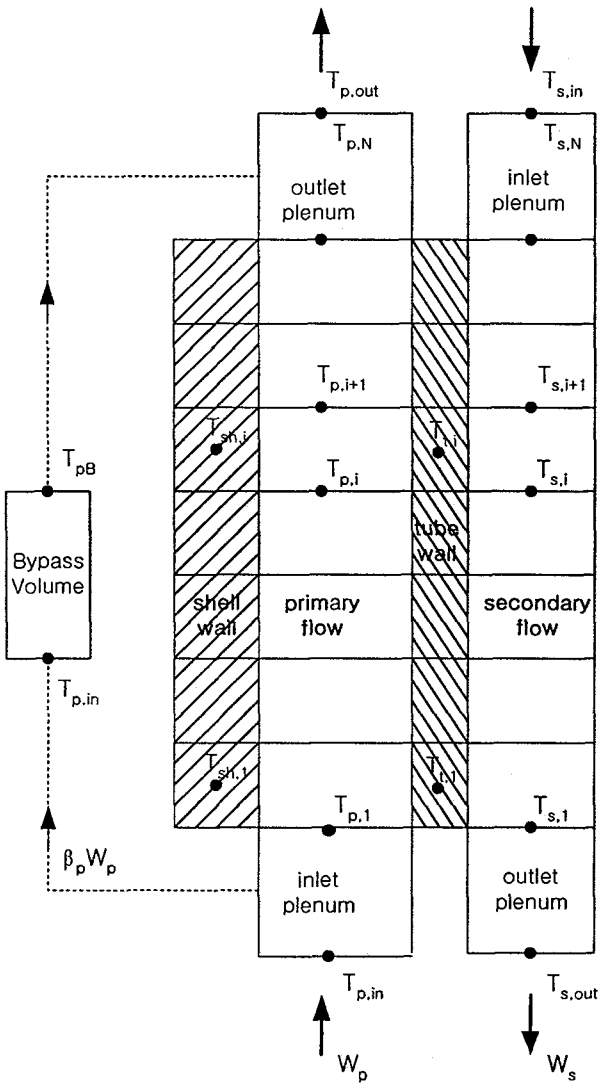

Fig. 4.2 Nodal Diagram for Thermal Balance

5. ELECTROMAGNETIC PUMP

The electromagnetic (EM) pump is modeled as a component. There are two pump choices available in the SSC-K code: centrifugal pump which was originally imbedded into the SSC-L, and an electromagnetic pump. Model description for the centrifugal pump is presented in the SSC-L code manual. In the SSC-K, an electromagnetic pump model is introduced for the KALIMER design.

5.1 Pump Models

The KALIMER design contains motor-generators on the primary pumps to extend the coastdown times of these EM pumps. Combination of EM pumps and motor-generators is included in SSC-K to handle this configuration. In the current KALIMER design a synchronous motor is running all of the time during normal operation, but the power to the EM Pump does not go through the motor as long as the normal pump power is available. If normal pump power is lost, then the motor becomes a generator, and a switch is thrown automatically to supply voltage from the motor-generator to the pump. The pump coastdown rate is then determined by the inertia of the motor. The motor is designed such that it will initially supply 60% of nominal voltage to the pump. Thus, when normal power is lost and the motor-generator power is switched on there is a sudden drop in pump head and flow followed by a gradual coastdown.

Pump Head

The pump head is correlated with an expression of the form

$$\overline{H} = (\overline{V}/\overline{f})^{3.5}\ h_n(\overline{W}/\overline{f}) - L_f\overline{W}^2 \qquad (5\text{-}1)$$

where

$$\overline{H} = H/Hr \qquad (5\text{-}2)$$

$$\overline{V} = V/Vr \qquad (5\text{-}3)$$

$$\bar{f} = f/fr \tag{5-4}$$

$$\bar{w} = w/wr \tag{5-5}$$

H = pump head
H_r = rated head
V= pump voltage
V_r= rated voltage
f = frequency
f_r = rated frequency
w = mass flow rate
w_r = rated mass flow rate
L_f = friction loss coefficient and
h_n is a head curve correlated as

$$h_n\ (\bar{w}/\bar{f}) = \sum_{j=1}^{5} a_j\ (\bar{w}/\bar{f})^{j-1} \tag{5-6}$$

with the coefficients a_j determined by a least-squares fit to the data.

Pump Efficiency

The pump efficiency, ε_f, is correlated as

$$\varepsilon_f = F(\bar{V})\ G(\bar{w}/\bar{f})\varepsilon_{fr} \tag{5-7}$$

with

$$F(\bar{V}) = \sum_{j=1}^{7} b_j\ \bar{V}^{j-1} \tag{5-8}$$

$$\begin{aligned} G(\bar{w}/\bar{f}) &= 0.01 && \text{if} \quad \bar{w}/\bar{f} \geq 5 \\ &= \sum_{j=1}^{9} c_j\ (\bar{w}/\bar{f})^{j-1} && \text{if} \quad \bar{w}/\bar{f} < 5 \end{aligned} \tag{5-9}$$

and ε_{fr} = rated efficiency

Pump Voltage

Before the cut-over to the motor-generator, the pump voltage is assumed to be constant at its rated value. Also, the frequency is constant at its rated value. Immediately after cut-over, the voltage drops to a fraction, V_{fr}, of its initial value. Then the voltage is proportional to the square of the frequency, so after cut-over the voltage is

$$\bar{V} = V_{fr}\ \bar{f}^2 \tag{5-10}$$

where

$$V_{fr} = 0.6 \tag{5-11}$$

Motor Speed

The equation for the motor speed, s, is

$$\frac{ds}{dt} = -\frac{(\tau_p + \tau_\ell)}{I} \tag{5-12}$$

where

τ_ρ = pump torque

τ_ℓ = friction loss

I = moment of inertia

Note that the motor speed and the pump frequency are the same:

$$f = s \tag{5-13}$$

The pump torque is given by

$$\tau_p = \frac{Hw}{\varepsilon_f \rho s} \tag{5-14}$$

where

ρ = liquid density

The friction loss in the motor is assumed to have the form

$$\tau_l = \tau_r L_m s \tag{5-15}$$

where L_m is a loss coefficient and τ_r, the rated torque.

5.2 Correlations to Pump Data

Experimental data has been fit by a least-squares fitting program to give the parameters listed in Table 5-1 for use in equations 5-6, 5-8, and 5-9. Also a value of .07592 is used for L_f in equation 5-1.

Table 5-1
Correlation Coefficients for Use with the LMR Pumps

j	a_j	b_j	c_j
1	1.333	-.148	0.
2	.996	7.110	-51.235
3	-2.498	-15.972	684.934
4	6.056	9.942	-3483.628
5	-4.611	12.024	9119.690
6	-	-18.536	-13449.761
7	-	6.577	11279.948
8	-	-	-5014.503
9	-	-	915.555

6. PASSIVE DECAY HEAT REMOVAL SYSTEM

6.1 Introduction

PSDRS (Passive Safety Decay Heat Removal System) is a heat removal feature in the KALIMER design which is characterized to cool the containment outer vessel with atmospheric air in passive manner. Fig. 6.1 exhibits the schematic of PSDRS. Atmospheric air comes in from the inlets located top of the containment, and flows down through the annulus gap between the air divider and the concrete wall. Then, it turns back upward passing through the other annulus gap between the containment outer surface and the air divider, and, finally, flows out through the stack with raised temperature by energy gained from cooling of the containment vessel. The air flow rate is determined from various parameters. Air temperature difference between two annulus channels, flow path or pressure drop of an orifice placed for flow control, friction exerted on the surfaces are main parameters affecting the flow rate.

It is important that the air divider should be made of high heat resistance material to maximize the temperature difference between the inner and outer channels. The gap between the reactor vessel and the containment vessel is filled with helium gas and thus radiation heat transfer prevails due to high temperature of these walls.

The significance of PSDRS in the KALIMER design is that it plays a role of the only heat removal system under total loss of heat sink accident. For this reason, its function is crucial to prevent the core damage, so that performance analysis as well as realistic modeling of the system may be a key issue to provide essential knowledge for safety evaluation of the KALIMER design.

6.2 PSDRS Modeling

6.2.1 Basic Assumptions

- Temperature in a wall is represented with one temperature except the air divider as shown in Fig. 6.1, because the wall thicknesses are thinner than those of gaps between them by roughly factor of 3 and more over the thermal resistances of the gaps are also relatively much higher. The air divider, however, is made of material with high thermal

resistance to reduce conduction across it.

- Air flow is calculated under assumption of quasi steady state, due to much smaller time constant than those of the walls. Therefore, it is assumed that air temperature varies axially along the flow channels.

- All walls and air channels are modeled with an equal mesh size which locates the same elevation in the axial direction. The axial heat conduction is ignored.

6.2.2 Governing Equations

Reactor vessel

The energy balance is set up using heat transfers from sodium or helium gas to the reactor vessel depending on the sodium level, and between reactor vessel inner and containment outer surfaces. e.g.

$$m_{w1}c_{w1}\frac{dT_{w1}}{dt} = h_{NW1}A_{NW1}(T_N - T_{W1}) + h_{W12}A_{W12}(T_{W2} - T_{W1}) \tag{6-1}$$

where,

m_{W1}, C_{W1} : mass and specific heat for the reactor vessel

T_N, T_{W1}, T_{W2} : temperatures of coolant or cover gas, reactor vessel, and containment vessel, respectively

h_{NW1} : heat transfer coef. between the inner surface of the reactor vessel and the coolant or cover gas

A_{NW1}, A_{W12} : corresponding heat transfer areas to the heat transfer coefficients

h_{W12} : heat transfer coef. between the reactor vessel and the containment vessel

$$\frac{1}{h_{w12}} = \frac{R_{w1}}{2} + \frac{1}{h_{CV12} + \varepsilon_{12}\,\sigma\,(T_{w1}+T_{w2})(T_{W1}^2+T_{W2}^2)} + \frac{R_{w2}}{2} \tag{6-2}$$

The approximation is made that R_{w1} and R_{w2} are lumped in with h_{CV12}, so

$$h_{w12} = h_{CV12} + \varepsilon_{12}\,\sigma\,(T_{w1}+T_{w2})(T_{W1}^2+T_{W2}^2) \tag{6-3}$$

where

$$\varepsilon_{12} = \frac{1}{\frac{1}{\varepsilon_{RV}} + \frac{1}{\varepsilon_{GVI}} - 1} \tag{6-4}$$

and

h_{CV12} = user-supplied convective heat transfer coefficient, RV to GV
(see 'User Manual')

ε_{RV} = emissivity of the reactor vessel wall

ε_{GVI} = emissivity of the guard vessel inner surface

σ = Stefan-Boltzmann Constant

R_{W1} = G_{RV} / k_{RV}

R_{W2} = G_{GV} / k_{GV}

G_{RV} = thickness of the reactor vessel

G_{GV} = thickness of the guard vessel

k_{RV} = thermal conductivity of guard vessel

k_{GV} = thermal conductivity of reactor vessel

Containment vessel

The containment temperature is determined by such terms as heat transfer from the reactor vessel, convection heat transfer to the up-flowing air, and radiation heat transfer directly to the inner surface of the air divider. Thus, the balance equation is led to

$$m_{w2}c_{w2}\frac{dT_{W2}}{dt} = h_{w12}A_{w12}(T_{W1} - T_{W2}) + h_{w23}A_{w23}(T_{W3} - T_{W2}) + h_{w2a}A_{w2a}(T_{a1} - T_{W2}) \tag{6-5}$$

The definitions of the coefficients used in this equation are the same notations as used in Eq. (6-1). However, h_{2a} denotes the heat transfer coefficient between the containment and down-flowing air, and A_{2a} is the outer surface area of the containment. T_{a1} is temperature of the up-flowing air. The heat transfer coefficient h_{23} is given by

$$\frac{1}{h_{w23}} = \frac{R_{w2}}{2} + \frac{1}{\varepsilon_{23}\,\sigma\,(T_{w2} + T_{w3})(T_{W2}^2 + T_{W3}^2)} \tag{6-6}$$

R_{w2} is neglected, so

$$h_{w23} = \varepsilon_{23}\,\sigma\,(T_{w2}+T_{w3})(T_{W2}^2+T_{W3}^2) \tag{6-7}$$

where

$$\varepsilon_{23} = \frac{1}{\frac{1}{\varepsilon_{GVO}}+\frac{1}{\varepsilon_{DI}}-1} \tag{6-8}$$

and

ε_{GVO} = emissivity of the guard vessel outer surface

ε_{DI} = emissivity of the air divider inner surface

$$\frac{1}{h_{w2a}} = \frac{R_{w2}}{2}+\frac{1}{h_{a1}} \tag{6-9}$$

again R_{w2} is neglected, so

$$h_{w2a} = h_{a1} \tag{6-10}$$

where the air heat transfer coefficient is

$$h_{a1} = \frac{k_a}{D_{ha1}} N_{u1} \tag{6-11}$$

k_a = air thermal conductivity

D_{ha1} = hydraulic diameter between the guard vessel and the air divider

N_{u1} = Nusselt number

$$N_{u1} = \begin{cases} C_1\,\mathrm{Re}_1^{C_2}\,P_{r1}^{0.4} & \text{if } \mathrm{Re}_1 \geq \mathrm{Re}_t \\ C_3 & \text{if } \mathrm{Re}_1 < \mathrm{Re}_t \end{cases} \tag{6-12}$$

$$\mathrm{Re}_1 = \frac{D_{ha1}\,w_a}{\rho_{a1}\,\mu_{a1}} \tag{6-13}$$

w_a = air flow rate

ρ_{a1} = air density

μ_{a1} = air viscosity

Pr_1 = Prandtl number

C_1, C_2, C_3 = user supplied correlation coefficients

C_1 ~ 0.023

C_2 ~ 0.8

C_3 ~ 3 – 8

Inner and outer surfaces of the air divider

Energy balance equation in the inner and outer surfaces of the air divider are given in similar manner and thus, it becomes

$$m_{w3}c_{w3}\frac{dT_{W3}}{dt} = h_{w34}A_{w34}(T_{W4}-T_{W3}) + h_{w23}A_{w23}(T_{W2}-T_{W3}) + h_{w3a}A_{w3a}(T_{a1}-T_{W3}) \quad (6\text{-}14)$$

$$m_{w4}c_{w4}\frac{dT_{W4}}{dt} = h_{w45}A_{w45}(T_{W5}-T_{W4}) + h_{w34}A_{w34}(T_{W3}-T_{W4}) + h_{w4a}A_{w4a}(T_{a2}-T_{W4}) \quad (6\text{-}15)$$

Here, T_{a2} represents temprature of the down-flowing air and heat transfer coefficients are given by

$$h_{w3a} = h_{a1} \quad (6\text{-}16)$$

$$h_{w4a} = h_{a2} \quad (6\text{-}17)$$

$$\frac{1}{h_{w5a}} = R_{w5} + \frac{1}{h_{2a}} \quad (6\text{-}18)$$

or

$$h_{w5a} = \frac{h_{2a}}{1 + R_{w5}\,h_{2a}} \quad (6\text{-}19)$$

$$h_{a2} = \frac{k_{a2}}{D_{ha2}} Nu_2 \tag{6-20}$$

Concrete wall

$$m_{w5}c_{w5}\frac{dT_{W5}}{dt} = h_{w56}A_{w56}(T_{W6} - T_{W5}) + h_{w45}A_{w45}(T_{W4} - T_{W5}) + h_{w5a}A_{w5a}(T_{a2} - T_{W5}) \tag{6-21}$$

Where, T_{W6} indicates the outer wall temperature of the concrete wall which always remains constant.

Temperatures of the up- and down-flowing air channels

The balance equations in the up- and down-flowing air channels are given as following equations, based on the assumptions described earlier.

$$w_a c_a \frac{dT_{a1}}{dz} = h_{wa2}A_{wa2}(T_{W2}(z) - T_{a1}(z)) + h_{wa3}A_{wa3}(T_{W3}(z) - T_{a1}(z)) \tag{6-22}$$

and

$$w_a c_a \frac{dT_{a2}}{dz} = h_{wa4}A_{wa4}(T_{W4}(z) - T_{a2}(z)) + h_{wa5}A_{wa5}(T_{W5}(z) - T_{a2}(z)) \tag{6-23}$$

Where, W_a denotes air flow rate and C_a does specific heat of air.

Calculation of air flow rate

Air flow rate is determined from gravitational force balance between down- and up-flowing air channels, and flow resistance along those channels. e.g.

$$\Delta p_{gr} = \int \rho g dz = g\{\rho_{in}\Delta z_{in} - \rho_{stack}\Delta z_{stack} + \sum_j \overline{\rho_{a2}}(j)\Delta z_j - \sum_j \overline{\rho_{a1}}(j)\Delta z_j - \rho_{in}(z_{st} - z_{in}) \tag{6-24}$$

and

$$\Delta p_{loss} = \sum \frac{w_a^2}{2\rho_a A_a^2}\left(f\frac{L}{D_h} + k_{or} \right) \tag{6-25}$$

where, (Z_{st} - Z_{in}) is the elevation difference between the inlet and stack, $\overline{\rho_a}(j)$ represents air density in j^{th} node, and K_{or} is defined as a form loss coefficient due to the geometry or orifice.

The friction factor is calculated as

$$f = \begin{cases} A_{fr}\,\mathrm{Re}^b & if \quad \mathrm{Re} \geq \mathrm{Re}_t \\ \dfrac{A_{fL}}{\mathrm{Re}} & if \quad \mathrm{Re} < \mathrm{Re}_t \end{cases} \tag{6-26}$$

where

Re = Reynolds number = $\dfrac{D_h W_a}{\mu_a A_a}$

μ_a = viscosity

A_{fr} = user-supplied turbulent friction factor coefficient (see 'User Manual')

b = user-supplied coefficient (see 'User Manual')

and

A_{fL} = user-supplied laminar friction factor coefficient

The value of Re_t, the Reynolds number for the transition from turbulent to laminar, is calculated by the code to make the friction factor continuous at the transition point.

$$A_{fr}\,\mathrm{Re}_t^{\,b} = \frac{A_{fL}}{\mathrm{Re}_t} \tag{6-27}$$

or

$$\mathrm{Re}_t = \frac{A_{fL}^{\frac{1}{1+b}}}{A_{fr}} \tag{6-28}$$

6.2.3 Solution Method

Schematic of solving the governing equations are presented in Fig. 6.2. Non-linear differential equations from Eqs. (6-1) to (6-5) are solved using Runge-Kutta Method [6-1], while Eqs. (6-6) and (6-7) can be solved with typical solution method of linear differential equation, if the axial wall temperature variations inside a node are ignored. The final solutions of these ordinary differential equations have a form of

$$T_{ai}(z') = T'_{ai} + (T_{ai}(0) - T'_{ai})e^{-\lambda_i z'} \tag{6-29}$$

where, i = 1,2,which correspond to up- and down-flowing channels, respectively

$$z' = z - z_j \tag{6-30}$$

$$T'_{a1} = f_2 T_{W2j} + f_3 T_{W3j} \tag{6-31}$$

$$f_2 = \frac{h_{w2a} A_{w2a}}{h_{w2a} A_{w2a} + h_{w3a} A_{w3a}} \tag{6-32}$$

$$f_3 = 1 - f_2 \tag{6-33}$$

$$\lambda_1 = \frac{h_{w2a} A_{w2a} + h_{w3a} A_{w3a}}{w_a C_a} \tag{6-34}$$

and above definitions for $T_{a2}(z')$ is similar.

Since the temperature, $T_{ai}(0)$, in Eq. (6-29) is defined at each node interface, so that a node temperature can be obtained by averaging the temperature profile within the length inside a node. Thus, the average value is calculated as

$$T_{aj} = \frac{\int_0^{\Delta z} T_{aj}(z')dz'}{\Delta z} \tag{6-35}$$

For the air temperature calculation, the balance Eqs. (6-24) and (6-25) becomes an algebraic equation. Thus, air temperature can be calculated straight forward once all coefficients are known.

6.3 PSDRS Program

Program 'PSDRS' consists of group-wised input variables. User should note that the sequence of input variables must be consecutive, otherwise there will be a problem to read the input. Error indication is not enough to find errors in the input lists easily at the present time and thus users should make sure of the card number and the number of input variables in a card. User also notes that units of all physical quantities should be given in SI units. Top view of the KALIMER PSDRS is shown in Fig. 6.3.

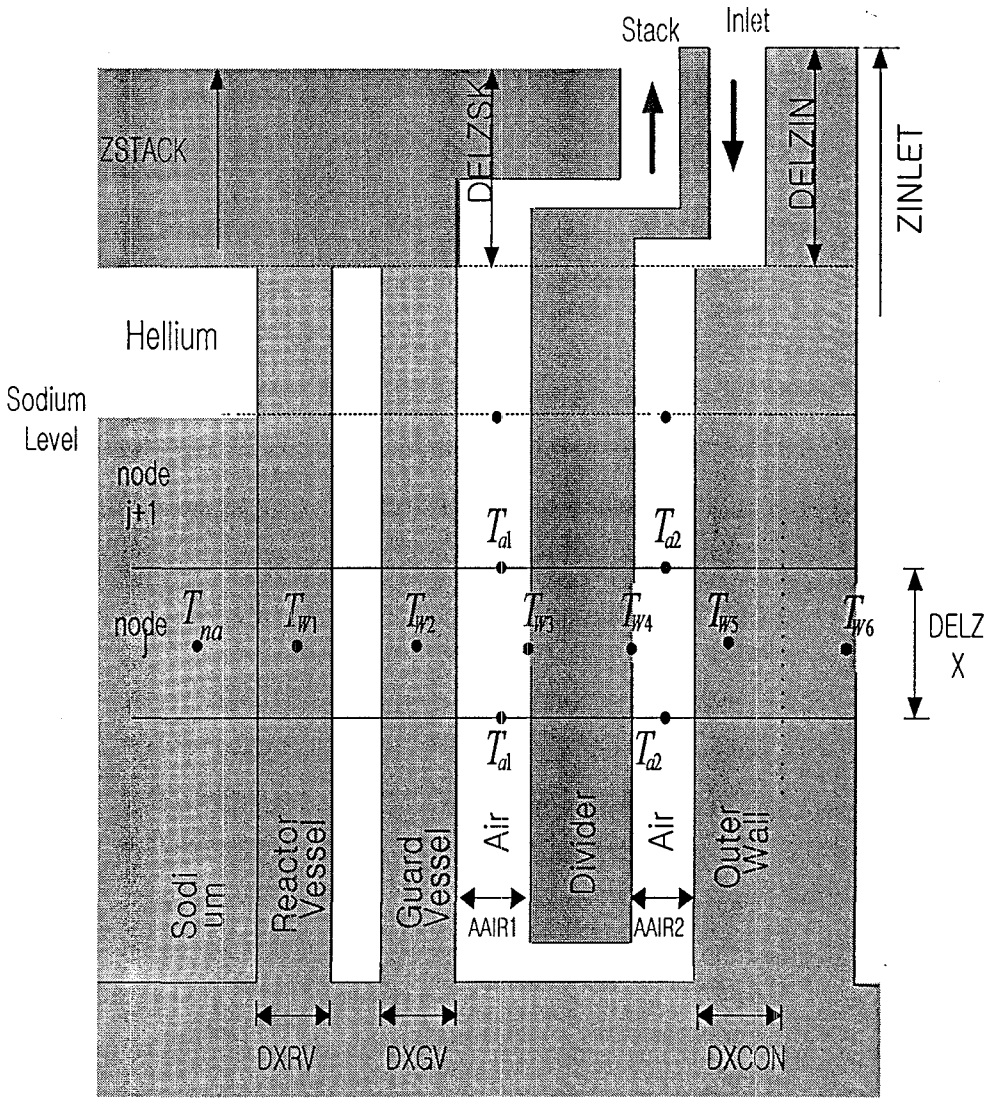

Fig. 6.1 PSDRS Model

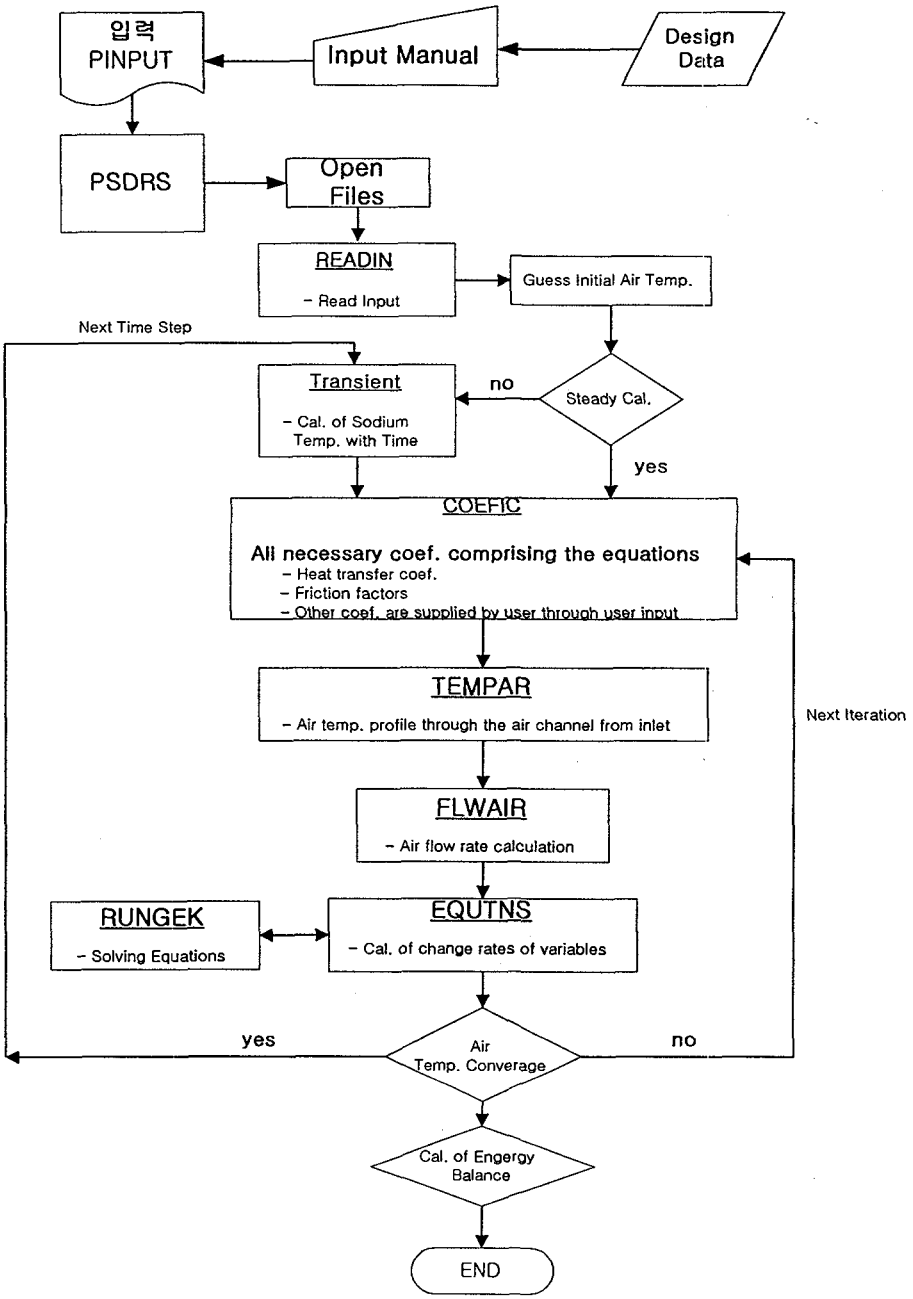

Fig. 6.2 Flowchart of PSDRS Program

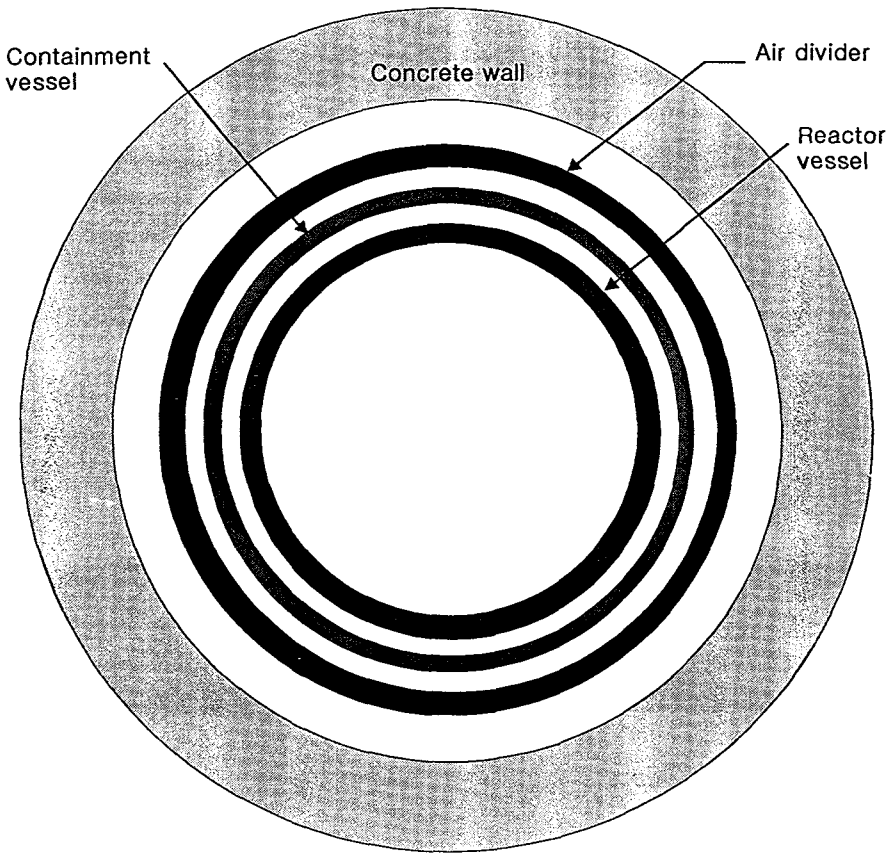

Fig. 6.3 Top View of KALIMER PSDRS

7. REACTIVITY MODELS

7.1 Introduction

One of the important KALIMER design features is inherent shutdown, which refers to the tendency of the reactor to transitions to a much lower power level whenever temperatures rise significantly. There are several reactivity feedbacks important in the inherent shutdown response for the metal cores, and the core is designed to provide strong, inherent, negative reactivity feedback with rising temperature. This feature, combined with the heat removal capability of the PSDRS, makes the KALIMER capable of safely withstanding severe undercooling or overpower accidents, even without scram.

Only when a major off-normal condition is encountered, combined with a postulated failure of the Plant Protective System (PPS), can serious accident consequences be predicted. The inherent shutdown characteristic must be tested against various postulated challenges if it is to be credited in the licensing arena.

The Super System Code (SSC), developed at BNL for analyzing LMR transients, was selected as a basis for the development of KALIMER safety analysis code SSC-K. Since the SSC code was used for the preparation of the PSAR for CRBRP which did not rely on the passive safety features including reactivity feedback effects, there exist only limited reactivity models within the code.

The objectives of the current task are (i) to develop a version of SSC-K code which has the capability of analyzing the inherent safety characteristics of the metal core, (ii) to gain experiences of the safety analysis for the unprotected accidents, and (iii) to identify action items for the further development of the reactivity, component and system models.

Reactivity feedback models have been developed for the SSC-K code in order to account for the effects due to Doppler, sodium density/void, fuel axial expansion, core radial expansion and control rod driveline expansion. These models will be used to establish a working version of the SSC-K code which is essential for the development of component and system models as the

KALIMER design progresses.

Attempts have been made for the application of the models in order to gain insight on the inherent safety characteristic under the postulated unprotected accident conditions. Reactivity models developed are not for actually generating a safety analysis results of KALIMER design but for the preparation of the further modeling efforts when the reactivity coefficients can be generated through a detailed neutronics calculation.

Efforts also have been made for the identification of the limitations and of the further modeling needs for the current version of the code through the preliminary safety analysis.

7.2 Reactor Kinetics

Nuclear reactor kinetics models predict the time behavior of the neutron population in a reactor core induced by changes in reactor multiplication. Diffusion model is capable of describing the time behavior of a nuclear reactor, provided the effects of delayed neutrons are included. However, such a model is too detailed for practical implementation in reactor kinetics analysis due to excessive computation requirements.

Point reactor kinetics approximations can be used more effectively for fast reactors than for thermal reactors because the neutron flux is more nearly separable in space and time for fast reactors. Fast reactor safety codes to date have therefore generally employed point kinetics, however, the reactivity feedback terms due to reactor temperature variations and material motion generally contain spatial effects.

7.2.1 Point Kintetics Equations

The total heat generation per unit volume $P(\vec{r}, t)$ is given as

$$P(\vec{r}, t) = P_f(\vec{r}, t) + P_d(\vec{r}, t) \tag{7-1}$$

where $P_f(\vec{r}, t)$ is the heat generation rate per unit volume due to nuclear fission and $P_d(\vec{r}, t)$ is the decay heat generation rate per unit volume.

While the spatial power distribution in a reactor core is of interest in the steady-state operation of the plant, the temporal power distribution is of utmost importance in day-to-day plant operation, reactor stability studies, and safety. The time-dependent portion of the fission power contribution is calculated by solving the space-averaged, one-energy group reactor kinetics equations. The one-energy group assumption is reasonable, particularly for a fast reactor. The space-averaged model is quite adequate since the core of an LMFBR responds, due to the relative smallness of the core and the large neutron migration area, more uniformly than a light water reactor core to changes in reactivity.

The point-kinetics equations may be expressed as

$$\frac{dN}{dt} = \frac{\rho - \beta_T}{\Lambda} N + \sum_{i=1}^{6} \lambda_i C_i \tag{7-2}$$

$$\frac{dC_i}{dt} = \frac{\beta_i}{\Lambda} N - \lambda_i C_i \quad (i = 1,2,..6) \tag{7-3}$$

where

N = neutron density (neutrons/m^3),
t = time(s),
ρ = *reactivity* ($\Delta k / k$),
β_T = effective delayed neutron fraction = $\sum_i \beta_i$,
Λ = prompt neutron generation time(s)
= prompt neutron lifetime / multiplication factor k,
λ_i = decay constnant for the i-th delayed neutron group(s^{-1}),
C_i = density of the i-th effective delayed neutron precursor
(precursors / m^3),
β_T = effective delayed neutron fraction for the i-the group.

It should be noted that for a particular isotopic composition of a reactor, a single set of λ_i and β_i values is obtained and utilized in the kinetics equations.

It is convenient to rewrite Eqs. (7-2) and (7-3) in a normalized form by defining the normalized neutron density, n(t) and concentration of the i-th group precursor, $c_i(t)$, as

$$n(t) = \frac{N(t)}{N(0)} \quad \text{and} \quad c_i(t) = \frac{C_i(t)}{C_i(0)}$$

Prior to the reactivity change, the derivative dC_i / dt in Eq. (7-3) is zero and

$$C_i(0) = \frac{\beta_i}{\lambda_i \Lambda} N(0)$$

By replacing $N(t)$ and $C_i(t)$ with $n(t)$ and $c_i(t)$, respectively, Eqs. (7-2) and (7-3) become

$$\frac{dn}{dt} = \frac{\rho - \beta_T}{\Lambda} n + \frac{1}{\Lambda} \sum_{i=1}^{6} \lambda_i c_i \tag{7-4}$$

$$\frac{dc_i}{dt} = \lambda_i (n - c_i) \qquad (i = 1,2,..6) \tag{7-5}$$

Perhaps the most serious approximation involved in the point reactor kinetics equations involves the assumption that the flux can be adequately represented by a single, time-independent spatial mode. When changes in core composition are sufficiently slow, as in fuel depletion or fission-product poisoning studies, one can perform an instantaneous steady-state criticality calculation of the shape function. For rapidly varying transients in which spatial effects are important, one is usually forced to solve the time-dependent neutron diffusion equation directly.

7.2.2 Prompt Jump Approximation

The direct integration of these equations requires very small timestep sizes due to the small numerical value of the generation time Λ. To assure numerical stability and accuracy, step sizes of approximately (100 to 1000)$\cdot \Lambda$ are required. Typically, Λ is about $= 6 \times 10^{-7}$s, therefore, the step sizes of the order of 0.00006 to 0.00006 s would be required.

The simplest way to circumvent this problem is to utilize the prompt jump approximation (PJA). This approximation makes use of the very fact that Λ is extremely small. By assuming the Λ approaches zero, the product $\Lambda(dn/dt)$ in Eq. (7-4) also approaches zero. It is also noted that for small values of reactivity, the rate of change of neutron density is sufficiently slow that

dn/dt is negligible compared to the two terms on the right hand side of Eq. (7-4). Thus, n may be directly solved for as

$$n = \frac{1}{\beta_T - \rho} \sum_i \lambda_i c_i \qquad (7\text{-}6)$$

This means that any disturbance in the reactivity (ρ) will be instantaneously reflected in the neutron density n jumps immediately to some initial level dependent on the size of the reactivity insertion.

Since dn/dt was assumed to be zero, the PJA is in excellent agreement (to within < 0.1%) with the exact solution for values of ρ less than +50 cents. It should be noted that this approximation gets even closer to the exact solution when the prompt neutron generation time is smaller.

The main drawback of using the PJA is the fact that agreement to the exact solution diminishes as ρ approaches β_T. It can be seen from Eq. (7-6) that n is discontinuous at $\rho = \beta_T$. To provide for these cases where ρ approaches β_T (or more conservatively, when $\rho > 50$ cents) an optional numerical method is included in SSC-K which solves the equations exactly.

7.2.3 Kagnove Method

To provide an exact solution to Eqs. (7-4) and (7-5), without integrating them directly, the method proposed by Kaganove was used in SSC. Here, Eqs. (7-5) are solved for c_i in terms of dc_i/dt and substituted into Eq. (7-4) such that

$$\frac{dn}{dt} = \frac{\rho n}{\Lambda} - \frac{1}{\Lambda} \sum_i \frac{\beta_i}{\lambda_i} \frac{dc_i}{dt}, \qquad (7\text{-}7)$$

The assumption is then made that over any integration step (Δt), the normalized power (n) and reactivity (ρ) may be represented by second-order polynomials. Thus,

$$n(t) = n_0 + n_1 t + n_2 t^2 \; ; \; 0 \le t \le \Delta t, \qquad (7\text{-}8)$$

$$\rho(t) = \rho_0 + \rho_1 t + \rho_2 t^2 \; ; \; 0 \le t \le \Delta t, \qquad (7\text{-}9)$$

where

n_0 = value of n at the end of previous timestep,

ρ_0 = value of ρ at the end of previous timestep

and n_1, n_2, ρ_1, ρ_2 are constants to be evaluated.

Eq. (7-5) is now integrated in a straightforward manner:

$$\int_0 d[c_i(\mu)e^{\lambda i\mu}] = \int_0 \lambda_i e^{\lambda i\mu} n(\mu) d\mu$$

Then

$$c_i(t) = c_{i0}e^{-\lambda it} + \lambda_i e^{-\lambda it} \int_0 e^{\lambda i\mu} n(\mu) d\mu \tag{7-10}$$

where

$$c_{i0} = c(t)|_{t=0}.$$

Making use of Eq. (7-8), Eq. (7-10) becomes

$$\begin{aligned} c_i(t) = c_{i0}e^{-\lambda it} + n_0(1 - e^{-\lambda it}) + \frac{n_1}{\lambda_i}(\lambda_i t - 1 + e^{-\lambda_i t}) \\ + \frac{n_2}{\lambda_i^2}(\lambda_i^2 t^2 - 2\lambda_i t - 2(1 - e^{-\lambda_i t}) \end{aligned} \tag{7-11}$$

Likewise, Eq. (7-7) becomes

$$n(t) - n(0) = \frac{1}{\Lambda}\int_0 \rho(\mu)\, n(\mu)\, d\mu - \frac{1}{\mu}\sum_i \frac{\beta_i}{\lambda_i}[c_i(t) - c_{i0}] \tag{7-12}$$

Upon substituting Eqs. (7-8) and (7-9) into Equation (7-12), one obtains

$$n_i(t) + n_2 t^2 = \frac{1}{\Lambda}(\rho_0 n_0 t + \rho_0 n_1 \frac{t^2}{2} + \rho_0 n_2 \frac{t^3}{3} + \rho_1 n_0 \frac{t^2}{2} + \rho_1 n_1 \frac{t^3}{3} + \rho_1 n_2 \frac{t^4}{4} + \rho_2 n_0 \frac{t^3}{3} + \rho_2 n_1 \frac{t^4}{4} + \rho_2 n_2 \frac{t^5}{5}) - \frac{1}{\Lambda}\sum_i \frac{\beta_i}{\lambda_i}[c_i(t) - c_{i0}] \quad (7\text{-}13)$$

The boundary conditions are then imposed that integral Eq. (7-13) be satisfied at the midpoint and end of the step (i.e., at $t = \Delta t/2t$ and $t = \Delta t$).

Thus, Eq. (7-13) yields two equations in the unknown n_1 and n_2. With the assumption that during any given timestep, the power and reactivity are functions of time only (i.e., decoupled), the solution in SSC will proceed as follows.

(a) using the predicted value of reactivity at $t = \Delta t$ and two previous values, the two constants ρ_1 and ρ_2 in Eq. (7-9) are calculated;
(b) using Eq. (7-13) solved at $\Delta t/2$ and Δt, the constants n_1 and n_2 are calculated;
(c) the predicted power may then be calculated using Eq. (7-8).

7.3 Reactivity Effects

Values for reactivity effects are required both for transient safety analysis and for control requirements during normal operation. Reactivity effects of importance in fast reactor design and safety include the Doppler effect, effects of sodium density changes or loss of sodium, effects of dimensional changes in core geometry, and long-term reactivity loss from fuel burnup.

The total reactivity at a given time, t, is the sum of as applied reactivity, $\rho_a(t)$ e.g., control rod movement, plus the sum of the various reactivity feedback contributions, $\rho_i(t)$:

$$\rho(t) = \rho_a(t) + \sum \rho_i(t) \quad (7\text{-}14)$$

As indicated in Fig. 7.1, the total reactivity is then incorporated into the point-kinetics model and used in the evaluation of the normalized time dependent factor for the fission and gamma heating. It should also be noted that the reactivity effects are inherently space-dependent. This is not only due to the fact that the temperatures vary spatially, but even for the same

temperatures the magnitude of the effect will depend on the location within the reactor. Since the point-kinetics equations suppress any spatial dependence, an appropriately weighted spatial integration of the evaluated local reactivity feedback effects must be performed.

In the following sections, models for various reactivity feedback effects are discussed. For the reactivity effects of dimensional changes in core geometry, fuel axial expansion, core radial expansion and control rod driveline expansion are considered.

Due to the unavailability of reactivity coefficients for KALIMER core designs at the present time, test runs have been performed for the SSC-K representation of the KALIMER for the preliminary verification of the reactivity models and for the better understanding of the reactor response under unprotected accident conditions.

7.3.1 Doppler Effect

It is important to have a prompt negative reactivity feedback that reverses a power transient if the reactor becomes prompt critical. Mechanical action by control rods is too slow after prompt criticality is reached. A prompt negative feedback is particularly important for fast reactors because two mechanisms, fuel compaction and sodium loss, have the potential to make the reactor superprompt critical.

The Doppler effect is the most important and reliable prompt negative reactivity effect in current thermal and fast reactor designs which utilize high fertile U238 material concentrations. Probably one of the better understood reactivity phenomena, the Doppler effect is due to the increased kinetic motion of the fuel atoms, as measured by an increase in fuel temperature, resulting in the broadening of cross-section resonances and increased resonance absorption.

The Doppler reactivity comes predominantly from the capture of low-energy neutrons. Ceramic-fueled reactors, due to the presence of oxygen or carbon in the fuel, have a soft enough neutron spectrum to have a large Doppler effect. The high density metal reactor, having no moderator in the fuel matrix, yields the hard neutron spectrum, and the flux in the principal Doppler resonance region (0.1 - 10 keV) is appreciably less than for the ceramic fueled reactor. Consequently, both oxide and carbide fueled fast reactors possess much higher Doppler

coefficients than metal fueled reactors. This represents one of the important advantages of ceramic over metal fuel.

7.3.1.1 Hard Spectrum Case

The Doppler coefficient, dk/dT, is defined as the change in multiplication factor, k, associated wit an arbitrary change in the absolute fuel temperature, T. For a reactor with hard neutron spectrum, such as a metal-fueled fast reactor, the theory for the effective Doppler cross section indicates that dk/dT should vary as $1/T^{3/2}$, i.e.,

$$\frac{dk}{dt} = \frac{\alpha^{DOP}}{T^{3/2}} \tag{7-15}$$

where α^{DOP} is the Doppler constant which is independent of temperature.

Eq. (7-15) may be integrated to yield

$$k - k_0 = 2\,\alpha^{DOP}\left(\frac{1}{\sqrt{T_0}} - \frac{1}{\sqrt{T}}\right) \tag{7-16}$$

where T_0 and T represent two different fuel temperatures and k_0 and k are the resulting multiplication factors. Rigorously, reactivity is defined as

$$\rho = \frac{k - 1}{k}$$

and changes in reactivity, $\Delta\rho$, as

$$\Delta\rho = \rho - \rho_0 = \frac{k - k_0}{k\,k_0}$$

For small reactivity changes, the Doppler effect is of the order of 10^{-4}.
With $k \approx 1$,

$$\Delta\rho \approx k - k_0$$

and the change in reactivity due to the Doppler effect $\Delta\rho^{DOP}$, can be written as

$$\Delta\rho^{DOP} = 2\,\alpha^{DOP}\left(\frac{1}{\sqrt{T_0}} - \frac{1}{\sqrt{T}}\right) \tag{7-17}$$

By definition, the reactivities are referenced to zero at steady state conditions, that is, $k_0 = 1$ and $\rho_0 = 0$, and the Doppler reactivity can be rewritten as

$$\rho^{DOP} = 2\,\alpha^{DOP}\left(\frac{1}{\sqrt{T_0}} - \frac{1}{\sqrt{T}}\right) \tag{7-18}$$

This is equation may be applied locally or regionally depending on how the temperatures and Doppler constant are defined. Specifically, in discrete notation, the local Doppler reactivity, ρ_{JK}^{DOP} is

$$\rho_{JK}^{DOP} = 2\,\alpha_{JK}^{DOP}\left(\frac{1}{\sqrt{T_{0JK}}} - \frac{1}{\sqrt{T_{JK}}}\right) \tag{7-19}$$

where

K = index of fuel channel

J = index of the axial level along the fuel channel

α_{JK}^{DOP} = the node-weighted Doppler constant for position JK

T_{0JK} = the reference fuel temperature at position JK

T_{JK} = the effcetive local temperature at position JK

The effective fuel temperature can be taken to be the volume-averaged fuel temperature which is defined as

$$T_{JK} = \frac{\sum_{I} V_{IJK} T_{IJK}}{\sum_{I} V_{IJK}} \tag{7-20}$$

where V_{IJK} is the fuel volume is channel K, axial slice J, between radial mesh I and I-1,

and T_{JK} is the local fuel temperature at this position. Figures 7.3 and 7.4 show the SSC-K representations of reactor core subassemblies and radial node within a fuel rod, respectively.

It should be noted that the Doppler constant in Eq. (7-19) is shown to be a space-dependent variable. Although α_{JK}^{DOP} will be a constant with respect to fuel temperature, there will be spatial variations due to different fuel types (e.g., enrichment, pin size, volume fractions of structural material, coolant, and fuel) and different sodium density. In the present model, α_{JK}^{DOP} will be a space-dependent parameter supplied by the user. Thus, the first concern relating to fuel type can be directly addressed.

The sodium density dependences is actually a neutron spectrum dependence- the harder the spectrum, the smaller the Doppler effect since there are less neutrons in the resonance range. The less sodium present, owing to density decreases or voids, implies a harder spectrum. To treat this effect, an effective isothermal sodium void fraction, X_{JK}^{Na}, is defined

$$X_{JK}^{Na} = \frac{\rho_{0JK}^{Na} - \rho_{JK}^{Na}}{\rho_{0JK}^{Na}} \tag{7-21}$$

where ρ_{JK}^{Na} is the local, time-dependent sodium density at position JK, and ρ_{0JK}^{Na} is the local reference sodium density. Thus, if β_{JK}^{DOP} and Ω_{JK}^{DOP} are the Doppler constants with and without sodium present, respectively, then the net Doppler constant can be approximated by

$$\alpha_{JK}^{DOP} = \beta_{JK}^{DOP}(1 - X_{Jk}^{Na}) + \Omega_{JK}^{DOP} X_{JK}^{Na} \tag{7-22}$$

To obtain an overall Doppler reactivity, ρ^{DOP}, for use in the point - Kinetics equation, a summation of Eq. (7-19). must be performed. Thus

$$\rho^{DOP} = \sum_{JK} \rho_{JK}^{DOP} = 2\sum_{JK} \alpha_{JK}^{DOP} \left(\frac{1}{\sqrt{T_{0JK}}} - \frac{1}{\sqrt{T_{JK}}}\right) \tag{7-23}$$

The value of the Doppler constants, β_{JK}^{DOP} and Ω_{JK}^{DOP} for each position JK, must be supplied by the user in units of reactivity $\Delta k/k$ for that mesh.

7.3.1.2 Soft Spectrum Case

Since the Doppler coefficient is found to vary with $1/T$ in a oxide-fueled fst reactor, this coefficient an be defined as

$$\frac{dk}{dT} = \frac{\alpha^{DOP}}{T} \tag{7-24}$$

where α^{DOP} is a temperature independent Doppler constant.

For a uniform change in fuel temperature from T_0 and T, Eq. (7-24) may be integrated to yield

$$k - k_0 = \alpha^{DOP} \ln(\frac{T}{T_0}) \tag{7-25}$$

where k and k_0 are resulting multiplication factors.

For small reactivity changes with $k \approx 1$, the Doppler reactivity effect can be calculated as

$$\rho^{DOP} = \alpha^{DOP} \ln(\frac{T}{T_0}) \tag{7-26}$$

which can be applied locally and rewritten as

$$\rho_{JK}^{DOP} = \alpha_{JK}^{DOP} \ln(\frac{T_{JK}}{T_{0JK}}) \tag{7-27}$$

To obtain an overall Doppler reactivity, ρ^{DOP}, for use in the point kinetics equation, a summation of Eq. (7-27) must be performed. Thus,

$$\rho_{JK}^{DOP} = \sum_{JK} \rho_{JK}^{DOP} = \sum_{JK} \alpha_{JK}^{DOP} \ln(\frac{T_{JK}}{T_{0JK}}) \tag{7-28}$$

where α_{JK}^{DOP} is also defined by Eq. (7-22).

Input requirements for the calculation of Doppler reactivity are β_{JK}^{DOP} and Ω_{JK}^{DOP} in $\Delta k/k$.

7.3.1.3 Other Models

ARIES code also calculates the Doppler reactivity coefficient by the Eq. (7-28) with temperatures in Rankines.

SASSYS code calculates the Doppler feedback reactivity, ρ^{DOP}, based on summation, over fuel axial nodes in all channels, the contribution for a node which is based on a mass weighted average fuel temperature, as well as on how much fuel and sodium are currently present in the node:

$$\begin{aligned}\rho_{DOP} &= \sum_{JK} \rho_{JK}^{DOP} \\ &= \sum_{JK} W_{JK} \frac{m_f^{JK}}{m_{f0}^{JK}} \left\{ \Omega_K^{DOP} + (\beta_K^{DOP} - \Omega_K^{DOP}) \frac{\bar{\rho}_{JK}}{\rho_{JK0}} \right\} \ln\left(\frac{T_{JK}}{T_{JKo}}\right)\end{aligned} \tag{7-29}$$

where

W_{JK} = Doppler weighting factor for axial node J in channel K. normalized for each channel

β_K^{DOP} = Doppler coefficient for channel K with all sodium present

Ω_K^{DOP} = Doppler coefficient for channel K with no sodium present

m_f^{JK} = fuel mass of the node JK

m_{f0}^{JK} = initial steady-state mass of fuel in the node JK

$\overline{\rho_{JK}}$ = average density of sodium in the node JK

$\overline{\rho_{JK0}}$ = initial steady-state density of sodium in the node JK

T_{JK} = average temperature of fuel in the node JK

T_{JK0} = initial steady-state temperature of fuel in the node JK

The valves for the unvoided and voided Doppler coefficient, β_K^{DOP} and Ω_K^{DOP}, for each channel, as well as the weighting factors are supplied by the user, based on neutronics calculations or experimental measurements.

7.3.2 Sodium Density Effect

The loss of sodium from a large fast reactor can result in a large positive reactivity effect. Sodium might be expelled from the core in the unlikely event of an unprotected transient, in which sodium boiling results from undercooling the reactor. This condition presents an important safety problem for an LMFBR, a problem not present in thermal reactors.

The sodium loss reactivity effect is exceedingly space-dependent. Sodium loss from the center of the core yields a highly positive reactivity effect, and sodium loss from near the edge gives a negative effect. The density decreases affect the reactivity of the reactor through two competing effects: increased leakage, which adds negative reactivity and is important away from the center of the core, and spectral hardening due to a decrease in the macroscopic sodium scattering cross-section which adds positive reactivity. The net effect depends primarily upon the location in the reactor.

In modeling this effect, both sodium density changes and voiding can be treated in a similar fashion. Basically, what is required along with the spatial sodium density distribution is a table of space-dependent sodium reactivity worths. The sodium density will be determined internally by SSC from knowledge of the sodium temperature distribution. However, the reactivity worths are user supplied.

There are several ways to present this reactivity effect depending on the form in which the reactivity worth data are known. For application in SSC, the following equation, which can treat either sodium density or voiding reactivity effects, is used

$$\rho^{Na} = \sum_{JK} \beta_{JK} M_{JK} \tag{7-30}$$

where ρ^{Na} is the overall sodium void reactivity coefficient for use in the point-kinetics equation, β_{JK} is the sodium reactivity worth in axial slice J, channel K, in units of reactivity per unit mass of sodium voided in segment JK, and is defined as

$$M_{JK} = (\rho_{0JK}^{Na} - \rho_{JK}^{Na})\, V_{JK}^{Na} \tag{7-31}$$

where ρ_{0JK}^{Na} is the local sodium density at reference temperature, ρ_{JK}^{Na} is the local average, time-dependent sodium density and V_{JK}^{Na} is the local coolant volume in segment JK.

Input requirements for the calculation of sodium void reactivity according to the Eq. (7-30) are the mesh weighted sodium void reactivity coefficients β_{JK} in $\Delta k/k$ per kg of sodium effectively voided.

The sodium void reactivity may also be calculated based on the changes in sodium temperatures as

$$\rho^{Na} = \sum_{JK} \beta_{JK} * (T_{JK}^{Na} - T_{0JK}^{Na}) \tag{7-32}$$

where β_{JK} is the sodium void reactivity coefficient in $\Delta k/k$ per K.
T_{JK}^{Na} is the sodium temperature at axial node J of channel K
and T_{0JK}^{Na} is the initial steady state sodium temperature at axial node J of channel K.

The ARIES code computers the sodium void reactivity as

$$\rho^{Na} = \sum_{JK} \alpha^{Na} \beta_{JK} * (T_{JK}^{Na} - T_{0JK}^{Na}) \tag{7-33}$$

where α^{Na} is the sodium volumetric expansion coefficient in $^{0}F^{-1}$
β_{JK} is the sodium void reactivity coefficient in $\Delta k/k$
and T_{JK}^{Na} and T_{0JK}^{Na} are sodium temperatures in ^{0}F

The sodium voiding model in SASSYS-1 and SAS4A is a multiple-bubble slug ejection model. The main purposes of this model are to predict the rate and extent of voiding for the voiding reactivity calculations and to predict the heat removal from the cladding surface after the onset of voiding for the fuel and cladding temperature calculations.

7.3.3 Axial Expansion Effect

A role of axial expansion of fuel in the normal solid fuel pin geometry is to provide a prompt negative reactivity feedback at the start of a power transient. This mechanism is the principal prompt negative feedback available in a metal-fueled fast reactor. Doppler feedback is

also available for the metal-fueled system, but it is relatively small due to the hard neutron spectrum. For a ceramic-fueled reactor, lack of structural integrity due to cracking in high burnup fuel renders the axial expansion mechanism somewhat unreliable so that more dependence is placed on the Doppler effect for a prompt negative feedback.

The fuel axial expansion increases the core height as temperatures rise, and changes the reactivity of the system by increasing the neutron leakage. The result is a rapid negative feedback contribution from an increase in fuel temperature, or a rapid positive feedback in response to a decrease in fuel temperature. The axial leakage changes only a little with axial fuel expansion, but the radial leakage does increase, thereby producing a negative reactivity effect, which can be shown as follows.

The criticality factor can be expressed as

$$k = k_\infty P_{NL} = k_\infty e^{-B^2 M^2} \tag{7-34}$$

where k is the product of the criticality factor for an infinite reactor, k_∞, and the fast neutron nonleakage probability, $e^{-B^2 M^2}$. For a cylindrical core,

$$k = k_\infty e^{-(B_z^2 + B_r^2) M^2} = k_\infty e^{[-(\pi/Z)^2 + (2.405/R)^2] M^2} \tag{7-35}$$

Now let us suppose that fuel expands axially as a result of increasing fuel temperature during the rise to full power or in a power transient. Radial fuel expansion may increase fuel pin diameters slightly but will have relatively little effect on radial expansion of the core. Bulk radial core expansion is governed primarily by the structure and hence, the coolant temperatures, together with the influence of the radial restraint system. Hence, the primary core expansion from increased fuel temperature is in the axial direction.

According to conventional reactor theory, the migration area varies with transport and total cross sections as

$$M^2 = \frac{1}{\sum_{tr} \sum_{t}} \propto \frac{1}{N^2}$$

where $\sum_{tr}$ and $\sum_{t}$ are effective transport and total cross sections that provide the correct nonleakage probability. N is the number density of fuel and structure atoms.

For a fixed number of fuel and structure atoms,

$$N \propto \frac{1}{V} \propto \frac{1}{R^2 Z}$$

where V = volume of the core
R = core radius
and Z = core height

Thus $M^2 \propto R^4 Z^2$, but now Z is the only dimension in V that changes during axial fuel expansion. Hence, the criticality factor can be presented in terms of the only parameter that is varying, Z, as

$$k = k_\infty e^{-C_1 R^4 Z^2 / Z^2} e^{-C_2 R^4 Z^2 / R^2} = k_\infty e^{-C_1} e^{-C_2 Z^2} \tag{7-36}$$

This result indicates that the axial leakage does not change with axial fuel expansion, but that the radial leakage does increase, thereby producing a negative reactivity effect.

An upper limit to the magnitude of this effect is obtained if it is assumed that the fuel pellets are free to move within the cladding. However, the actual mechanisms for expansion are difficult to model, especially for ceramic fuel. Fuel pellet cracking or friction between the pellet surface and inner clad wall will reduce the expansion significantly. On the other hand, if the fuel pellets are not stacked in perfect contact within the clad, then there may be negative fuel expansion if the fuel pellets settle. Physics calculations for CRBRP indicate a maximum overall reactivity of -.18 ¢/mil of fuel axial expansion. The range of this effect is quoted to be +.025 ¢/mil to -.18 ¢/mil owing to the uncertainties involved in the expansion mechanism.

The lack of strong Doppler coefficient for metal fuels, which is caused by the characteristic hard neutron spectrum, has historically been compensated for by the presence of a reliable axial expansion coefficient. The ternary U-Pu-Zr fuel swells out to contact the HT9 cladding material

around 2-3% atom burnup. After the fuel-clad lockup occurs, the fuel thermally expands according to the thermal expansion of the clad material. This is because the strength of metal fuel is very limited, and thus its expansion is dominated by the clad expansion. Experiments have shown that a 4% axial elongation is possible in the 1.9 to 5.3% burnup range.

The reactivity effect due to the thermal expansion usually decreases with the increase in reactor core size.

There are three models in the SSC-K code available for the evaluation of fuel axial reactivity coefficient. Free fuel expansion model, which gives the upper limit to the axial expansion reactivity, assumes that the fuel expands freely in the axial direction, and fuel - cladding contact is ignored. Uncertainties in the axial reactivity coefficient are accounted for by the uncertainty factor, and this is the original model present in the SSC-L code.

Force balance controlled expansion model assumes that the fuel is in contact with the clad, which is the most likely state for the metal-fueled core since the fuel is in an unlocked state only briefly. The fuel elongation is calculated by using an average strain, weighted with Young's modulus.

Another model is the one for ARIES code, which is based upon the fuel and clad temperature variations. Axial expansion may be optionally calculated based upon clad temperatures for conservative analyses of postulated accident conditions.

The simple model of the SASSYS code is based on a few assumptions. During the transient, if the cladding expands faster than the fuel, then the fuel-cladding gap opens, and the fuel can expand freely in the axial direction. If the fuel expands faster than the cladding, then the fuel binds with the cladding, and the axial expansion is determined by balancing the axial forces between the fuel and cladding.

7.3.3.1 Free Fuel Expansion Model

The reactivity due to fuel axial expansion, ρ^{AX} is based on a model which parallels the treatment of sodium density reactivity effects:

$$\rho^{AX} = \sum_{JK} C_{JK} N^{*}_{JK} \tag{7-37}$$

where C_{JK} is the user-supplied fuel reactivity worth in axial slice J, channel K, in units of reactivity, $\Delta k/k$, per unit mass of fuel effectively voided from segment JK, and N^{*}_{JK} is the effective mass of fuel voided in segment *JK*.

An expression for the evaluation of N^{*}_{JK} is derived based on the logic that as the fuel temperature increases, the fuel expands axially according to

$$Z_{JK} = [1 + \alpha\,(T_{JK} - T_{0JK})]\, Z_{0JK} \tag{7-38}$$

where α is the linear fuel expansion coefficient in units of $cm/cm\,K$ and T_{JK} is volume - averaged fuel temperature. To conserve mass, an axial increase in the fuel length implies a decrease in the fuel density ρ_{JK}, which can be expressed as

$$\rho_{0JK}\, Z_{0JK} = \rho_{JK}\, Z_{JK} \tag{7-39}$$

or

$$\rho_{0JK} - \rho_{JK} = \rho_{0JK} \left[\frac{\alpha(T_{JK} - T_{0JK})}{1 + \alpha(T_{JK} - T_{0JK})} \right] \tag{7-40}$$

The difference in density times the original fuel volume, V_{0JK}, will give the amount of fuel voided from location, *JK*, N_{JK},

$$N_{JK} = (\rho_{0JK} - \rho_{JK})\, V_{0JK}\, \rho_{0JK} \left[\frac{\alpha(T_{JK} - T_{0JK})}{1 + \alpha(T_{JK} - T_{0JK})} \right] \tag{7-41}$$

The effective amount of fuel voided from location *JK*, N^{*}_{JK}, and the resulting net reactivity effect associated with fuel axial expansion are given as

$$N^{*}_{JK} = e\, N_{JK} \tag{7-42}$$

$$\rho^{AX} = e \sum_{JK} C_{JK} N_{JK} \tag{7-43}$$

where e is a user-supplied constant that accounts for the fact that the present model does not account for the uncertainties associated with the mode of fuel expansion and does not explicitly evaluate the increase in reactivity because the fuel that was calculated to be voided from location *JK* actually causes a net increase in axial fuel height, reducing leakage. A recommended upper limit for e is given to be 0.3 for oxide fuels.

For the calculation of fuel axial expansion reactivity, a user needs to supply C_{JK}, the fuel reactivity worth in axial slice J, channel K, in units of reactivity *(Δk/k)* per kg of fuel effectively voided from segment *JK*.

7.3.3.2 Force Balance Controlled Expansion Model

This model assumes that the fuel is locked and expands with clad. The reactivity worth is determined from the difference between the initial fuel length and the elongated length at any given time.

The axial expansion reactivity coefficient dk/dz is defined as

$$\frac{dk}{dz} = \frac{\alpha^{AX}}{z} \tag{7-44}$$

where α^{AX} is an axial expansion constant in units of Δk. This equation may be integrated to yield

$$\rho^{AX} = \alpha^{AX} \ln \left(\frac{z}{z_0}\right) \tag{7-45}$$

In discrete notation

$$\rho^{AX} = \sum_k \rho_K^{AX} = \sum_K \alpha_K^{AX} \ln\left(\frac{z_k}{z_{0k}}\right) \tag{7-46}$$

where

α_K^{AX} = an axial expansion constant for channel K in units of Δk

z_k = the elongated axial length of channel K

z_{0k} = the axial length of channel K at reference temperature T_o

By definition, the effective strain ($\Delta l / l$) of K-th channel, ξ_k, can be expressed as

$$\xi_k = \frac{z_k - z_{0k}}{z_{0k}} \tag{7-47}$$

and rewritten as

$$\bar{\alpha}(T) = \alpha_0 + \alpha_1 T \tag{7-48}$$

The effective strain of channel K can be calculated by using an average strain, weighted with Young's modulus as

$$\begin{aligned} \xi_k &= \frac{1}{z_{0k}} \sum_J z_{0JK}\, \xi_{Jk} \\ &= \frac{1}{z_{0k}} \sum_J z_{0JK} \left(\frac{\xi_f Y_f A_f + \xi_c Y_c A_c}{Y_f A_f + Y_c A_c} \right)_{JK} \end{aligned} \tag{7-49}$$

where

K	= index of channel
J	= index of the axial position along the channel
z_{0JK}	= the axial length of segment *JK* at reference temperature
Y	= Young's modulus
A	= Nominal cross-sectional area

and subscripts *f* and c represent fuel and clad, respectively.

The strains of fuel and clad can be obtained from

$$\xi^f_{JK} = \alpha^f \, (T^f_{JK} - T^f_{0JK}) \tag{7-50}$$

$$\xi^c_{JK} = \alpha^c \, (T^c_{JK} - T^c_{0JK}) \tag{7-51}$$

where

α^f = the thermal expansion coefficient of the fuel
α^c = the thermal expansion coefficient of the clad
T^f_{JK} = the average temperature of fuel in segment JK
T^c_{JK} = the average temperature of clad in segment JK
T_0 = the reference temperature

Input requirements for this model are as follows:

α^f = the thermal expansion coefficient of the fuel
α^c = the thermal expansion coefficient of the clad
Y = Young's modulus for fuel and clad
α^{AK}_K = axial expansion constant in units of Δk

α^f and α^c are currently calculated in subroutine TEXP, while Y and α^{AK}_K are provided in subroutine GROW5T of SSC-K.

7.3.3.3 Other Models

ARIES code adopts a fuel-clad expansion model as

$$\rho^{AX} = \sum_{JK} \left[\alpha^C \rho^C_{JK} \, (T^{Na}{}_{JK} - T^{Na}{}_{0JK}) + \alpha^F \rho^F_{JK} \, (T^F{}_{JK} - T^F{}_{0JK}) \right] \tag{7-52}$$

where α^C = the cladding linear expansion coefficient in $^0F^{-1}$

α^F = the fuel linear expansion coefficient in $^0F^{-1}$

ρ^C_{JK} = the cladding axial expansion reactivity coefficient in Δk

ρ^F_{JK} = the fuel axial expansion reactivity coefficient in Δk

Axial fuel expansion can also be calculated based on cladding temperature as

$$\rho^{AX} = \sum_{JK} (\alpha^C \rho^C_{JK} + \alpha^C \rho^F_{\rho JK}) (T^{Na}_{JK} - T^{Na}_{0JK}) \quad (7\text{-}53)$$

Usually, Eq. (7-52) is used when analyzing undercooling events and Eq. (7-53) is used for conservative analyses of transient overpower events.

It is assumed in SASSYS code that before the start of the transient, a combination of fuel cracking, fuel re-structuring, and stress relaxation cause the gap between the fuel and the cladding to close, but there is little contact force between the fuel and cladding. During the transient, if the cladding expands faster than the fuel, then the fuel-cladding gap opens, and the fuel can expand freely in the axial direction. If the fuel expands faster than the cladding, then the fuel binds with the cladding, and the axial expansion is determined by balancing the axial forces between the fuel and cladding. Slip between fuel and cladding is ignored in this case.

The reactivity calculation is based on the user-supplied local fuel reactivity worth, in units of reactivity, $\Delta k / k$, per unit mass of fuel effectively voided from the segment.

7.3.4 Radial Expansion Effect

7.3.4.1 SSC-K Model

Radial fuel expansion due to increasing fuel temperature may increase fuel pin diameters slightly but will have relatively little effect on radial expansion of the core. Bulk radial core expansion is governed primarily by the structure and, hence, the coolant temperatures, together with the influence of the radial restraint system.

The core assemblies are held by their nosepieces in the receptacles, and by the load pads near the top of the assemblies which are surrounded by a core restraint ring attached to the core barrel, as shown in Fig. 7.6. The separation of the assemblies is maintained by an intermediate plane of load pads at an elevation above the active core. The intermediate load pads above the core are not restrained by a former ring attached to the core barrel. Thus, the core assemblies are free to bow as dictated by temperature differences and their metallurgical condition.

The radial dimension of the core is largely determined by the assembly spacing. This spacing is

determined by the grid plate below the core and by two sets of load pads above the core.

The redial expansion reactivity coefficient, dk/dr, can be defined as

$$\frac{dk}{dr} = \frac{\alpha^R}{r} \tag{7-54}$$

where α^R is a radial expansion constant in units of Δk. This equation may be integrated to yield

$$\rho^R = \alpha^R \ln(\frac{r}{r_0}) \tag{7-55}$$

where

r = the radial dimension of core at transient temeprature

r_0 = the initial steady-state radial dimension of core

By definition, the effective strain ($\Delta l/l$), ξ, can be expressed as

$$\xi = \frac{r - r^0}{r^0}$$

and rewritten as

$$\frac{r}{r^0} 1 + \xi$$

Thus

$$\rho^R = \alpha^R \ln(1 + \xi) \tag{7-56}$$

The coefficients α^R, for radial expansion effect, were calculated assuming a uniform increase over the core radius. However, the above core load pad (ACLP) responds to core exit sodium temperature while the grid plate (GP) responds to the core inlet temperature. This causes non-uniform expansion and the worth for each component must be weighted. From geometrical considerations, the split is W_{LP} for ACLP and W_{LP} for GP. Hence, the radial expansion reactivity can be calculated as

$$\rho^R = \alpha^R \ln(1 + W_{LP}\,\xi_{LP} + W_{GP}\,\xi_{GP}) \tag{7-57}$$

where

W_{LP} = geometrical weighting factor for the ACLP

W_{GP} = geometrical weighting factor for the GP

The strain of the ACLP can be calculated as

$$\xi_{LP} = \sum_{K} N^{K} \xi_{LP}^{K} \tag{7-58}$$

where

K = index of the fuel channel

N^{K} = number of subassemblies in K-th channel across core radius layout as shown in Fig. 7.6

ξ_{LP}^{K} = strain $(\Delta r / r)$ for ACLP of channel K

The strains of the ACLP and the GP for channel K can be obtained as

$$\xi_{LP}^{K} = \alpha_{LP}(T_{avg}^{K} - T_{0}^{K}) \tag{7-59}$$

$$\xi_{GP} = \alpha_{GP}(T^{GP} - T_{0}^{GP}) \tag{7-60}$$

where

α_{LP} = the thermal expansion coefficient of the ACLP

α_{GP} = the thermal expansion coefficient of the GP

T_{0}^{K} = the initial steady state temperature of the ACLP at K-th channel

T_{avg}^{K} = the volume-averaged temperature of the ACLP at K-th channel

T_{0}^{GP} = the initial steady state temperature of the GP

T^{GP} = the temperature of the GP.

7.3.4.2 Other Models

The ARIES code computes the thermal expansion reactivity coefficient as a sum of contributions from the fuel axial expansion, core radial expansion, and bowing effects. A Global radial expansion reactivity coefficient is utilized for the core radial expansion effect.

Two radial expansion feedback models are available in SASSYS-1: a simple model and a more detailed model.

The simple model assumes that

1. The reactivity feedback is determined solely by thermal expansions of the grid support plate and load pad region, with all regions having the same thermal expansion coefficient.

2. The displacement of the core mid-plane is sufficient to estimate the reactivity feedback from the radial core expansion.

3. All of the subassembly load pads are in contact throughout the transients.

The equations actually used in SASSYS are

$$\rho^{AX} = C_{rc} \left[\Delta T_{in} + \frac{XMC}{XAC} \left(\Delta T_{SLP} - \Delta T_{in}\right)\right] \tag{7-61}$$

where

C_{rc} = coefficient, \$/K
ΔT_{in} = changes in coolant inlet temperature
XMC = distance from nozzle support point to core mid-place
XMC = distance from nozzle support point to above ACLP
ΔT_{SLP} = changes in average structure temperature at ACLP

This model was not explicitly set up to account for subassembly bowing or flowering of the core, but the user can set arbitrary values for C_{rc} and XMC/XMC. Therefore, if the bowing reactivity effect is proportional to ΔT_{SLP} or the ΔT_{SLP} - ΔT_{ϵ}, then bowing reactivity can be accounted for by adjusting C_{rc} and XMC/XAC.

The simple model, however, does not explicitly account for subassembly bowing, and is not capable of calculating changes in core loading conditions during the course of a transient. In a more detailed model, rather than maintaining the cylindrical shape associated with a uniform core dilation, an axial profile of core radius is calculated. During a transient, the changes in the axial profile are used in conjunction with a worth curve for radial core expansion, such as the one obtained with NUBOW-3D code, to yield the reactivity feedback.

7.3.5 Control Rod Driveline Expansion Effect

Thermal expansion of the drives due to a rise in core outlet temperature will cause the control rods to be inserted further into the core, providing a negative reactivity component. On the other hand, if the control rod drives are supported on the vessel head, and if the core is supported by the vessel walls, then heating the vessel walls will either lower the core or raise the control rod drive supports, leading to a positive reactivity component. The effect of vessel expansion needs to be analyzed carefully for the KALIMER design which adopts PSDRS.

A simple one node treatment is used for calculating the temperature of the control rod drives.

$$M_{cr} C_p^{cr} \frac{dT_{cr}}{dt} = h_{cr} A_{cr} (T_{Na}^{cr} - T_{cr}) \tag{7-62}$$

where

M_{cr} = mass of the control rod drives, kg

C_p^{cr} = specific heat of the control rod drives, J/kg K

T_{cr} = control rod drive temperature, K

t = time, sec

h_{cr} = heat transfer coefficient between coolant and control rod drive, W/m^2 K

A_{cr} = heat transfer area, m^2

T_{Na}^{cr} = coolant temperature in the upper plenum region, K

In finite difference equation form, the above equation becomes

$$M_{cr} C_p^{cr} \frac{T_{cr}(t) - T_{cr}(t - \Delta t)}{\Delta t} = h_{cr} A_{cr} \{(T_{Na}^{cr}(t) - T_{cr}(t)\} \tag{7-63}$$

or

$$T_{cr}(t) = \frac{T_{cr}(t - \Delta t) + d_{cr} T_{Na}^{cr}(t)}{1 + d_{cr}} \tag{7-64}$$

where

$$d_{cr} = \frac{\Delta t \, h_{cr} A_{cr}}{M_{cr}}$$

$$Z_{cr}^{0} = Z_{cr}^{ref} \{1 + \alpha_{cr} T_B(t) + \frac{H(t) - Z_j(t)}{H(t)} T_A(t)$$

$Z_j(t)$ = penetration height into upper mixing plenum of average core exit flow, m

$H(t)$ = height of sodium in upper mixing plenum above top of core, m

$T_A(t)$ = temperature of sodium in upper mixing zone of upper outlet plenum, K

$T_B(t)$ = temperature of sodium in lower mixing zone of upper outlet plenum, K

For calculation of $T_{Na}^{cr}(t)$, two-zone mixing model of SSC-K is used during transient. However, a single-zone perfect mixing model is used at steady state, and the control rod drives and coolant in the upper plenum region are assumed to be in thermal equilibrium. That is,

$$T_{cr}(0) = T_1$$

where T_1 is the vessel sodium outlet temperature in K.

At steady state, the length of control rod drive can be calculated as

$$Z_{cr}^{0} = Z_{cr}^{ref} \{1 + \alpha_{cr}(T_{cr}(0)) * (T_{cr}(0) - T_{cr}^{ref})\} \quad (7\text{-}65)$$

where

Z_{cr}^{0} = steady state length of control rod drive immersed in sodium, m

Z_{cr}^{ref} = reference length of control rod drive immersed in sodium, m

≈ reference height of sodium in upper mixing plenum above top of core, m

α_{cr} = linear coefficient of thermal expansion for control rod drive, m/m K

T_{cr}^{ref} = reference control rod drive temperature, K

Expansion of the control rod drive from the steady state length can be expressed as

$$\Delta Z_{cr} = Z_{cr}^{0} * \alpha_{cr}(T_{cr}(t)) * \{(T_{cr}(t) - T_{cr}^{0}\} \quad (7\text{-}66)$$

For vessel expansion,

$$M_{vs} C_p^{vs} \frac{dT_{vs}}{dt} = h_{vs} A_{vs} (T_{Na}^{vs} - T_{vs}) \quad (7\text{-}67)$$

where

M_{vs} = mass of the reactor vessel, kg

C_p^{vs} = specific heat of the reactor vessel, J/kg K

T_{vs} = temperature of the reactor vessel, K

t = time, sec

h_{vs} = heat transfer coefficient between the coolant and the reactor vessel, W/m^{2}K

A_{vs} = heat transfer area, m^2

T_{Na}^{vs} = coolant temperature adjacent to the reactor vessel, K

Above equation can be solved for the reactor vessel temperature T_{vs} as

$$T_{vs}(t) = \frac{T_{vs}(t-\Delta t) + d_{vs} T_{Na}^{vs}(t)}{1+d_{vs}} \tag{7-68}$$

where

$$d_{vs} = \frac{\Delta t\, h_{vs} A_{vs}}{M_{vs} C_p^{vs}}$$

$T_{Na}^{vs}(t) \simeq T_{BPM}(t)$

= mean coolant temperature in upper region of bypass, K

$T_{vs}(0) = T_{Na}^{vs}(0)$

The vessel height at steady state can be calculated as

$$Z_{vs}^0 = Z_{vs}^{ref} \{1 + \alpha_{vs}(T_{vs}(0))\,(T_{vs}(0) - T_{vs}^{ref})\} \tag{7-69}$$

where

Z_{vs}^0 = reactor vessel height at steady state, m

Z_{vs}^{ref} = reference vessel height, m

≈ reference sodium level from bottom of reactor vessel, m

α_{vs} = linear coefficient of thermal expansion for reactor vessel, m/m K

T_{vs}^{ref} = reference reactor vessel temperature, K

Expansion of the reactor vessel from the steady state height can be expressed as

$$\Delta Z_{vs} = Z_{vs}^{0} * \alpha_{vs}(T_{vs}(t) * \{T_{vs}(t) - T_{vs}^{0}\} \quad (7\text{-}70)$$

Thus the effective control rod driveline expansion can be calculated as

$$\Delta Z = \Delta Z_{cr} - \Delta Z_{vs} \quad (7\text{-}71)$$

Reactivity for control rod driveline expansion is calculated as

$$\rho^{CR} = C^{CR} \Delta Z \quad (7\text{-}72)$$

where C^{CR} is the user-supplied coefficient for control rod driveline expansion in $\Delta k/k$ per m.

Control rod driveline expansion model of the SASSYS-1 code is similar to the one described above.

7.4 Input Requirements for Reactivity Feedback Models

For the generation of the reactivity coefficients by the core design group of the KALIMER design team, descriptions of each model with the definition of the reactivity coefficient are summarized below. Discussions with the core design group for the SSC-K reactivity feedback models will be based on the following descriptions which will be included in the Design Data Request for the Safety Analysis.

7.4.1 Doppler Effect

Reactivity coefficients need to be provided for one of the models described below or for any other model suggested by the core design.

Model 1

$$K\rho^{DOP} = \sum_{JK} \rho_{JK}^{DOP} = 2\sum_{JK} \alpha_{JK}^{DOP} \left(\frac{1}{\sqrt{T_{0JK}}} - \frac{1}{\sqrt{T_{JK}}}\right) \quad (7\text{-}73)$$

$$\alpha_{JK}^{DOP} = \beta_{JK}^{DOP}(1 - X_{JK}^{Na}) + \Omega_{JK}^{DOP} X_{JK}^{Na} \quad (7\text{-}74)$$

where

K = index of the fuel channel

J = index of the axial level along the fuel channel

T_{0JK} = the initial steady state fuel temperature at position JK

T_{JK} = the effective local temperature at position JK

X_{JK}^{Na} = an effective isothermal sodium void fraction

Input Requirements:

β_{JK}^{DOP} = Doppler coefficient with Na present for node JK, $\Delta k / k$

Ω_{JK}^{DOP} = Doppler coefficient without Na present for node JK, $\Delta k / k$

Typically, twelve axial nodes are used for the entire length of the fuel rod: two for lower blanket or shielding, six for active fuel, and four for upper gas plenum.

Model 2

$$\rho^{DOP} = \sum_{JK} \rho_{JK}^{DOP} = \sum_{JK} \alpha_{JK}^{DOP} \ln \left(\frac{T_{JK}}{T_{0JK}}\right) \tag{7-75}$$

$$\rho^{DOP} = \beta_{JK}^{DOP}(1 - X_{JK}^{Na}) + \Omega_{JK}^{DOP} X_{JK}^{Na} \tag{7-76}$$

Input Requirements:

β_{JK}^{DOP} = Doppler coefficient with Na present for node JK, $\Delta k / k$

Ω_{JK}^{DOP} = Doppler coefficient without Na present for node JK, $\Delta k / k$

Model 3

$$\begin{aligned} \rho^{DOP} &= \sum_{JK} \rho_{JK}^{DOP} \\ &= \sum_{JK} W_{JK} \frac{m_f^{JK}}{m_{f0}^{JK}} \{\Omega_K^{DOP} + (\beta_K^{DOP} - \Omega_K^{DOP}) \frac{\bar{\rho}_{JK}}{\bar{\rho}_{JK0}}\} \ln\left(\frac{T_{JK}}{T_{JK0}}\right) \end{aligned} \tag{7-77}$$

where

m_f^{JK} = fuel mass of the node JK

m_{f0}^{JK} = initial steady-state mass of fuel in the node *JK*

$\overline{\rho_{JK}}$ = average density of sodium in the node *JK*

$\overline{\rho_{JK0}}$ = initial steady-state density of sodium in the node *JK*

T_{JK} = average temperature of fuel in the node *JK*

T_{JK0} = initial steady-state temperature of fuel in the node *JK*

Input Requirements:

W_{JK} = Doppler weighting factor for node JK, normalized for each channel

β_{JK}^{DOP} = Doppler coefficient for channel K with all sodium present

Ω_{JK}^{DOP} = Doppler coefficient for channel K with no sodium present

7.4.2 Sodium Density Effect

Reactivity coefficients need to be provided for one of the models described below or for any other model suggested by the core design.

Model 1

$$\rho^{Na} = \sum_{JK} \beta_{JK} M_{JK} \tag{7-78}$$

where M_{JK} is the effective mass of sodium voided in the segment JK.

Input Requirements:

β_{JK} = sodium void reactivity coefficient for axial slice J of channel

Model 2

$$\rho^{Na} = \sum_{JK} \beta_{JK} * (T_{JK}^{Na} - T_{0JK}^{Na}) \tag{7-79}$$

Input Requirements:

β_{JK} = sodium void reactivity coefficient for the axial slice J of channel K, $\Delta k / k$ / K

Model 3

$$\rho^{Na} = \sum_{JK} \alpha^{Na} \beta_{JK} * (T_{JK}^{Na} - T_{0JK}^{Na}) \quad (7\text{-}80)$$

Input Requirements:

α^{Na} = sodium volumetric expansion coefficient in ^{o}F-1

β_{JK} = sodium void reactivity coefficient for the node JK in $\Delta k / k$

7.4.3 Axial Expansion Effect

Reactivity coefficients need to be provided for one of the models described below or for any other model suggested by the core design.

Model 1

$$\rho^{AX} = e \sum_{JK} C_{JK} N_{JK} \quad (7\text{-}81)$$

where N_{JK} is the mass of fuel voided from segment JK.

Input Requirements:

e = a user-supplied constant that accounts for the uncertainties associated with the mode of fuel expansion

C_{JK} = fuel reactivity worth in axial slice, J, channel K, in $\Delta k/k$ per unit mass fuel effectively voided from segment JK

Model 2

$$\rho^{AX} = \sum_K \rho_K^{AX} = \sum_K \alpha_K^{AX} \ln\left(\frac{Z_K}{Z_{0k}}\right) \tag{7-82}$$

where

z_K = the elongated axial fuel length of channel K

z_{0k} = the axial fuel length of channel K at reference temperature T_0

Input Requirements:

α_K^{AX} = an axial expansion reactivity coefficient for channel K in units of Δk

Model 3

$$\rho^{AX} = \sum_{JK}[\alpha^C \rho_{JK}^C (T^{Na}{}_{JK} - T^{Na}{}_{0JK}) + \alpha^F \rho_{JK}^F (T^F{}_{JK} - T^F{}_{0JK})] \tag{7-83}$$

Input Requirements:

α^C = the cladding linear expansion coefficient in K^{-1}

α^F = the fuel linear expansion coefficient in K^{-1}

ρ_{JK}^C = the cladding axial expansion reactivity coefficient in Δk

ρ_{JK}^F = the fuel axial expansion reactivity coefficient in Δk

7.4.4 Radial Expansion Effect

Reactivity coefficients need to be provided for one of the models described below or for any other model suggested by the core design.

Model 1

$$\rho^R = \alpha^R \ln (1 + W_{LP}\, \xi_{LP} + W_{GP}\, \xi_{GP}) \tag{7-84}$$

where ξ_{LP} and ξ_{GP} are the strains of Above Core Load Pad (ACLP) and Grid Plate (GP), respectively.

Input Requirements:

α^R = the radial expansion reactivity coefficient in units of Δk
W_{LP} = geometrical weighting factor for the ACLP
W_{GP} = geometrical weighting factor for the GP

Model 2

$$\rho^{AX} = C_{rc}[\Delta T_{in} + \frac{XMC}{XAC}(\Delta T_{SLP} - \Delta T_{in})] \quad (7\text{-}85)$$

where

ΔT_{in} = changes in coolant inlet temperature
XMC = distance from GP to core mid-place
XAC = distance from GP to ACLP
ΔT_{SLP} = changes in average structure temperature at ACLP

Input Requirements:

C_{rc} = the radial expansion reactivity coefficient, \$/K

7.4.5 Control Rod Driveline Expansion Effect

Reactivity coefficients need to be provided for the model described below or for any other model suggested by the core design.

$$\rho^{CR} = C^{CR}(\Delta Z_{cr} - \Delta Z_{vs}) \quad (7\text{-}86)$$

where ΔZ_{cr} and ΔZ_{vs} are the changes in CRDL and reactor vessel height, respectively.

Input Requirements:

C^{CR} = CRDL expansion reactivity coefficient in $\Delta k/k$ per m

7.5 Flowcharts

Figure 7.9 shows the modularized structure of the reactivity feedback subroutines of SSC-K. Each box contains subroutine names, which are underlined, and a brief description of their functions. All subroutines shown in the figure are implemented into the SSC-K code except for GEM5T which will be developed for the analysis of gas expansion modules in the core.

7.6 GEM Model

Gas Expansion Modules (GEMs) are added to KALIMER core in order to supplement the negative reactivity feedback that develops once the primary pump has been tripped. When the pumps trip and the pressure drops, the sodium within the GEMs at the active core elevation is displaced by Helium gas, thus increasing the leakage of neutrons from the core and subtracting about [TBD] cents of reactivity, assuming all 6 GEMs function properly.

The GEM is essentially an empty hexagonal cross section duct, sealed at the top, open at the bottom and connected to the high pressure in the inlet plenum of the core as shown in Fig. 7.7. When the pumps are at full flow, the plenum pressure compresses the gas in the GEM cavity. When the flow decreases, the trapped Helium expands and drops the sodium level into the core region. As a result, fewer neutrons are scattered back into the core region. The reactivity effect increases as the gas expands into the core and remains constant once the gas liquid interface drops below the core region.

The objective of this study is to develop a simple model for the analysis of the reactivity effects introduced by the GEM, and to identify the areas of further improvement.

7.6.1 Current GEM Model

In order to calculate the sodium level in the GEM, the following equations are solved. As shown in Fig. 7.8, the total length of GEM is occupied by the Helium gas and primary sodium as

$$h_g + h_l = h_t \tag{7-87}$$

where

h_g = axial length of Helium gas in GEM, m

h_l = axial length of sodium in GEM, m

h_t = total axial length of GEM, m

Since there is no sodium flow through the GEM, the pressure of sodium at the core inlet plenum can be expressed as

$$P_g + \rho g h_l = P_i \tag{7-88}$$

where

P_g = GEM gas pressure, Pa

P_i = pressure of sodium at core inlet plenum, Pa
= (pressure of sodium at bottom of core)
– (gravitational pressure drop along the orifice inlet zone)

ρ = average density of sodium in GEM, kg/m^3

g = gravity, m/s^2

The equation of state for ideal gas is applied for the Helium gas in the GEM as

$$P_g\ A\ h_g = \left(\frac{M_g}{W_g}\right) R\ T_g \tag{7-89}$$

where

A = cross sectional area of GEM, m^2

M_g = mass of Helium gas in GEM, kg

W_g = melecular weight of Helium gas, kg/mole

R = universal gas constant, J/K mole

T_g = temperature of Helium gas in GEM, K

Unknowns in the Eqs. (7-87) to (7-89) are h_g, h_l, and P_g.

The average density of sodium in GEM, ρ, is assumed to be the density corresponding to the average temperature of sodium in adjacent subassemblies.

The gas temperature, T_g, closely follows the GEM duct temperature which is determined by considering the heat transfer between the neighboring subassemblies and the GEM. For simplicity, the gas temperature is assumed to be the average of the temperatures of duct walls of adjacent subassemblies.

Equations (7-87) to (7-89) can be rearranged to give a quadratic equation for the axial length of Helium gas in GEM, h_g, which is calculated at each time step. The worth of the GEMs when the sodium level is equal to, or greater than, the top of the core is zero. When the level reaches the bottom of the core, the maximum worth of GEM is inserted. Intermediate values of reactivity are interpolated linearly from the sodium level in the GEMs.

Subroutine GEM5T of SSC-K code has been developed to calculate the level of sodium inside GEM and the negative reactivity inserted. GEM5T is called by REAC5T which drives the overall reactivity calculations.

7.6.2 GEM Model Improvement

A GEM model, which will be used for the analysis of LOF accident, has been developed for SSC-K code, and reasonable results have been obtained through test runs. Due to the lack of detailed design data, including dimensions, sodium levels at various operating regimes, mass of Helium gas inside GEM, and GEM reactivity worth as a function of sodium level, a simplified model was developed first in order to study the effectiveness of GEM under LOF accident conditions.

Following are the items which need further work for the current GEM model:

- Currently the sodium density inside the GEM is assumed to be the axial average of the neighboring channels. Sensitivity study is needed to investigate the effect of sodium density on the sodium level. If needed, the GEM model will be modified so that the axial sodium density is calculated considering inter-assembly heat transfer.

- The temperature of the GEM gas is assumed to the average of the structural temperature of neighboring channels. Improvement of the current GEM model can be achieved by calculating the GEM gas temperature as

$$c_p \, M_g \frac{dT_g}{dt} = Q \qquad (7\text{-}90)$$

where

c_p = Specific heat of GEM gas, J/kg*K

Q = Heat from conduction from neighboring channels, watts

- In addition to the model improvement described above, more detailed design data are essential for the analysis of GEM effect.
  - GEM worth curve : sodium level vs reactivity
  - Sodium level at various operating regimes
  - Mass of GEM gas

- The effect of primary pump coastdown can be investigated and generate the requirements for the coastdown.

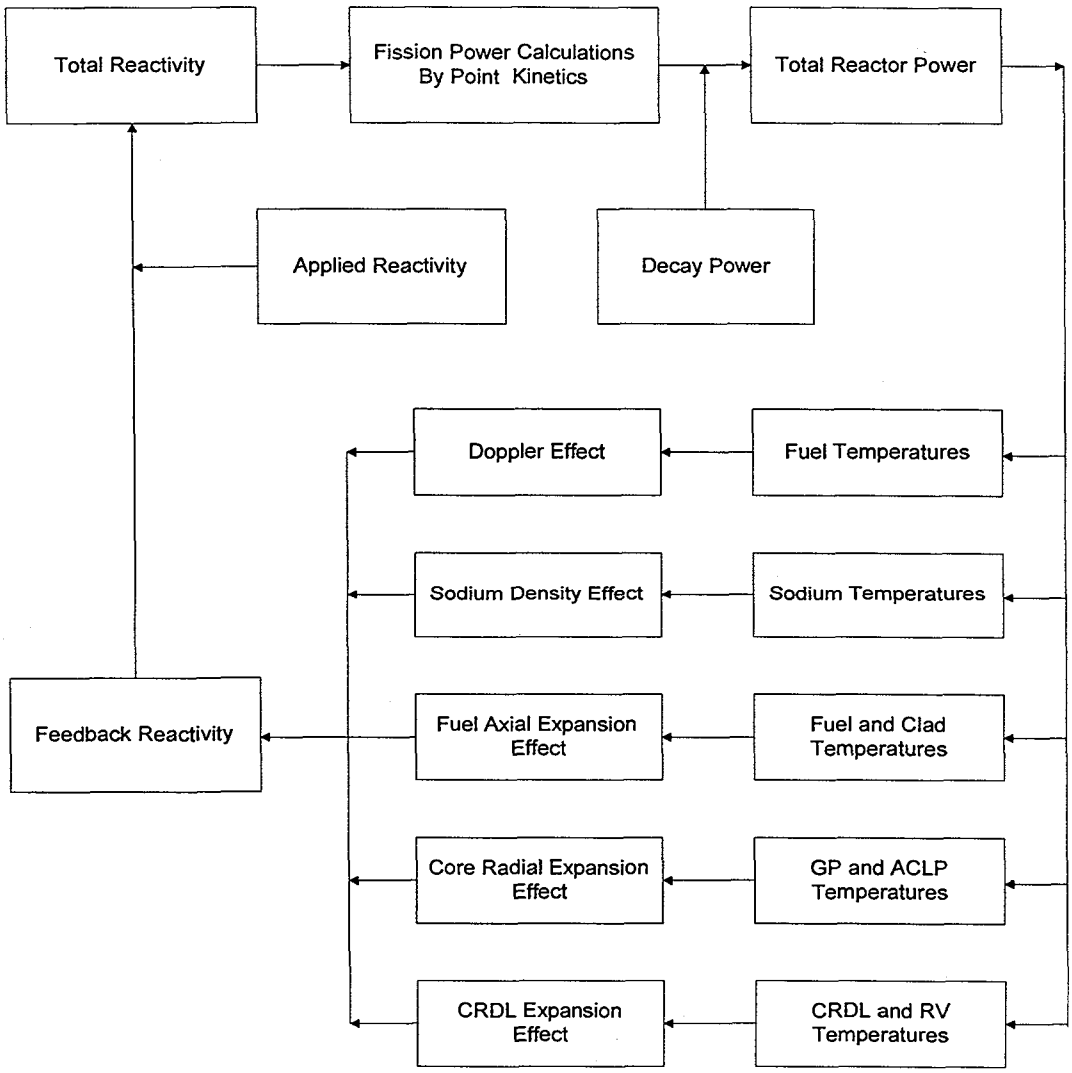

Fig. 7.1 Overall Scheme for Calculating Total Reactor Core Power

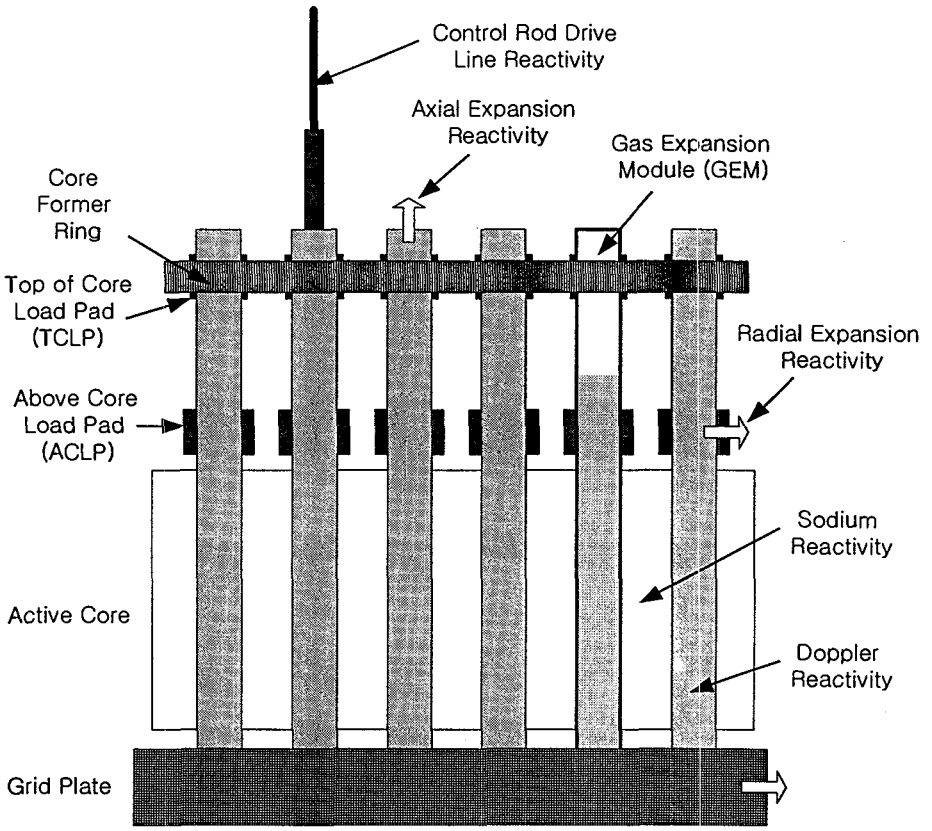

Fig. 7.2 Components of Reactivity Feedback Effect

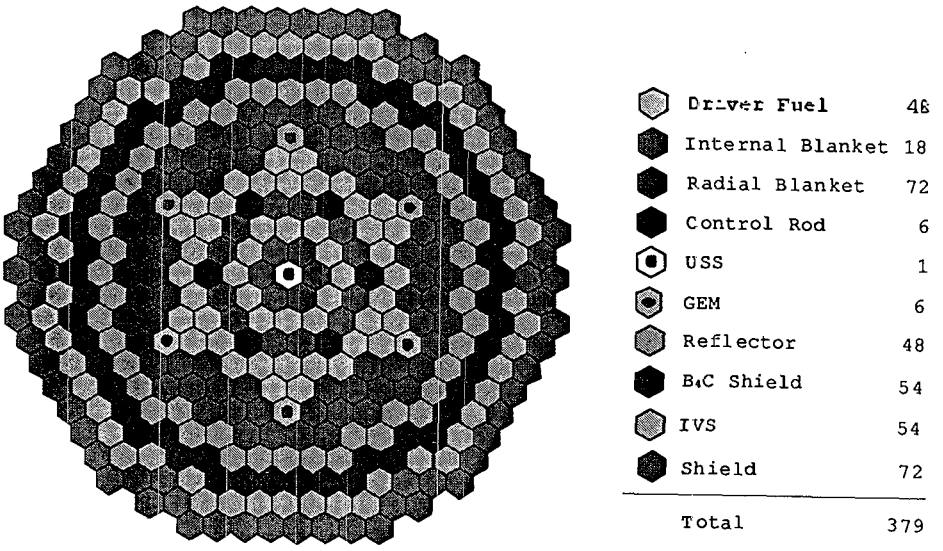

Fig. 7.3 Schematic of Core Layout for Reactivity Model Development

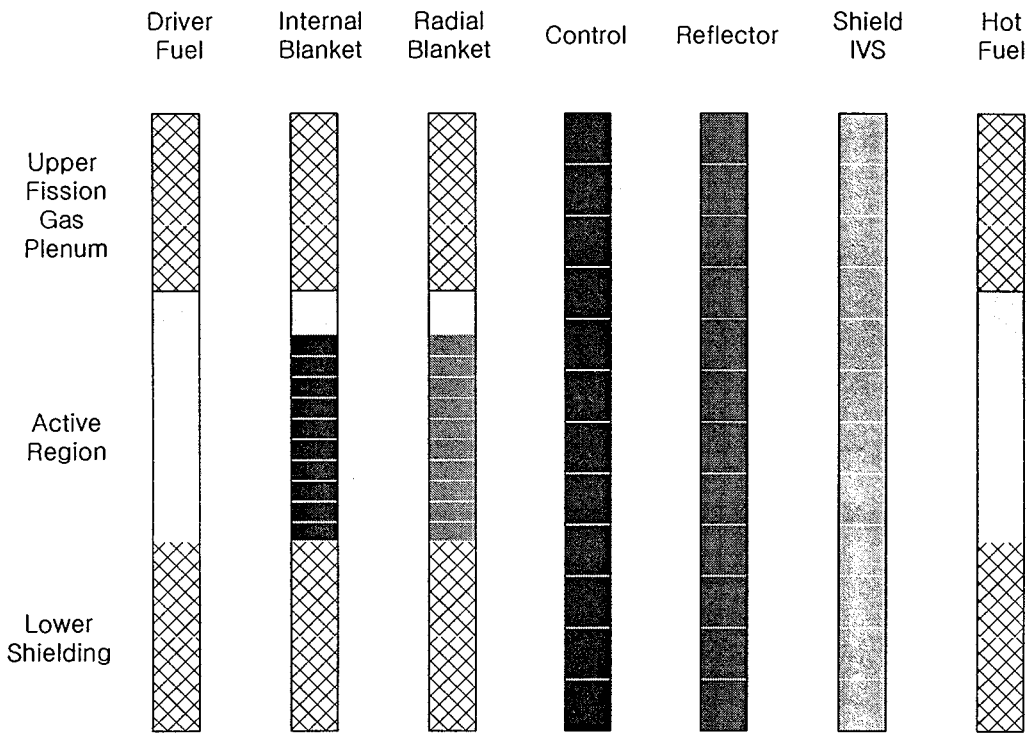

Fig. 7.4 SSC-K Representation of Core Subassemblies

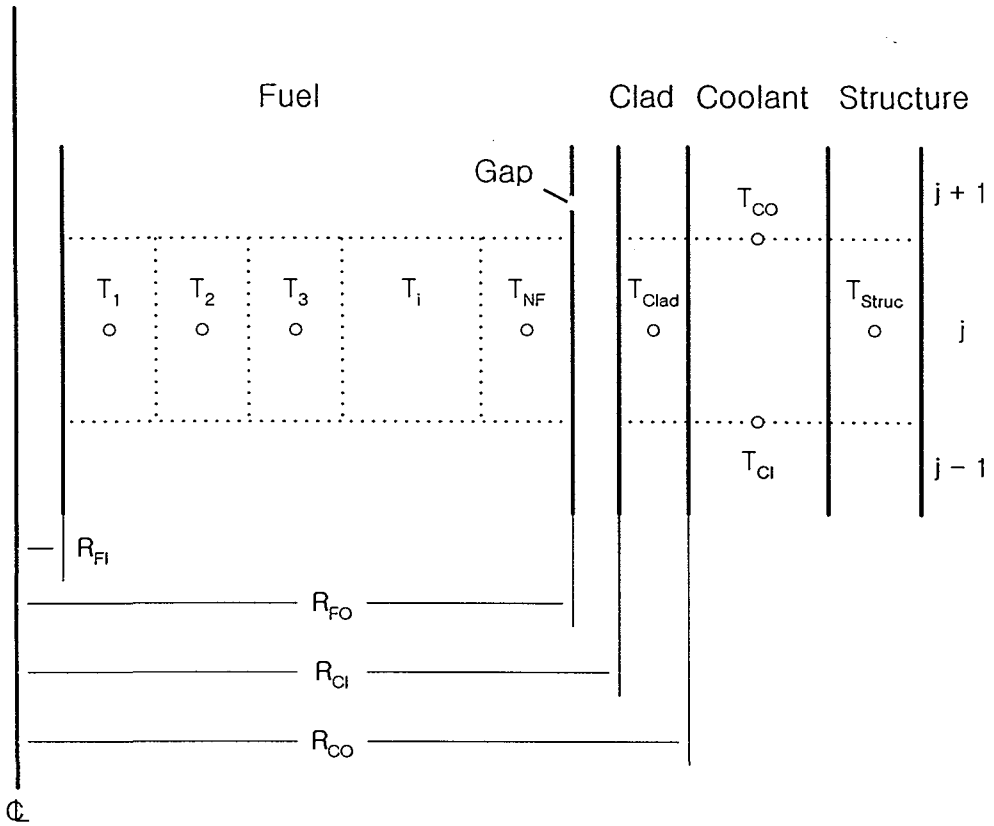

Fig. 7.5 SSC-K Representation of Fuel Rod

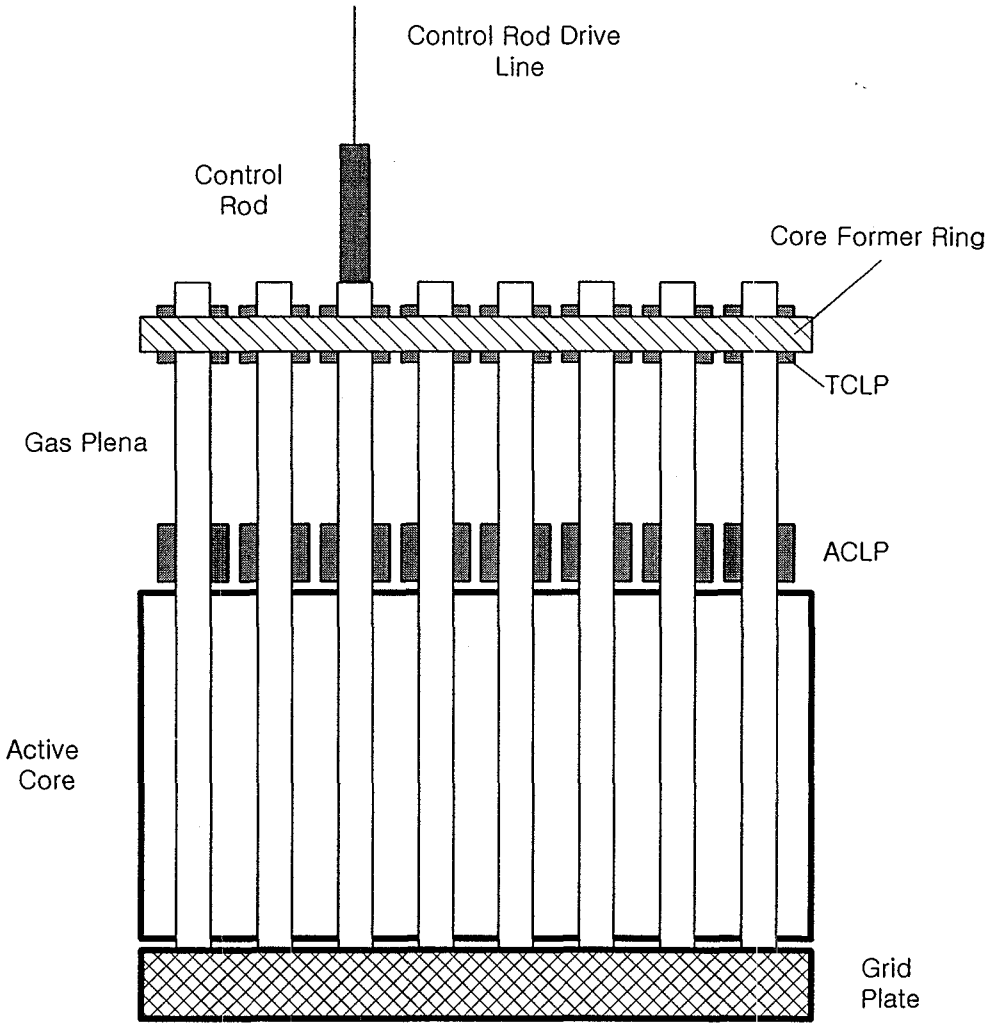

Fig. 7.6 Typical Core Restarint System

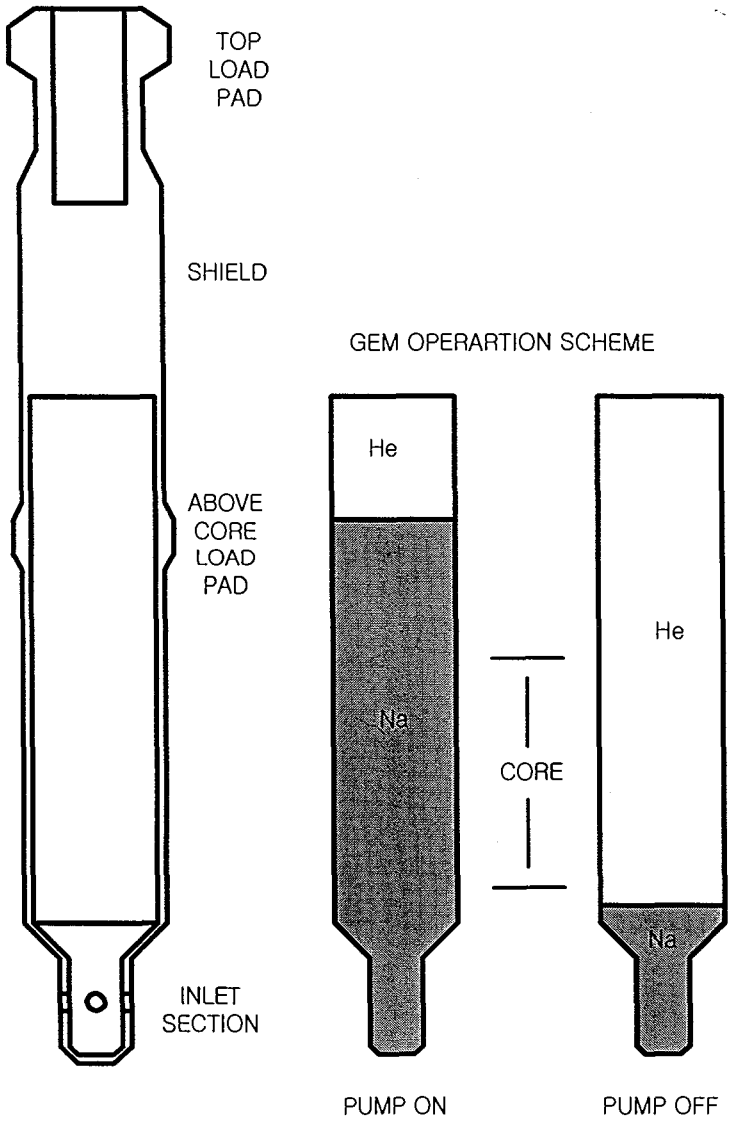

Fig. 7.7 GEM Operation Scheme

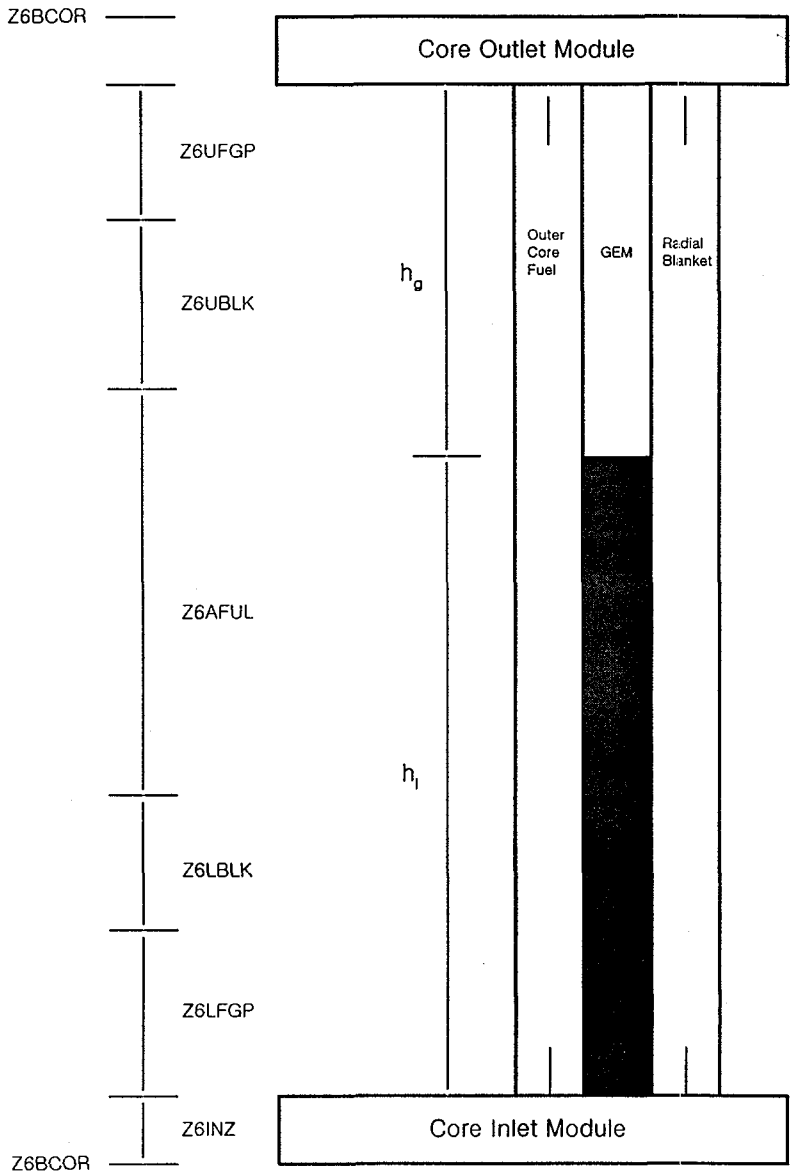

Fig. 7.8 Schematic for GEM Model Development

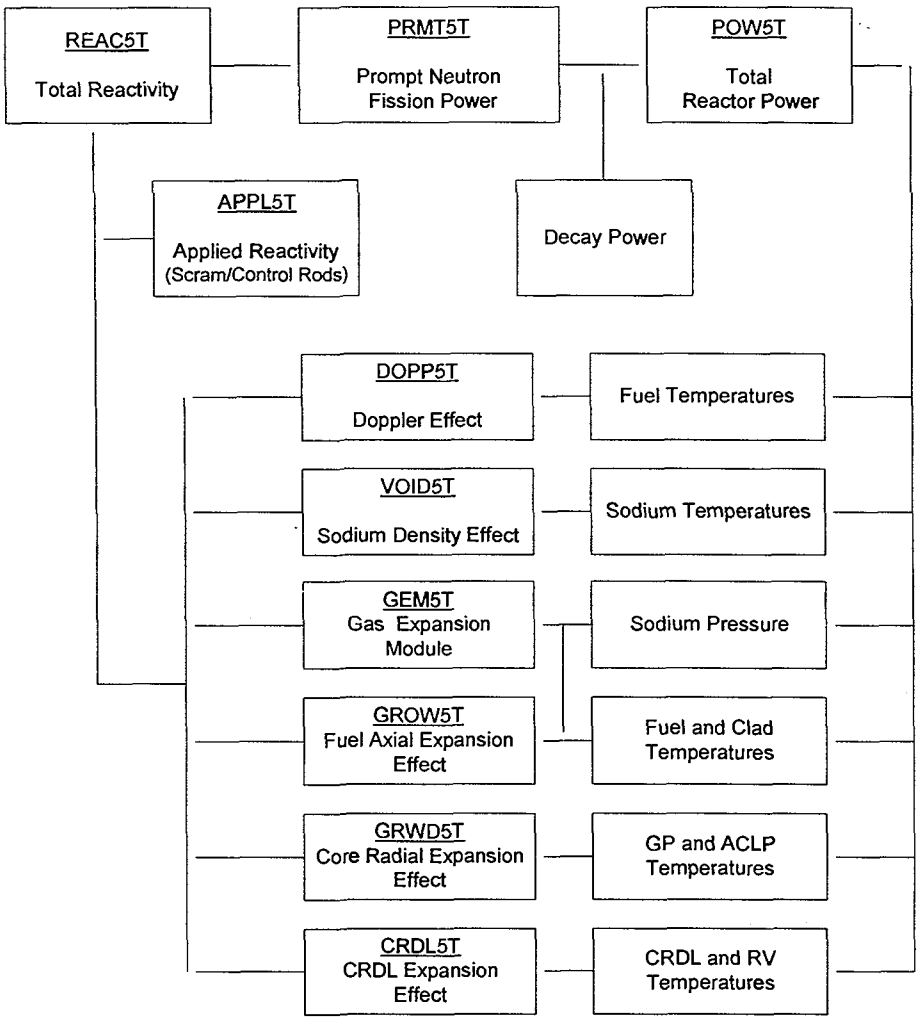

Fig. 7.9 Flow Diagram of Reactivity Feedback Calculation for SSC-K

8. CONSTITUTIVE LAWS AND CORRELATIONS

A number of constitutive laws and correlations are required in order to execute the SSC code. T collection or part of these data may be overwritten by the user. This section describes collections of data that have he approach taken is based on providing the best available data into the code. The entire been incorporated so far. All of the correlations and numerical values used are in SI units.

8.1 Constitutive Laws

The required thermo-physical and transport properties for all of the materials of interest are provided for in the form of correlations. Reasonable values for the coefficients in these correlations are provided in SI units. These values may be changed by the user through input cards. Various constitutive laws are grouped according to materials.

8.1.1 SSC-L Properties

8.1.1.1 Core and Blanket Fuel

Thermal Conductivity (W/m K)

The thermal conductivity of mixed oxide [8-1] core (UO_2-20 w/o Puo_2) and blanket (oxide) materials is given by the following relation:

$$K(T,P) = \frac{k_0(1-P)}{1+(k_4+k_3P)P}\frac{1}{k_1+k_2T} + k_3T^3 \qquad (8\text{-}1)$$

Where typical values for k_0, k_1, k_2, k_3, k_4 and k_5 are noted in Table 8-1, and P is the fractional porosity (= 1- fractional density).

Specific Heat Capacity (J/ kg K)

The specific heat capacity of mixed-oxide [8-2] core and blanket materials is given by the following relations:

$$c_p(T) = c_0\left[1 + c_1T + c_2T^2 + c_3T^3 + \frac{c_6}{T^2}\right] \qquad \text{for } T < T_1 \qquad (8\text{-}2)$$

$$c_p(T) = c_p(T_1) + \frac{c_p(T_2) - c_p(T_1)}{T_2 - T_1}(T - T_1) \qquad \text{for } T_1 < T \le T_2 \qquad (8\text{-}3)$$

$$c_p(T) = c_4 + c_5T \qquad \text{for } T > T_2 \qquad (8\text{-}4)$$

where values of various parameters are noted in Table 8-1, and

$$c_p(T_1) = c_0\left[1 + c_1T_1 + c_2T_1^2 + c_3T_1^3\right] \qquad (8\text{-}5)$$

and

$$c_p(T_2) = c_4 + c_5T_2 \qquad (8\text{-}6)$$

Table 8-1

Parameters on Fuel Thermal Conductivity and Specific Heat Correlations

Parameter	Fuel material	Blanket material
k_0	113.3	113.3
k_1	0.78	0.78
k_2	0.02935	0.02935
k3	$6.600*10^{-13}$	$6.60*10^{-13}$
k4	1	1
k5	10	10
P	input	input
C_0	194.319	194.319
C_1	$1.3557*10^{-3}$	$1.3557*10^{-3}$
C_2	$-9.3301*10^{-7}$	$-9.3301*10^{-7}$
C_3	$2.4482*10^{-10}$	$2.4482*10^{-10}$
C_4	502.951	502.951
C_5	0	0
C_6	0	0
T_1	3020.0	3020.0
T_2	3060.0	3060.0

Coefficient of Thermal Expansion (m/m K)

The average linear coefficient if thermal expansion from T_0 to T for core and blanket materials is represented by the following equation [8-3, 8-4]:

$$\bar{\alpha}(T) = \alpha_0 + \alpha_1 T \qquad \text{for} \quad T \le T_3 \tag{8-7}$$

For higher temperatures, the average liner coefficient of thermal expansion is given by the following relation:

$$\bar{\alpha}(T) = \alpha_2 \qquad \text{for} \quad T \ge T_4 \tag{8-8}$$

For intermediate temperatures,

$$\bar{\alpha}(T) = \bar{\alpha}(T_3) + \left[\frac{\bar{\alpha}(T_4) - \bar{\alpha}(T_3)}{T_4 - T_3}\right](T - T_3) \qquad \text{for} \quad T_3 < T < T_4 \tag{8-9}$$

where

$$\bar{\alpha}(T_3) = \alpha_0 + \alpha_1 T_3 \tag{8-10}$$

$$\bar{\alpha}(T_4) = \alpha_2 \tag{8-11}$$

and other parameters are noted in Table 8-2

Density (kg/m^3)

The core and blanket fuel materials density is given by the following set of correlations:

$$\rho(T,P) = \frac{\rho_0(1-P)}{\left[1 + \bar{\alpha}(T)(T - T_0)\right]^3} \qquad \text{for} \quad T_0 \le T \le T_3 \tag{8-12}$$

$$\rho(T,P) = \rho(T_3,P) + \frac{\rho(T_4,P) - \rho(T_3,P)}{T_4 - T_3}(T - T_3) \qquad \text{for } T_3 < T \le T_4 \qquad (8\text{-}13)$$

$$\rho(T,P) = \frac{\rho_1}{\left[1 + \bar{\alpha}(T)(T - T_4)\right]^3} \qquad \text{for } T > T_4 \qquad (8\text{-}14)$$

where P is the fractional porosity. The above correlations imply that (a) the core fuel density for different restructured regions have the same temperature dependence below fuel solidus temperature (T_3), and (b) the molten fuel density, i.e., density beyond its liquids temperature (T_4), does not depend upon its pre-molten fractional density. The following two equations are noted for the sake of clarity:

$$\rho(T_3,P) = \frac{\rho_0(1-P)}{\left[1 + \bar{\alpha}(T_3)(T_3 - T_0)\right]^3} \qquad (8\text{-}15)$$

$$\rho(T_4,P) = \rho_1 \qquad (8\text{-}16)$$

The average linear coefficient of thermal expansion is already noted above; other parameters are noted in Table 8-2.

Table 8-2

Parameters in Fuel Coefficient of Thermal Expansion, Density and Emissivity Correlations

parameter	Fuel material	Blanket material
α_0	$5.706*10^{-6}$	$5.7506*10^{-6}$
α_1	$2.997*10^{-9}$	$2.997*10^{-9}$
α_2	$3.1*10^{-5}$	$3.1*10^{-5}$
T_0	295.4	295.4
T_3	3020.0	3020.0
T_4	3060.0	3060.0
ρ_0	$11.04*10^3$	$10.0*10^3$
ρ_1	$8.733*10^3$	$8.744*10^3$
P	input	input
e_0	0.75	0.75
e_1	$5*10^{-5}$	$5*10^{-5}$
T_5	400.0	400.0

Emissivity (Dimensionless)

The core and blanket material emissivity [8-5] is given by the following correlations:

$$e = e_0 \qquad \text{for} \quad T \le T_5 \tag{8-17}$$

and

$$e = e_0 + e_1 (T - T_5) \qquad \text{for} \quad T > T_5 \tag{8-18}$$

where e_0, e_1 and T_5 are given in Table 8-2 .

8.1.1.2 Cladding and Structural Materials

For stainless steel, the default material for cladding and structure, the thermal conductivity (W/m-k) [8-6], specific heat (J/kg K) [8-6], and the average linear coefficient of thermal expansion (m/m-K) [8-7], are represented by polynomial fits of data. These equations, for temperatures up to melting point, are given by the following:

$$k(T) = k_0 + k_1 T + k_2 T^2 + k_3 T^3 \tag{8-19}$$

$$c_p(T) = c_0 + c_1 T + c_2 T^2 + c_3 T^3 \quad \text{and} \tag{8-20}$$

$$\alpha(T) = \alpha_0 + \alpha_1 T + \alpha_2 T^2 \tag{8-21}$$

where values for various parameters for both cladding and structural materials are noted in Table 8-3. The structural or cladding material density is related to the average thermal coefficient of linear expansion as follows:

$$\frac{\rho(T)}{\rho_0} = \frac{1}{\left[1 + a(T)(T - T_0)\right]^3} \tag{8-22}$$

where ρ_0 is the density at temperature T_0 .

The cladding and structural emissivity [8-8] are given by the following relations:

$$e = e_0 \qquad \text{for } T \le T_1 \tag{8-23}$$

and

$$e = e_0 + e_1(T - T_1) \qquad \text{for } T > T_1 \tag{8-24}$$

where values for e_0, e_1 and T_1 are also noted in Table 8-3 .

Table 8-3
Parameters for Cladding and Structural Material Properties

Parameter	Cladding material	Structural material
K_0	9.01748	9.01748
K_1	$1.62997*10^{-2}$	$1.62997*10^{-2}$
K_2	$-4.80329*10^{-6}$	$-4.80329*10^{-6}$
K_3	$2.18422*10^{-9}$	$2.18422*10^{-9}$
C_0	380.962	380.962
C_1	0.535104	0.535104
C_2	$-6.10413*10^{-4}$	$-6.10413*10^{-4}$
C_3	$3.02469*10^{-7}$	$3.02469*10^{-7}$
P_0	8127.87	8127.87
a_c	$1.7887*10^{-5}$	$1.7887*10^{-5}$
a_1	$2.3977*10^{-9}$	$2.3977*10^{-9}$
a_2	$3.2692*10^{-13}$	$3.2692*10^{-13}$
T_0	298.15	298.15
e_0	0.55	0.55
e_1	$2.5*10^{-4}$	$2.5*10^{-4}$
T_1	400	400

8.1.2 Constitutive Laws for SSC-K

8.1.2.1 Metal Fuel Properties

Original SSC-L code has a collection of thermo-physical and transport properties for

selected materials, however, additional properties are necessary for materials which will be used for KALIMER design. Table shows properties which are provided in the SSC-K code:
E denotes properties which are in the original code, and N denotes newly added properties.

	UO_2-20 w/o PuO_2	U-Zr-Pu	Stainless steel	HT9	Modified Subroutines
K, W/m K	E	N	E	N	gama5s, gama5t stem5s
C_p, J/kg K	E	N	E		prop5t
α, m/m K	E	N	E	N	alfa5s, prop5t
ρ, kg/m^3	E	N	E	N	prop5t
E	E		E		

Detailed description of changes is summarized below:

- Equations with fixed coefficients are inserted in the subroutines, and input parameters are dummies.
- For general material types, input requirements and block data need to be modified.

Thermal Conductivity

Material (ID)	Input		Thermal Conductivity		Changes
	Parameter	Subroutine	Parameter	Subroutine	
Blanket (40-49)	C4K0 ~ C4K → C5KF	CALC7R	COND5K	GAMA5S GAMA5T STEM5S	MOX → U-Pu-Z
Fuel (50-59)	C5K0 ~ C5K → C5KF	〃	COND5K	GAMA5S GAMA5T STEM5S	MOX → U-Pu-Z
Clad (60-69)	C6K0 ~ C6K → C6KF	〃	COND6K	GAMA5S GAMA5T STEM5S	SS → HT9
Structure (70-79)	C7K0 ~ C7K → C7KF	〃	COND7K	GAMA5T STEM5S	SS → HT9

Specific Heat Capacity

Material (ID)	Input		Specific heat		Changes
	Parameter	Subroutine	Parameter	Subroutine	
Blanket (40-49)	C4C0 C4CT2 → C5CF	CALC7R	HCAP5C	PROP5T	MOX → U-Pu-Z
Fuel (50-59)	C5C0 C5CT2 → C5CF	〃	HCAP5C	PROP5T	MOX → U-Pu-Z
Clad (60-69)	C6C0 ~ C6C → C6CF	〃	HCAP6C	PROP5T	(SS → HT9)
Structure (70-79)	C7C0 ~ C7C → C7CF	〃	HCAP7C	PROP5T	(SS → HT9)

Thermal Expansion Coefficient

Material (ID)	Input		Thermal expansion coefficien		Changes
	Parameter	Subroutine	Parameter	Subroutine	
Blanket (40-49)	C4A0 C4AT2 → C5AF	CALC7R	ALFA5A	ALFA5S PROP5T GROW5T	MOX → U-Pu-Z
Fuel (50-59)	C5A0 C5AT2 → C5AF	〃	ALFA5A	ALFA5S PROP5T GROW5T	MOX → U-Pu-Z
Clad (60-69)	C6A0 C6AT1 → C6AF	〃	ALFA6A	ALFA5S PROP5T GROW5T	SS → HT9
Structure (70-79)	C7A0 ~ C7A → C7AF	〃	ALFA7A	ALFA5S PROP5T	SS → HT9

- Note that functions TEXFUEL and TEXCLAD, which were used in subroutine GROW5T for fuel rod expansion, have been replaced by the relations given in subroutines ALFA5S and PROP5T.

Density

Material (ID)	Input		Thermal expansion coefficien		Changes
	Parameter	Subroutine	Parameter	Subroutine	
Blanket (40-49)	C4D0 ~ C4D → C5DF	CALC7R	DENS5D	PROP5T	MOX → U-Pu-Z
Fuel (50-59)	C5D0 ~ C5D → C5DF	"	DENS5D	PROP5T	MOX → U-Pu-Z
Clad (60-69)	C6D0 C6DF	"	DENS6D	PROP5T	SS → HT9
Structure (70-79)	C7DT0 C7D0 → C7DF	"	DENS7D	PROP5T	SS → HT9

Thermal Conductivity of U-Zr-Pu Alloys (Unirradiated) [8-9]

$$k_0 = A + BT + CT^2 \tag{8-25}$$

where

k_0 = thermal conductivity, W/m K

$$A = 17.5\left[\frac{1-2.23W_z}{1+1.61W_z} - 2.62W_p\right] \tag{8-26}$$

$$B = 1.54\times10^{-2}\left[\frac{1+0.061W_z}{1+1.61W_z} + 0.90W_p\right] \tag{8-27}$$

$$C = 9.38\times10^{-6}\left(1-2.70W_p\right) \tag{8-28}$$

W_z = Zr weight fraction

W_p = Pu weight fraction

and

T = temperature, K

For design calculations, an uncertainty of 20% is recommended.

Thermal Conductivity of U-Zr-Pu Alloys (Irradiated) [8-9]

$$f_p = \frac{k}{k_0} = \frac{(1-P)}{(1+\beta P)} \tag{8-29}$$

where P = porosity fraction referenced to initial fuel volume and β=1.7

The minimum value of f_p is taken as 0.5 ± 0.1 and the long-time value is 0.7 ± 0.1 to reflect the influence of sodium logging and fuel hot pressing. For design purposes an uncertainty of $\pm 32\%$ is recommended after porosity interlinkage.

Specific Heat of U-Zr-Pu Alloys [8-10]

$$C_p = \left[1.359 + 0.05812T + 1.086 \times 10^6 T^{-2}\right] / \left(238 \times 10^{-3}\right) \tag{8-30}$$

where

C_p = specific heat capacity for U-10 wt % Zr, J/kg K

T = temperature, K

Linear Thermal Expansion Coefficient of U-Zr-Pu Alloys [8-11]

$$\alpha_l = \frac{1}{L_0}\left(\frac{L-L_0}{T-T_0}\right) = \left(\frac{\Delta L}{L_0}\right)\frac{1}{T-T_0} = \left(\frac{\Delta L}{L_0}\right)\frac{1}{T-293} \tag{8-31}$$

where

α_l = linear thermal expansion coefficient of U-10 wt % Zr, m/m K

$$\frac{\Delta L}{L_0} = 0.01 \times \left[-0.424 + (1.658 \times 10^{-3} T) - (1.052 \times 10^{-6} T^2) + (1.115 \times 10^{-9} T^3)\right] \tag{8-32}$$

for $293 \le T \le 900K$.

Density of U-Zr-Pu Alloys:

$$\rho = \left(16.02 \times 10^3\right) \times \left[1.0122 - \left(4.629 \times 10^{-5} T\right) + \left(2.438 \times 10^{-8} T^2\right) - \left(2.805 \times 10^{-11} T^3\right)\right] \qquad (8\text{-}33)$$

for $293 \le T \le 900K$

where ρ = density of U-10 wt % Zr, kg/m^3

Thermal Conductivity of HT9 [8-12]

$$k = 29.65 - 6.668 \times 10^{-2} T + 2.184 \times 10^{-4} T^2 - 2.527 \times 10^{-7} T^3 + 9.621 \times 10^{-11} T^4 \qquad (8\text{-}34)$$

where k = thermal conductivity, W/m K
T = temperature, K.

Thermal Expansion of HT9 [8-13]

$$\alpha_l = \frac{1}{L_0}\left(\frac{L - L_0}{T - T_0}\right) = \left(\frac{\Delta L}{L_0}\right)\frac{1}{T - T_0} = \left(\frac{\Delta L}{L_0}\right)\frac{1}{T - 293} \qquad (8\text{-}35)$$

where

α_l = linear thermal expansion coefficient of HT9, m/m K

$$\frac{\Delta L}{L_0} = 0.01 \times \left[-0.16256 + \left(1.62307 \times 10^{-4} T\right) + \left(1.42357 \times 10^{-6} T^2\right) - \left(5.50344 \times 10^{-10} T^3\right)\right] \qquad (8\text{-}36)$$

for $293 \le T \le 1050K$

Density of HT9 [8-14]

$$\rho = \left[7.778 - 3.07 \times 10^{-4} (T - 273)\right] \times 10^3 \quad \text{for } 273 \le T \le 1073K \qquad (8\text{-}37)$$

where ρ = density, kg/m^3
T = temperature, K

8.1.2.2 Limitations and Future Work

- For the heat transfer coefficient of fuel-clad gap, the contact resistance h_g of input Vessel 20 is used in subroutines gama5s and gama5t whether the metal fuel contacts cladding inner surface or not. This is a reasonable assumption since the metal fuel swells rapidly by irradiation and contacts the clad inner surface at about 2 a/o burnup. There is a need to check the radial fuel expansion.

- Material properties of control rod are necessary for the calculation of the reactivity feedback effects in subroutine crdl5t which needs to be updated.

- A set of material properties data is built into the code. The data required to alter the default values of the material properties provided within SSC-K, or to create new material properties, are input to the code through input records MATDAT 10-19 for sodium, 40-49 for blanket, 50-59 for fuel, 60-69 for cladding, and 70-79 for structural materials. (cf. SSC-L manual Sections 5.1 and 7.7) Temporarily, equations for thermal conductivity, specific heat, linear thermal expansion coefficient, and density of U-Zr-Pu and HT9 are implemented in the subroutines, and hence related coefficients in MATDAT records are dummies.

- With the update of SSC-K input file using the most up-to-date KALIMER design data, a code-to-code comparison with a core T-H design code for the in-core heat transfer would provide confidence in the SSC-K predictions.

- Friction factor and heat transfer correlations for rod bundles also need to be reviewed in comparison with the core T-H design for consistency in in-core heat transfer analysis.

8.1.3 Control Rod Material

For the control rod material (born carbide), the thermal conductivity (W/mK), the specific heat (J/kgK), the average linear thermal coefficient of expansion (m/mK), and the density (kg/m^3) are represented by polynomial fits [8-15]. These equations are:

$$k(T) = \frac{k_0(1-P)}{(1+k_4P)} \frac{1}{k_1 + k_2 T} \tag{8-38}$$

$$c_p(t) = c_0\left(1 + c_1 T + c_6 / T^2\right) \tag{8-39}$$

$$\bar{\alpha}(T) = \alpha_0 + \alpha_1 T \tag{8-40}$$

and

$$\rho(T) = \frac{\rho_0(1-P)}{\left[1 + \bar{\alpha}(T)(T - T_0)\right]^3} \tag{8-41}$$

These equations are similar in form to Equations (8-1), (8-2), (8-7) and (8-12), respectively. Values for the various parameters are noted in Table 8-4, and P is the porosity, which is an input quantity read in with the control rod geometric data. These correlations are valid in the temperature range from 500 K to 1250 K.

8.1.4 Sodium

All of the required thermo-physical properties for liquid sodium and sodium vapor are taken from Golden and Tokar [8-16]. These are noted as follows:

Thermal Conductivity (W/mK)

The thermal conductivity of liquid sodium is given by the following equation:

$$k(T) = k_0 + k_1 T + k_2 T^2 \tag{8-42}$$

where

$$k_0 = 109.7 \ ,$$
$$k_1 = -6.4499 * 10^{-2}$$
$$k_2 = 1.1728 * 10^{-5} \ .$$

Specific Heat Capacity (J/gK)

The specific heat capacity at constant pressure for liquid sodium is given by

$$c_p(T) = c_0 + c_1 T + c_2 T^2 \tag{8-43}$$

where

$$c_0 = 1630.22 \quad ,$$
$$c_1 = -0.83354 \quad ,$$
$$c_2 = 4.62838 * 10^{-4} \quad .$$

Table 8-4
Parameters for Control Rod Material Properties

Parameter	Value
K_0	334.13
K_1	21.6178
K_2	0.05381
K_3	0.0
K_4	2.2
K_5	0.0
C_0	1741.79
C_1	$2.34856*10^{-4}$
C_2	0.0
C_3	0.0
C_4	0.0
C_5	0.0
C_6	-46,634.7
a_0	$-1.4886*10^{-3}$
a_1	$4.124*10^{-6}$
P_0	2381.0
T_0	295.4

Enthalpy (J/kg)

The enthalpy of saturated liquid sodium is given by

$$h_s(T) = h_0 + h_1 T + h_2 T^2 + h_3 T^3 \tag{8-44}$$

where

$$h_0 = -6.7511*10^4$$
$$h_1 = 1630.22,$$
$$h_2 = -0.41674,$$
$$h_3 = 1.54279*10^{-4}.$$

For unsaturated liquid sodium, the enthalpy is written as

$$h = h_s - \frac{p_s}{\rho_s} + \frac{p}{\rho}, \tag{8-45}$$

where the saturation vapor pressure (P_s) and the liquid sodium density (P_s) are given in the following equations. For incompressible sodium,

$$\rho(T, P_s) = \rho(T) = \rho_s(T) \quad ;$$

hence, Equation (8-45) becomes

$$h = h_s - \frac{p_s - p}{\rho} \tag{8-46}$$

For most purposes, the liquid sodium enthalpy may be approximated by the saturation value.

In SSC-K we also need to compute liquid sodium temperature from its enthalpy value. Although it is computed iteratively in the code by inverting Eq. (8-44), an approximate correlation is given by the following:

$$T = c_0 + c_1 h_s + c_2 h_s^2 + c_3 h^3{}_s + c_4 h_s^4 \tag{8-47}$$

where

$$c_0 = 55.5057,$$
$$c_1 = 5.56961*10^{-4},$$
$$c_2 = 2.17341*10^{-10},$$
$$c_3 = -7.27069*10^{-17},$$

and

$$c_4 = 4.41118*10^{-24}.$$

Saturation Vapor Pressure (Pa or N/m^2)

The saturation vapor pressure of sodium is expressed by the following two equations:

$$\log 10 P_S = p1 + p2/T + p3\log_{10} T \qquad \text{for} \quad T \le T_1 \qquad (8\text{-}48)$$

and

$$\log 10 p_S = P4 + P5/T + P6\log_{10} T \qquad \text{for} \quad T > T_1 \qquad (8\text{-}49)$$

where

P_1= 11.35977 ,
P_2= -5567.0 ,
P_3= -0.5 ,
P_4= 11.68672 ,
P_5= -5544.97 ,
P_6= -0.61344 ,

and

T_1= 1144.2 .

The saturation temperature of liquid sodium as a function of pressure is given by the following equation [8-17]:

$$T_S = \frac{c_0}{\ln\left(9.869*10^{-6}P\right) - c_1} \qquad (8\text{-}50)$$

where

C_0=-1213.0
C_1=10.51

and P is the pressure in N/m^2 .

Density (kg/m^3)

The density of saturated liquid sodium is given by the following relation:

$$p_S(T) = \rho_0 + \rho_1 T + \rho_2 T^2 + \rho_3 T^3 \qquad \text{for} \quad T_1 \le T \le T_2 \qquad (8\text{-}51)$$

where ,

$$\rho_0 = 1011.597$$
$$\rho_1 = -0.22051,$$
$$\rho_2 = -1.92243*10^{-5},$$
$$\rho_3 = 5.63769*10^{-9},$$
$$T_1 = 370.9,$$

and ,

$$T_2 = 1644.2 \ .$$

The density of unsaturated liquid sodium is related to that of saturated liquid through a compressibility factor (β_T), as follows:

$$\rho(T,P) = \rho_S(T)\exp[\beta_T(p - p_S)] \tag{8-52}$$

where $\rho_s(T)$ is given by Equation (8-51) and P_S is given by Equations (8-48) or (8-49). If incompressibility is assumed, $\beta_T = 0$. Hence,

$$\rho(t,p) = \rho(T) = \rho_S(T) \tag{8-53}$$

Dynamic Viscosity (Pl, i.e. ,N s/m^2)

The dynamic viscosity of liquid sodium is represented as

$$\log_{10} n = c_1 + \frac{c_2}{T} + c_3 \log_{10} T \tag{8-54}$$

where

C_1=-2.4892 ,
C_2=220.65 ,

and

C_3=-0.4925 .

Heat of Vaporization (J/kg)

The heat of vaporization, fitted over the range 1150 to 1500 K is given by the following equation [8-17]:

$$\lambda(T) = \lambda_0 + \lambda_1 T + \lambda_2 T^2 \tag{8-55}$$

where

$$\lambda_0 = 4.40241 * 10^6,$$
$$\lambda_1 = -17.5055,$$
$$\lambda_2 = -0.380184.$$

Specific Heat Capacity (J/kg K)

The specific heat capacity at constant pressure for sodium vapor was fitted over the range 1150 to 1500 K, and is given by the equation [8-17]:

$$c_{pv}(T) = c_0 + c_1 T + c_2 T^2 \tag{8-56}$$

where

$$c_0 = 4.4015 * 10^3,$$
$$c_1 = -2.2987,$$
$$c_2 = 6.347 * 10^{-4}.$$

Density (kg/m^3)

The density of sodium vapor is given by the following equation:

$$\rho_V = \frac{pA(T)}{T} \tag{8-57}$$

in which the factor A(T) was fitted over the range 1150 to 1600 K and is given by the equation [8-17]:

$$A(T) = a_0 + a_1 T + a_2 T^2 \tag{8-58}$$

where

$$a_0 = 3.27317*10^{-3},$$
$$a_1 = -8.72393*10^{-7},$$
$$a_2 = 6.07353*10^{-10}.$$

Enthalpy (J/kg)

At a given reference pressure p, the sodium saturation temperature T_S is first calculated. The liquid saturation enthalpy $h_l(T_S)$ and heat of vaporization $\lambda(T_S)$ are then calculated. The vapor enthalpy is then given by the equation

$$h_V(T) = h_l(T_S) + \lambda(T_S) + h_{V1}(T - T_S) + h_{V2}(T - T_S)^2 + h_{V3}(T - T_S)^3 \qquad (8\text{-}59)$$

where

$$h_{V1} = 4.4015*10^3,$$
$$h_{V2} = -1.14935,$$
$$h_{V3} = 2.11567*10^{-4},$$

$\lambda(T_S)$ is given by Eq.(8-55), and $h_l(T_S)$ is given by Eq.(8-44).

8.1.5 Water and Steam

The constitutive relations for water are currently given by correlations where the properties are evaluated as a function of enthalpy (H) and pressure (P) [8-18].

Enthalpy of Saturated Liquid (J/kg)

The enthalpy of saturated water is given by

$$H_l(p) = a_0 + a_1 p + a_2 p^2 + a_3 p^3 + a_4 p^4 + a_5 p^5 \qquad (8\text{-}60)$$

where

$$
\begin{aligned}
a_0 &= 5.7474 * 10^5, \\
a_1 &= 2.09206 * 10^{-1}, \\
a_2 &= -2.8051 * 10^{-8}, \\
a_3 &= 2.38098 * 10^{-15}, \\
a_4 &= -1.0042 * 10^{-22}, \\
a_5 &= 1.6587 * 10^{-30},
\end{aligned}
$$

and P is pressure in N/m^2.

Enthalpy of Saturated Vapor

The enthalpy of saturated steam is given by

$$H(p) = b_0 + b_1 p + b_2 p^2 + b_3 p^3 + b_4 p^4 \tag{8-61}$$

where

$$
\begin{aligned}
b_0 &= 2.7396 * 10^6, \\
b_1 &= 3.7588 * 10^{-2}, \\
b_2 &= -7.1640 * 10^9, \\
b_3 &= 4.2002 * 10^{-16}, \\
b_4 &= -9.8507 * 10^{-24}.
\end{aligned}
$$

Temperature of Compressed Liquid (K)

The temperature of compressed liquid is given by

$$T(H, p) = c_0(p) + c_1(p) H + c_2(p) H^2 + c_3(P) H^3 \tag{8-62}$$

where

$$
\begin{aligned}
c_0(p) &= c_{00} + c_{01} p, \\
c_1(p) &= c_{10} + c_{11} p, \\
c_2(p) &= c_{20} + c_{21} p, \\
c_3(p) &= c_{30} + c_{31} p,
\end{aligned}
$$

and the coefficients c_{ij} are given in Table 8-5.

Temperature of Superheated Vapor (K)

The temperature of superheated steam is given by

$$T(H,p) = d_0(p) + d_1(p)H + d_2(p)H^2 \tag{8-63}$$

where

$$d_0(p) = d_{00} + d_{01}p + d_{02}p^2,$$
$$d_1(p) = d_{10} + d_{11}p + d_{12}p^2,$$
$$d_2(p) = d_{20} + d_{21}p + d_{22}p^2,$$

and the coefficients d_{ij} are given in Table 8-6.

Density of Compressed Liquid (kg/m^3)

The density of compressed water is given by

$$D(H,p) = f_1 + f_2H^2 + f_3H^4, \quad \text{for} \quad H \le 6.513*10^5 J/kg \tag{8-64}$$

$$D(H,p) = f_4 + \frac{f_5}{H - f_6}, \quad \text{for} \quad H > 6.513*10^5 J/kg \tag{8-65}$$

The coefficients f_j are given in Table 8-7.

Table 8-5

Values of Coefficients for Temperature of Compressed Liquid Water

Coefficient	Value
C_{00}	$2.7291*10^{2}$
C_{01}	$-1.5954*10^{-7}$
C_{10}	$2.3949*10^{-4}$
C_{11}	$-5.1963*10^{-13}$
C_{20}	$5.9660*10^{-12}$
C_{21}	$1.2064*10^{-18}$
C_{30}	$-1.3147*10^{-17}$
C_{31}	$-5.6026*10^{-25}$

Table 8-6

Values of Coefficients for Temperature of Compressed Water Vapor

Coefficient	Value
d_{00}	$6.5659*10^{+2}$
d_{10}	$-5.2569*10^{-4}$
d_{20}	$1.6221*10^{-10}$
d_{01}	$9.9066*10^{-5}$
d_{11}	$-3.4406*10^{-11}$
d_{21}	$1.8674*10^{-18}$
d_{02}	$-2.1879*10^{-12}$
d_{32}	$7.0081*10^{-19}$
d_{22}	$-1.4567*10^{-26}$

Table 8-7

Values of Coefficients for Density of Compressed Liquid Water

Coefficient	Value
f_1	$999.65+4.9737*10^{-7}*p$
f_2	$-2.5847*10^{-10}+6.1767*10^{-19}*p$
f_3	$1.2696*10^{-22}-4.9223*10^{-31}*p$
f_4	$1488.64+1.3389*10^{-6}*p$
f_5	$1.4695*10^{9}+8.85736*p$
f_6	$3.20372*10^{6}+1.20483*10^{-2}*p$

Density of Superheated Vapor (kg/m^3)

The density of superheated steam is given by

$$D(H,p)=\frac{1}{g_0(p)+g_1(p)H} \tag{8-66}$$

where

$$g_0(p)=g_{00}+g_{01}p+g_{02}/p,$$
$$g_1(p)=g_{10}+g_{11}p+g_{12}/p;$$

and

$$g_{00}=-5.1026*10^{-5},$$
$$g_{01}=1.1208*10^{-10},$$
$$g_{02}=-4.4506*10^{+5},$$
$$g_{10}=-1.6893*10^{-10},$$
$$g_{11}=-3.3980*10^{-17},$$
$$g_{12}=2.3058*10^{-1}.$$

Specific Heat of Compressed Liquid (J/m^{3}K)

The specific heat of compressed water is given by

$$c_p(H,p)=\frac{1}{a_0(p)+a_1(p)H+a_2(p)H^2} \tag{8-67}$$

where

$$a_0(p)=a_{00}+a_{01}p,$$
$$a_1(p)=a_{10}+a_{11}p,$$
$$a_2(p)=a_{20}+a_{21}p;$$

and

$$a_{00}=2.3949*10^{-4},$$
$$a_{01}=-5.1963*10^{-13},$$
$$a_{10}=1.1932*10^{-11},$$
$$a_{11}=2.4127*10^{-18},$$
$$a_{20}=-3.9441*10^{-17},$$
$$a_{21}=-1.6808*10^{-24}.$$

Specific Heat of Superheated Vapor (J/m^3K)

The specific heat of superheated steam is given by

$$c_P(H,p)=\frac{1}{b_0(p)+b_1(P)H} \tag{8-68}$$

where

$$b_0(p)=b_{00}+b_{01}p+b_{02}p^2,$$
$$b_1(p)=b_{10}+b_{11}p+b_{12}p^2;$$

and

$$b_{00}=-5.2569*10^{-4},$$
$$b_{01}=-3.4406*10^{-11},$$
$$b_{02}=7.0081*10^{-19},$$
$$b_{10}=3.2441*10^{-10},$$
$$b_{11}=3.7348*10^{-18},$$
$$b_{12}=-2.9134*10^{-26}.$$

Viscosity of Compressed Liquid (Ns/m^2)

The viscosity of compressed water is given by

$$n(H,p)=c_0+c_1x+c_2x^2+c_3x^3+c_4x^4-\left(d_0+d_1E+d_2E^2+d_3E^3\right)(p-p_1) \qquad H\le H_1 \tag{8-69}$$

$$n(H,p)=e_0(H)+e_1(H)(p-p_1) \qquad H_1<H<H_2 \tag{8-70}$$

$$n(H,p)=f_0+f_1z+f_2z^2+f_3z^3+f_4z^4 \qquad H\ge H_2 \tag{8-71}$$

where

$$X=g_0(H-g_1),$$
$$E=g_2(H-g_3),$$
$$Z=g_4(H-g_5),$$
$$e_0(H)=e_{00}+e_{01}H+e_{02}H^2+e_{03}H^3,$$
$$e_1(H)=e_{10}+e_{11}H+e_{12}H^2+e_{13}H^3,$$

and the coefficients are given in Table 8-8.

Table 8-8
Values of Coefficients for Viscosity of Compressed Liquid Water

Coefficient	Value
C_0	$1.2995*10^{-3}$
C_1	$-9.2640*10^{-4}$
C_2	$3.8105*10^{-4}$
C_3	$-8.2164*10^{-5}$
C_4	$7.0224*10^{-6}$
d_0	$-6.5959*10^{-12}$
d_1	$6.763*10^{-12}$
d_2	$-2.8883*10^{-12}$
d_3	$4.4525*10^{-13}$
e_{00}	$1.4526*10^{-3}$
e_{01}	$-6.9881*10^{-9}$
e_{02}	$1.5210*10^{-14}$
e_{03}	$-1.2303*10^{-20}$
e_{10}	$-3.8064*10^{-11}$
e_{11}	$3.9285*10^{-16}$
e_{12}	$-1.2586*10^{-21}$
f_{13}	$1.2860*10^{-27}$
f_0	$3.0260*10^{-4}$
f_1	$-1.8366*10^{-4}$
f_2	$7.5671*10^{-5}$
f_3	$-1.6479*10^{-5}$
f_4	$1.4165*10^{-6}$
H_1	$2.76*10^{5}$
H_2	$3.94*10^{5}$
P_1	$6.8946*10^{5}$
g_0	$8.5813*10^{-6}$
g_1	$4.2659*10^{4}$
g_2	$6.4845*10^{-6}$
g_3	$5.5359*10^{4}$
g_4	$3.8921*10^{-6}$
g_5	$4.0147*10^{5}$

Viscosity of Superheated Vapor (Ns/m^2)

The viscosity of superheated steam is given by

$$n(H,p) = (a_0 + a_1 T) - D(b_0 + b_1 T) \qquad \text{for} \quad T \le 300K \qquad (8\text{-}72)$$

$$n(H,P) = (a_0 + a_1 T) + (c_0 + c_1 T + c_2 T^2 + c_3 T^3) D + D(d_0 + d_1 T + d_2 T^2 + d_3 T^3)(e_0 + eD + eD) \quad \text{for} \quad 300 < T < 375K \qquad (8\text{-}73)$$

$$n(H,p) = (a_0 + a_1 T) - D(e_0 + e_1 D + e_2 D^2) \qquad \text{for} \quad T \ge 375K \qquad (8\text{-}74)$$

where

$$T = T_V(H,p) - 273.15,$$
$$D = D_V(H,p),$$

and the coefficients are given in Table 8-9.

Table 8-9
Values of Coefficients for Viscosity of Superheated Water Vapor

Coefficient	Value
a_0	$4.07*10^{-8}$
a_1	$8.04*10^{-6}$
b_0	$1.858*10^{-1}$
b_1	$5.9*10^{-10}$
C_0	$-2.885*10^{-6}$
C_1	$2.427*10^{-8}$
C_2	$-6.7893*10^{-11}$
C_3	$6.3170*10^{-14}$
d_0	$1.76*10^{2}$
d_1	-1.6
d_2	$4.8*10^{-3}$
d_3	$-4.7407*10^{-6}$
e_0	$3.53*10^{-8}$
e_1	$6.765*10^{-11}$
e_2	$1.021*10^{-14}$

Conductivity of Compressed Liquid (W/mK)

The thermal conductivity of compressed water is given by

$$k(H,p) = a_0 + a_1 X + a_2 X^2 + a_3 X \tag{8-75}$$

where

$$X = \frac{H}{5.815*10^5}$$

and

$$a_0 = 5.7374*10^{-1},$$
$$a_1 = 2.5361*10^{-1},$$
$$a_2 = -1.4547*10^{-1},$$
$$a_3 = 1.3875*10^{-2}.$$

Conductivity of Superheated Vapor (W/mK)

The thermal conductivity of superheated steam is given by

$$k(H,p) = X + D(Z + \frac{cD}{T^{4.2}}), \tag{8-76}$$

where

$$T = T(H,p) - 273.15,$$
$$D = D(H,p),$$
$$X = z_0 + a_1 T + a_2 T^2 + a_3 T^3,$$
$$Z = b_0 + b_1 T + b_2 T^2,$$

and

$$c = 2.1482E5,$$
$$a_0 = 1.76*10^{-2},$$
$$a_1 = 5.87*10^{-5},$$
$$a_2 = 1.04*10^{-7},$$
$$a_3 = -4.51*10^{-11},$$

$$b_0 = 1.0351*10^{-4},$$
$$b_1 = 4.198*10^{-7},$$
$$b_2 = -2.771*10^{-11}.$$

In addition to the properties listed above, various partial derivatives of many of the functions were required. These are obtained by analytically differentiating the appropriate correlations.

8.2 Correlations

The required pressure drop and heat transfer correlations for the range of interest are included in this section. Representative valves for various curve-fitted parameters are noted in SI units.

8.2.1 Friction Factor Correlations

8.2.1.1 Pressure Drop in Pipe

In the SSC-K code, the Darcy-Weisbach friction factor, *f*, is computed from correlations for laminar and turbulent flows with interpolation in the transition regime. There are two turbulent flow fiction factor models. The first model computes the turbulent friction factor using an engineering approximation to the well-known Colebrook-White correlation, while the second model uses an exponential friction with user's input coefficients. The frictional pressure drop in the different subchannels of core is calculated by specifying different friction factors. However the default friction law which applies globally throughout the system is specified in the function of FRIC in the SSC-K code.

The friction pressure drop across a pipe of length L, when the developing flow region can be ignored, is given by

$$\Delta P_{friction} = \int_{z_{in}}^{z_{out}} \left(-\frac{dp}{dz} \right) = P_{in} - P_{out} = \frac{f\,L}{D_h} \frac{\rho U^2}{2} \tag{8-77}$$

where D_h is the hydraulic or equivalent diameter in the case on non-circular channels, defined as

$$D_h = \frac{4\,(flow\ area)}{wetted\ parameter} \tag{8-78}$$

and U is the velocity. The friction factor f, depends on the Reynolds number (Re) of the flow, and the surface roughness (e) of the pipe or channel. Curves of f vs. Re for various values of surface roughness are provided in the Moody chart. The surface roughness typically runs from 10^{-3} for a small commercial grade tube $1.5*10^{-6}$ for a very large drawn tube or pipe. For commercial steel, e=0.000046 m. It is most likely that the reactor pipes will be even smoother than this (see Table 8-10).

The curves for turbulent flow in the Moody chart [8-19] are generated by the Colebrook-White equation [8-20].

$$\frac{1}{\sqrt{f}} = -2.0\log_{10}\left(\frac{e/D_h}{3.7} + \frac{2.51}{\mathrm{Re}\sqrt{f}}\right) \tag{8-79}$$

In the SSC-L code, a simplified form of friction factor [8-20] rather than the above-mentioned transcendental equation is desired, and the following explicit relation for f, which is accurate to within 5%, was coded.

$$f = 0.0055\left\{1 + \left[20000\frac{e}{D_h} + \frac{10^6}{\mathrm{Re}}\right]^{1/3}\right\} \tag{8-80}$$

Table 8-10
Roughness of various piping materials

Material	e (m)
Drawn tubing	$1.5*10^{-6}$
Commercial steel	$4.6*10^{-5}$
Wrought iron	$4.6*10^{-5}$
Asphalted cast iron	$1.2*10^{-4}$
Galvanized iron	$1.5*10^{-4}$
Cast iron	$2.6*10^{-4}$
Concrete	$3*10^{-4}$ to $3*10^{-3}$
Riveted steel	10^{-3} to 10^{-2}

For smooth pipes, the above equation is reduced to

$$f = 0.0055 + 0.55(\mathrm{Re})^{-1/3} \tag{8-81}$$

According to comparison for computing efficiency in calculating f from either two equations, the Levy's approximate representation [8-21], Eq. (8-80), was found to be 25% more efficient. Since the friction factor needs to be evaluated for each node section of each pipe run, this can result in substantial savings in computing time every times step.

In the SSC-K code, the friction factors for each flow regime are calculated using the following correlations. The friction factor model is simply an interpolation scheme linking the laminar, laminar-turbulent transition, and turbulent flow regimes. The laminar friction factor is calculated as

$$f_L = \frac{64}{\mathrm{Re}}, \qquad 0 \le \mathrm{Re} \le 2000 \tag{8-82}$$

where *Re* is the Reynolds number, The friction factor in the transition region between laminar and turbulent flows is computed by linear interpolation as

$$f_{L,T} = \left(\frac{\mathrm{Re}-2000}{3000-2000}\right)\left[f_{T,3000} - f_{L,2000}\right], \quad 2000 < \mathrm{Re} < 3000 \tag{8-83}$$

where $f_{L,2000}$ is the laminar friction factor at a Reynolds number of 2000, $f_{T,3000}$ is the turbulent friction factor at a Reynolds number of 3000, and the interpolation factor is defined to lie between zero and one.

The turbulent friction factor is given by the Zigrang-Sylvester [8-22] approximation to the Colebrook-White correlation as,

$$\frac{1}{\sqrt{f_T}} = -2\log_{10}\left\{\frac{e/D_h}{3.7} + \frac{2.51}{\mathrm{Re}}\left[1.14 - 2\log_{10}\left(\frac{e}{D_h} - \frac{21.25}{\mathrm{Re}^{0.9}}\right)\right]\right\}, \quad \mathrm{Re} \ge 3000 \tag{8-84}$$

or by

$$f_T = A + B\,\mathrm{Re}^{-C} \tag{8-85}$$

where e is the surface roughness, A, B, and C are user input constants, and the other variables have been defined previously. The Zigrang-Sylvester equation has the advantage that it is an explicit relation for the friction factor, while the Colebrook-White correlation is a transcendental function requiring iteration for the determination of the friction factor. The Zigrang-Sylvester approximation to the Colebrook-White correlation for turbulent flow, has a mean square error of 0.1% and a maximum deviation of 0.5% when compared to the Colebrook-White correlation over the ranges $0.5 \geq e/D_h \geq 10^{-5}$ and $10^7 \geq Re \geq 2500$.

It should be noted that the Moody charts are generated based on isothermal fluid flow. In the presence of heat transfer at the wall, either the fluid properties, such as viscosity and density should be evaluated at a film temperature. The film temperature is assumed to be average of wall temperature (T_w) and bulk temperature of coolant (T_b). The computed value for f should be modified as follows.

$$f_{\text{modified}} = f\left(\frac{\mu_w}{\mu_b}\right)^n \tag{8-86}$$

where n is constant. Generally, for steady-state flow in a pipe, $f_{\text{modified}} = f$. These two values are different under transient condition, however, the difference is considered small enough to be neglected.

Pressure losses due to fittings, valves, bends, contractions, and expansions are computed from

$$\Delta P_g = K\frac{\rho \overline{U}^2}{2} \tag{8-87}$$

where U is the average velocity in the smaller cross section if there is a change in cross section in the fitting involved. These objects cause the flowing fluid to lose energy owing to a sudden change of cross section or change of direction. Such a loss in energy proportional to square of velocity, and unlike wall friction, has little if any dependence upon Reynolds number and relative roughness. In general, the effects of fittings and valves are evaluated by the velocity-head-loss coefficient K. These data can be obtained from typical pipe fittings and other changes

as shown in Table 8-11 [8-23].

Table 8-11

Form Loss Coefficient for Various Flow Restrictions

Parameter		K	Reference velocity
Pipe entrance from a plenum			
Well rounded entrance to pipe		0.04	In pipe
Slightly rounded entrance to pipe		0.23	In pipe
Sharp-edged entrance		0.50	In pipe
Projecting pipe entrance		0.78	In pipe
Pipe exit to plenum			
Any pipe exit		1.0	In pipe
Sudden changes in cross-sectional area			
Sudden contraction		$0.5(1-\beta^2)$	Downstream
Sudden expansion		$1-\beta^2$	Upstream
where $\beta = \frac{\text{small cross-sectional area}}{\text{large cross-sectional area}}$			
Fittings	$(L/D)_{equiv}$		
90° Standard elbow	30	0.35-0.9	
90° Large-radius elbow	20	0.2-0.6	
45° Standard elbow	16	0.17-0.45	
Standard tree (flow through run)	20	0.2-0.6	
Standard tree (flow through branch)	60	0.65-1.7	
Valves (various types)			
Fully open		0.15-15.0	
Half-closed			

8.2.1.2 Pressure Drop in Wire-Wrapped Rod Bundles

Methods of calculating pressure drop in core assemblies in LMFBR are similar to conventional approaches. The pressure drop across a core assembly consists of (i) entrance and exit pressure losses between the vessel plena and the core internals, (ii) the friction pressure drop along the fuel rods, and (iii) the form losses due to the presence of spacers. The entrance and exit losses are those due to a sudden change in flow area. loss through assembly inlet nozzle, rod bundle, assembly outlet, etc. Generally, empirically determined pressure-loss correlations have been used for wire-wrapped rod bundle applications. Attention here is focused on the friction along the wire-wrapped rod bundles.

(1) Engel, Markley, and Bishop

Based on limited experimental data, Engel, Markley, and Bishop [8-24] have recommended the following generalized correlation for hexagonal fuel assembly applicable in the range $P/D < 1.23$ and $H < 30$ cm.

$$f = \frac{A}{\mathrm{Re}}(1-\chi)^{1/2} + \frac{0.48}{\mathrm{Re}^{0.25}}\chi^{1/2} \tag{8-88}$$

where

$$\chi = 0.0, \qquad \text{for} \quad \mathrm{Re} \le 400,$$

$$\chi = \frac{\mathrm{Re}-400}{4600}, \qquad \text{for} \quad 400 < \mathrm{Re} < 5000$$

$$\chi = 1.0, \qquad \text{for} \quad \mathrm{Re} \ge 5000$$

and the coefficient A is a function of wire-wrap lead H and pitch to rod diameter ratio.

$$A = \frac{320}{\sqrt{H}}(P/D)^{1.5} \tag{8-89}$$

Note that the wire-wrap lead H in above equation is in centimeters.

(2) Chan and Todreas

Chan and Todreas [8-25] developed the following generalized correlations applicable to a wide range of wire-wrapped hexagonal fuel assemblies.

$$f = \frac{C_{19}}{\mathrm{Re}} \qquad \text{for} \quad \mathrm{Re} \le 400 \tag{8-90}$$

$$f = \frac{C_{19}}{\mathrm{Re}}\left(1 + C_{16}\,\mathrm{Re}^{1.222}\right)^{0.671} \qquad \text{for} \quad \mathrm{Re} > 400 \tag{8-91}$$

Here, *Re* is the bundle Reynolds number and the coefficient C_{18} and C_{19} are functions of the number of rods in a bundle *N*, pitch to rod (pin) diameter ratio *P/D*, and lead length to rod (pin) diameter ratio *H/D*.

$$C_{18} = A(N)^{B}(P/D)^{C}(H/D)^{E} \tag{8-92}$$

$$C_{19} = 251(N)^{0.007}(P/D)^{0.997}(H/D)^{-0.354} \tag{8-93}$$

The values of the constant *A*, *B*, *C*, and *E* are given in Table 8-12.

Table 8-12
Values of Constants in Equation (8-92)

D ≥ 0.35 inch	D < 0.35 inch	Note
A = 0.00221	A = 0.000584	1. 4 H/D
B = 0.166	B = 0.185	for 2. P/D 1.2 & 8 H/D
C = 8.297	C = 8.247	3. P/D 1.343 & 12 H/D
E = -1.457	D = -1.818	
A = 0.0000395	A = 0.000278	
B = 0.063	B = -0.084	for others
C = 0.174	C = 0.289	
E = 0.178	D = -0.268	

For hexagonal assembly, the flow area and hydraulic diameter D_h, can be calculated using the relationships:

$$\text{Flow area} = \frac{\sqrt{3}}{2}\left(d_{f-f}\right)^2 - \frac{N\pi}{4}\left(D^2 + D_w^2\right) \tag{8-94}$$

$$\text{Perimeter} = \left(2\sqrt{3}d_{f-f}\right) + \pi N\left(D + D_w\right) \tag{8-95}$$

Here, d_{f-f} is the distance between the flat surfaces of hexagonal assembly, D is the pin diameter, D_w is wire-wrap diameter, and n is the number of pins in a bundle.

(3) Experiments for fuel assemblies of CRBR and FFTF

In the Clinch River Breeder Reactor (CRBR) plant, there are several different types of hexagonal rod bundles. The important geometrical characteristics of these bundles are presented in Table 8-13. Based on the experimental measurements [8-26-29], several different correlations for friction factor are recommended for CRBR and Fast Flux Test facility (FFTF) fuel assemblies. The same correlations are applicable to both FFTF and CRBR fuel assemblies. Three sets of correlations for friction factors of in-core assemblies are available in the SSC-K code.

Table 8-13
Important Parameters of CRBR Hexagonal Assemblies

Assembly	No. of pins	P/D	H/D	D(mm)	D_h(mm)
Fuel	217	1.24	51.74	5.842	3.254
Blanket	61	1.072	7.905	12.852	3.399
Primary control	37	1.05	21.18	15.291	6.862
Secondary control	31	1.05	10.87	14.036	15.981
Reactor shield	19	1.0	-	25.197	1.357

Fuel Assemblies (L6ATYP≠ 2 or 3)

$$f = Min\left\{\frac{84}{\text{Re}}, 0.5\right\} \qquad \text{for} \quad \text{Re} \le 800 \tag{8-96}$$

$$f = \frac{0.316}{\text{Re}^{0.25}}\left(1.029 + \frac{2837}{\text{Re}^{1.24}}\right) \qquad \text{for} \quad \text{Re} > 800 \tag{8-97}$$

Blanket Assemblies (L6ATYP= 2)

$$f = Min\left\{\frac{110}{\mathrm{Re}}, 0.5\right\} \qquad \text{for} \quad \mathrm{Re} < 400 \qquad (8\text{-}98)$$

$$f = \frac{110}{\mathrm{Re}}\sqrt{1-\frac{\mathrm{Re}-400}{4600}} + \frac{0.48}{\mathrm{Re}^{0.25}}\sqrt{\frac{\mathrm{Re}-400}{4600}} \qquad \text{for} \quad 400 \le \mathrm{Re} < 5000 \qquad (8\text{-}99)$$

$$f = \frac{0.48}{\mathrm{Re}^{0.25}} \qquad \text{for} \quad \mathrm{Re} > 5000 \qquad (8\text{-}100)$$

Control Assemblies (L6ATYP= 3)

$$f = Min\left\{\frac{84}{\mathrm{Re}}, 0.5\right\} \qquad \text{for} \quad \mathrm{Re} < 800 \qquad (8\text{-}101)$$

$$f = \frac{84}{\mathrm{Re}} + \left(0.316\mathrm{Re}^{-0.25} - 84\mathrm{Re}\right)\frac{(\mathrm{Re}-800)}{1200} \qquad \text{for} \quad 800 \le \mathrm{Re} < 2000 \qquad (8\text{-}102)$$

$$f = 0.316\mathrm{Re}^{-0.25}\left(\frac{1.034}{(P/D)^{1.24}} + 29.7(P/D)^{6.94}\frac{\mathrm{Re}^{0.086}}{(P/D)_w^{2.239}}\right)^{0.885} \qquad \text{for} \quad \mathrm{Re} \ge 2000 \qquad (8\text{-}103)$$

Here, *P/D* is assembly pitch to diameter ratio and $(P/D)_w$ is wire wrap pitch to diameter ratio. Constants *A* and *B* are supplied by user as input.

For the inlet orifice region and bypass region, SSC-K uses the following corrections.

$$f = Min\left\{\frac{96}{\mathrm{Re}}, 0.5\right\} \qquad \text{for} \quad \mathrm{Re} < 2000 \qquad (8\text{-}104)$$

$$f = 0.316\mathrm{Re}^{-0.25} \qquad \text{for} \quad \mathrm{Re} \ge 2000 \qquad (8\text{-}105)$$

8.2.2 Heat Transfer Correlations

Heat transfer correlations for liquid metal turbulent flow in channels or rod bundles are in the form of:

$$Nu = A + B(Pe)^C \tag{8-106}$$

where the Peclet number *Pe,* is the product of the Reynolds and Prandtl numbers. A, B, and C are constants that depend on the geometry and the boundary conditions. The constant C is a number close to 0.8. The constant A reflects the fact that significant transfer in liquid metals occurs even as Re goes to zero.

(1) Circular tube

The following relations hold for the boundary conditions cited and fully developed flow conditions.

Lyon's correlation for constant heat flux along and around the tube [8-30]

$$Nu = 7 + 0.025Pe^{0.8} \tag{8-107}$$

Seban and Shimazaki's correlation for uniform axial wall temperature and uniform radial heat flux [8-31]

$$Nu = 5.0 + 0.025Pe^{0.8} \tag{8-108}$$

Aoki's correlation [8-32]

$$Nu = 6.0 + 0.025\left(\bar{\phi}Pe\right)^{0.8} \tag{8-109}$$

where

$$\bar{\phi} = \frac{0.014\left[1 - \exp(-71.8\chi)\right]}{\chi} \tag{8-110}$$

$$\chi = \frac{1}{\mathrm{Re}^{0.45}\,\mathrm{Pr}^{0.2}} \tag{8-111}$$

In the laminar region,

$$Nu = 4.36 \qquad \text{for} \quad \mathrm{Re} \le 3000 \tag{8-112}$$

(2) Parallel plates

For fully developed flow [8-33],
For constant heat flux through one wall only (the other is adiabatic)

$$Nu = 5.8 + 0.02\,Pe^{0.8} \tag{8-113}$$

For constant heat flux through both walls, a graphic correction factor for the heat transfer coefficient was supplied by Seban [8-33].

(3) Concentric annuli

For fully developed flow and boundary condition of uniform heat flux in the wall when $D_2/D_1 > 1.4$.

$$Nu = 5.25 + 0.0188\,Pe^{0.8}\left(\frac{D_2}{D_1}\right)^{0.3} \tag{8-114}$$

If D_2/D_1 is close to unity, the use of Eq. (8-113) for parallel plate was recommended by Seban [8-33].

(4) Rod bundles

The non-uniformity of the subchannel shape creates substantial azimuthal variation of *Nu*. Also in finite rod bundles the turbulent effects in a given subchannel affect adjacent subchannels differently depending on the location of the subchannels with respect to the duct boundaries. Therefore the value of *Nu* is a function of position within the bundle. However, overall heat transfer correlations are provided in this section.

The liquid metal heat transfer correlations for forced convection in a rod bundle have been developed by many researchers. These experimental have been compared with the experimental data by Kazimi [8-34].

Westinghouse [8-35]

For $1.4 \geq P/D \geq 1.1$ and $5000 \geq Pe \geq 10$

$$Nu = 4.0 + 0.33(P/D)^{3.8}(Pe/100)^{0.86} + 0.16(P/D)^{5.0} \tag{8-115}$$

Modified Schad [8-35]

For $1.5 \geq P/D \geq 1.1$ and $1000 \geq Pe \geq 150$: Turbulent flow regime

$$Nu = \left[-16.15 + 24.96(P/D) - 8.55(P/D)^2\right] Pe^{0.3} \tag{8-116}$$

For $150 \geq Pe$: Lamina flow regime

$$Nu = 4.496\left[-16.15 + 24.96(P/D) - 8.55(P/D)^2\right] \tag{8-117}$$

Garber and Rieger [8-36]

For the shell side in the IHX, the following correlations are used in SSC-K;

For $1.95 \geq P/D \geq 1.25$ and $3000 \geq Pe \geq 150$

$$Nu = \left[0.25 + 6.2(P/D)\right] + \left[0.32(P/D) - 0.007\right](Pe)^{0.8-0.024(P/D)} \tag{8-118}$$

For $Pe < 110$

$$Nu = \left[0.25 + 6.2(P/D) + 0.32(P/D) - 0.007\right](110)^{0.8-0.024(P/D)} \tag{8-119}$$

Borishcnskii et al. [8-37]

For $1.5 \geq P/D \geq 1.1$ and $2000 \geq Pe \geq 200$

$$Nu = 24.15 \log\left[-8.12 + 12.76(P/D) - 3.65(P/D)^2\right] + 0.0174\left[1 - \exp 6(1 - P/D)\right]\left[Pe - 200\right]^{0.9} \quad (8\text{-}120)$$

For $1.5 > P/D > 1.1$ and $200 \geq Pe$

$$Nu = 24.15 \log\left[-8.12 + 12.76(P/D) - 3.65(P/D)^2\right] \quad (8\text{-}121)$$

Currently In the SSC-K code, Aoki's correlation is used for liquid metal flow in a pipe, Graber-Rieger correlation for the shell side in the intermediate heat exchanger (IHX), and Modified- Schad correlation for Rod bundles. Table 8-14 summarizes the correlations used for both SSC-L and SSC-K.

Table 8-14
Comparison of correlations used for SSC-L and SSC-K

	SSC-L	SSC-K
Friction Factor	For pipe o Moody Chart, Levy model For in-core assembly o CRBR specific experiments for Fuel, Blanket and Control assemblies	For pipe o Zigrang-Sylvester approximation For in-core assembly o Engel, Markley, and Bishop o Chan and Todeas o Generalized FFTF experiments
Heat Transfer Coeffi.	For circular tube o Theoretical Nu for laminar flow o Aoki for turbulent flow For IHX shell-side o Graber and Rieger For rod bundle o Modified Schad for both laminar and turbulent flows	For circular tube o Theoretical Nu for laminar flow o Aoki for turbulent flow o Lyon for const. heat flux o Seban and Shimazaki for const. temperature For IHX shell-side o Graber and Rieger For rod bundle o Westinghouse o Kazimi and Carelli o Borishanskii

The heat transfer correlations for water/steam are given for four different modes of heat transfer. The first mode of heat transfer is forced convection. The Nusselt number for nucleate boiling is given as [8-38]:

$$Nu = 0.023\,\mathrm{Re}^{0.8}\,\mathrm{Pr}^{0.4} \tag{8-122}$$

The heat transfer for nucleate boiling is given as [8-39]:

$$h = S \bullet h_{NB} + F \bullet h_C \tag{8-123}$$

where the nucleate boiling coefficient h_{NB} is given as:

$$h_{NB} = 0.00122 \left\{ \frac{K_l^{0.79} C_l^{0.45} \rho_l^{0.49}}{\Omega^{0.5} \mu_l^{0.29} \lambda_{fg}^{0.24} \rho^{0.24}} \right\} \Delta p^{0.75} \tag{8-124}$$

where

C_l = specific heat of liquid
K_l = thermal conductivity of liquid
Ω = surface tension
λ_{fg} = latent heat of vaporization, and
ΔP = difference in saturation pressure corresponding to the wall superheat.

The Reynolds number correction factor F, and the nucleate boiling suppression factor S are represented as:

$$F = \begin{cases} 2.84 \left(\dfrac{1}{X_{tt}} \right)^{0.45}, & \dfrac{1}{X_{tt}} < 2. \\ 2.57 + 0.7643 \dfrac{1}{X_{tt}}, & \dfrac{1}{X_{tt}} \geq 2. \end{cases} \tag{8-125}$$

$$S = \begin{cases} 1.05 - 1.3*10^{-5}\,\mathrm{Re}, & \mathrm{Re} \leq 2.5*10^4 \\ 0.83 - 4.3*10^{-6}\,\mathrm{Re}, & 2.5*10^4 < \mathrm{Re} \leq 10^5 \\ 0.32 \exp(-1.92*10^{-6}\,\mathrm{Re}), & 10^5 < \mathrm{Re} \leq 6*10^5 \\ 0.09 & \mathrm{Re} > 6*10^5 \end{cases} \tag{8-126}$$

and

$$Re=Re_l F^{1.25}$$

Where X_{tt} is the Lockhart/Martinelli [8-40] parameter:

$$\frac{1}{X_{tt}} = \left(\frac{X}{1-X}\right)^{0.9} \bullet \left(\frac{\rho_l}{\rho_v}\right)^{0.5} \bullet \left(\frac{\mu_v}{\mu_l}\right)^{0.10} \tag{8-127}$$

The convection coefficient h_C is calculated from the Dittus Boelter equation based on liquid thermodynamic properties [8-38].

The heat transfer for film boiling regime is given as [8-41]:

$$Nu = 0.0193\,\mathrm{Re}_l^{0.8}\,\mathrm{Pr}_l^{1.23}\left(\frac{\rho_B}{\rho_g}\right)^{0.68}\left(\frac{\rho_l}{\rho_g}\right)^{0.068}, \tag{8-128}$$

where subscripts l and g denote, respectively, liquid and vapor phase at saturation and subscript $_B$ indicates a bulk property of the steam/water mixture.

For superheat steam, the following heat transfer correlation for forced convection is used [8-42]:

$$Nu = 0.0133\,\mathrm{Re}^{0.84}\,\mathrm{Pr}^{0.333}. \tag{8-129}$$

The steam/water quality at the DNB point is given by [8-43]:

$$X_{DNB} = \frac{4.38*10^4 \rho_l}{H_{lg}\rho_g\sqrt{G/1350.0}} \qquad \text{for } q > 6.3*10^5, \tag{8-130}$$

or

$$X_{DNB} = \frac{4.38*10^4 \upsilon_l \bullet \left(5.3*10^5/q\right)^{1.5}}{H_{lg}\rho_g\sqrt{G/1350.0}} \qquad \text{for } q < 6.3*10^5 \tag{8-131}$$

where H_{lg} is the latent heat of vaporization (J/kg), G is the mass flow rate per unit area (kg/s m^2), and q is in W/m^2.

9. TWO-DIMENSIONAL HOT POOL MODEL

9.1 Introduction

During a normal reactor scram, the heat generation is reduced almost instantaneously while the coolant flow rate follows the pump coastdown. This mismatch between power and flow results in a situation where the core flow entering the hot pool is at a lower temperature than the temperature of the bulk pool sodium. This temperature difference leads to thermal stratification. Thermal stratification can occur in the hot pool region if the entering coolant is colder than the existing hot pool coolant and the flow momentum is not large enough to overcome the negative buoyancy force. Since the fluid of hot pool enters IHXs, the temperature distribution of hot pool can alter the overall system response. Hence, it is necessary to predict the pool coolant temperature distribution with sufficient accuracy to determine the inlet temperature conditions for the IHXs and its contribution to the net buoyancy head. Therefore, in this section two-dimensional hot pool model is developed instead of existing one-dimensional model to predict the hot pool coolant temperature and velocity distribution more accurately and is applied to the SSC-K code.

9.2 Theory

9.2.1 Governing Equations

The governing equations for conservation of mass, momentum, energy, turbulent kinetic energy and rate of turbulent kinetic energy dissipation for $k-\varepsilon$ turbulence model in a generalized coordinate system x^j can be written as follows;

$$\frac{\partial}{\partial x^1}(rU_1)+\frac{\partial}{\partial x^2}(rU_2) = 0 \tag{9-1}$$

$$\frac{\partial}{\partial t}(rJ\rho u_1)+\frac{\partial}{\partial x^1}\left[rU_1u_1-\frac{r}{J}(\mu+\mu_t)\left\{\frac{\partial u_1}{\partial x^1}B_1^1+\frac{\partial u_1}{\partial x^2}B_2^1+b_1^1w_1^1+b_2^1w_1^2\right\}+rb_1^1p\right]$$
$$+\frac{\partial}{\partial x^2}\left[rU_2u_1-\frac{r}{J}(\mu+\mu_t)\left\{\frac{\partial u_1}{\partial x^1}B_1^2+\frac{\partial u_1}{\partial x^2}B_2^2+b_1^2w_1^1+b_2^2w_1^2\right\}+rb_1^2p\right]=0. \tag{9-2}$$

$$\frac{\partial}{\partial t}(rJ\rho u_2)+\frac{\partial}{\partial x^1}\left[rU_1u_2-\frac{r}{J}(\mu+\mu_t)\left\{\frac{\partial u_2}{\partial x^1}B_1^1+\frac{\partial u_2}{\partial x^2}B_2^1+b_1^1w_2^1+b_2^1w_2^2\right\}+rb_2^1p\right] \tag{9-3}$$

$$\begin{aligned}&\frac{\partial}{\partial t}(rJ\rho T)+\frac{\partial}{\partial x^1}\left[rU_1T-\frac{r}{J}\left(\frac{\mu}{P_r}+\frac{\mu_t}{P_{r_t}}\right)\left\{\frac{\partial T}{\partial x^1}B_1^1+\frac{\partial T}{\partial x^2}B_2^1\right\}\right]\\&+\frac{\partial}{\partial x^2}\left[rU_2T-\frac{r}{J}\left(\frac{\mu}{P_r}+\frac{\mu_t}{P_{r_t}}\right)\left\{\frac{\partial T}{\partial x^1}B_1^2+\frac{\partial T}{\partial x^2}B_2^2\right\}\right]=0.\end{aligned} \tag{9-4}$$

$$\begin{aligned}&\frac{\partial}{\partial t}(rJ\rho k)+\frac{\partial}{\partial x^1}\left[rU_1k-\frac{r}{J}\left(\mu+\frac{\mu_t}{\sigma_k}\right)\left\{\frac{\partial k}{\partial x^1}B_1^1+\frac{\partial k}{\partial x^2}B_2^1\right\}\right]\\&+\frac{\partial}{\partial x^2}\left[rU_2k-\frac{r}{J}\left(\mu+\frac{\mu_t}{\sigma_k}\right)\left\{\frac{\partial k}{\partial x^1}B_1^2+\frac{\partial k}{\partial x^2}B_2^2\right\}\right]=rJ(G-\rho\varepsilon)\end{aligned} \tag{9-5}$$

$$\begin{aligned}&\frac{\partial}{\partial t}(rJ\rho\varepsilon)+\frac{\partial}{\partial x^1}\left[rU_1\varepsilon-\frac{r}{J}\left(\mu+\frac{\mu_t}{\sigma_\varepsilon}\right)\left\{\frac{\partial \varepsilon}{\partial x^1}B_1^1+\frac{\partial \varepsilon}{\partial x^2}B_2^1\right\}\right]\\&+\frac{\partial}{\partial x^2}\left[rU_2\varepsilon-\frac{r}{J}\left(\mu+\frac{\mu_t}{\sigma_\varepsilon}\right)\left\{\frac{\partial \varepsilon}{\partial x^1}B_1^2+\frac{\partial \varepsilon}{\partial x^2}B_2^2\right\}\right]=rJ\left(C_{\varepsilon1}\frac{\varepsilon}{k}G-C_{\varepsilon2}\rho\frac{\varepsilon^2}{k}\right)\end{aligned} \tag{9-6}$$

where

$$U_i=\rho u_k b_k^i,\quad B_m^j=b_k^jb_k^m,\quad w_j^i=\frac{\partial u_i}{\partial x^k}b_j^k \tag{9-7}$$

and

$$\mu_t=C_\mu\rho\frac{k^2}{\varepsilon} \tag{9-8}$$

$$G=\frac{\mu_t}{J^2}\left[2\left\{\frac{\partial u_1}{\partial x^1}b_1^1+\frac{\partial u_1}{\partial x^2}b_1^2\right\}^2+2\left\{\frac{\partial u_2}{\partial x^1}b_2^1+\frac{\partial u_2}{\partial x^2}b_2^2\right\}^2\right.$$

$$+\left\{\frac{\partial u_1}{\partial x^1}b_2^1+\frac{\partial u_1}{\partial x^2}b_2^2+\frac{\partial u_2}{\partial x^1}b_1^1+\frac{\partial u_2}{\partial x^2}b_1^2\right\}^2+2\frac{u_2^2}{r^2}\ ] \tag{9-9}$$

$$C_{\varepsilon_1}=1.44,\quad C_{\varepsilon_2}=1.92,\quad P_{r_t}=0.9,\quad C_\mu=0.09,\quad \sigma_k=1.0,\quad \sigma_\varepsilon=1.3 \tag{9-10}$$

In above equations u_i, T, k, ε denote two cylindrical velocity components, temperature, turbulent kinetic energy and rate of turbulent kinetic energy dissipation respectively. The geometric coefficients b_i^j represent the cofactors of $\partial y^i/\partial x^j$ in the Jacobian matrix of the coordinate transformation, J stands for the determinant of the Jacobian matrix, y^i is the cylindrical coordinate system and ρ, μ, p, P_r denote density, viscosity, pressure and Prandtl number respectively.

9.2.2 Discretization of Governing Equation

The solution domain is divided into a finite number of quadrilateral control volumes and the discretization of the governing equation is performed following the finite volume approach. The convection terms are approximated by a higer-order bounded scheme HLPA developed by Zhu [9-1] and the unsteady terms are treated by the backward differencing scheme.

9.2.3 Momentum Interpolation Method

In the present study, the Rhie and Chow's scheme [9-2] is modified to obtain a converged solution for unsteady flows which is independent of the size of time step and relaxation factors. The momentum equations are solved implicitly at the cell-centered locations in the Rhie and Chow's scheme. The discretized form of momentum equations for the cell-centered velocity components can be written as follows with the under-relaxation factors expressed explicitly;

$$u_{1,P}=(H_{u_1})_P+(D_{u_1}^1)_P(P_w-P_e)_P+(D_{u_1}^2)_P(P_s-P_n)_P+(E_{u_1})_P u_{1,P}^{n-1}+(1-\alpha_{u_1})u_{1,P}^{l-1} \tag{9-11}$$

$$u_{2,P}=(H_{u_2})_P+(D^1_{u_2})_P(P_w-P_e)_P+(D^2_{u_2})_P(P_s-P_n)_P+(E_{u_2})_P u^{n-1}_{2,P}+(1-\alpha_{u_2})u^{l-1}_{2,P} \quad (9\text{-}12)$$

where

$$H_{u_i}=\alpha_{u_i}\left\{\sum A^{u_i}_{nb}u_{i,nb}+(S^{u_i}_c\,\Delta V)\right\}\Big/A^{u_i}_P \quad (9\text{-}13)$$

$$D^j_{u_i}=\alpha_{u_i}rb^j_i/A^{u_i}_P \quad (9\text{-}14)$$

$$E_{u_i}=\frac{\alpha_{u_i}\rho\Delta V}{\Delta t}\Big/A^{u_i}_P \quad (9\text{-}15)$$

$$A^{u_i}_P=\sum A^{u_i}_{nb}-S^{u_i}_P\Delta V+\frac{\rho\Delta V}{\Delta t} \quad (9\text{-}16)$$

and α_{u_i} are the under-relaxation factors for u_i velocity components and the superscripts $n-1$, $l-1$ denote the previous time step and iteration level, respectively. The discretized form of momentum equations for the cell-face velocity component, for example u_1 at the east face, can be written as follows;

$$u_{1,e}=(H_{u_1})_e+(D^1_{u_1})_e(P_P-P_E)+(D^2_{u_1})_e(P_{se}-P_{ne})+(E_{u_1})_e u^{n-1}_{1,e}+(1-\alpha_{u_1})u^{l-1}_{1,e} \quad (9\text{-}17)$$

In the present modified Rhie and Chow's scheme, this cell-face (the east face) velocity component is obtained explicitly through the interpolation of momentum equations for the neighboring cell-centered cylindrical velocity components. Following assumptions are introduced to evaluate this cell-face velocity component.

$$(H_{u_1})_e\approx f^+_e(H_{u_1})_E+(1-f^+_e)(H_{u_1})_P \quad (9\text{-}18)$$

$$(D^2_{u_1})_e(P_{se}-P_{ne})\approx f^+_e(D^2_{u_1})_E(P_s-P_n)_E+(1-f^+_e)(D^2_{u_1})_P(P_s-P_n)_P \quad (9\text{-}19)$$

$$\frac{1}{(A_P^{u_1})_e} \approx \frac{f_e^+}{(A_P^{u_1})_E} + \frac{(1-f_e^+)}{(A_P^{u_1})_P} \tag{9-20}$$

where f_e^+ is the geometric interpolation factor defined in terms of distances between nodal points. Similar assumptions can be introduced for evaluating the velocity components at the north face. Using above assumptions, the velocity component $u_{1,e}$ can be obtained as follows;

$$\begin{aligned} u_{1,e} = & \left[f_e^+ u_{1,E} + (1-f_e^+) u_{1,P} + (D_{u_1}^1)_e (P_P - P_E) - f_e^+ (D_{u_1}^1)_E (P_w - P_e)_E \right. \\ & \left. - (1-f_e^+)(D_{u_1}^1)_P (P_w - P_e)_P \right] + (1-\alpha_{u_1}) \left[u_{1,e}^{l-1} - f_e^+ u_{1,E}^{l-1} - (1-f_e^+) u_{1,P}^{l-1} \right] \\ & + \frac{\alpha_{u_1} \rho}{\Delta t} \left[\frac{(\Delta V)_e}{(A_P^{u_1})_e} u_{1,e}^{n-1} - f_e^+ \frac{(\Delta V)_E}{(A_P^{u_1})_E} u_{1,E}^{n-1} - (1-f_e^+) \frac{(\Delta V)_P}{(A_P^{u_1})_P} u_{1,P}^{n-1} \right] \end{aligned} \tag{9-21}$$

The term in the first bracket of right hand side of Eq. (9-11) is the original Rhie and Chow's scheme [9-2]. Majumdar [9-3] has revealed that omission of the term in the second bracket leads to a converged solution that is relaxation factor dependent. Recently, Choi [9-4] added the term in the last bracket to obtain the converged solution that is independent of the size of time step and relaxation factors for unsteady flow calculations.

9.2.4 Solution Algorithm

The SIMPLEC algorithm by Van Doormal and Raithby [9-5] is used for pressure-velocity coupling in the present study. In this algorithm the momentum equations are implicitly solved at cell-centered locations using Eqs. (9-1) and (9-2). Then the cell-face velocities are evaluated by Eq. (9-11). Since these starred velocities do not satisfy the continuity equation unless the pressure field is correct, they should be corrected to satisfy the continuity equation during the iteration process. The following velocity correction equations are assumed in the SIMPLEC algorithm.

$$u'_{1,e} = u_{1,e} - u^*_{1,e} = (D^1_{u_1})_e (P'_P - P'_E) / \left[1 - \alpha_{u_1} (\sum A^{u_1}_{nb} / A^{u_1}_P)_e\right] \tag{9-22}$$

$$u'_{2,e} = u_{2,e} - u^*_{2,e} = (D^1_{u_2})_e (P'_P - P'_E) / \left[1 - \alpha_{u_2} (\sum A^{u_2}_{nb} / A^{u_2}_P)_e\right] \tag{9-23}$$

Inserting above equations into the continuity equation leads to a pressure correction equation. After solving the pressure correction equation, the cell-face velocities are corrected by above equations and the cell-centered velocities are corrected by following equations.

$$u'_{1,P} = u_{1,P} - u^*_{1,P} = \left[(D^1_{u_1})_P (P'_w - P'_e) + (D^2_{u_1})_P (P'_s - P'_n) \right] / \left[1 - \alpha_{u_1} (\sum A^{u_1}_{nb} / A^{u_1}_P)_P\right] \tag{9-24}$$

$$u'_{2,P} = u_{2,P} - u^*_{2,P} = \left[(D^1_{u_2})_P (P'_w - P'_e) + (D^2_{u_2})_P (P'_s - P'_n) \right] / \left[1 - \alpha_{u_2} (\sum A^{u_2}_{nb} / A^{u_2}_P)_P\right] \tag{9-25}$$

The pressure correction equations as well as other algebraic equations of momentum equations, energy equation and turbulent transport equations are solved by the strongly implicit procedure by Stone [9-6] in the present study.

9.2.5 Treatment of Boundary Conditions

At the inlet both the velocity components and turbulent quantities are prescribed. At the outlet the zero gradient conditions are imposed while the velocity components are adjusted to satisfy the overall mass conservation. At the symmetry line the symmetry conditions are imposed. At the wall node both the velocity components are set to zero. For the near-wall control volumes, the wall shear-stress vector is expressed as a function of the nodal velocity component parallel to the wall. The wall shear stress is again decomposed in two components along u_1 and u_2, respectively, to be used as source terms in the corresponding momentum equations. The wall function method is used for the near-wall nodes.

9.3 Modeling

As shown in Fig. 9.1, in the case of one-dimensional model the steady-state hot pool coolant temperature is calculated in MAIN9S using the input values from MAIN9R and the transient hot pool temperature is calculated in MAIN9T. In UPLS6T the hot pool energy variation is calculated and is corrected by prediction-correction method in INTG1T. And then correct hot pool temperature is fixed in UQIV1T. Therefore, two-dimensional hot pool coolant temperature is calculated by coupling the developed two-dimensional hot pool model with UPLS6T

As shown in Fig. 9.2, the developed two-dimensional hot pool model consists of three subprograms, i.e, BFC, FLOW2D and UFLOW2D. In BFC the grid is generated automatically. In FLOW2D steady-state hot pool coolant temperature and velocity distributions are calculated and are used as input values of UFLOW2D. In the UFLOW2D coupled with UPLS6T, the transient hot pool coolant temperature and velocity distributions are calculated. In Figs. 9.3 and 9.4, the flowcharts of each subprogram are illustrated.

The main functions of the subprograms are as follows;

BF	grid generation module
BINDEX	calculate location adress for the near boundary nodes
BKIND	define various boundary conditions
BOUNDP	extrapolate pressure at boundary nodes
BOUNDS	call appropriate boundary conditions
CDFLUX	calculate cross-derivative fluxes
COEFF	calculation of algebraic coefficients of transport equations HLPA scheme on non-uniform grid
COFCON	calculate coefficients for pressure correction equation and face convective fluxes using momentum interpolation (SIMPLEC)
CWCS	initializing mass fluxes
FLOSOL	solving all the conservation equations transient
GEOMET	calculate geometric coefficients and center-points of control volume
INFORM	printing important informations
INP	read input variables
INPUT	read input variables

MFLOW2D	numerical solution of incompressible flows on a nonorthogonal grid using momentum interpolation method - steady
MUFLOW2D	numerical solution of incompressible flows on a nonorthogonal grid using momentum interpolation method - transient
OUTPUT	print output variables
PDTST	calculate pressure difference
PRINT	print major output
PROPS	calculate fluid properties
PVFC	correct velocity, flux and pressure
SFLOSOL	solving all the conservation equations - steady
SOLVE	numerical scheme: Stone's strongly implicit method - transient
SOURCE	calculation of sources for the conservation equations
SSOLVE	numerical scheme: Stone's strongly implicit method - steady
SSTART	initialize some variables - steady
START	initialize some variables - transient
SUSER	user define module - steady
TPLOT	plotting module
USER	user define module - transient

9.4 Sample Run

9.4.1 Constant Inlet Temperature Increase

The KALIMER design is a pool-type system, with the entirety of the primary heat transport system contained within the reactor vessel. During normal operation, the sodium core inlet and outlet temperatures are 386℃ and 530℃, and the other initial conditions used and important system parameters are listed in Table 9-1. In the case of two-dimensional model, the hot pool is modeled as shown in Fig. 9.5. The input parameters of the two-dimensional hot pool model named HP2D are core outlet temperature and flowrate. In the model, the temperature and velocity distributions in the hot pool are calculated.

Firstly, in the case of constant inlet temperature increase, we compare the prediction accuracy between one- and two-dimensional hot pool model. During normal operation, the sodium bulk temperature of the hot pool is 530℃ and flowrate is 2143.1kg/sec. Also the sodium

velocity distribution in the hot pool is shown in Fig. 9.6. In the case that the hot pool sodium inlet temperature increases from 530℃ to 647℃ suddenly, the hot pool sodium temperature increases until it reaches to the inlet temperature. As shown in Fig. 9.7, the temperature behaviors of the both models are quite different. In the one-dimensional model, the outlet temperature increases slowly and immediately, and is reached to 645℃ after 420 seconds. However, in the two-dimensional model, the outlet temperature is not changed until 20 seconds and then increases steeply. The outlet temperature is reached to 645℃ after 250 seconds.

In two-dimensional model, the outlet sodium temperature is affected by the inlet sodium temperature change after several tens of seconds during normal operation and is more actual qualitative prediction than one-dimensional model. The time delay can alter the overall reactor system response, so that it is necessary to predict the hot pool sodium temperature distribution with sufficient accuracy.

9.4.2 Unprotected Transient Overpower Events

An unprotected transient overpower (UTOP) event results when positive reactivity is inadvertently inserted into the core and there is a failure to scram. The limiting case assumption is that all the control rods are accidently removed. The event is initiated from full power. The control rods are assumed to begin withdrawing with a speed of 0.67 cents per second. The control rod stops are set to limit the withdrawal worth to 10 cents. The UTOP transient results for hot pool temperatures, power and flow in both cases of one- and two-dimensional models are shown in Figs. 9-8 through 9-10. As shown in Fig. 9.6, the power reaches a peak of 1.130 and 1.124 times the rated power at 34 and 27 seconds into the transient, and begins to level off at 1.019 and 1.021 times the rated power in the case of one- and two-dimensional model cases, respectively.

In the case of one-dimensional model, the hot pool inlet temperature increases from a normal value of 530℃ to a peak of 551℃ and outlet temperature increases from 530℃ to a peak of 543℃ and then the inlet and outlet temperatures are reestablished at around 542℃, which is 12℃ above the initial temperature, as shown in Fig. 9.9. On the other hand, in the case of two-dimensional model, the hot pool inlet temperature increases from 530℃ to 550℃ and outlet temperature increases from 530℃ to 546℃, and then the inlet and outlet temperatures are

reestablished at around 543℃, which is 13℃ above the initial temperature. The outlet temperature is not affected by the inlet coolant until 25 seconds.

As a result of this comparison, it is considered that the time delay effect of the hot pool affects the core inlet sodium temperature. And then core inlet sodium temperature change affects the reactivity feedback and reactor power also. Therefore, it seems that the two-dimensional modeling of the hot pool can predict the overall reactor system response more realistic than one-dimensional model.

Table 9-1

Initial and Key Operating Parameters

Power (MWth)	392.2
Number of IHTS loops	2
Cover gas pressure (MPa)	0.1013
Primary sodium flowrate (kg/s)	2143.1
Primary sodium core outlet temperature (℃)	530.0
Primary sodium core inlet temperature (℃)	386.2
Number of Primary pumps	4
Intermediate sodium flowrate (kg/s)	1803.6
IHX-IHTS inlet temperature (℃)	339.7
IHX-IHTS outlet temperature (℃)	511.0
Number of IHXs	4
Number of SGs	2
Steam flowrate (kg/s)	155.5
Steam temperature (℃)	483.2
Steam pressure (MPa)	15.5

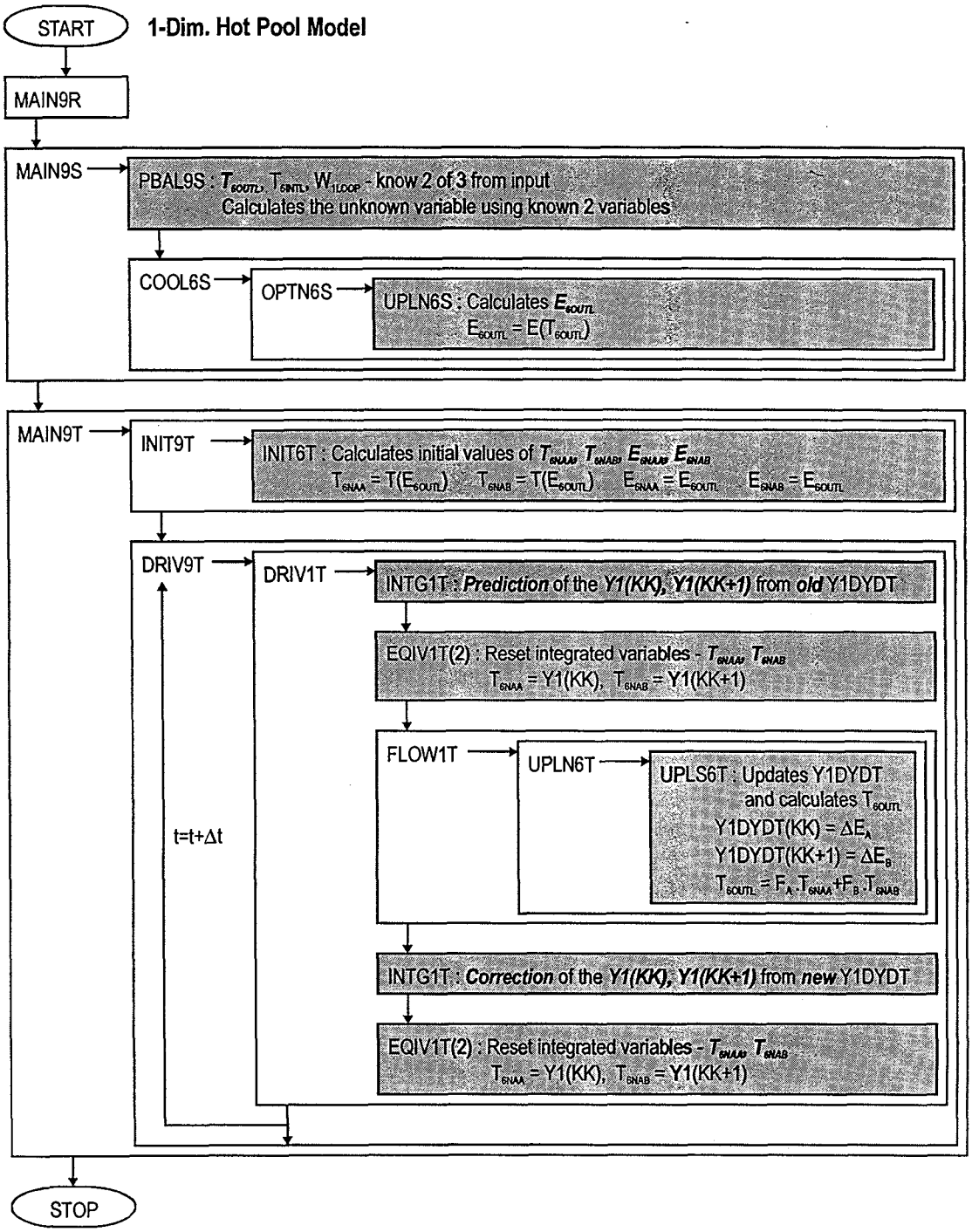

Fig. 9.1 Flowchart of One-dimensional Hot Pool Model

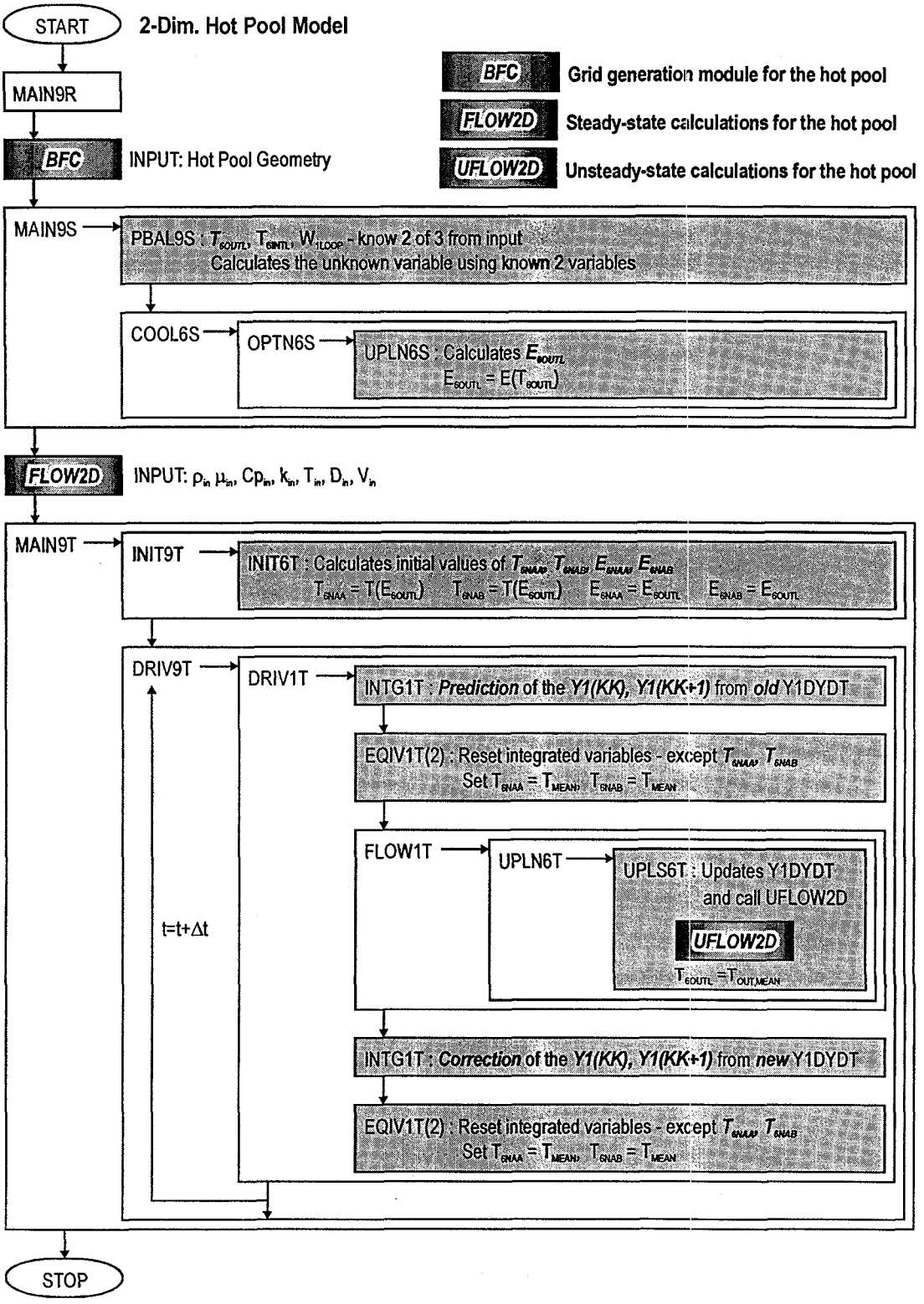

Fig. 9.2 Flowchart of Two-dimensional Hot Pool Model

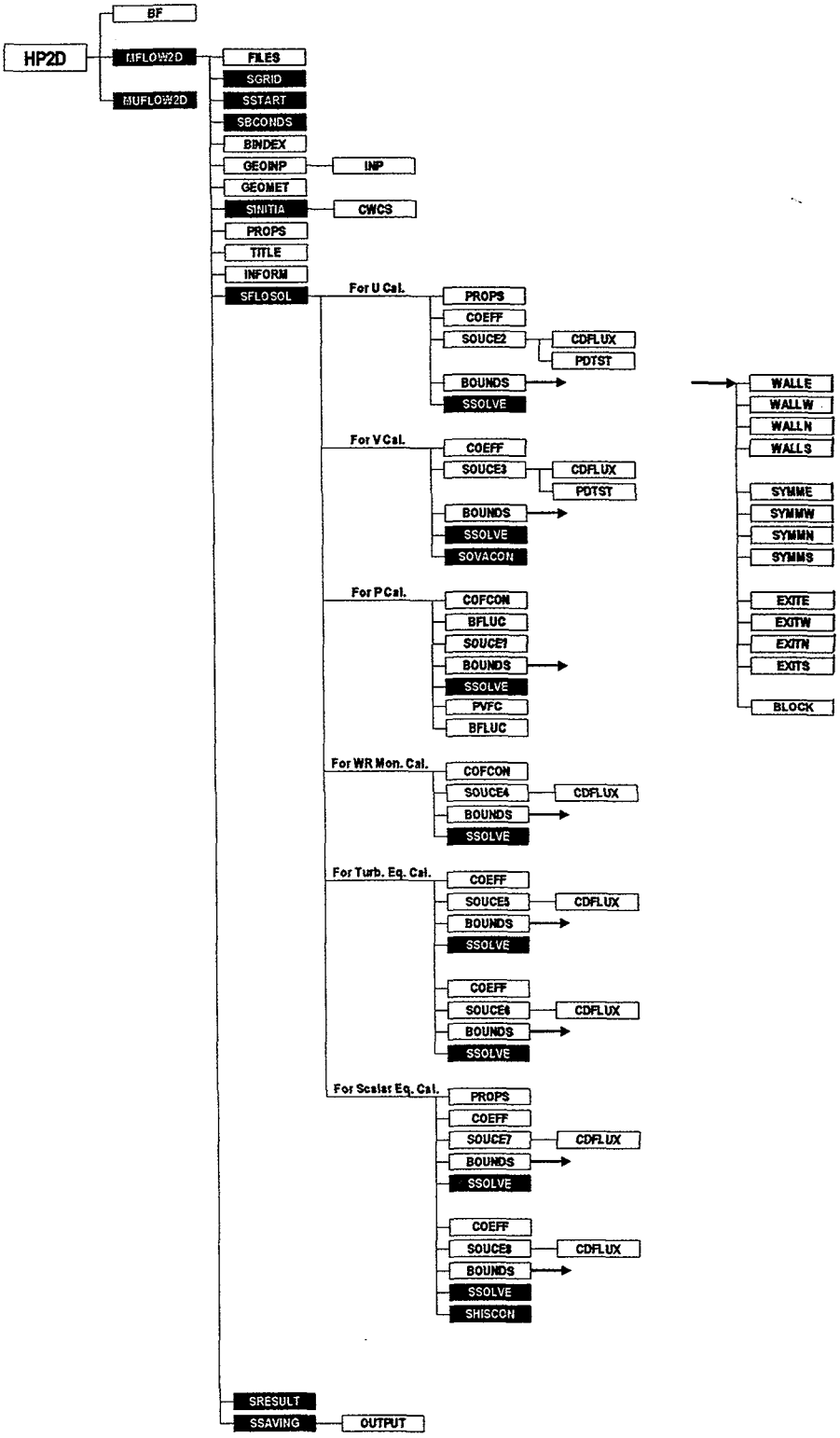

Fig. 9.3 Flowchart of HP2D; Steady-State

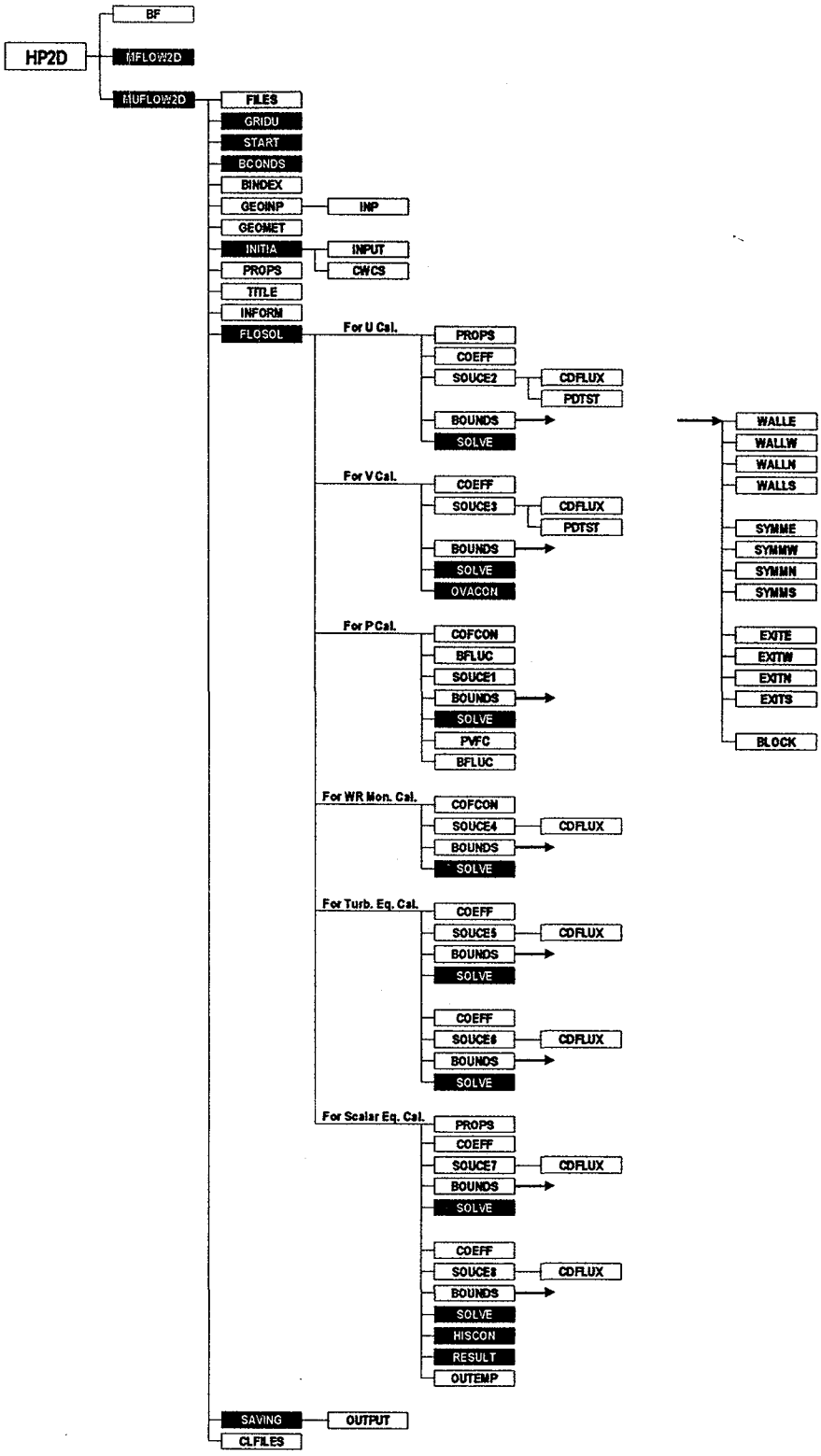

Fig. 9.4 Flowchart of HP2D; Transient

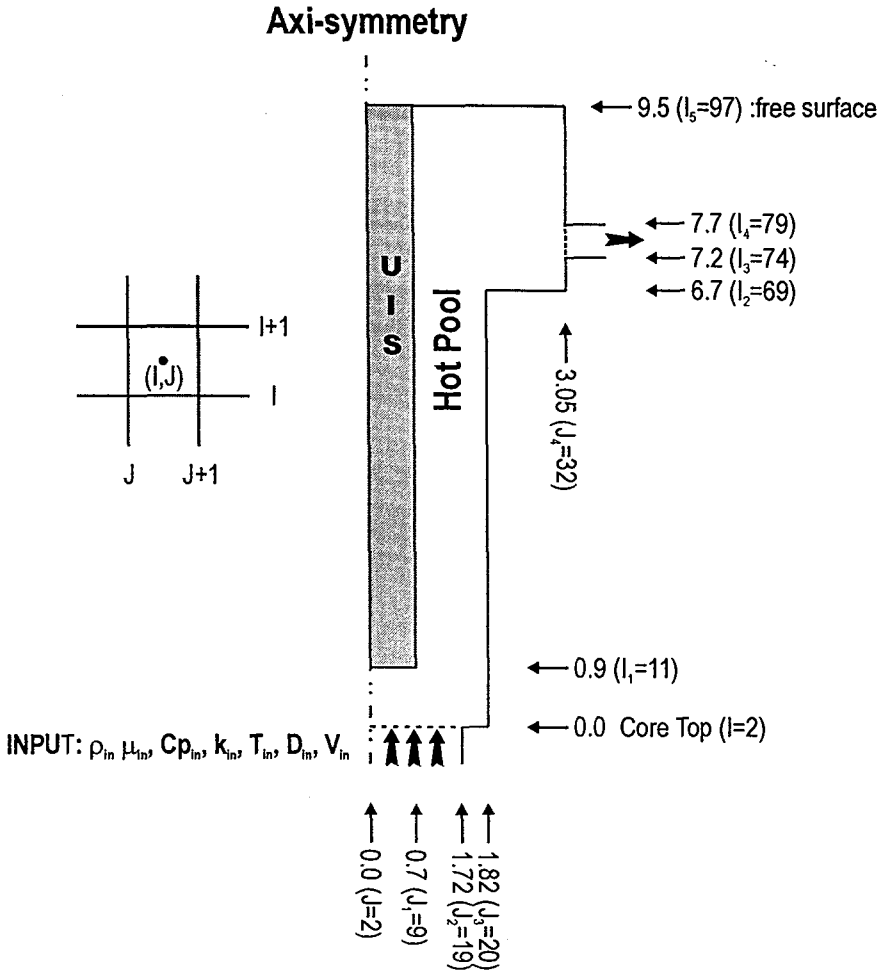

Fig. 9.5 Two-Dimensional Hot Pool Model

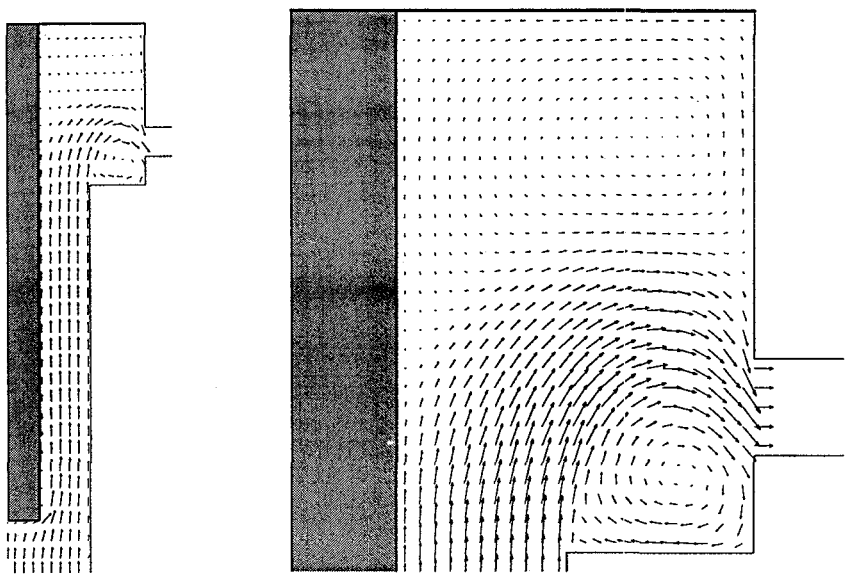

Fig. 9.6 Sodium Velocity Distribution in Hot Pool during Normal Operation

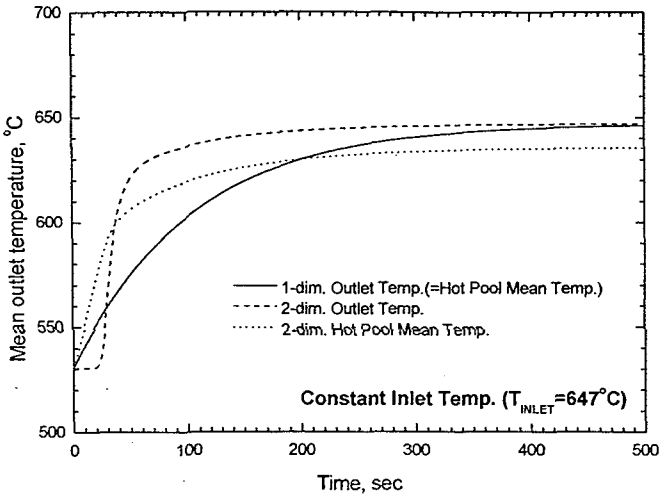

Fig. 9.7 Hot Pool Sodium Outlet Temperatures

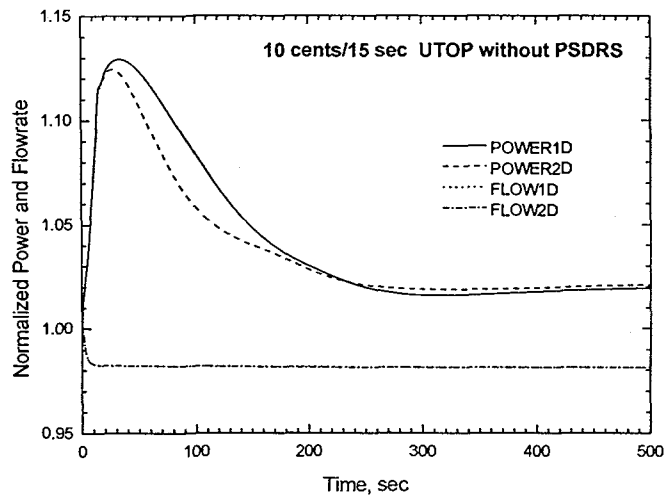

Fig. 9.8 Power and Flow during 10 Cent UTOP

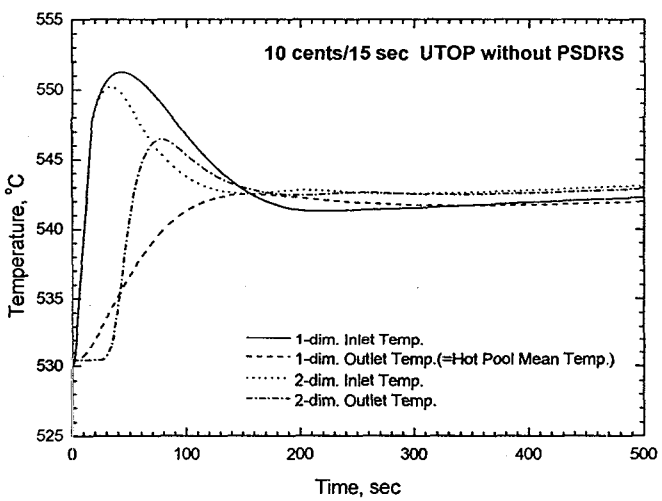

Fig. 9.9 Hot Pool Temp. during 10 Cent UTOP

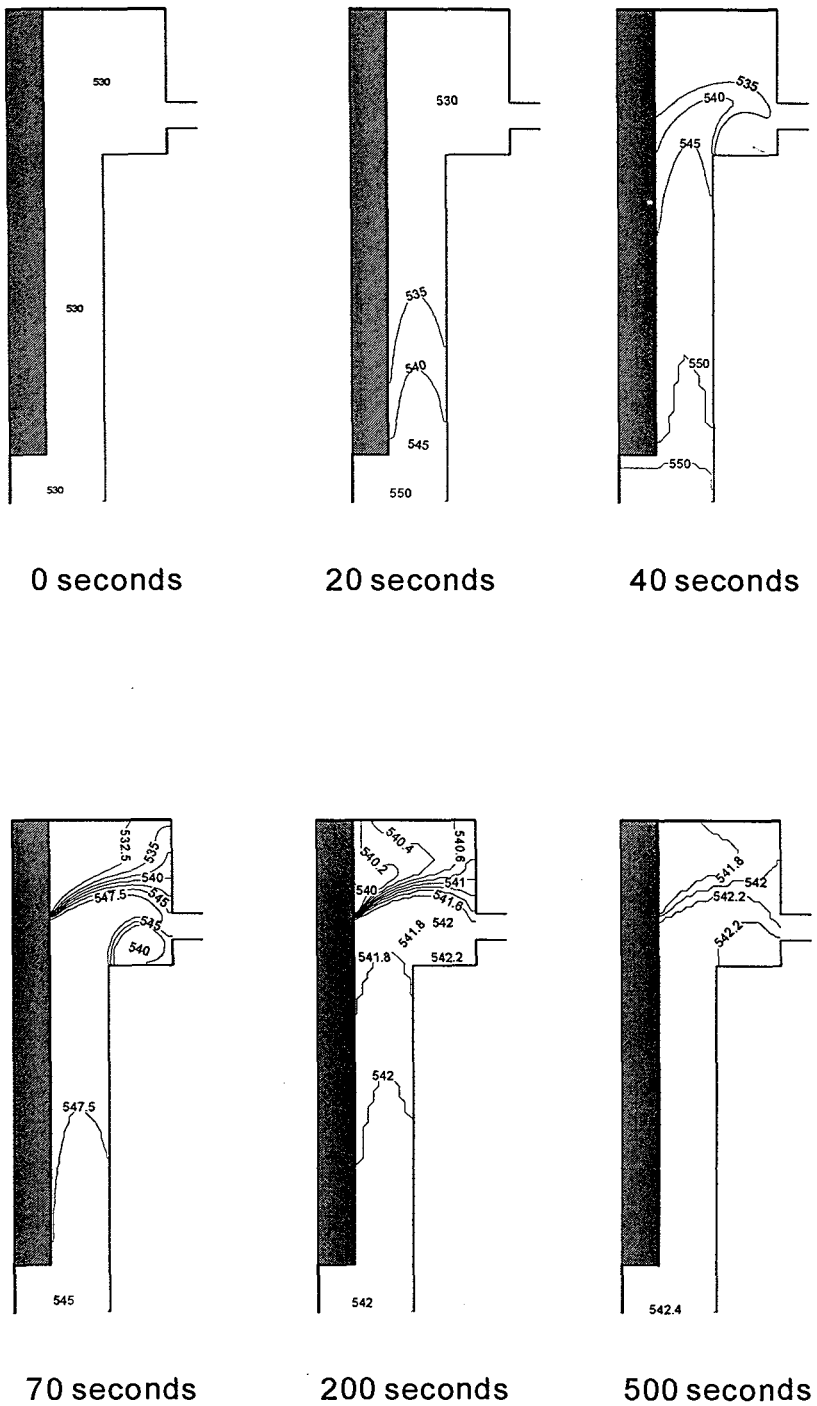

Fig. 9.10 Hot Pool Temperature Distribution during 10 Cent UTOP

REFERENCES

1-1 C. K. Park, et. al. "KALIMER Design Concept", KAERI/TR-888/97.

1-2 J. G. Guppy, et al., "Super System Code – An Advanced Thermohydraulic Simulation Code for Transients in LMFBRs," NUREG/CR-3169, BNL, (1983).

6-1 Lee W. Johnson et al, "Numerical Analysis", Addson-Wesley Publishing Company

8-1 LIFE-II Committee, ANL, Priv. Comm, (1973).

8-2 R.G. Gibbym, L. Leibowitz, J.F. Kerrisk and D.G Clifton, "Analytical Expressions for Enthalpy and Hear Capacity for Uranium-Plutonium Oxide," HEDL-TME 73-60, June (1973).

8-3 B.F. Rubin, "Summary of (U, Pu) O_2 properties and Fabrication Methods, "GEAP-1582, (November 1970).

8-4 M.F. Lyons, et al., "U O_2 Properties Affecting Performance," Nucl. Eng. & Design 21, 167 (1972).

8-5 Thermophysical Properties of Matter, "Thermal Radioactive Properties of Non-Metallic Solids," Vol. 8 edited by Y.S. Touloukian (1972).

8-6 "Mechanical and Physical Properties of the Austenitic Chromium-Nickel Stainless Steels at Elevated Temperature," The International Nickel Company, Inc., New York (1963).

8-7 C.S. Kim, "Thermophysical Properties of Stainless Steel," ANL 78-55 (1975).

8-8 J. Humphries, "On the Thermal Emittance of Stainless Steels," J. of British Nucl. Energy Soc. 1, 271 (1974).

8-9 ~ 8-14 blank

8-15 "A Compilation of Boron Carbide Design Support Data for LMFBR Control Elements," HEDL-TME 78-19 (1975).

8-16 G.H. Golden and J.V. Tokar, "Thermophysical Properties of Sodium," ANL-7323 (August 1967).

8-17 F.E. Dunn, G.J. Fischer, T.J. Heams, P.A. Pizzica, N.A. McNeal, W.R. Boh1 and S.M. Prestein, "The SAS2A LMFBR Accident Analysis computer Code," ANL-8138 (October 1974).

8-18 W. Wulff, et al., "Development of a Computer Code for Thermal hydraulics of Reactors (THOR)," Fifth Ouarterly Progress Report, Sect. 3.2, BNL-NUREG-50534 (July 1976).

8-19 C.F. Bonill, "Fluid Flow in Reactor Systems," Nuclear Engineering Handbook, pp. 9-30, edited by H. Etherington, McGraw-Hill book Company, Inc., New York (1958).\

8-20 C. F. Colebrook, "Turbulent Flow in Pipes with Particular Reference to the transition Region Between Smooth and Rough Pipe Laws," Journal of Institution Civil Engineers, Vol.11, pp.133-156. (1939).

8-21 S. Levy, "Fluid Flow," Ch. 15 in The Technology of Nuclear Reactor Safety, Vol. 2, edited by T.J. Thompson and J.G. Beckerly, the M.I.T. Press, Cambridge, Massachusetts (1973).

8-22 J. Zigrang and N. D. Sylvester, "A Review of Explicit Friction Factor Equations," Trans ASME, J. Energy Resources Technology, Vol.107, pp.280-283 (1985).

8-23 N. E. Todreas and M.S. Kazimi, Nuclear System I – Thermal Hydraulic Fundamentals, Hemisphere Publishing Corp. (1990).

8-24 F. C. Engel, R. A. Markley, and A. A. Bishop, "Laminar, Transition, and Turbulent Parallel Flow Pressure Drop Across Wire-Wrap-Spaced Rod Bundles," Nucl. Sci. Eng., Vol.69. pp.290-296 (1979).

8-25 Y. N. Chan and N. E. Todreas, "A Simple LMFBR Axial Flow Friction Factor Correlation," MIT Report DOE/ET/37240-92TR, Rev.I (1982).

8-26 HEDL-TI-76049, "Covered pressure drop flow test / Crossflow mixing test" (1976).

8-27 W. L. Thorne, HEDL-TC-812, "Pressure drop measurements in FFTF fuel vibration tests" (1977).

8-28 W. L. Throne, HEDL-TC-824, "Pressure drop measurements from fuel assembly vibration test" (1977).

8-29 PSAR-1975, "Preliminary safety analysis report," Clinch River Breeder Reactor Project with amendment through (1982).

8-30 N. Lyon, "Liquid metal heat transfer coefficients," Chem. Engn. Prog. Vol.47, p.75 (1951).

8-31 R. A. Seban and T. Shimazaki, "Heat Transfer to a Fluid Flowing Turbulently in a Smooth Pipe with Walls at Constant Temperature," ASME Paper, 50-A-128 (1950).

8-32 S. Aoki, "Current Liquid-Metal Hear Transfer Research in Japan," Progress Metals Flowing In-Line Through Tube Bundles," Progress in Hear & Mass Transfer, Vol. 7, pp. 569-573, edited by O.E. Dwyer, Pergamon Press, Inc., Elmsford, New York (1973).

8-33 R. A. Seban, "Heat Transfer to a Fluid Flowing Turbulently between Parallel Walls and Asymmetric Wall Temperatures," Trans. ASME, Vol.72, p.789 (1957).

8-34 S. Kazimi, "Heat Transfer Correlation for Analysis of CRBRP Assemblies," WARD-D-0034 (April 1974).

8-35 M. S. Kazimi and M. D. Carelli, "Heat Transfer Correlation for Analysis of CRBRP Assemblies," Westinghouse Report, CRBRP-ARD-0034 (1976).

8-36 H. Graber and M. Rieger, "Experimental Study of Heat Transfer to Liquid Metals Flowing In-line through Tube Bundles," Prog. Heat Mass Transfer, Vol.7, p.151 (1973.)

8-37 V. M. Borishanskii, M. A. Gotorsky, and E. V. Firsova, "Heat Transfer to Liquid Metal Flowing Longitudinally in Wetted Bundles of Rods," atomic energy, Vol.27, p.549 (1969).

8-38 F.W. Dittus and L.K. Boelter, Univ. of Calif. Publs. Eng. 2, 433 (1930).

8-39 J.G. Chen, "Correlation for Boiling Hear Transfer to Saturated Fluids in convective Flow," I&EC Process Design and Development 5, 322 (1966).

8-40 R.W. Lockhart, and R.C. Martinelli, "Proposed Correlation of Data for Isothermal Two-Phase, Two-Component Flow in Pipes," Chem. Eng. Prog. 45(1), 39 (1949).

8-41 A.A. Bishop, R.O. Sandberg and L.S. Tong, "Forced convection Hear Transfer at High Pressure after Critical Hear Flux," ASME Paper 68-HT-31 (1965).

8-42 J.B. Heineman, " An Experimental Investigation of Heat Transfer to Superheated Steam in Round and Rectangular Channels," ANL-6213 (1960).

8-43 R.B. Harty, "Modular Steam Generator Final Project Report," TR-097-330-010 (September 1974).

9-1 J. Zhu, "A Low-Diffusive and Oscillation Free Convection Schemes", Communications in Applied Numerical Methods, Vol. 7, pp. 225-232 (1991).

9-2 C. M. Rhie and W. L. Chow, "Numerical Study of the Turbulent Flow Past an Airfoil with Trailing Edge Separation", AIAA Journal, Vol. 21, pp. 1525-1532 (1983).

9-3 S. Majumdar, "Role of Underrelaxation in Momentum Interpolation for Calculation of Flow with Nonstaggered Grids", Numerical Heat Transfer, Vol. 13, pp. 125-132 (1988).

9-4 S. K. Choi, "Note on the Use of Momentum Interpolation Method for Unsteady Flows", Numerical Heat Transfer, Part A, Vol. 36, pp. 545-550 (1999).

9-5 J. P. Van Doormal and G. D. Raithby, "Enhancements of the SIMPLE Method for Predicting Incompressible Fluid Flows", Numerical Heat Transfer, Vol. 7, pp. 147-163 (1984).

Appendix A SSC-K INPUT DESCRIPTION

The basic component of the SSC-K input is the input record. These records are grouped on a modular basis to form subdivisions of the input, which in turn are referred to as data files. Each data file has been assigned a file name to delimit as well as to identify the file partitioning. The entire sequence of input records constitutes the input file.

File name:

VESSEL	Core and in-vessel components
NALOOP	Primary and secondary heat transport system
MINETD	Steam generator and balance-of-plant
OPDATA	Overall plant operating conditions
MATDAT	material properties
OLDATA	User initiated program control
TRNDAT	Conditions to initiate transient scenario
PSDRS	Passive decay heat removal system

In-Vessel Data (VESSEL)

Geometric and hydraulic data required to specify the core and in-vessel components

Rec.	Variable	Description	Unit
1	**L6RTYP**	Reactor type 0 = loop type, 1 = pool type	
	N6CHAN	Number of channels being simulated	
	N5RTYP	Number of rod types	
	N5ASEC(L)	Number of axial sections (slices) of each rod type (L=1,N5RTYP)	
	N5NFR(K)	Number of radial fuel nodes in an axial slice of each channel (K=1,N6CHAN)	
2	**L6ATYP(K)**	Rod type assigned to each channel. Also used for friction factor correlation. See Eqs. 5.71-5.73 for acceptable type	

		selections (K=1,N6CHAN):	
		2 for blanket assemblies, 3 for control assemblies	
3	**F6TPOW(K)**	Fraction of total power in each channel	
		(K=1,N6CHAN)	
4	**F6FLOW(K)**	Fraction of total vessel flow in each channel	
		(K=1,N6CHAN)	
5	**N5ASSY(K)**	Number of assemblies represented by each channel	
		(K=1,N6CHAN)	
6	**A6ROD(K)**	Sodium flow area per rod in each channel	
		(K=1,N6CHAN)	[m^2]
8	**Y6HYDR(K)**	Hydraulic diameter of each coolant channel	
		(K=1,N6CHAN)	[m]
11	**X5FIR(K)**	Fuel inner radius of each channel (K=1,N6CHAN)	[m]
12	**X5FOR(K)**	Fuel outer radius of each channel (K=1,N6CHAN)	[m]
13	**X5CLIR(K)**	Cladding inner radius of each channel (K=1,N6CHAN)	[m]
14	**X5CLOR(K)**	Cladding outer radius of each channel (K=1,N6CHAN)	[m]
15	**X5LBIR(K)**	Lower blanket inner radius of each channel	
		(K=1,N6CHAN)	[m]
16	**X5LBOR(K)**	Lower blanket outer radius of each channel	
		(K=1,N6CHAN)	[m]
17	**X5UBIR(K)**	Upper blanket inner radius for each channel	
		(K=1,N6CHAN)	[m]
18	**X5UBOR(K)**	Upper blanket outer radius for each channel	
		(K=1,N6CHAN)	[m]
19	**F5ASTR(K)**	Fractional heat transfer area of structure used per	
		channel (K=1,N6CHAN)	
20	**H5NOGP(K)**	Heat transfer coeff. for fuel-clad contact for each	
		channel (K=1,N6CHAN)	[W/K,m^2]
21	**P5FGAS(K)**	Fission gas pressure for each channel	
		(K=1,N6CHAN)	[N/m^2]
23	**L6WOPT**	Flow fraction option indicator	
		0 - fractions known, 1 - fractions unknown	
	F6LSA4(K)	Total K-loss coeff. at top of each channel	
		(K=1,N6CHAN)	
	F6LSBP	Bypass flow K-loss coeff.	
	P6DSGN	When L6WOPI=0, Actual nozzle to nozzle pressure	

		drop	[N/m^2]
		When L6WOPI=1, Core design delta-P (used in P6INLT guess)	[N/m^2]
	W6DSGN	Design core flow rate	[kg/s]
	N6PMAX	Maximum iteration for pressure calculation	
	N6FLMX	Maximum iterations for flow calculation	
	F6CONV	Convergence criterion (relative)	
	F6WSTP	Maximum flow fraction change allowed per iteration	
	P6STEP	Maximum pressure change allowed per iteration Note: Non-zero value(s) need be assigned only when L6WOPT=1.	[N/m^2]
24	**V6LP**	Volume of lower plenum	[m^3]
	B6LPMC	Mass heat capacity of metal in lower plenum	[J/K]
	H6LPUA	Overall heat transfer coefficient in lower plenum	[W/K]
	A6LPLF	Cross-sectional flow area of lower plenum	[m^2]
	F6PKLP	If >0, total K-loss coeff. from inlet nozzle elevation to core bottom. If <0, total K-loss press. drop from inlet nozzle elevation to core bottom.	
25	**L5MESH**	Fuel radial mesh indicator: 0 - equal radius, 1 - equal area	
	T5REF	Temperature at which the rod dimensions are referenced	[K]
26		set as 0	
27	**Z6REF**	Reference elevation of reactor vessel	[m]
		Refer to Fig.1.1 for the below variables	
	Z6INOZ	Elevation of vessel inlet nozzle above Z6REF	[m]
	Z6BCOR	Elevation of bottom of core above Z6REF	[m]
	Z6TCOR	Elevation of top of core above Z6REF	[m]
	Z6UPLN	Elevation of initial upper plenum sodium level above Z6REF	[m]
	Z6ONOZ	Elevation of vessel outlet nozzle above Z6REF (loop) or elevation of IHX inlet nozzle above Z6REF (pool)	[m]
	Z6UPTL	Elevation of top of thermal liner above Z6REF	[m]
	Z6VSTP	Elevation of top of vessel above Z6REF	[m]
28	**A6GL**	Area between gas and liquid in vessel upper plenum (same as flow cross-sectional area)	[m^2]

	A6GM1	Area between gas and metal 1 in vessel upper plenum	[m^2]
	A6GM2	Area between gas and metal 2 in vessel upper plenum	[m^2]
	A6GM3	Area between gas and metal 3 in vessel upper plenum	[m^2]
	A6LM1	Area between liquid and metal 1 in vessel upper plenum	[m^2]
	A6LM2	Area between liquid and metal 2 in vessel upper plenum	[m^2]
	A6JET	Area of core jet flow	[m^2]
	H6GAS	Heat transfer coeff. for cover gas in upper plenum	[W/Km^2]
	H6LNA	Heat transfer coeff. at interface of two sodium zones in upper plenum	[W/Km^2]
	H6INF	Heat transfer coeff. at interface of two sodium zones in upper plenum	[W/Km^2]
	Z6CHIM	Length of chimney above core outlet	[m]
	F6PKUP	If >0, total K-loss coeff. from core top to outlet nozzle elevation. If <0, total K-loss P-drop from core top to outlet nozzle elevation.	[N/m^2]
	F6LEAK	Fraction of bypass flow leaking directly into upper plenum from lower bypass region	
	B6UMC1	Mass heat capacity of metal 1 in upper plenum	[J/K]
	B6UMC2	Mass heat capacity of metal 2 in upper plenum	[J/K]
	B6UMC3	Mass heat capacity of metal 3 in upper plenum * See 3.1.3 Upper Plenum of SSC-K Manual for descriptions of Metals 1, 2 and 3.	[J/K]
29	**A6LFBP**	Flow area of lower region of bypass channel	[m^2]
	A6UFBP	Flow area of upper region of bypass channel	[m^2]
	Y6LRBP	Hydraulic diameter of lower bypass region channel	[m]
	Y6URBP	Hydraulic diameter of upper bypass region channel	[m]
	F6INBP	If >0, total K-loss coeff. at bypass inlet. If <0, total K-loss P-drop at bypass inlet.	[N/m^2]
	H6ABP	Overall heat transfer coeff. between upper bypass region sodium and liner	[W/K]
30	**F6FRC1**	Coeff. used in friction factor correlation for rod bundles (Eq. 8-71)	
	F6FRC2	Coeff. used in friction factor correlation for rod bundles (Eq. 8-71)	
	F6NUC1	Coeff. used in Nu number correlation (Forced	

		convection - Rod Bundle) (Eq. 8-75)	
	F6NUC2	Coeff. used in Nu number correlation (Forced convection - Rod Bundle) (Eq. 8-75)	
	F6NUC3	Coeff. used in Nu number correlation (Forced convection - Rod Bundle) (Eq. 8-75)	
	F6NUC4	Exp. used in Nu number correlation (Forced Convection - Rod Bundle) (Eq. 8-75)	
31	**Y6HYOZ(K)**	Hydraulic diameter of inlet orifice zone of each channel (K=1,N6CHAN) Note: Of the three parameters Y6HYOZ, P6FINZ, and F6ZINZ, two must be non-zero. The other is zero for each channel.	[m]
32	**F6LSA(1,K)**	K-loss pressure at inlet orifice zone for each channel (K=1,N6CHAN)	
	F6LSA(2,K)	K-loss pressure at assembly outlet for each channel (K=1,N6CHAN) Note: If value positive, the actual K-loss factor. If value negative, the K-loss pressure drop. Note: Data for this consists of a series of paired points. The index K is incremented over the set of all data required. That is, F6LSA(1,1), F6LSA(2,1), F6LSA(1,2), etc.	$[N/m^2]$
33	**P6FINZ(K)**	Pressure drop due to friction across the inlet orifice zone for each channel (K=1,N6CHAN) Note: Of the three parameters Y6HYOZ, P6FINZ, and F6ZINZ, two must be non-zero. The other is zero for Each channel.	$[N/m^2]$
34	**F6ZINZ(K)**	Fraction of assembly inlet orifice zone length (Z6INZ) assigned to each channel (K=1,N6CHAN) Note: Of the three parameters Y6HYOZ, P6FINZ, and F6ZINZ, two must be non-zero. The other is zero for each channel.	
39		set to 0.	
41		set to (N6CHAN), 0	
101 - 199		(Implied rod type dependency, L = Number - 100)	
	Z6LFGP	Axial length of lower fission gas plenum region of L-th rod type	[m]

Z6LBLK	Axial length of lower blanket region of L-th rod type	[m]
Z6AFUL	Axial length of active fuel region of L-th rod type	[m]
Z6UBLK	Axial length of upper blanket region of L-th rod type	[m]
Z6UFGP	Axial length of upper fission gas plenum region of L-th rod type	[m]
N6LFGP	Number of axial coolant nodes in lower fission gas plenum region of L-th rod type	
N6LBLK	Number of axial coolant nodes in lower blanket region of L-th rod type	
N6AFUL	Number of axial coolant nodes in active fuel region of L-th rod type	
N6UBLK	Number of axial coolant nodes in upper blanket region of L-th rod type	
N6UFGP	Number of axial coolant nodes in upper fission gas plenum region of L-th rod type	
F6PD	Pitch to diameter ratio of L-th rod type	
F6PWD	Pitch to diameter ratio for wire wrap of L-th rod type	
L5CLMT	Index of cladding material of L-th rod type	
L5STMT	Index of structural material of L-th rod type	
L5LBMT	Index of lower blanket material of L-th rod type	
F5DLBU	Fractional unrestructured grain density of lower blanket of L-th rod type	
F5DLBE	Fractional equiaxed grain density of lower blanket of L-th rod type	
F5DLBC	Fractional columnar grain density of lower blanket of L-th rod type	
L5AFMT	Index of active fuel material of L-th rod type	
F5DAFU	Fractional unrestructured grain density of active fuel of L-th rod type	
F5DAFE	Fractional equixed grain density of active fuel for L-th rod type	
F5DAFC	Fractional columnar grain density of active fuel for L-th rod type	
L5UBMT	Index of upper blanket material of L-th rod type	
F5DUBU	Fractional unrestructured grain density of upper blanket of L-th rod type	
F5DUBE	Fractional equxiaxed grain density of upper blanket of	

	L-th rod type	
F5DUBC	Fractional columnar grain density of upper blanket of L-th rod type	
N5AROD	Number of rods per assembly of L-th rod type	
Y5WIRE	Wire wrap diameter of L-th rod type	[m]
Y5FLAT	Hex-Can flat-to-flat inner diameter of L-th rod type	[m]
X5HXCN	Total Hex-Can wall thickness of L-th rod type	[m]
Z6INZ	Length of the inlet hydraulic orifice zone of L-th rod type	[m]
201 - 299	(Implied channel dependency, K = Number - 200)	
F5PAX(J)	Axial power fraction for each node in the K-th channel (J=N5ASEC(L5ATYP(K)))	
301 - 399	(Implied channel dependency, K = Number - 300)	
F5PRAD(I)	Fuel power fraction in each radial fuel node in the K-th Channel (I=N5NFR(K)) Note: No axial dependence	
401 - 499	(Implied channel dependency, K = Number - 400)	
F5PWR5	Fraction of power generated in the K-th channel deposited directly into the fuel	
F5PWR6	Fraction of power generated in the K-th channel deposited directly into the clad	
F5PWR1	Fraction of power generated in the K-th channel deposited directly into the coolant	
501 - 599	(Implied channel dependency, K = Number - 500)	
L5GAS(I)	Index of each fission gas type in the K-th channel	
F5GAS(I)	Mole fraction of each fission gas in the K-th channel Note: Data for this consists of a maximum of 3 paired points. The index I is incremented over the set of all data required for the That is, L5GAS(1), F5GAS(1), L5GAS(2), F5GAS(2), etc.	

Sodium Loop Data (NALOOP)

Geometric and hydraulic data required to specify the primary and secondary loop piping, pumps and IHX.

Rec.	Variable	Description	Unit
1		Must be the first in file NALOOP	
	N1LOOP	Number of primary loops simulated	
	N1PIPE	Number of pipes in primary loop	
	N1NODE(J)	Number of nodes in each pipe of primary loop (J=1,N1PIPE)	
	N2PIPE	Number of pipes in intermediate loop	
	N2NODE(J)	Number of nodes in each pipe of intermediate loop (J=1,N2PIPE) Note: There exists an implied maximum number of data elements for any record. At present this limit is 99. This may restart the heat transport system nodalization.	
2	**F1LUMP(K)**	Number of actual loops in each simulated loop (K=1,N1LOOP)	
100	**N1TUBE**	Number of tubes in IHX	
	Y1TUB1	Inner diameter of IHX tubes	[m]
	Y1TUB2	Outer diameter of IHX tubes	[m]
	A1IHX	Flow area on primary side of IHX	[m^2]
	V1BYP	Volume of sodium in IHX primary bypass	[m^3]
	V1IHX	Volume of sodium in IHX primary heat exchange region	[m^3]
	B1SHEL	Mass of IHX shell	[kg]
	A1SHEL	Heat transfer area of IHX shell	[m^2]
	F1POD	Pitch-to-diameter ratio for IHX tube bundle	
	H1FLP	Fouling resistance on outer (primary) surface of tubes	[m^2 K/W]
	H1FLS	Fouling resistance on inner (secondary) surface of tubes	[m^2 K/W]
	L1STRC	Primary loop structural material ID	
101	**L1FDIR**	IHX flow indicator: 1 = parallel flow in IHX, -1 = counter flow	
	L1KP	Input option indicator: 0 = P1PDHX specified, 1 = F1LOSS(JIHX) specified	
	F1IN	Primary inlet loss coefficient for IHX	

	F1OUT	Primary outlet loss coefficient for IHX	
	L1KS	Input option indicator: 0 = P2PDHX specified, 1 = F2LOSX specified	
	F2INHX	Inlet loss coefficient to IHX secondary side	
	F2EXPN	Loss coefficient for expansion from tubes to outlet region in IHX	
	F2CONT	Loss coefficient for contraction from inlet plenum to tubes in IHX	
	F2OUHX	Outlet loss coefficient from IHX secondary side	
102	**X1PLEN(1)**	Length of IHX primary inlet plenum	[m]
	X1PLEN(2)	Length of IHX primary outlet plenum	[m]
	X2PLEN(1)	Length of IHX intermediate inlet plenum	[m]
	X2PLEN(2)	Length of IHX intermediate outlet plenum	[m]
	V1PLEN(1)	Sodium volume of IHX primary inlet plenum	[m^3]
	V1PLEN(2)	Sodium volume of IHX primary outlet plenum	[m^3]
	V2PLEN(1)	Sodium volume of IHX intermediate inlet plenum	[m^3]
	V2PLEN(2)	Sodium volume of IHX intermediate outlet plenum	[m^3]
103	**R1PLEN(1)**	The angle of flow in IHX primary inlet plenum	[deg]
	R1PLEN(2)	The angle of flow in IHX primary outlet plenum	[deg]
	R2PLEN(1)	The angle of flow in IHX secondary inlet plenum	[deg]
	R2PLEN(2)	The angle of flow in IHX secondary outlet plenum	[deg]
104	**X2DOWN**	Length of IHX central downcomer region	[m]
	Y2DOWN	Inner diameter of IHX central downcomer	[m]
	R2DOWN	The angle of flow in the IHX central downcomer	[deg]
105	**T1CONV**	Convergence criterion for temperatures in IHX	[K]
	F1EPS	Roughness of primary loop piping	[m]
	F2EPS	Roughness of intermediate loop piping	[m]
111	**I1FAIL**	Mode of primary check valve: 0 - working, 1 - failed	
	I1TYPE	Type of primary check valve	
	P1PCV	Backpressure for check valve to close	[N/m^2]
	F1CVAL(1)	Check valve charact. coeff. for positive flow w/ open valve (Eq. 3.2-71)	[m^4]
	F1CVAL(2)	Check valve charact. coeff. for positive flow w/ open valve (Eq. 3.2-71)	[m^4]
	F1CVAL(3)	Check valve charact. coeff. for positive flow w/ open valve (Eq. 3.2-71)	[m^4]

112	**Z1HEDR**	Rated head of primary pump	[m]
	U1OMGR	Rated speed of primary pump	[rpm]
	Q1FLOR	Rated volumetric flow rate of primary pump	[m^3/s]
	T1ORKR	Rated torque of primary pump	[N-m]
	Z1RTOT	Height of primary pump tank if L6RTYP ≠1	[m]
		Height of cold pool region from pump inlet to top of Reactor vessel if L6RTYP=1 (pool type)	
	A1RES	Cross-sectional area of primary pump tank	[m^2]
		Dummy value if L6RTYP=1	
	Q1PYTQ	Pump torque under pony motor operation	[N-m]
	V6BPMP	Cold pool volume below pump inlet if L6RTYP=1	[m^3]
		Dummy value if L6RTP≠1	
	Z6IHXP	Height from pump inlet to IHX exit if L6RTYP=1	[m]
		Dummy value if L6RTP≠1	
	A6IHXP	Cross sectional area of cold pool region between pump inlet and IHX exit if L6RTYP=1	[m^2]
		Dummy value if L6RTP≠1	
	A6OVRF	Cross sectional area of cold pool region above IHX exit if L6RTYP=1	[m^2]
		Dummy value if L6RTP≠1	
		* Refer to Fig.1.1 for Z1RTOT,A1RES, V6BPMP, Z6IHXP, A6IHXP, and A6OVRF	
122	**Z2HEDR**	Rated head of intermediate pump	[m]
	U2OMGR	Rated speed of intermediate pump	[rpm]
	Q2FLOR	Rated volumetric flow rate of intermediate pump	[m^3/s]
	T2ORKR	Rated torque of intermediate pump	[N-m]
	Z2RTOT	Height of intermediate pump tank	[m]
	A2RES	Cross-sectional area of intermediate pump tank	[m^2]
	Z2TTOT	Height of surge tank	[m]
	A2TANK	Cross-sectional area of surge tank	[m^2]
	Q2PYTQ	Pump torque under pony motor operation	[N-m]
1001	**L1PUMP**	Pipe number preceding pump in primary loop	
	L1CV	Pipe number preceding check valve in primary loop	
	L1IHX	Pipe number of IHX in primary loop	
	L2PUMP	Pipe number preceding pump in intermediate loop	
	L2TANK	Pipe number preceding expansion tank in intermediate loop	

	L2SG	Pipe number preceding evaporator in intermediate loop	
1002	**F1BETA**	Primary bypass fraction through IHX	
	N1ACTV	Number of active (unplugged) tubes in IHX of loop	
	P1PDHX	Pressure drop over IHX primary side	[N/m^2]
10003	**P2PDHX**	Pressure drop over secondary side of IHX	[N/m^2]
	F2LOSX	Loss coefficient for secondary side of IHX	
1101 - 1199		(Implied (Primary loop) pipe dependency, J = Number - 1100)	
	F1LOSS	Loss coefficient for J-th pipe in primary loop	
	X1PIPE	Length of J-th pipe in primary loop	[m]
	Y1PIPE	Inner diameter of J-th pipe in primary loop Note: For IHX, enter primary side hydraulic diameter.	[m]
	Y1THIK	Thickness of J-th pipe wall in primary loop Note: This value is ignored for IHX primary pipe.	[m]
	R1SIN(I)	Angle of primary flow at each node in J-th pipe of loop (I = 1, N1NODE(N1PIPE(J)))	[deg]
1201 - 1299		(Implied (Intermed. loop) pipe dependency, J = Number - 1200)	
	F2LOSS	Loss coefficient for J-th pipe in intermediate loop	
	X2PIPE	Length of J-th pipe in intermediate loop	[m]
	Y2PIPE	Inner diameter of J-th pipe in intermediate loop	[m]
	Y2THIK	Thickness of J-th pipe wall in intermediate loop	[m]
	R2SIN(I)	Angle of intermediate flow at each node of J-th pipe of loop (I = 1, N2NODE(N2PIPE(J)))	[deg]

MINET DATA (MINETD)

Steam Generator and Balance of Plant Data. All data required to specify the steam generator system (including balance of plant) and its associated sodium-side interfaces.

Rec.	Variable	Description	Unit
1		Pipe Geometric	
	MODID	Module ID assigned to pipe	
	INLETID	Port identifier assigned to inlet port	
	OUTLETID	Port identifier assigned to outlet port	
	X3MOD	Length of module	[m]
	Y3ID	Diameter of module	[m]
	E3PSI	Surface roughness factor, roughness/surface	
	N3NODE	Number of nodes to be used for module	
	N3PATH	Number of parallel units being represented	
101		Valve Geometric	
	MODID	Module ID assigned to valve	
	INLETID	Port identifier assigned to inlet port	
	OUTLETID	Port identifier assigned to outlet port	
	X3MOD	Length of module (Pipe-like portion)	[m]
	Y3ID	Diameter of module (Pipe-like portion)	[m]
	E3PSI	Surface roughness factor, roughness/surface	
	N3NODE	For valve, must use 1 node	
	N3PATH	Number of parallel units being represented	
	A3VMAX	Maximum flow area thru valve when open	[m^2]
	S3VMIN	Minimum valve position, relative, must be GT 0.0	
	F3STOA	Factor, position to area, AREA=POSITN**F3STOA	
201		Pump Geometric	
	MODID	Module ID assigned to pump	
	INLETID	Port identifier assigned to inlet port	
	OUTLETID	Port identifier assigned to outlet port	
	X3MOD	Length of module (Pipe-like portion)	[m]
	Y3ID	Diameter of module (Pipe-like portion)	[m]
	E3PSI	Surface roughness factor, roughness/surface	
	N3NODE	Number of nodes, for pump use 1 node	
	N3PATH	Number of parallel units being represented	
301		Heat exchanger geometric	

	MODID	Module ID assigned to heat exchanger	
	INLETID	Port ID assigned to inlet port, inside tube	
	OUTLETID	Port ID assigned to outlet port, inside tube	
	X3MOD	Length of module (Active heat transfer length)	[m]
	Y3ID	Inner diameter of heat transfer tubes	[m]
	E3PSI	Surface roughness factor inside tubes	
	N3NODE	Number of axial nodes to be used	
	N3PATH	Number of parallel units being represented	
	INLETID	Port ID assigned to inlet port, outside tube	
	OUTLETID	Port ID assigned to outlet port, outside tube	
	Y3OD	Outer diameter of heat transfer tube	[m]
	F3TBPD	Pitch to diameter ratio (Tube spacing / Diameter)	
	N3TUBE	Number of tubes per heat exchanger	
	M3TYPE	Material type in tubing	
	I3GRID	Number of tubes equal-distant from center tube, 1, 4, 6	
	D3COIL	Helical coil diameter, 0 for straight tubes	[m]
	F3ITOO	Ratio of flow length inside tube to outside	
	Y3CORO	Diameter of core tube (Zero of none)	
	M3CORT	Material type of core tube	
	M3STRC	Material type of heat exchanger shell and structure	
	A3STRC	Surface area between structure - fluid, sum - path	[m^2]
	B3STRC	Mass of structure, summed over parallel paths	[kg]
		M3TYPE, M3CORT, M3STRC Options;	
		1 - St Steel, 2- 2.25 Ch-Mly, 3- Admrlty,	
		4- 90-10 Cu-Ni 8- 80-20 Cu-Ni, 6- 70-30 Cu-Ni,	
		7- Monel, 8-Inconnel 9- Carbon Steel,	
		10- Aluminum	
401		Inlet boundary module geometric	
	MODID	Module ID assigned to inlet boundary	
	OUTLETID	Port ID assigned to BND outlet (System Inlet)	
402		Outlet boundary module geometric	
	MODID	Module ID assigned to outlet boundary	
	INLETID	Port ID assigned to BND inlet (System Outlet)	
501		Volume geometric	
	MODID	Module ID assigned to volume	
	L3VSHP	Component shape,	
		1=vertical cylinder or box, 2=horizontal cylinder	

	V3VOL	Volume within module (Portion of component)	[m^3]
	Y3VOL	Total height of component	[m]
	F3VMIN	Relative height of module low point with respect to component	
	F3VMAX	Relative height of module high point with respect to component	
	Z3VOL	Elevation of component vertical midpoint	[m]
	N3PATH	Number of parallel units being represented	
	L3PSEP	1=homogeneous, 2=separated phases, 3=1SS-2TRN	
511		Volume inlet port geometric	
	MODID	Module ID assigned to volume	
	INLETID	Port ID assigned to incoming volume port	
512		Volume outlet port geometric	
	MODID	Module ID assigned to volume	
	OUTLETID	Port ID assigned to outgoing volume port	
601		Turbine stage geometric	
	MODID	Module ID assigned to turbine stage	
	INLETID	Port ID assigned to inlet port	
	OUTLETID	Port ID assigned to outlet port	
	ALPHA	Absolute angle of approach steam with respect to blade, eg-15	[deg]
801		Network geometric	
	MODID	Module ID of any boundary or accumulator in network	
	IFTYPN	Fluid type, 1-H2O, 2-Sodium, 3-Air, 4-NaK	
901		Junction	
	Z3J	CTN Elevation of interface between module ports	[m]
	MODID1	Module ID of first module	
	PORTID1	Port ID of first module	
	MODID2	Module ID of second module	
	PORTID2	Port ID of second module	
1001		Pipe performance	
	MODID	Module ID of pipe	
	F3KMI	Loss coefficient (K) for module	
1101		Valve performance (If choked, must isolate)	
	MODID	Module ID of valve	
	F3KMI	Module loss coefficient - pipe-like section	
	F3VALV	Loss coefficient across valve opening	

	I3CHOK	Choke flow option, 0-none, 1-choking expected	
	J3VPRS	Volume where pressure taken, not used= -999	
	P3VOPN	Pressure at which valve trips open	[Pa]
	S3VOPN	Valve opening time constant	[s]
	P3VCLO	Pressure at which valve trips shut	[Pa]
	S3VCLO	Valve closing time constant	[s]
		** Alternate use of last parameters ** For check valve	
		J3VPRS=0 for check valve	
		P3VOPN=flow/path [kg/s] to open	
		P3VCLO=flow/path [kg/s] to close	
1201		Pump performance	
	MODID	Module ID of pump	
	F3KMI	Module loss coefficient	
	W3REFF	Reference flow rate (per unit)	[kg/s]
	H3REF	Reference pump head	[m]
	F3REF	Reference pump speed	[rpm]
	A3PUMP	(1) HEAD(SPEED,FLOW)=H3REF*(SPEED/F3REF)**2	
		(2) *(A3PUMP(1)+A3PUMP(2)*WRATIO	
		(3) +A3PUMP(3)*WRATIO**2+A3PUMP(4)*WRATIO**3	
		(4) +A3PUMP(5)*WRATIO**4)	
		(5) where WRATIO=W/(W3REFF*(SPEED/F3REF))	
	S3PTAU	Pump coastdown time constant, SPD=SPD0*E-T/TAU	[s]
	S3PSEZ	Pump seizure time after trip	[s]
1301		Heat exchanger performance	
	MODID	Module ID of heat exchanger	
	F3KMI	Module loss coefficient, inside tubes	
	F3KMO	Module loss coefficient, outside tubes	
	I3LVTI	DNB/DRYOUT option,	
		1-DNB, 2-DRYOUT, 3-X=0.75	
	I3LVTO	Same as I3LVTI, but applied outside tubes	
	F3CCFL	Flow direction, 1=parallel, 0=cross, -1=counter	
1601		Turbine performance	
	MODID	Module ID for turbine	
	I3TTYP	Turbine stage type, 1=impulse, 2=impuls-react	
	E3FGEN	Efficiency to electrical grid	
	W3TREF	Reference flow rate	[kg/s]
	P3ITRF	Reference inlet pressure	[Pa]

	P3OTRF	Reference outlet pressure	[Pa]
	T3ITRF	Reference inlet temperature	[K]
	R3TSRF	Reference speed	[rpm]
	S3TTAU	Coastdown time constant, SPD=SPD0*EXP(-T/TAU)	
	S3TSEZ	Seizure time (After Trip)	[s]
2001		Pipe initial condition (All QMOD's subject to adjust.)	
	MODID	Module ID of pipe	
	Q3MOD	Heat put into module, sum over parallel units	[J/s]
2101		Valve initial condition	
	MODID	Module ID of valve	
	Q3MOD	Heat put into module, sum over parallel units	[J/s]
	S3VPOS	Initial stem position, relative, 0=closed, 1=open	
2201		Pump initial condition	
	MODID	Module ID of pump	
	Q3MOD	Heat put into module, sum over parallel units	[J/s]
	F3PUMP	Initial pump speed	[rpm]
2301		Heat exchanger initial condition	
	MODID	Module ID of heat exchanger	
	Q3MOD	Total heat transfer, out to in, sum over parallel units	[J/s]
2401		Boundary module initial condition	
	MODID	Module ID of boundary	
	K3EBST	Boundary status, 0=inlet, 1=floating, 2=fixed	
	K3EBC	E3BC flag, 1=enthalpy, 2=temperature, 3=quality	
	E3BC	Enthalpy, temperature, or quality (If H2O)	[J/KG] or [K]
	W3BC	Mass flow (total) used for inlets only	[kg/s]
	P3BC	Pressure used for outlets only	[Pa]
2501		Volume initial condition	
	MODID	Module ID of volume	
	Q3MOD	Heat put into module, sum over parallel units	[J/s]
	F3LQLV	Relative liquid level vs component height	
	P3VOL	Estimated volume pressure at steady state	[Pa]
2511		Volume outlet port initial condition	
	MODID	Module ID of volume	
	OUTLETID	Outlet port ID of volume	
	W3VOUT	Estimate of flow exiting, sum over parallel path	[kg/s]
2601		Turbine stage initialization	

	MODID	Module ID of turbine stage	
	R3TS	Initial turbine speed	[rpm]
	Q3MOD	Work done on turbine stage	[J/s]
3011		Pipe heat input table (Repeat 2 and 3 entries)	
	MODID	Module ID of pipe	
	S3QT	Time of table entry	[s]
	Q3MDT	Heat input for corresponding time	[J/s]
3111		Valve heat input table (Repeat 2 and 3 entries)	
	MODID	Module ID of valve	
	S3QT	Time of table entry	[s]
	Q3MDT	Heat input for corresponding time	[J/s]
3121		Valve position table - optional (Repeat entries 2 and 3)	
	MODID	Module ID of valve	
	S3VTIM	Time of valve position table entry	[s]
	S3VPSN	Relative valve stem position	
3201		Pump transient (Can be over-ruled by 3221D)	
	MODID	Module ID of pump	
	S3PTRP	Time at which pump is tripped	[s]
3211		Pump heat input table (Repeat entries 2 and 3)	
	MODID	Module ID of pump	
	S3QT	Time of table entry	[s]
	Q3MDT	Heat input at corresponding time	[J/s]
3221		Pump speed table - optional (Repeat entries 2 and 3)	
	MODID	Module ID of pump	
	S3PTIM	Time of table entry	[s]
	R3PMPT	Pump speed at corresponding time	[rpm]
3411		Boundary condition table (Repeat entries 4, 5, and 6)	
	MODID	Module ID of boundary	
	I3BCTP	Key, 1=flow specified, 2=pressure specified	
	K3ETAB	Key for ETAB, 1=enthalpy, 2=temperature, 3=quality	
	S3TAB	Time of table entry	[s]
	E3TAB	Enthalpy, temperature, or quality entry	[J/kg] or [K]
	P3WTAB	Flow or pressure table entry	[kg/s] or [Pa]
3511		Volume heat input table (Repeat 2, 3 entries)	
	MODID	Module ID of volume	

	S3QT	Time of table entry	[s]
	Q3MDT	Heat input at corresponding time	[J/s]
3601		Turbine trip (Can be overruled by 3611D)	
	MODID	Module ID of turbine stage	
	S3TSTP	Turbine trip time	[s]
3611		Turbine speed table - optional (Repeat entries 2 and 3)	
	MODID	Module ID of turbine stage	
	S3TSTB	Time of turbine speed table entry	[s]
	R3TSTB	Turbine speed at corresponding time	[rpm]
4000		Run control card	
	S3END	End of transient simulation	[s]
4100		Print control (Repeat entries 3 and 4)	
	L3PRON	Step number to start frequent prints, -1 for SS	
	L3PRNT	Keys print detail, 1=brief, 2=middle, 3=detailed	
	S3PRIN	Print interval	[s]
	S3PLIM	Time limit for corresponding print interval value	[s]
4200		Context save control	
	L3REST	Context restore control,	
		0=no restore, 1=restore context	
	N3SINT	Context save control, defines print count between saves	

OPDATA

Initial overall plant operating conditions and specification of plant balance initialization logic.

Rec.	Variable	Description	Unit
1	**P9OP**	Reactor power	[W]
	N9LOOP	Number of operating loops present in plant	
2	**T6OUTL**	Vessel sodium outlet temperature	[K]
	T6INLT	Vessel sodium inlet temperature	[K]
		cf. TRNDAT 8015, T81REF	
	W1LOOP	Sodium flow rate in primary loop	[kg/s]
		cf. TRNDAT 8015, W81REF	
		Note: Of the three parameters in this, two must be specified as known (denoted by entering values greater than zero) while the other one is assumed unknown (denoted by entering a value less than zero) and will be calculated by SSC. The unknown value to be entered need not be too precise; it can be an approximate initial guess.	
3	**T2IHXI**	IHX intermediate sodium inlet temperature	[K]
	T2IHXO	IHX intermediate sodium outlet temperature	[K]
	W2LOOP	Sodium flow rate in intermediate loop	[kg/s]
		cf. TRNDAT 8015, W82REF	
		Note: Of the three parameters in this one must be specified as known (denoted by entering values greater than zero) while the others are assumed unknown (denoted by entering a value less than zero) and will be calculated by SSC. The accuracy of the initial guesses for this are more important.	
4	**P1GASI**	Initial cover gas pressure in each primary pump tank	[N/m^2]
	P2GASI	Initial cover gas pressure in each intermediate loop	[N/m^2]
	Z2TANK	Height of coolant in surge (expansion) tank	[m]
	T1PUMP	Temperature rise across primary pump	[K]
	T2PUMP	Temperature rise across intermediate pump	[K]
5	**L1EPRT**	Primary and intermediate loop detailed print option; 1= report, 0= no report	

L3PRNT	SG detailed print option; 1 - 4 = low to high detail report, 0 = no report
L5PRNT	Detailed in vessel temp. distribution print option; 1 = report, 0 = no report
L6PRNT	In-vessel fluid dynamics detailed print option; 1 = report, 0 = no report

MATDAT

A set of material properties data is built into the code. The data required to alter the default values of the material properties, or to create new material properties, are input to the code through data file MATDAT.

Rec.	Variable	Description	Unit
10		Material properties for sodium	
40 – 49		Material properties for blanket	
50 - 59		Material properties for fuel	
60 - 69		Material properties for cladding	
70 - 79		Material properties for structural material	
80 - 89		Material properties for cover gas	

TRNDAT Transient scenario data

Rec.	Variable	Description	Unit
1001	**L1PONY(K)**	Primary loop pony motor status;	
		1 = motor is on, 0 = motor is off (K = 1,N1LOOP)	
	F1PONY	Primary pony motor speed fraction of rated speed	
	Q1NRTA	Primary pump inertia [KG*M2]	
1002	**L2PONY(K)**	Secondary loop pony motor status;	
		1 = motor is on, 0 = motor is off (K = 1,N1LOOP)	
	F2PONY	Secondary pony motor speed fraction of rated speed	
	Q2NRTA	Secondary pump inertia	[kg,m^2]
1003	**L1GV(K)**	Guard vessel option;	
		0 = no guard vessel, 1 = reactor vessel outlet,	
		2 = RV inlet, 3 = pump inlet, 4 = pump outlet,	
		5 = IHX inlet , 6 = IHX outlet (K = 1, N1LOOP)	
	V1MINR	R.V. guard vessel volume at level with break	[m^3]
	Z1MAXR	R.V. guard vessel maximum level that can be reached	
		by coolant	[m]
	F1GVR(1)	R.V. guard vessel volume to level coeff.	
	F1GVR(2)	R.V. guard vessel volume to level coeff.	
	F1GVR(3)	R.V. guard vessel volume to level coeff.	
	V1MINP	Pump guard vessel volume at level with pipe break	[m^3]

	Z1MAXP	Pump guard vessel maximum level that can be reached by coolant	[m]
	F1GVP(1)	Pump guard vessel volume to level coeff.	
	F1GVP(2)	Pump guard vessel volume to level coeff.	
	F1GVP(3)	Pump guard vessel volume to level coeff.	
	V1MINX	IHX guard vessel volume at level with pipe break	[m^3]
	Z1MAXX	IHX guard vessel maximum level that can be reached by coolant	[m]
	F1GVX(1)	IHX guard vessel volume to level coeff.	
	F1GVX(2)	IHX guard vessel volume to level coeff.	
	F1GVX(3)	IHX guard vessel volume to level coeff.	
	V1MAX	Maximum volume that can be filled in guard vessel in any location	[m^3]
1004	**I1FAIL(K)**	Primary check valve status; 0 = working, 1 = failed (K = 1, N1LOOP)	
1101 - 1199		(Implied primary loop dependency, J = number - 1100)	
	J1BREK	Primary loop pipe number containing break	
	N1NBRK	Number of nodes in broken primary pipe upstream of break	
	X1BREK	Length of primary pipe upstream of break	[m]
	F1LSBK	Loss coefficient at primary break	
	A1BREK	Break area in primary pipe	[m^2]
	A1GAP	X-sectional area between broken primary pipe and guard vessel	[m^2]
	S1BREK	Time of primary pipe break Note: This series is specified only for loop(s) containing break(s).	[s]
1201 - 1299		(Implied secondary loop dependency, J = number - 1200)	
	J2BREK	Secondary loop pipe number containing break	
	N2NBRK	Number of nodes in broken secondary pipe upstream of break	
	X2BREK	Length of primary pipe upstream of break	[m]
	F2LSBK	Loss coefficient at secondary break	
	A2BREK	Break area in secondary pipe	[m^2]
	A2GAP	X-sectional area between broken secondary pipe and guard pipe	[m^2]
	S2BREK	Time of secondary pipe break	[s]

		Note: This series is specified only for loop(s) containing break(s).	
3101	**MODID**	Module ID of boundary	
	N3TAB	Number of table entries on corresponding 3111	
	I3BCTP	Boundary condition type; 1 = flow, 2 = pressure	
3111	**MODID**	Module ID of boundary	
	S3TAB(I)	Time for table entry	[s]
	E3TAB(I)	Enthalpy [J/KG] or temperature [K] for table entry	
	P3WTAB(I)	Pressure [Pa] of flow [kg/s] for table entry	
		Note: Data is entered as a user defined series of paired points.	
3201	**MODID**	Module ID of volume (Accumulator)	
	N3VOLT	Number of table entries on corresponding 3211	
3211	**MODID**	Module ID of volume	
	S3VOLT(I)	Time for table entry	[s]
	Q3VOLT(I)	Heat input to all parallel volumes	[J/s]
		Note: Data is entered as a user defined series of paired points.	
3301	**MODID**	Module ID of valve	
	N3VALT(I)	Number of table entries on corresponding 3311	
	N3VCAS	PPS/PCS option; 0 = Ignore PPS/PCS, 1 = Accept PPS/PCS signal Note: At present, N3VCAS must be set equal to zero.	
3311	**MODID**	Module ID of valve	
	S3VALT(I)	Time for table entry	[s]
	S3VPST(I)	Valve stem position; 0 = Full closed, 1 = Full open Note: Data is entered as a user defined series of paired points.	
3401	**MODID**	Module ID of pump	
	N3PUMT(I)	Number of table entries on corresponding 3411	
	S3PTRP	Pump trip time	[s]
	N3PCAS	PPS/PCS option; 0 = Ignore PPS/PCS, 1 = Accept PPS/PCS signal Note: At present, N3PCAS must be set equal to zero.	
3411	**MODID**	Module ID of pump	
	S3PUMT(I)	Time for table entry	[s]
	R3PUMT(I)	Relative pump speed; 0 = Full stop, 1 = Full speed	

		Note: Data is entered as a user defined series of paired points.	
5001	**L5POPT**	Transient power flag; 0 = Prompt jump approximation, 1 = exact	
	N5DNGP	Number of delayed neutron groups (Maximum of 6)	
	C5LN	Prompt neutron generation time	[s]
5002	**F5PFIS(K)**	Fractional power in each channel and bypass due to fission heating (K = 1,N6CHAN+1)	
5003	**F5BETA(N)**	Fraction of N-th effective delayed neutron group (0<N<7)	
5004	**C5LMDA(N)**	Decay constant of N-th delayed neutron group (0<N<7)	
5005	**F5PBPD(I)**	Fractional transient decay power in bypass	
	S5PBPD(I)	Transient postscram time for decay power in bypass	[s]
		Note: Data is assigned as a user defined series of paired points of up to 25 pairs	
5101 - 5199		(Implied channel dependency, K= Number - 5100)	
	F5PD(I)	Fractional transient decay power in K-th channel	
	S5PD(I)	Transient postscram time for decay power in K-th channel	[s]
		Note: Data is assigned as a user defined series of paired points of up to 25 pairs	
5201 - 5299		(Implied channel dependency, K= Number - 5200)	
	F5BDOP(J)	Mesh weighted Doppler reactivity coefficient with sodium present for K-th channel (J=1,N5SLIC(K))	[ρ]
5301 - 5399		(Implied channel dependency, K= Number - 5300)	
	F5GDOP(J)	Mesh weighted Doppler reactivity coefficient w/o sodium present for K-th channel (J=1,N5SLIC(K))	[ρ]
5401 - 5499		(Implied channel dependency, K= Number - 5400)	
	F5VWGT(J)	Mesh weighted sodium void reactivity coefficient for K-th channel (J=1,N5SLIC(K))	[ρ/kg]
5501 - 5599		(Implied channel dependency, K= Number - 5500)	
	F5AWGT(J)	Mesh weighted fuel axial expansion reactivity coefficient for K-th channel (J=1,N5SLIC(K))	[ρ/kg]
6001	**L6MIX**	Upper Plenum Mixing type option; 1= one zone mixing, 2= two zone mixing	

	L6FLOW	Flow redistribution option; 0 = No flow redistribution, 1 = Flow redistribution	
	T6SUPH	Super heat temperature If set .LT. 0.0, thermal expansion model will be used in boiling calculations. If set .GE. 0.0, single mass flow rate will be used in boiling calculations.	
6002	**L6CGAS**	Cover gas pressure option; 1 = constant mass, 2 = constant pressure 3 = constant feed/bleed rate	
	Q6CGFB	Cover gas feed/bleed rate	[kg/s]
	P6CGFB	Cover gas pressure change required to actuate feed/bleed valve	[N/m^2]
8001	**N8PCSD**	Number of feedback cascades in the reactor power controller	
	N8CBNK	Number of primary control rod banks	
8002	**L8PUMP(J)**	Manual/Auto pump trip flag; 1 = manual, 0 = auto (J=1,(4*N1LOOP+1)) Note: Parameters are assigned on a subsystem/component basis. That is, data assignments are made for the pump in primary loop 1, the pump in primary loop 2 (if needed), and so on, up to the pump in primary loop "N1LOOP". The data for all "N1LOOP" primary loop pumps is followed by corresponding series for the secondary loop(s) and each of two dummy steam generator pumps. Data for the last pump is assigned to the turbine. Pump trips for the steam generator and turbine must be set through RECORD 3401.	
8003	**S8TDLY(J)**	Pump trip time delay after an automatic PPS signal (J=1,(4*N1LOOP+1)) Note: Parameters are assigned on a subsystem and component basis. That is, data assignments are made for the pump in primary loop 1, the pump in primary loop 2 (if needed), and so on, up to the pump in primary loop "N1LOOP". The data for all "N1LOOP" primary loop pumps is followed by corresponding series for the secondary loop(s) and each of two dummy steam generator pumps. Data for the last pump is assigned to the	[s]

		turbine. Pump trips for the steam generator and turbine must be set through RECORD 3401.	
8004	**S8MANP(J)**	Time at which pumps are to be tripped manually (J=1,(4*N1LOOP+1)) and time at which IHX are to be isoltaed manually * Note: Parameters are assigned on a subsystem/component basis. That is, data assignments are made for the pump in primary loop 1, the pump in primary loop 2 (if needed), and so on, up to the pump in primary loop "N1LOOP". The data for all "N1LOOP" primary loop pumps is followed by corresponding series for the secondary loop(s) and each of two dummy steam generator pumps Data for the last pump is assigned to the turbine. Pump trips for the steam generator and turbine must be set through RECORD 3401.	[s]
8005	**F8PD1**	Fractional power demand at time S8DT1	
	F8PD2	Fractional power demand at time S8DT2	
	S8DT1	Time at which the load demand starts changing	[s]
	S8DT2	Time at which the load demand reaches a constant level	[s]
8006	**F8RSCR**	Reactivity worth due the secondary control rods (Eq. 3.4-30)	[$]
	F8RSDM	Cold shutdown margin of reactivity (Constant) (Eq. 3.4-30)	[$]
	Z8SRMX	Maximum insertion limit of the secondary control rods corresponding to F8SRMX (Eq. 3.4-31)	[m]
	F8SRMX	Maximum reactivity worth of the secondary control rods (Eq. 3.4-31)	[$]
	F8RSTP	Reactivity worth of the primary system stuck rod (Eq. 3.4-38A)	[$]
	F8RSTS	Reactivity worth of the secondary system stuck rod (Eq. 3.4-38B)	[$]
8007	**C8A0**	Coefficients for a 6th degree polynomial (Eq. 3.4-37)*	
	C8A1	Coefficients for a 6th degree polynomial (Eq. 3.4-37)*	
	C8A2	Coefficients for a 6th degree polynomial (Eq. 3.4-37)*	
	C8A3	Coefficients for a 6th degree polynomial (Eq. 3.4-37)*	
	C8A4	Coefficients for a 6th degree polynomial (Eq. 3.4-37)*	
	C8A5	Coefficients for a 6th degree polynomial (Eq. 3.4-37)*	

	C8A6	Coefficients for a 6th degree polynomial (Eq. 3.4-37)*	
	C8B0	Coefficients for a 6th degree polynomial (Eq. 3.4-37)**	
	C8B1	Coefficients for a 6th degree polynomial (Eq. 3.4-37)**	
	C8B2	Coefficients for a 6th degree polynomial (Eq. 3.4-37)**	
	C8B3	Coefficients for a 6th degree polynomial (Eq. 3.4-37)**	
	C8B4	Coefficients for a 6th degree polynomial (Eq. 3.4-37)**	
	C8B5	Coefficients for a 6th degree polynomial (Eq. 3.4-37)**	
	C8B6	Coefficients for a 6th degree polynomial (Eq. 3.4-37)**	
	S8DSPT	Maximum time range of validity of polynomials for the primary rods	[s]
	F8ZSPT	Fractional portion of the scram rods at which we shift to second polynomial fit Note: * This polynomial describes the primary rod position as a function of time after scram with the rods fully out. ** This polynomial describes the primary rod position as a function of time after scram with the rods partially inserted.	
8008	**C8C0**	Coefficients for a 6th degree polynomial (Eq. 3.4-37)*	
	C8C1	Coefficients for a 6th degree polynomial (Eq. 3.4-37)*	
	C8C2	Coefficients for a 6th degree polynomial (Eq. 3.4-37)*	
	C8C3	Coefficients for a 6th degree polynomial (Eq. 3.4-37)*	
	C8C4	Coefficients for a 6th degree polynomial (Eq. 3.4-37)*	
	C8C5	Coefficients for a 6th degree polynomial (Eq. 3.4-37)*	
	C8C6	Coefficients for a 6th degree polynomial (Eq. 3.4-37)*	
	S8DSST	Maximum time range of validity of polynomials for the secondary rods Note: This polynomial describes the secondary rod position as a function of time after scram. Since the secondary rods are assumed to be fully out, only one polynomial is used.	[s]
8009	**S8RI1**	Time at which the reactivity insertion starts	[s]
	S8RI2	Time at which the reactivity insertion ends	[s]
	F8RI1	Reactivity at the start of the insertion (Corresponding to S8RI1)	[$]
	F8RI2	Reactivity at the end of the insertion (Corresponding to S8RI2)	[$]
8010	**F8VMAX(I)**	Maximum fractional valve opening	

		(I=1,(N1LOOP+3)) (Eq. 3.4-57)*	
	F8TRMA(I)	Maximum valve trim (I=1,(N1LOOP+3)) (Eq. 3.4-57)*	
		Note: * Data is entered as a series of paired points.	
		The index "I" is incremented over the set of all required	
		data. The required valve sequencing is:	
		- Main feed water control valve (one entry per loop)	
		- Throttle valve, Bypass valve, Motor operated relief valve	
8011	**F8VMIN(I)**	Minimum fractional valve opening	
		(I=1,(N1LOOP+3)) (Eq. 3.4-57)*	
	F8TRMN(I)	Minimum valve trim (I=1,(N1LOOP+3))	
		(Eq. 3.4-57)*	
		Note: * Data is entered as a series of paired points.	
		The index "I" is incremented over the set of all required	
		data. The req uired valve sequencing is:	
		Main feed water control valve (one entry per loop)	
		Throttle valve, Bypass valve, Motor operated relief valve	
8012	**S8OPEN(I)**	Valve opening time (I=1,(N1LOOP+3))	[s]
		(Eq. 3.4-57)	
		Note: The required valve sequencing is:	
		Main feed water control valve (one entry per loop)	
		Throttle valve, Bypass valve, Motor operated relief valve	
8013	**S8CLOS(I)**	Valve closing time (I=1,(N1LOOP+3)) (Eq. 3.4-57)	
		Note: The required valve sequencing is:	[s]
		- Main feed water control valve (one entry per loop)	
		- Throttle valve, Bypass valve, Motor operated relief valve	
8014	**C8TIME(I)**	Time constants used in computing sensor measurement	
		time lags (I=1,3+5*N1LOOP)	[s]
		Note: These constants correspond to the following sensors:	
		- Reference pressure	
		- Sodium level	
		- IHX outlet temperature (one entry per loop)	
		- Evaporator inlet temperature (one entry per loop)	
		- Feed water flow rate (one entry per loop)	
		- Steam flow rate (one entry per loop)	
		- Steam drum level (one entry per loop)	
		- Reactor outlet nozzle temperature	
8015	**U81REF**	Refence 100 % power, primary loop pump speed	[rpm]

	U82REF	Reference 100 % power, intermediate loop pump speed	[rpm]
	W81REF	Reference 100 % power, primary loop sodium mass flow rate, cf. OPDATA 2, W1LOOP	[kg/s]
	W82REF	Reference 100 % power, intermediate loop sodium mass Flow rate, cf. OPDATA 3, W2LOOP	[kg/s]
	T8RREF	Reference 100 % power, core mixed mean outlet temperature	[K]
	T81REF	Reference 100 % power, reactor vessel sodium inlet Temperature, cf. OPDATA 2, T6INLT	[K]
	T8TREF	Reference 100 % power, cold shutdown temperature	[K]
	P86REF	Refence 100 % power, reactor inlet plenum pressure	[N/m^2]
	P8TREF	Reference 100 % power, turbine inlet pressure	[N/m^2]
	P8DPRF	Reference 100 % power, pressure drop across feedwater valve	[N/m^2]
	W8FWRF	Reference 100 % power, feedwater flow rate	[kg/s]
	W8STRF	Reference 100 % power, steam flow rate	[kg/s]
8016	**L8AVLP(I)**	Protective functions examined by the primary shutdown system, (I=1,J: 0<J<21)	
8017	**L8AVLS(I)**	Protective functions examined by the secondary shutdown system, (I=1,J: 0<J<21)	
8018	**L8FUNP(I)**	Protective functions operative for primary shutdown system (I=1,J: 0<J<21) Note: At least one must be operative.	
8019	**L8FUNS(I)**	Protective functions operative for secondary shutdown system (I=1,J: 0<J<21) Note: At least one must be operative.	
8020	**L8PMAN**	Manual/auto scram flag for the primary shutdown system, 1 - manual, 0 - auto	
	S8PDLY	Primary shutdown system scram time delay after an automatic PPS signal	[s]
]	**S8PMAN**	Time at which primary shutdown system is to be manually tripped Note: Selection of manual scram does not prevent an automatic scram. To prevent an automatic scram from the primary shutdown system, S8PDLY should be set to a long time.	[s]
8021	**L8SMAN**	Manual/auto scram flag for the secondary shutdown	

		system; 1- manual, 0 - auto	
	S8SDLY	Secondary shutdown system scram time delay after an automatic PPS signal	[s]
	S8SMAN	Time at which secondary shutdown system is to be Manually tripped Note: Selection of manual scram does not prevent an automatic scram. To prevent an automatic scram from the secondary shutdown system, S8SDLY should be set to a long time.	[s]
8101	**F86SFX**	Fractional high neutron flux (PPS setting) (Eq. 3.4-2)	
8106	**Z86SNA**	Reactor vessel sodium level PPS setting (Eq. 3.4-10)	
8107	**C8PET**	Setpoint constant for steam to feedwater ratio function (PPS function 7) (Eq. 3.4-11)	
8108	**T82SHX**	IHX outlet temperature PPS setting (Eq. 3.4-12)	[K]
8110	**C8PG1**	Constant used in determining the setpoint for the primary to intermediate flow ratio (PPS function 10) (Eq. 3.4-14)	
	C8PG2	Constant used in determining the setpoint for the primary to intermediate flow ratio (PPS function 10) (Eq. 3.4-14)	
	C8PG3	Constant used in determining the setpoint for the primary to intermediate flow ratio (PPS function 10) (Eq. 3.4-14)	
	C8PG4	Constant used in determining the setpoint for the primary to intermediate flow ratio (PPS function 10) (Eq. 3.4-14)	
	C8PG5	Constant used in determining the setpoint for the primary to intermediate flow ratio (PPS function 10) (Eq. 3.4-14)	
	C8PG6	Constant used in determining the setpoint for the primary to intermediate flow ratio (PPS function 10) (Eq. 3.4-14)	
8111	**Z83SMX**	Setpoint steam drum maximum water level PPS setting (Eq. 3.4-15)	[m]
	Z83SMN	Setpoint steam drum water level PPS setting (Eq. 3.4-15)	
8112	**T83SEV**	PPS setting evaporator exit sodium temperature (Eq. 3.4-16)	[K]
8113	**T86SNZ**	PPS setting reactor outlet nozzle temperature (Eq. 3.4-17)	[K]
8114	**F81SFL**	Primary pump PPS setting (Eq. 3.4-18)	
8115	**F82SFL**	Intermediate pump speed PPS setting (Eq. 3.4-18)	
8200	**F8HFXL**	High flux limiter (Fraction of 1)	
	F8CRDZ	Control rod dead zone (Fraction of 1)	

8102	**C8PA1**	Constants used in determining the setpoint for flux delayed flux function when RHO is greater than 0 (PPS function 2) (Eq. 3.4-3)
	C8PA2	Constants used in determining the setpoint for flux delayed flux function when RHO is greater than 0 (PPS function 2) (Eq. 3.4-3)
	C8PA3	Constants used in determining the setpoint for flux delayed flux function when RHO is greater than 0 (PPS function 2) (Eq. 3.4-3)
	C8PA4	Constants used in determining the setpoint for flux delayed flux function when RHO is greater than 0 (PPS function 2) (Eq. 3.4-3)
	C8PA5	Constants used in determining the setpoint for flux delayed flux function when RHO is greater than 0 (PPS function 2) (Eq. 3.4-3)
	C8PB1	Constants used in determining the setpoint for flux delayed flux function when RHO is less than 0 (PPS function 2) (Eq. 3.4-3)
	C8PB2	Constants used in determining the setpoint for flux delayed flux function when RHO is less than 0 (PPS function 2) (Eq. 3.4-3)
	C8PB3	Constants used in determining the setpoint for flux delayed flux function when RHO is less than 0 (PPS function 2) (Eq. 3.4-3)
	C8PB4	Constants used in determining the setpoint for flux delayed flux function when RHO is less than 0 (PPS function 2) (Eq. 3.4-3)
	C8PB5	Constants used in determining the setpoint for flux delayed flux function when RHO is less than 0 (PPS function 2) (Eq. 3.4-3)
8103	**C8PC1**	Constant used in determining the setpoint for flux-sqrt (Pressure) function (PPS function 3) (Eq. 3.4-8)
	C8PC2	Constant used in determining the setpoint for flux-sqrt (Pressure) function (PPS function 3) (Eq. 3.4-8)
	C8PC3	Constant used in determining the setpoint for flux-sqrt (Pressure) function (PPS function 3) (Eq. 3.4-8)
8104	**C8PD1**	Constant used to determine the setpoint for primary to

		intermediate speed ratio function (PPS function 4) (Eq. 3.4-9)	
	C8PD2	Constant used to determine the setpoint for primary to intermediate speed ratio function (PPS function 4) (Eq. 3.4-9)	
	C8PD3	Constant used to determine the setpoint for primary to intermediate speed ratio function (PPS function 4) (Eq. 3.4-9)	
	C8PD4	Constant used to determine the setpoint for primary to intermediate speed ratio function (PPS function 4) (Eq. 3.4-9)	
	C8PD5	Constant used to determine the setpoint for primary to intermediate speed ratio function (PPS function 4) (Eq. 3.4-9)	
	C8PD6	Constant used to determine the setpoint for primary to intermediate speed ratio function (PPS function 4) (Eq. 3.4-9)	
8201	**MODID**	PPS/PCS module identifier*	
	Z8CRIN	Initial position of the primary control rods. May vary from 0.0 (Fully inserted) to the value assigned Z8CRMX (Fully withdrawn) (Eq. 3.4-34)	[m]
	Z8CRMX	Maximum insertion limit of the primary control rods (Eq. 3.4-34)	[m]
	Z8SAT	Primary control rod saturation position	[m]
	Z8LOCR	Lower position of the rod bank before the next bank movement begins	[m]
	Z8CRUP	Upper position of the rod bank before the next bank movement begins	[m]
	U8CRDN	Primary control rod downward velocity (negative value) (Eq. 3.4-36)	[m/s]
	U8CRUP	Primary control rod upward velocity (positive value) (Eq. 3.4-36)	[m/s]
	F8ROMX	Maximum reactivity of the primary control rod banks (Eq. 3.4-34)	[$]
		Note: A MODID is a three (3) digit code designed to uniquely identify a PCS controller. Since a control rod bank is defined with neither sub-system nor loop	

		dependencies, digits one (1) and three (3) are by convention always assigned a value of zero (0). The remaining digit (2) designates the bank to which the data is associated. It's value will range from one (1) to the user defined maximum number of control rod banks (N8CBNK) which is found on record 8001	
8301	**MODID**	PPS/PCS module identifier *	
	M8MOTR	Motor type flag (0/1, squirrel cage/wound rotor)	
	N8POLE	Number of pairs of poles for squirrel cage type motor (Eq. 3.4-43)	
	Q8FRER	100% reference frequency of the motor-generator set	[Hz]
	C8PCS	Constants associated with the pump drive system (Eq. 3.4-40)	
	C8ACT	Actuator constants (Eq. 3.4-44)	
	F8HSPL	Pump high speed limit	
	R8MAX	Maximum resistance of the liquid rheostat actuator (Eq. 3.4-51)	[Ω]
	R8ROT	Motor resistance (Eq. 3.4-50)	[Ω]
	U8SRPM	Synchronous speed of the sodium pumps (Eq. 3.4-53)	[rpm]
		Note: * A MODID is a three (3) digit code designed to uniquely identify a PCS controller. Since there is only one driver per pump and one pump per loop, the second digit of the pump controller MODID is superfluous and is by convention always assigned a value of zero (0). The first digit of the MODID code is assigned on a subsystem basis. A pump driver in a primary heat transport system is assigned a value of one. (1) while the secondary system counterpart is assigned a value of two (2). The plant loop is identified by the MODID's last digit. It's range of valid values is one (1) through the maximum number of loops simulated (N1LOOP).	
8400	**N8CSCD(I)**	Number of flow controller cascades associated with each subsystem component (I=1,(4*N1LOOP+3))	
		Note: The following cascade sequencing is assumed:	
		- Primary heat transport system (one entry for each loop)	
		- Secondary heat transport system (one entry for each loop)	

		- Feedwater water pump (one entry for each loop)	
		- Feedwater valve (one entry for each loop)	
		- Throttle valve	
		- Bypass valve	
		- Relief valve	
8401	**MODID**	PPS/PCS module identifier*	
	M8FLAG	Controller mode flag (0/1, automatic/manual) (Figure 3.4-3)	
	F8GAIN	Controller gain (Eq. 3.4-22)	
	F8REPT	Integral controller repetition rate	[1/s]
	C8TIME	Time constants (Eq. 3.4-22)	[s]
	F8ROLU	Integral limiter (Upper limit)	
	F8ROLD	Integral limiter (Lower limit)	
	F8DBND	Dead band (Fraction of 1)	
	X8PM	Manual adjustable setpoints for controllers	
	C8TIME	Time constants	[s]
	C8FP	Flow controller part load profile coefficients for load dependent set points	
		Note: A MODID is a three (3) digit code designed to uniquely identify a PCS controller. The first digit denotes the subsystem/component. It may assume values of one (1) through eight (8) in accordance with the following definition:	
		1 - Primary heat transport system	
		2 - Secondary heat transport system	
		3 - Feedwater pump	
		4 - Feedwater valve	
		5 - Throttle valve	
		6 - Bypass valve	
		7 - Relief valve	
		8 - Power controller	
		Digit two (2) identifies a cascade within a subsystem. It is assigned a value of one(1) to a user defined maximum. For subsystems 1 through 7, this maximum is defined by a corresponding entry on the REORD 8400. The maximum number of power controllers(subsystem 8) is defined on RECORD 8001. The plant loop is	

		identified by the last digit of the MODID. It's range is zero (0) through the maximum number of loops simulated (N1LOOP). A valve of zero (0) in the third digit indicates no loop dependency. By convention, a zero (0) is always assigned to the third digit of power controller MODID.	
9001	**S9LAST**	Total problem simulation time	[s]
	S9MAXA	Maximum time step allowed	[s]
	S9MINA	Minimum timestep allowed	[s]
	S9SINT	Master clock interval at which a restart dump will occur	[s]
	S9PINT(J)	Master clock interval at which a system report will be generated.	[s]
	S9PINT(J+1)	Master clock time after which the corresponding S9PINT is no longer valid.	[s]
		Note: The index J is incremented over the set of paired points. There may be as many pairs (intervals) as the users find necessary.	
		S9PINT(1) is imposed from time 0.0 to S9PINT(2). S9PINT(3) is then used from the master clock time S9PINT(2) to S9PINT(4). Similarly, S9PINT(5) is used from S9PINT(4) to S9PINT(6), and so on.	
		It should be apparent that S9PINT(4) must be strictly greater than S9PINT(2), and S9PINT(6) must be strictly greater than S9PINT(4), and so on.	
		There is quite a bit of latitude permitted in the selection Of print intervals, but they must be carefully chosen (see section 7.8)	
9002	**F1EMXA**	Relative accuracy acceptance limit for loop thermal calculations	
	F1WMXA	Relative accuracy acceptance limit for loop hydraulic calculations	
	F5MAXA	Relative accuracy acceptance limit for fuel calculations	
	F6MAXA	Relative accuracy acceptance limit for in-vessel coolant calculations	
9003	**F1ICDA**	Relative interface condition acceptance limit for loop hydraulic calculations	
	F6ICDA	Relative interface condition acceptance limit for in-vessel coolant calculations	

9004	**L1ECAL**	Loop thermal option; 1 - module is called, 0 - module is not called
	L1WCAL	Loop hydraulic option; 1 - module is called, 0 - module is not called
	L3CALL	Steam generator option; 1 - module is called, 0 - module is not called
	L5CALL	Fuel option; 1 - module is called, 0 - module is not called
	L6CALL	In-vessel option; 1 - module is called, 0 - module is not called
	L8CALL	PCS option; 1 - module is called, 0 - module is not called
9005	**L1EPRT**	Loop thermal report option; 0 - no report, 1 - report is generated
	L1WPRT	Loop hydraulic report option; 0 - no report, 1 - report is generated
	L3PRNT	Steam generator report option; 0 - no report, 1-4 - report is generated with correspondingly greater detail
	L5PRNT	Fuel report option; 0 - no report, 1 - report is generated
	L6PRNT	In-vessel coolant report option; 0 - no report, 1 - report is generated
	L8PRNT	PPS/PCS report option; 0 - no report, 1 - report is generated
9006		set to 0
9008	**L9DMPZ**	Dump labeled common before initialization; 1 - yes, 0 - no
	L9DMPI	Dump labeled common after initialization; 1 - yes, 0 - no
	L9DMPL	Dump labeled common after last time step; 1 - yes, 0 - no
	L9TBLD	Dump container array table information; 1 - yes, 0 - no Note: This is currently valid only on CDC installations.

TRNREG

May be used to alter a transient proceeding from a restart at simulation time greater than zero. Corresponds to TRNDAT RECORDs 9001 and 9005.

Rec.	Variable	Description	Unit
101	**S9LAST**	Total problem simulation time [s]	
	S9MAXA	Maximum time step allowed [s]	
	S9MINA	Minimum time step allowed [s]	
	S9SINT	Master clock interval at which a restart dump will occur	[s]
	S9PINT(J)	Master clock interval at which a system report will be generated.	[s]
	S9PINT(J+1)	Master clock time after which the corresponding S9PINT is no longer valid.	[s]
		Note: The index J is incremented over the set of paired points. There may be as many pairs (intervals) as the users find necessary.	
	I	S9PINT(1) is imposed from time 0.0 to S9PINT(2). S9PINT(3) is then used from the master clock time S9PINT(2) to S9PINT(4). Similarly, S9PINT(5) is used from S9PINT(4) to S9PINT(6), and so on. It should be apparent that S9PINT(4) must be strictly greater than S9PINT(2), and S9PINT(6) must be strictly greater than S9PINT(4), and so on. There is quite a bit of latitude permitted in the selection Of print intervals, but they must be carefully chosen (see section 7.8)	
105	**L1EPRT**	Loop thermal report option; 0 - no report, 1 - report is generated	
	L1WPRT	Loop hydraulic report option; 0 - no report, 1 - report is generated	
	L3PRNT	Steam generator report option; 0 - no report, 1-4 - report is generated with correspondingly greater detail	
	L5PRNT	Fuel report option;	

0 - no report, 1 - report is generated

L6PRNT In-vessel coolant report option;
0 - no report, 1 - report is generated

L8PRNT PPS/PCS report option;
0 - no report, 1 - report is generated

OLDATA:

Exercise of other than default program control for the generation and subsequent use of restart data files.

PSDRS

Passive Decay Heat Removal System (PSDRS)

Rec.	Variable	Description	Unit
0	**Title**	The character of the problem title should not exceed 80 characters and there is no need for a card number.	
1		5 integer, 2 real numbers	
	ICARD(1)	Card identification number (= 1)	
	NTRAN	Steady Option Flag (0 = Steady cal./Otherwise, Number of steps for transient temperature variation)	
	ITRIP	PSDRS Trip Flag in 'driv9t.f' in SSC-K (= 0 : No Trip, Otherwise, Skip PSDRS Transient Calculation)	
	SEND	Steady calculation end time	
	NEQUTN	Number of equations to be solved (= 7)	
	JNODES	Total axial node numbers – same numbers for all components *Two air channels, namely, down-flow and up-flow Channels have JNODES each	
	DELT	Maximum time-step	[s]
2		3 integers, 3 real numbers	
	ICARD(2)	Card identification number (= 2)	
	TEND	Transient end time	[s]
	TPRINT	Major printing time	[s]
	JW	Node number where the temp. is to be monitored with time	
	NITER	Maximum allowable iteration number for air temperature convergence	
	CRIT	Convergence criteria for air temperature calculation	
3		4 integers	
	KTRAN(I)	Number of transient steps for each variable (3 consecutive numbers), I = 1, 3	[s]
4		1 integer, 2*KTRAN(1) real numbers	
	ICARD(4)	Card identification number (= 4)	
	TRANS(1,I)	Sodium level initiating time , I =1, KTRAN(1)	[s]
	XLSODM(I)	Sodium level inside the reactor vessel at the initiating time (I =1, KTRAN(1))	[m],

5		1 integer, 2*KTRAN(2) real numbers	
	ICARD(5)	Card identification number (= 5)	
	TRANS(2,I)	Sodium temp. initiating time, I =1,.KTRAN(2)	[s]
	TEMPNA(I)	Sodium temp. inside the Rx vessel at the initiating time I =1, KTRAN(2)	[°C],
6		1 integer, 2*KTRAN(3) real numbers	
	ICARD(6)	Card identification number (= 6)	
	TRANS(1,I)	Cover gas initiating time, I =1, KTRAN(3)	[s]
	TEMPHE(I)	Cover gas (HE) temp. inside the Rx vessel at the initiating time, I =1, KTRAN(3)	[°C]
7		1 integer, 6 real numbers	
	ICARD(7)	Card identification number (= 7)	
	DXRV	Thickness of reactor vessel	[m]
	DXGV	Thickness of guard vessel	[m]
	DXCON	Thickness of concrete wall	[m]
	DHGVFI	Hydraulic diameter between guard vessel and finned shell	[m]
	HRX	Height of active reactor vessel	[m]
	DHRX	Hydraulic Diameter of the inner Rx vessel	[m]
8		1 integer, 6 real numbers	
	ICARD(8)	Card identification number (= 8)	
	ZINLET	Height of air channel inlet to the ref. position	[m]
	DELZIN	Length of air channel inlet	[m]
	AREAIN	Air channel inlet area	[m^2]
	DHINLT	Hydraulic diameter of inlet air channel	[m]
	AAIR2	Down-flowing air channel area	[m^2]
	DHADWN	Hydraulic diameter of down-flowing air channel	[m]
9		1 integer, 6 real numbers	
	ICARD(9)	Card identification number (= 9)	
	ZSTACK	Height of air channel stack to the ref. position	[m]
	DELZSK	Length of air channel stack	[m]
	AREASK	Air flow area of stack	[m^2]
	DHSTCK	Hydraulic dia. of stack	[m]
	AAIR1	Up-flowing air channel area	[m^2]
	DHAUP	Hydraulic diameter of up-flowing air channel	[m]
10		1 integer, 3 real numbers	
	ICARD(10)	Card identification number (= 10)	

	AREAFR	Turbulence friction factor	
	BCONST	Constant to be used for boundary Reynold number between turbulent flow and laminar flow	
	AREAFL	Laminar friction factor	
11		1 integer, 6 real numbers	
	ICARD(11)	Card identification number (= 11)	
	ANW01	Vessel inner heat transfer area per unit length	[W/m]
	AW012	Circumference between reactor vessel and guard vessel	[W/m]
	AW023	Circumference between guard vessel and inner finned shell	[W/m]
	AW034	Circumference between inner finned shell and outer finned shell	[W/m]
	AW045	Circumference between outer finned shell and Concrete	[W/m]
	AW056	Circumference of concrete wall between the positions of TEMPW5(J) and TEMPW6	[W/m]
12		1 integer, 4 real numbers	
	ICARD(12)	Card identification number (= 12)	
	AW02A	Outer circumference of guard vessel	[W/m]
	AW03A	Inner circumference of finned shell	[W/m]
	AW04A	Outer circumference of finned shell	[W/m]
	AW05A	Inner circumference of concrete	[W/m]
13		1 integer, 2 real numbers	
	ICARD(13)	Card identification number (= 13)	
	FKORI1	Form Loss Coefficients for Orifices in the up-flowing channel	
	FKORI2	Form Loss Coefficients for Orifices in the down-flowing channel	
14		1 integer, 1 real numbers	
	ICARD(14)	Card identification number (= 14)	
	HCONHE	Vessel inner heat transfer coef. between Hellium and vessel wall	[W/m^2-°C]
15		1 integer, JNODES real numbers	
	ICARD(15)	Card identification number (= 15)	
	HCV12(J)	Heat transfer coef. between reactor vessel and guard vessel, J=1, JNODES	[W/m^2-°C]

16		1 integer, 2 real numbers	
	ICARD(16)	Card identification number (= 16)	
	HW034	Heat transfer coef. between inner node and outer node of divider	[W/m^2-°C]
	HW056	Heat transfer coef. between concrete and constant heat sink	[W/m^2-°C]
17		1 integer, 5 real numbers	
	ICARD(17)	Card identification number (= 17)	
	WLMASS(I)	Mass per unit length for each wall	[Kg/m]
18		1 integer, 10 real numbers	
	ICARD(18)	Card identification number (= 18)	
	WLSPEC(I)	Specific heat for each wall	[J/Kg-°C]
	WLCONK(I)	Thermal conductivity for each wall	[W/m-°C]
19		1 integer, 7 real numbers	
	ICARD(19)	Card identification number (= 19)	
	EPSRV	Emissivity on reactor vessel wall	
	EPSGVI	Emissivity on guard vessel inner wall	
	EPSGVO	Emissivity on guard vessel outer wall	
	EPSFSI	Emissivity on finned shell inner wall	
	EPSFSO	Emissivity on finned shell outer wall	
	EPSOW	Emissivity on concrete wall	
	CONCK	Thermal conductivity of concrete	[W/m-°C]
20		1 integer, 4 real numbers	
	ICARD(20)	Card identification number (= 20)	
	TEMPIN	Inlet air temperature	[°C]
	TEMPW6	Constant concrete outer wall temperature	[°C]
	WAIR0	Initial user guessing air flow rate	[kg/s]
21		1 integer, 2 real numbers	
	ICARD(21)	Card identification number (= 21)	
	XLSODM1	Initial sodium level in the reactor vessel	[m]
	TEMPNA1	Initial sodium temp. in the reactor vessel	[°C]
	TEMPHE1	Initial cover gas (Helium) temp. in the reactor vessel	[°C]
22		1 integer, JNODES real numbers	
	ICARD(22)	Card identification number (= 22)	
	TEMP1	Reactor vessel initial temp.	[°C]
	TEMP2	Guard vessel initial temp.	[°C]
	TEMPA	Upflow air initial temp.	[°C]

TEMP3	Divider inner node initial temp.	[°C]
TEMP4	Divider shell outer node initial temp.	[°C]
TEMP5	Concrete inner node initial temp.	[°C]

APPENDIX B Subroutines in SSC-K

The SSC-K code has a modularized structure. The code is divided into three major sequentially disjointed processes of MAIN9R, MAIN9S, and MAIN9T as shown in Fig. B.1. These routines are the main driver programs and are called in succession by the controller routine. Each performs a unique set of tasks and is executed only once for any given case. It should be noted that the modules necessary to describe the characteristics of the pool design and reactivity models for metallic fuel were changed or added to the SSC-K code. The remainder of the code was obtained from the SSC-L library.

The flow chart of each of the drivers, along with its associated subroutines, is shown in Figs. B.1 through B.5. Note on these figures that subroutines designated by an underline are the changed or added ones for SSC-K. A brief description of all subroutines used in SSC-K, except for the MINET code portion, is presented in Appendix B.

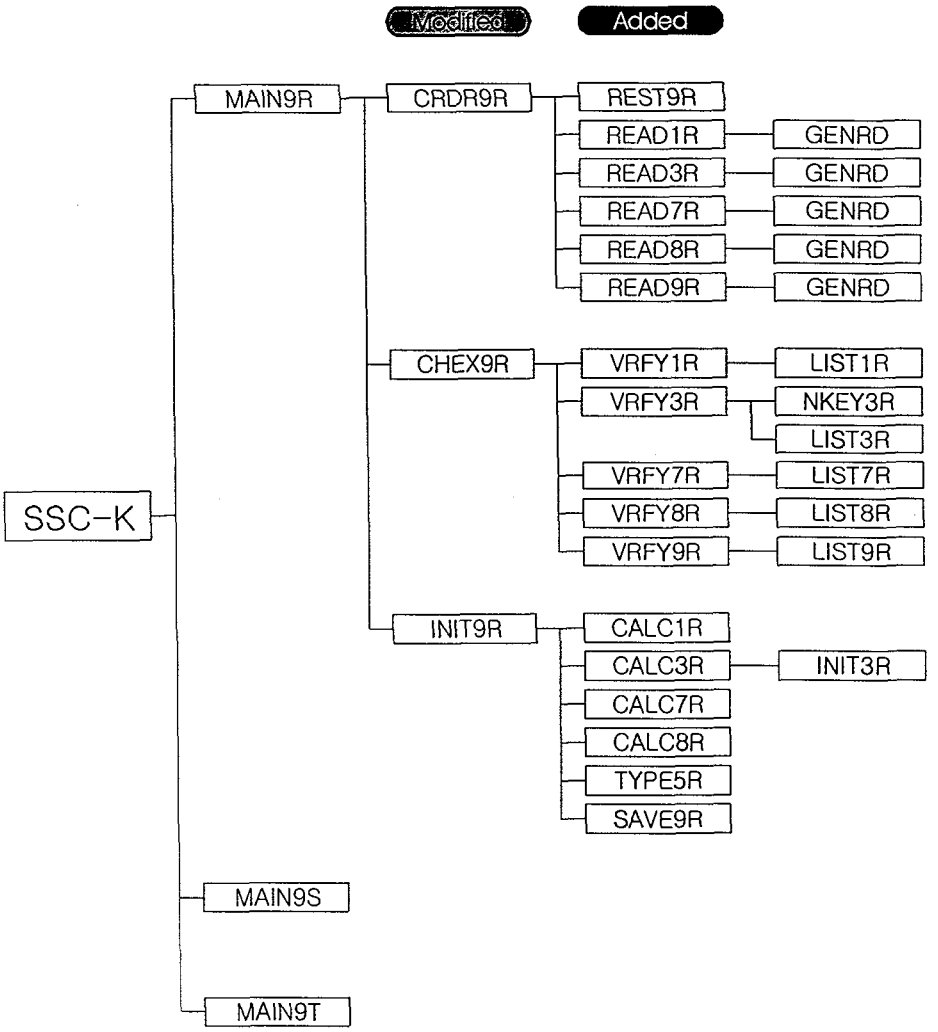

Fig. B.1 Subroutines for Input Processing

MAIN9R	main driver for the input initialization module
CRDR9R	primary controller for the processing of initialization data. It calls the free-format reader routines
REST9R	reads a program generated file for the re-initialization of labeled common in the event of a restart
READ1R	processes the input for the initialization of the primary and secondary loop module
GENRD	general purpose reader routine
READ3R	processes input for the initialization of the steam generator module
GENRD	general purpose reader routine
READ7R	processes input for the initialization of the in-vessel module
GENRD	general purpose reader routine
READ8R	processes input for the initialization of the plant balance routine
GENRD	general purpose reader routine
READ9R	processes input for the initialization of the material property parameters
GENRD	general purpose reader routine
CHEX9R	calls for the verification routines
VRFY1R	validates the data processed by the corresponding READ routines
LIST1R	lists the data processed by the corresponding READ routines
VRFY3R	validates the data processed by the corresponding READ routines
NKEY3R	assists in the decoding of steam generator input
LIST3R	lists the data processed by the corresponding READ routines
VRFY7R	validates the data processed by the corresponding READ routines
LIST7R	lists the data processed by the corresponding READ routines
VFRY8R	validates the data processed by the corresponding READ routines
LIST8R	lists the data processed by the corresponding READ routines
VRFY9R	validates the data processed by the corresponding READ routines
LIST9R	lists the data processed by the corresponding READ routines
INIT9R	calls a series of intermediate data management routines
CALC1R	manipulates certain primary and secondary loop input data / initializes subsequent loop structures
CALC3R	loads the input data into the data arrays
INIT3R	initializes certain steam generator constants
CALC7R	sets slice-type dependent arrays and determines normalized axial and radial power distribution
CALC8R	interprets the coded iterative scheme for establishing the initial plant balance
TYPE5R	loads channel-dependent parameters for use in the slice-type-dependent in-vessel modules
SAVE9R	generates an ordered file for a re-initialization restart

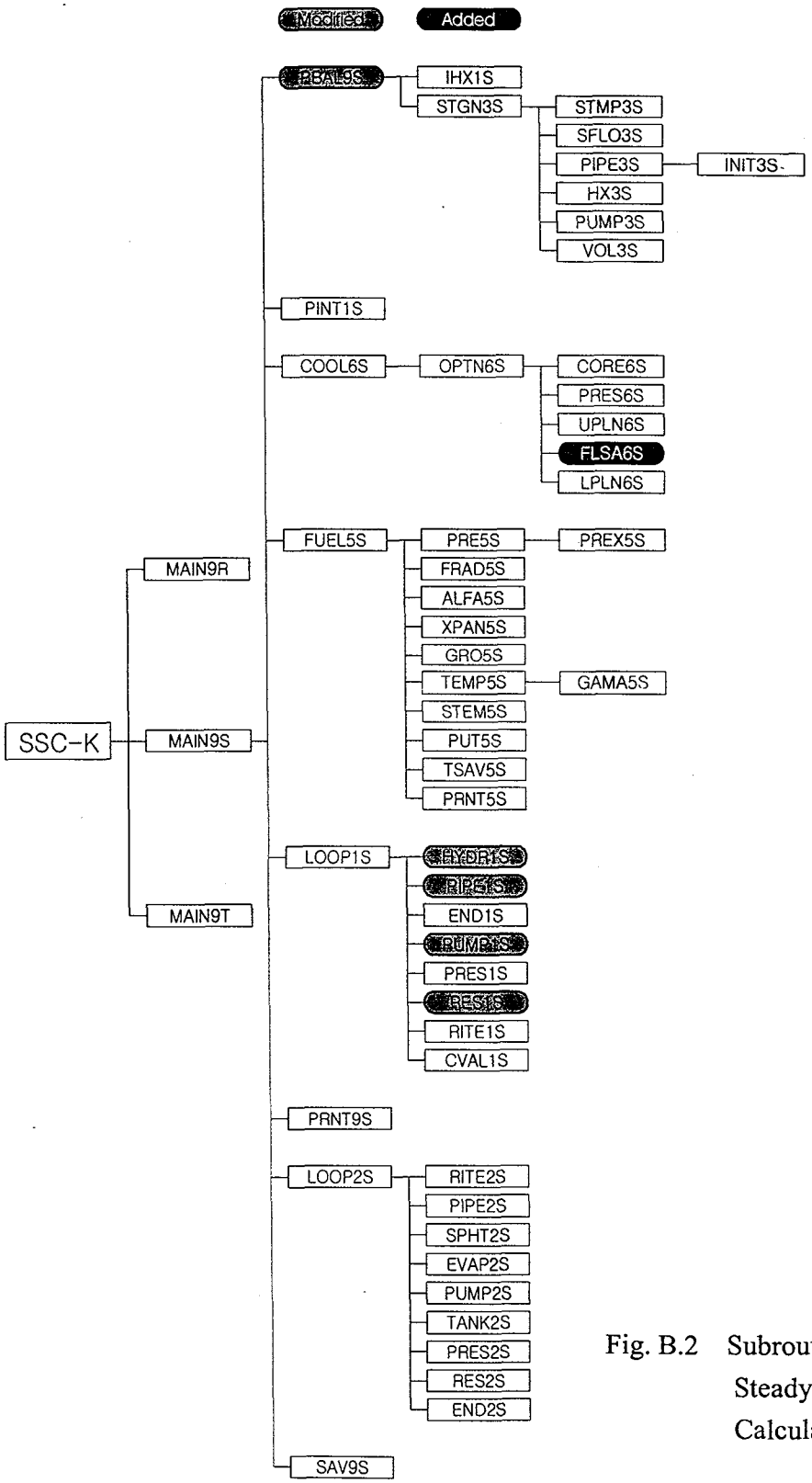

Fig. B.2 Subroutines for Steady-State Calculation

MAIN9S	main driver for the steady-state calculations
PBAL9S	performs the global thermal balance for the whole plant
IHX1S	solves the steady-state energy equations for the IHX. IHX1S and HYDR1S are the only interface between the primary and intermediate loop
STGN3S	main driver for the SG calculations
STMP3S	determines the sodium inlet temperature
SFLO3S	determines the sodium flow rate per tube
PIPE3S	computes the pressure at the exit of a pipe
INIT3S	loads initial guesses for steam pressures, mass flow rates, enthalpies and heat transfer rates. Values for pressure and mass are user-input. Initial enthalpies and heat transfer rates are zeroed, as ENET3S is called soon after INIT3S.
HX3S	performs the heat exchanger model calculations. It determines the pressure drop in the inlet plenum of the heat exchanger, calls the routines which determines the enthalpy and pressure distributions in the heat transfer tube, and calculates the pressure drop in the outlet plenum of the heat exchanger. It determines the location of the DNB point and adjusts the total heat transfer area to produce specified outlet conditions.
PUMP3S	computes the pump outlet pressure at rated pump speed or the pump speed if the pump outlet pressure is specified
VOL3S	calculates the mixed mean enthalpy in a volume based on the liquid level and the pressure specified in the volume
PINT1S	interfaces the in-vessel and primary loop pressures
COOL6S	driver module for in-vessel coolant calculations
OPTN6S	computes the steady-state channel flow rate distribution or pressure loss coefficients
CORE6S	core coolant: It calculates axial temp., enthalpy gradients, friction factors, heat transfer coefficients and pressures each node in each channel
PRES6S	determines the nodal pressures in each reactor coolant channel
UPLN6S	coolant module: calculates upper plenum temp. exit quality, outlet, and top of core pressures and finds pressure loss factors for each channel
FLSA6S	calculates pressure equalization loss coefficient at top of assembly
LPLN6S	lower plenum module: initializes values of temperature, enthalpy, and pressure for the first axial nodal interface of each channel. It calculates pressures at the bottom of the core
FUEL5S	driver module for fuel heat conduction calculations. It treats a fuel slice as the basic computational element, calls all major fuel computational modules, and controls convergence
PRE5S	performs the initialization for FUEL5S by obtaining data computed by other modules. Among others, it sets the proper rod nodal

	temperature to T6COOL(J,K), places the heat transfer coefficient for the slice in a local variable HCOOL, initializes tags for restructuring and calls PREX5S to initialize nodal distances at temperature T5REF
PREX5S	initializes nodal distances for either equal radius increments or equal area increments of the rod slice
FRAD5S	calculates the average power generation for all radial nodes in any core channel slice
ALFA5S	calculates the coefficient of thermal expansion for each node in the fuel slice
XPAN5S	adjusts radii due to thermal expansion for each node in the fuel slice
GRO5S	sets pointers for restructuring in the slice
TEMP5S	calculates the steady-state radial temperature distribution in the rod and cladding for any slice
GAMA5S	calculates the thermal conductivity for fuel and clad nodes for the slice and heat transfer coefficients for the interfaces
STEM5S	calculates the temperature of the fuel rod structure and fission gas plenum for steady-state
PUT5S	moves the calculated steady-state values for the slice into storage locations
TSAV5S	determines the average temperature in each rod slice except fission gas plenum slice
PRNT5S	prints steady-state results for the fuel calculations
LOOP1S	drives the primary loop steady-state calculations. It interprets the logical variables in order to select the proper calling sequence to the various subroutines. This routine also copies the results of the computations for loop-1 into the arrays for the rest of the loop
HYDR1S	solves the steady-state hydraulic momentum equations for both primary and secondary sides of the IHX
PIPE1S	solves the steady-state energy and momentum equations for pipe J in the primary coolant loop
END1S	calculates the temperature boundary conditions for the sub-pipe in the primary loop and accounts for the temperature rise across pump, as well as IHX plena temperatures at the proper locations
PUMP1S	determines pump pressure rise by matching it with overall load in the primary circuit. It then sets up the polynomial equation for pump head and calls ROOT1U to calculate pump operating speed
RES1S	computes the height of coolant in the primary pump tank, and the mass of cover gas above the coolant level
RITE1S	prints the primary loop steady-state solution
CVAL1S	computes the steady-state pressure drop over the check valve
PRNT9S	prints a plant-wide steady-state summary of results
LOOP2S	drives the intermediate loop steady-state computation. The rest of the description is the same as for LOOP1S

RITE2S	prints the secondary loop steady-state solution
PIPE2S	solves the steady-state energy and momentum equations for pipe J in the intermediate coolant loop
SPHT2S	calculates the pressure drop or loss coefficient on the shell side of the superheater
EVAP2S	calculates the pressure drop or loss coefficient on the shell side of the evaporator
PUMP2S	determines pump pressure rise by matching it with overall load in the intermediate circuit
TANK2S	computes the pressure in the loop at the location of the surge tank, and further, calculates the mass of gas in the surge tank
PRES2S	determines the pressure at pipe end points around the intermediate loop
RES2S	computes the height of coolant in the intermediate pump tank, and the mass of cover gas above the coolant level
END2S	sets the inlet temperature and mass flow rate boundary conditions for pipe J+1 in the intermediate coolant loop
SAV9S	creates an ordered file containing information necessary to re-initialize all common blocks to computed steady-state values

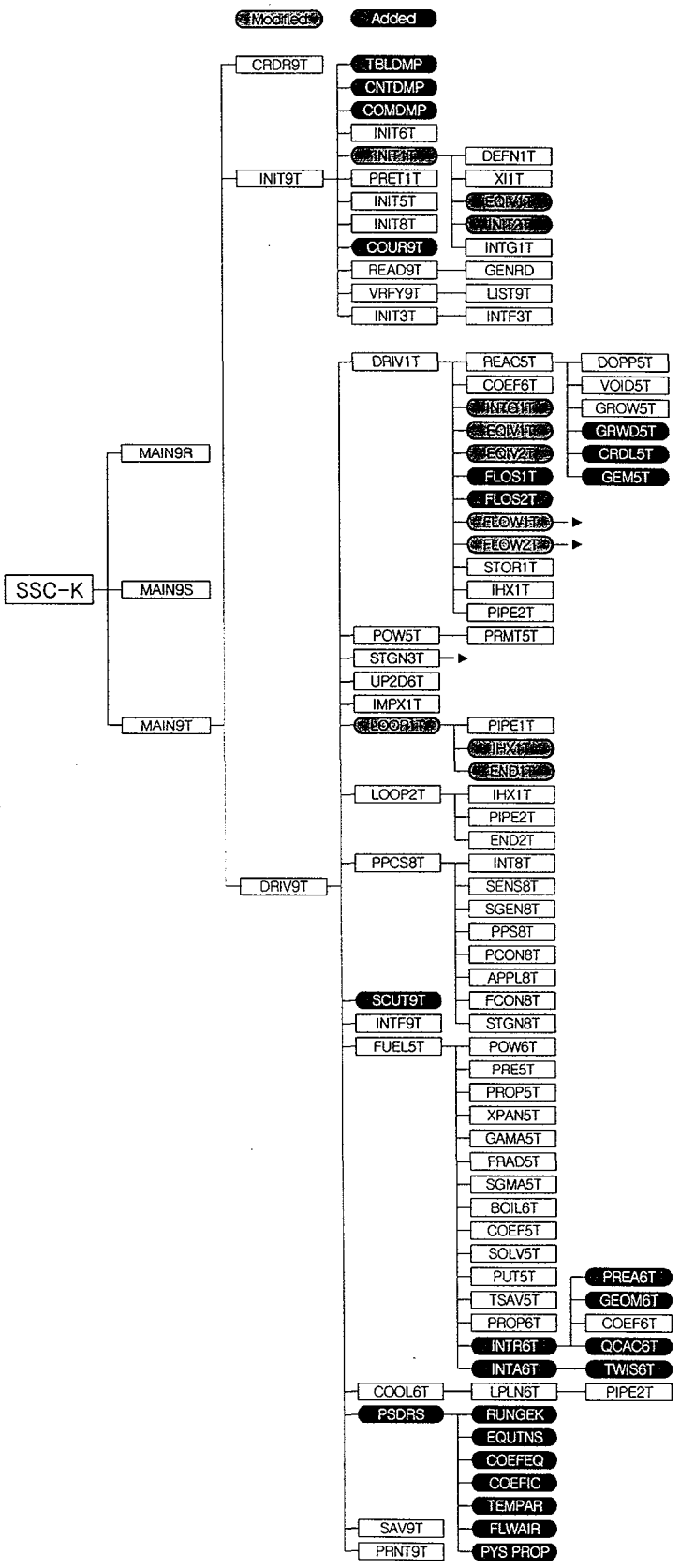

Fig. B.3 Subroutines for Transient Calculation

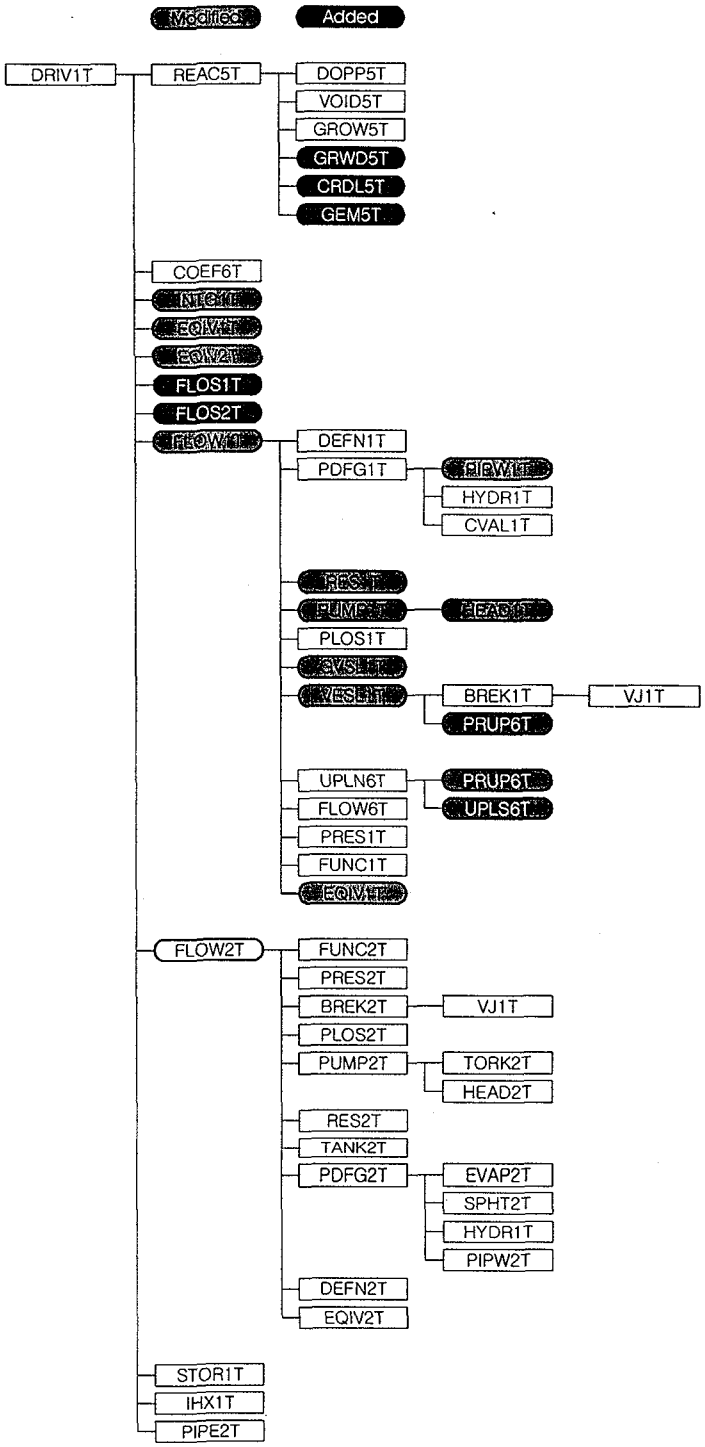

Fig. B.3 Subroutines for Transient Calculation (Continued)

MAIN9T	overall driver routine for the transient calculations
CRDR9T	
INIT9T	intermediate controller for the transient initialization routines
TBLDMP	lists global container allocations
CNTDMP	list all global locations in the container
COMDMP	
INIT6T	initiates variables used by the in-vessel coolant hydraulics modules
INIT1T	sets variables needed for the first call to the primary loop hydraulic integration scheme
DEFN1T	defines pipe flow rates, and input and output pump flow rates for primary loop
XI1T	
EQIV1T	equivalences the names of primary loop variables and their time intervals in terms of names in the integrating subroutine
INIT2T	sets variables needed for the first call to the secondary loop hydraulic integrating routine
INTG1T	advances the hydraulic equations using the predictor-corrector method of the Adams type
PRET1T	initializes the primary and secondary loop variables for the thermal calculations
INIT5T	initializes variables used in the fuel and reactivity calculations
INIT8T	initializes values used in the PPS/PCS subroutines
COUR9T	calculates Courant condition for all channels
READ9T	reads free-format card-image input for the initialization of transient parameters
GENRD	general purpose reader routine
VRFY9T	validates the data processed by the READ9T routine against the criteria established in the data dictionary
LIST9T	lists the data processed by READ9T
INIT3T	initializes transient variables used by the steam generator modules
INTF3T	interfaces the required boundary conditions between all intermediate sodium loops and all steam generator heat exchanger
DRIV9T	driver routine for the transient calculations. It also handles the overall time step control
DRIV1T	driver for heat transport system transient hydraulics
REAC5T	initiates calls to other modules to obtain the various applied and

	feedback reactivity contributions
DOPP5T	calculates the reactivity feedback due to Doppler effect
VOID5T	calculates the reactivity feedback due to sodium voiding
GROW5T	calculates the reactivity feedback due to axial expansion
GRWD5T	calculates the reactivity feedback due to radial expansion
CRDL5T	calculates the reactivity feedback due to CRDL expansion
GEM5T	calculates the reactivity feedback due to GEM
COEF6T	calculates coefficients for the various pressure loss terms used in FLOW6T
INTG1T	advances the hydraulic equations using the predictor-corrector method of the Adams type
EQIV1T	equivalences the names of primary loop variables and their time derivatives in terms of names used in the integrating subroutine
EQIV2T	equivalences the names of intermediate loop variables and their time derivatives in terms of names used in the integrating subroutine
FLOS1T	calls subroutines to integrate implicit hydraulic differential equations
FLOS2T	calls subroutines to integrate implicit hydraulic equations in intermediate loop
FLOW1T	sets proper calling sequence to primary loop hydraulic computation submodules
DEFN1T	defines pipe flow rates, and input and output pump flow rates for primary loop
PDFG1T	sets the logic to compute pressure losses across different elements of primary loops
PIPW1T	computes pressure losses in pipe sections in primary loops
HYDR1T	computes transient hydraulics in IHX
CVAL1T	computes the pressure loss across the check valve
RES1T	computes variables and time derivatives for level in primary pump reservoir
PUMP1T	computes primary pump variables and time derivative for pump speed
HEAD1T	computes head of primary pumps and defines its operational region
PLOS1T	computes pressure losses in appropriate sections of primary loop from the losses in individual components
GVSL1T	computes coolant level in guard vessel, pressure external to break,

	and time derivative for accumulated volume of coolant in the guard vessel
VESL1T	calculates certain algebraic relationships at the vessel-loop(s) interface(s) and within the vessel which are used in the hydraulic computations
BREK1T	computes pressures at eventual break in primary loop
VJ1T	determines velocity of jet out of a pipe break
PRUP6T	calculates the vessel outlet pressure and core top pressure for the one-dimensional two zone upper plenum model
UPLN6T	one-dimensional two zone upper plenum model
PRUP6T	calculates the vessel outlet pressure and core top pressure for the one-dimensional two zone upper plenum model
UPLS6T	updates the time derivatives for sodium level, sodium temperatures in two mixing zones, cover gas temperature, and temperature of the inner structure, thermal liner and vessel
FLOW6T	simulates the flow redistribution model. It calculates the mass flow rate in each channel and bypass channel
PRES1T	sets inlet and outlet pressures of uniform mass flow rate sections in primary loops
FUNC1T	calculate the time derivatives of differential equations for primary loop hydraulics
EQIV1T	equivalences the names of primary loop variables and their time derivatives in terms of names used in the integrating subroutine
FLOW2T	sets proper calling sequence to intermediate loop hydraulic computation submodules
FUNC2T	calculate the time derivatives of differential equations for intermediate loop hydraulics
PRES2T	sets inlet and outlet pressures of uniform mass flow rate sections in intermediate loops
BREK2T	computes pressures at eventual break in intermediate loop
VJ1T	determines velocity of jet out of a pipe break
PLOS2T	computes pressure losses in appropriate sections of intermediate loop from the losses in individual components
PUMP2T	computes intermediate pump variables and time derivatives for pump speed
TORK2T	computes hydraulic and friction torques for intermediate pumps
HEAD2T	computes head of intermediate pumps and defines its operational

	region
RES2T	computes variables and time derivatives for level in intermediate pump reservoir
TANK2T	computes pressures and time derivatives for level in surge tank
PDFG2T	sets the logic to compute pressure losses across different elements of intermediate loops
EVAP2T	computes pressure loss across the shell side of evaporator
SPHT2T	computes pressure loss across the shell side of superheater
HYDR1T	computes transient hydraulics in IHX
PIPW2T	computes pressure losses in pipe sections in intermediate loops
DEFN2T	defines pipe flow rates, and input and output pump flow rate for intermediate loop
EQIV2T	equivalences the names of intermediate loop variables and their time derivatives in etrms of names used in the integrating subroutine
STOR1T	stores the intermediate updated values of flow rate
IHX1T	solves transient energy equations in the IHX
PIPE2T	solves transient energy equations in the intermediate loop piping
POW5T	serves as the driver for the rod transient fission power generation calculations
PRMT5T	handles the advancement in time of the fission power generation
STGN3T	main driver for the steam generator calculation. It calls routines which computes accumulator conditions, backsubstitutes accumulator conditions to advance flow sequence variables, and determines the maximum change in water side variables during this step
UP2D6T	2D upper plenum model
IMPX1T	–
LOOP1T	main driver for transient thermal calculations in primary loop
PIPE1T	solves transient energy equations in the primary loop piping
IHX1T	solves transient energy equations in the IHX
END1T	sets transient thermal boundary conditions from one pipe to the next in primary loop
LOOP2T	main driver for transient thermal computations in intermediate loop
IHX1T	solves transient energy equations in the IHX
PIPE2T	solves transient energy equations in the intermediate loop piping
END2T	sets transient thermal boundary conditions from one pipe to the next

	intermediate loop
PPCS8T	main driver for the PPS/PCS transient calculations
INT8T	interfaces the PPS/PCS modules to the rest of SSC by fetching the actual values of the desired process variables for cascade selection for reactor power control and normalizing them against their respective 100% steady-state values. It also calls other subroutines to do similar calculations for PPS, flow controllers and the steam generator controllers
SENS8T	takes the actual sensed values from the controller cascades and compensates them for the inherent time lags imposed by the measuring devices
SGEN8T	calculates the load-dependent setpoints as governed by the supervisory controller, using the user specified second-order polynomial coefficients
PPS8T	subdriver routine for the plant protection system
PCON8T	simulates the reactor power control and the control rod drive mechanism. It also calculates the reactivity worth of the reactor control rods
APPL8T	calculates the scram reactivity worth of the primary and/or secondary control rods utilizing the user supplied polynomial coefficients for rod position as a function of time after reactor scram
FCON8T	simulates the sodium flow-speed control and the pump drive mechanism
STGN8T	subdriver for steam generator controller routines
SCUT9T	controls timestep after scram
INTF9T	checks the adequacy of all extrapolated interface conditions
FUEL5T	driver for the fuel rod and structure calculations. By calling series of modules in succession; it calculates, quantities such as temperature and radii of the fuel, cladding, and structure nodes
POW6T	calculates power to coolant for use in COOL6T
PRE5T	transfers the temperature from storage arrays into local scratch arrays for the particular slice in question, at the start of each time-step
PROP5T	calculates all properties for the fuel (rod) heat conduction calculations
XPAN5T	recalculates the radii of the fuel and cladding, necessary because of the thermal expansion of the radial nodes. Two methods are

	employed in calculating radii, equal area increment, and equal radii increment calculating radii; equal area increment, and equal radii increment
GAMA5T	calculate the thermal conductivity and emissivity for fuel and clad nodes and also computes the heat transfer coefficient for gaseous mixtures in the gap
FRAD5T	calculates average power for all radial nodes in any rod slice. It also calculates the power generation multiplier to be used later in calculating the transient volumetric power generation
SGMA5T	calculates the volumetric heat source for the fuel (rod) nodes, clad, coolant and structure in an axial slice
BOIL6T	calculates liquid and bubble temperature in upper and lower slugs
COEF5T	calculates appropriate coefficients for the transient temperature calculations of fuel rod
SOLV5T	solves the fuel (rod) matrix equation using Gaussian elimination with fuel pivoting
PUT5T	at the time this module is invoked, all formal calculations of the fuel and clad and structure have been completed for that timestep and for the given axial node. This module then move all temperatures and radii so far calculated from local scratch variables into storage arrays for subsequent timesteps
TSAV5T	calculates certain fuel slice dependent quantities required in GROW5T, DOPP5T, and VOID5T
PROP6T	calculates all properties used in the in-vessel coolant energy and fluid dynamics subroutines
INTR6T	main driver for interassembly heat transfer
PREA6T	calculates channel flow area
GEOM6T	
COEF6T	calculates coefficients for the various pressure loss terms used in FLOW6T
QCAC6T	calculates interassembly heat transfer
INTA6T	calculates interassembly heat transfer
TWIS6T	calculates interassembly heat transfer
COOL6T	driver for the transient coolant calculations. It provides initial conditions; determines step size; and then employs several submodules to calculate temperature, pressure, enthalpy, and mass flow rate of the coolant in all axial nodes of all channels. It then

	stores values for fuel calculations
LPLN6T	performs transient lower plenum calculations. It extrapolates boundary conditions. It determines its procedure by calculating coolant and metal temperature and pressures at the bottom of the core
PIPE2T	solves transient energy equations in the intermediate loop piping
PSDRS	PSDRS 해석
RUNGEK	비선형 미분방정식의 해 구함
EQUTNS	온도 변화율에 대한 지배방정식의 정의
COEFEQ	지배방정식의 항 계수 결정
COEFIC	지배방정식을 구성하는 물리계수의 계산
TEMPAR	노드의 평균온도 계산
FLWAIR	공기 유동량 계산
PSY PROP	각종 물성치 계산
SAV9T	creates an ordered file containing information necessary to re-initialize all common blocks to a given master clock solution
PRNT9T	main printing routine for the transient

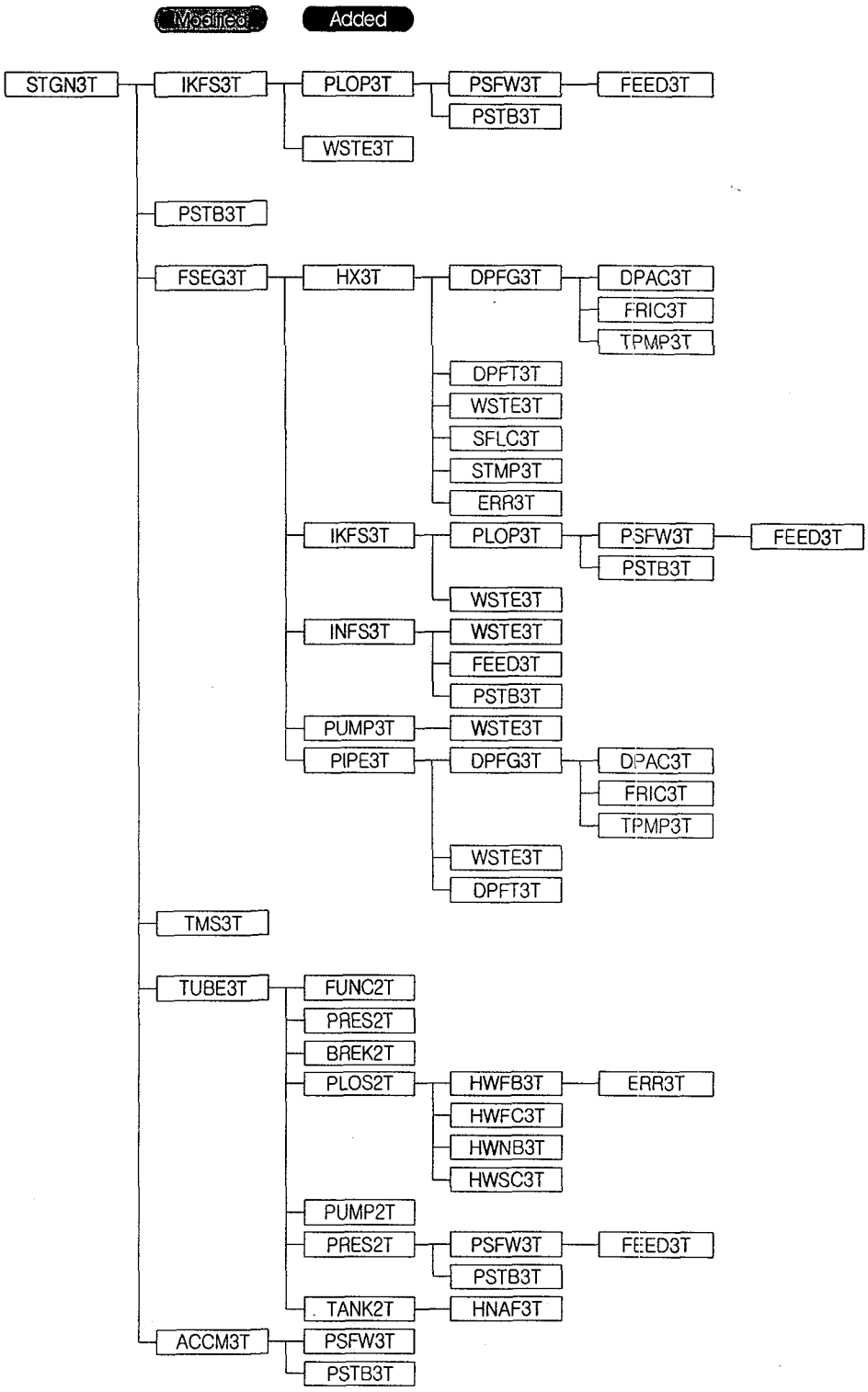

Fig. B.4 Subroutines for Steam Generator (MINET Portion)

STGN3T	main driver for the steam generator calculation. It calls routines which computes accumulator conditions, backsubstitutes accumulator conditions to advance flow sequence variables, and determines the maximum change in water side variables during this step
IKFS3T	determines pointers for all arrays needed in the flow segment calculations
PLOP3T	determines reference pressure for a flow segment
PSFW3T	determines reference pressure for a flow segment
FEED3T	determines reference coefficients for feedwater flow rate
PSTB3T	determines turbine inlet pressure
WSTE3T	determines water properties as function of enthalpy and pressure
PSTB3T	determines turbine inlet pressure
FSEG3T	main driver for flow segment calculations
HX3T	determines coefficients for energy and flow equation for water side of heat exchanger and advances sodium temperature
DPFG3T	determines coefficients of total flow resistance in control volume
DPAC3T	determines the coefficients of momentum flux pressure loss in control volume
FRIC3T	determines friction factor as function of Reynolds number and surface roughness
TPMP3T	determines two-phase friction multiplier on the water/steam side of the steam generator
DPFT3T	determines coefficients of pressure drop in a fitting using form loss coefficient
WSTE3T	determines water properties as function of enthalpy and pressure
SFLC3T	
STMP3T	determines sodium temperature at heat exchanger inlet from boundary conditions
ERR3T	writes error message
IKF3T	
PLOP3T	determines reference pressure for a flow segment
PSFW3T	determines reference pressure for a flow segment
FEED3T	determines reference coefficients for feedwater flow rate
PSTB3T	determines turbine inlet pressure
WSTE3T	determines water properties as function of enthalpy and pressure
INFS3T	

WSTE3T	determines water properties as function of enthalpy and pressure
FEED3T	determines reference coefficients for feedwater flow rate
PSTB3T	determines turbine inlet pressure
PUMP3T	determines coefficients for energy and flow equations for a pump
WSTE3T	determines water properties as function of enthalpy and pressure
PIPE3T	determines coefficients for energy and flow equations for a pipe
DPFG3T	determines coefficients of total flow resistance in control volume
DPAC3T	determines the coefficients of momentum flux pressure loss in control volume
FRIC3T	determines friction factor as function of Reynolds number and surface roughness
TPMP3T	determines two-phase friction multiplier on the water/steam side of the steam generator
WSTE3T	determines water properties as function of enthalpy and pressure
DPFT3T	determines coefficients of pressure drop in a fitting using form loss coefficient

TMS3T

TUBE3T	calculates surface heat fluxes and tube wall temperatures in heat exchanger
FUNC2T	calculates the time derivatives of differential equations for intermediate loop hydraulics
PRES2T	sets inlet and outlet pressures of uniform mass flow rate sections in intermediate loops
BREK2T	computes pressures at eventual break in intermediate loop
PLOS2T	computes pressure losses in appropriate sections of intermediate loop from the losses in individual components
HWFB3T	determines heat transfer coefficient in film boiling
ERR3T	writes error message
HWFC3T	determines heat transfer coefficient in forced convection to liquid
HWNB3T	determines heat transfer coefficient in nucleate boiling of subcooled or saturated water
HWSC3T	determines heat transfer coefficient in forced convection to super-heated steam
PUMP2T	computes intermediate pump variables and time derivative for pump speed
PRES2T	sets inlet and outlet pressures of uniform mass flow rate sections in intermediate loops

PSFW3T	determines reference pressure for a flow segment
FEED3T	determines reference coefficients for feedwater flow rate
PSTB3T	determines turbine inlet pressure
TANK2T	computes pressures and time derivative for level in surge tank
HNAF3T	computes sodium side surface heat transfer coefficient
ACCM3T	calculates coefficients for accumulator, eliminates flow segment terms for accumulator equations, and advances the accumulator variables
PSFW3T	determines reference pressure for a flow segment
PSTB3T	determines turbine inlet pressure

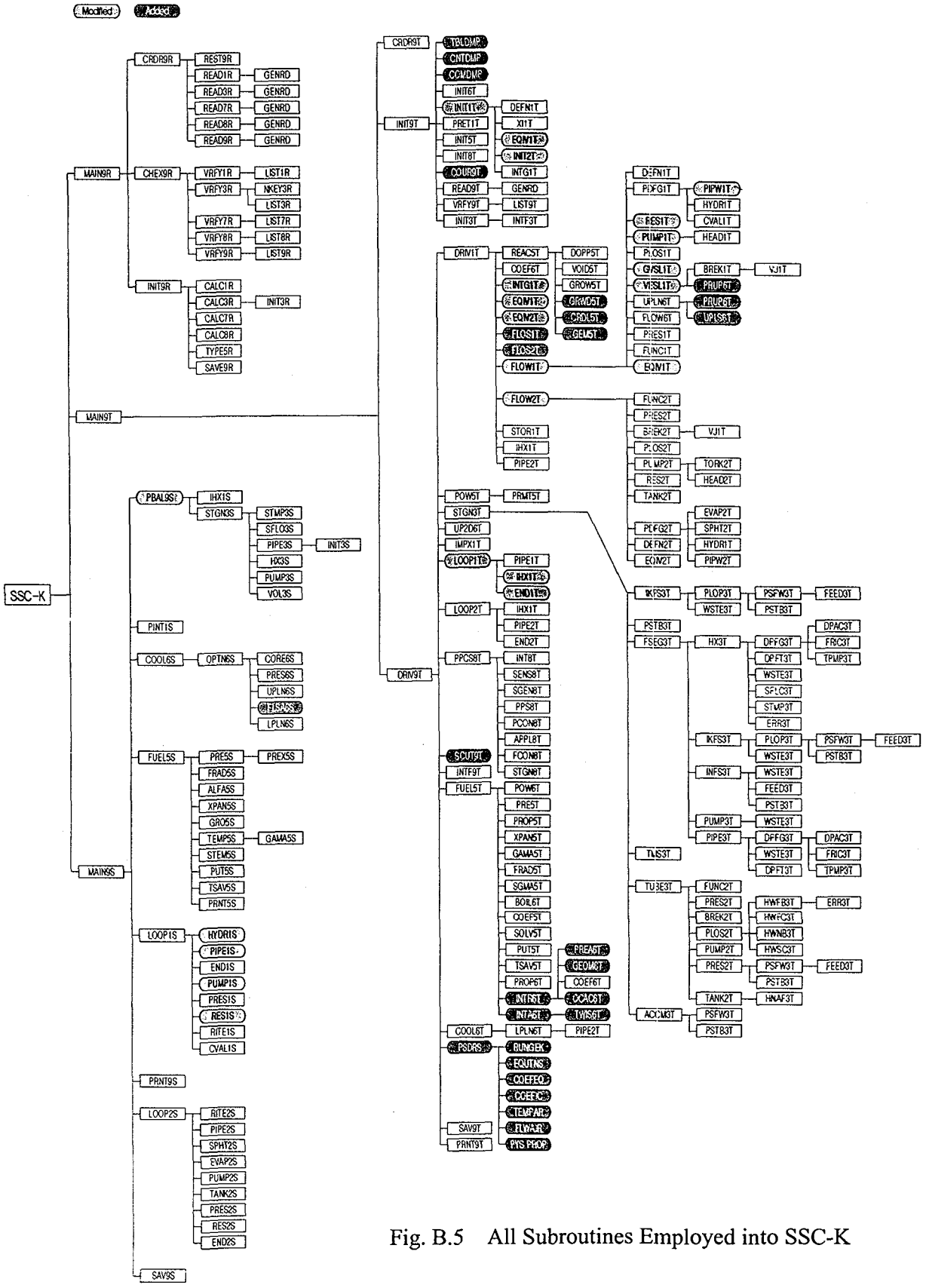

Fig. B.5 All Subroutines Employed into SSC-K

BIBLIOGRAPHIC INFORMATION SHEET

Performing Org. Report No.	Sponsoring Org. Report No.	Standard Report No.	INIS Subject Code
KAERI/TR-1619/2000			

Title / Subtitle	SSC-K Code User's Manual
Main Author	Y. M. Kwon (KALIMER Technology Development Team)
Researcher and Department	Y. B. Lee, W. P. Chang, D. Hahn (KALIMER Technology Development Team)

Publication Place	Taejon	Publisher	KAERI	Publication Date	2000. 7
Page	270 p.	I11. & Tab	Yes(O), No( )	Size	29.7 cm
Note					

Classified	Open(o), Restricted( ), Class Document	Report Type	Technical Report
Sponsoring Org.	ROK MOST	Contract No.	

Abstract (15-20 Lines)

The Supper System Code of KAERI (SSC-K) is a best-estimate system code for analyzing a variety of off-normal or accidents in the heat transport system of a pool type LMR design. It is being developed at Korea Atomic Energy Research Inititution (KAERI) on the basis of SSC-L, originally developed at BNL to analyze loop-type LMR transients. SSC-K can handle both designs of loop and pool type LMRs. SSC-K contains detailed mechanistic models of transient thermal, hydraulic, neutronic, and mechanical phenomena to describe the response of the reactor core, coolant, fuel elements, and structures to accident conditions. This report provides an overview of recent model developmentsvfor the SSC-K computer code, focusing on phenomenological model descriptions for new thermal, hydraulic, neutronic, and mechnaical modules. A comprehensive description of the models for pool-type reactor is given in Chapters 2 and 3; the steady-state plant characterization, prior to the initiation of transient is described in Chapter 2 and their transient counterparts are discussed in Chapter 3. In Chapter 4, a discussion on the intermediate heat exchanger (IHX) is presented. The IHX model of SSC-K is similar to that used in the SSC-L, except for some changes required for the pool-type configuration of reactor vessel. In Chapter 5, an electromagnetic (EM) pump is modeled as a component. There are two pump choices available in SSC-K; a centrifugal pump which was originally imbedded into the SSC-L, and an EM pump which was introduced for the KALIMER design. In Chapter 6, a model of passive safety decay heat removal system (PSDRS) is discussed, which removes decay heat through the reactor and containment vessel walls to the ambient air heat sink. In Chapter 7, models for various reactivity feedback effects are discussed. Reactivity effects of importance in fast reactor include the Doppler effect, effects of sodium density changes, effects of dimensional changes in core geometry. Finally in Chapter 8, constitutive laws and correlations required to execute the SSC-K are described. It is noted that the user's manual will be revised later with the further development of SSC-K.

Subject keywords (About 10 words)	LMFBR, SSC-K, Safety Analysis Code

서 지 정 보 양 식					
수행기관보고서번호	위탁기관보고서번호	표준보고서번호	INIS 주제코드		
KAERI/TR-1619/2000					
주제 / 부제	SSC-K 전산코드 사용자 지침서				
주저자 및 부서명	권영민 (KALIMER 기술개발팀)				
연 구 자 및 부 서 명	이용범, 장원표, 한도희 (KALIMER 기술개발팀)				
출 판 지	대 전	발행기관	한국원자력연구소	발행년	2000. 7
페 이 지	270 p.	도 표	있음(O), 없음( )	크 기	29.7 cm
참고사항					
비밀여부	공개(o), 대외비( ), _급비밀	보고서종류	기술보고서		
연구위탁기관	과학기술부	계약번호			
초록 (15-20 줄내외)	한국원자력연구소 (KAERI)는 Pool 형 액체금속로인 KALIMER 의 다양한 비정상 조건 및 사고를 분석하기 위하여 최적열수력 전산코드인 SSC-K (Supper System Code of KAERI)를 개발하고 있다. SSC-K 는 미국 BNL 에서 루프형 액체금속로의 안전해석을 위해 개발된 SSC-L 을 기반으로 하여 KALIMER 와 같은 풀형 원자로에 적용할 수 있도록 개발되었다. 현재 SSC-K 코드는 루프형과 풀형의 액체금속로를 모두 모의할 수 있다. SSC-K 는 과도상태의 열수력, 핵 및 기계적 모델을 포함하고 있으므로 사고시 노심과 냉각재, 핵연료의 거동 및 구조물의 온도변화를 모의할 수 있다. 본 보고서는 SSC-K 를 위하여 새로이 개발된 여러 현상학적인 모델들을 기술하고 있으며 부록에는 코드입력에 대한 설명을 포함하고 있다. 풀형 원자로 열수력 계산을 위해 개발된 정상상태 및 과도상태의 모델을 2 장과 3 장에 상세히 설명하였다. 4 장에는 기존 SSC-L 코드의 IHX 모델을 풀형의 원자로 구성에 적합하도록 변경된 중간열전달교환기 (IHX) 모델에 대해서 기술하였다. 5 장에는 전자펌프 모델을 설명하였으며, SSC-K 는 기존의 원심펌프 외에 KALIMER 설계에 도입된 전자펌프 모델을 선택적으로 사용 가능하다. 6 장에는 노심에서 발생되는 붕괴열을 원자로 벽면과 압력용기 벽면을 통하여 주변의 공기로 제거하는 PSDRS 모델을 기술하였다. 7 장에는 도플러와 소듐밀도 변화에 의한 반응도 모델 및 노심의 기하학적 변형에 의한 여러 반응도 궤환 모델에 대하여 설명하였다. 마지막으로 8 장에는 SSC-K 에 사용되는 상관식 및 물성치에 대하여 기술하였다. 시험계산을 통하여 개발된 SSC-K 코드의 예측능력에 대한 타당성을 정성적으로 확인하였다. 전형적인 액체금속로 사고들에 대하여 SSC-K 를 사용한 안전해석 결과는 별도의 보고서로 발간될 예정이다. 시험해석 결과에 의하면 개발된 SSC-K 코드는 향후 KALIMER 예비 안전해석에 사용할 수 있을 것으로 판단된다				
주제명 키워드 (10 단어내외)	LMFBR, SSC-K, Safety Analysis Code				